THÈSE

Pour obtenir le grade de

Docteur

Délivré par l'**École Nationale Supérieure de Chimie**

Préparée au sein de l'école doctorale **Sciences Chimiques Balard**
Et de l'unité de recherche **ICG -Equipe CTMM**

Spécialité: **Chimie Théorique**

Présentée par **Nicola Scafuri**

Ligand electronic influence in Pd-catalyzed C-C coupling processes.

Soutenue le 09/12/2016 devant le jury composé de

Mme Karinne Miqueu	DR	Universitè de Pau et des Pays de l Adour	Rapporteur
M Stuart Macgregor	PR	Heriot-Watt University of Edinburgh	Rapporteur
M Michel Etienne	PR	Université de Toulouse	Examinateur
M Jean-Marc Campagne	PR	École Nat. Sup. Chimie Montpellier	Examinateur
M Eric Clot	DR	Université Montpellier	Direct. de Thèse

Summary: The main objective of the present thesis is to get a better understanding of the Pd-catalyzed cross-coupling reactions, using the tools of computational chemistry. In particular, a detailed mechanistic study of all the possible reaction paths was carried out with different supporting ligands at palladium (phosphines and N-heterocyclic carbenes) in order to understand the elctronic influence of the latter on the three main steps: oxidative addition, transmetalation and reductive elimination. To probe the electronic influence of the ligands, the well-known *Natural Bond Orbital* (NBO) analysis and the innovative *Charge Displacement via Natural Orbital for Chemical Valence* (NOCV) were used. In addition, two computational studies of Pd-catalyzed transformations were carried out in collaboration with some experimental groups: hydrophosphonylation of alkenes and direct arylation of fluorinated substrated aromatic rings. The main purpose of these studies was to identify the factors at the origin of the regioselectivity observed.

Keywords: threorical chemistry, catalysis, DFT calculations.

Résumé: L'objectif principal de cette thèse est de pervenir, au moyen des méthodes de la chimie computationelle, à une meilleure compréhension des processus de couplage catalysés par le palladium. Una attention toute particulière a été apportée a l'étude de l'influence électronique des ligands du palladium (phoshpines ou carbène N-héterocyclique) sur les profils énérgetique des trois principales transformations: addition oxydante, transmetallation et élimination réductrice. Pour quantifier cette influence électronique, deux méthodes d'analyse différentes ont été utilisées: NBO (*Natural Bond orbital*) et NOCV (*Charge Displacement via Natural Orbital for Chemical Valence*). La méthode NBO est calssique alors que la méthode est plus recent. Il convnait pour cette dernière de tester sa pertinence pour le probléme étudié.

De plus, en collaboration avec différent groupes d'expérimentateurs, le mécanisme de deux réactions catalysées au palladium ont été étudiés: hydrophosphonylation du styrène et arlyation directe de dérivés aromatiques fluorés. Dans chacun des cas, l'objectif principal était d'indentifier les facteurs à l'origine des régiosélectivités observés.

Mots clés: chimie theorique, catalyse, calculs DFT.

Contents

Chapter 1

Palladium Catalyzed Cross-Coupling Reactions

1.1 Introduction

Cross-coupling processes have a rich and intriguing history originating in the 19^{th} century. The early discoveries of the metal-mediated homocoupling processes, for example Ullmann and Kharasch, originally inspired chemists to ponder over the possibility of forming carbon-carbon bond selectively between two different, rather than two identical, structural fragments. The issue of selectivity in cross-coupling reactions is of decisive significance, since a number of possible side reactions (e.g. homocoupling, isomerization, β-hydride elimination and functional group interferences) must be avoided to develop a practical method for use in organic synthesis. The introduction of palladium to this chemistry by Richard Heck, who developed coupling reactions of aryl compounds in the presence of either stoichiometric or catalytic amounts of palladium(II) in the late 1960s (Figure 1.1), designates a breakthrough toward the fascinating area of palladium-catalyzed carbon-carbon bond forming reactions.[1] Today, palladium catalyzed reactions provide extraordinarily useful and widely applied tools for organic synthesis. Famous representatives are the Heck,[2] Negishi[3] and Suzuki-Miyaura[4] reactions whose importance and excellence in organic chemistry were acknowledged by awarding the Nobel Prize in Chemistry in 2010.[5] The award of the 2010 Nobel Prize in Chemistry to Richard Heck, Ei-ichi Negishi and Akira Suzuki was a monumental event that was applauded by chemists worldwide: indeed the pioneering work in the 1960s and 1970s of the three Nobel Prize winners has led to cross-coupling reactions nowadays becoming extremely valuable and reliable transformations in complex natural product syntheses, and even more importantly for numerous pharmaceutical and agrochemical applications, as well as for the production of new materials. The work of the three Nobel Prize winners ushered in a new era in organic chemistry, which stimulated dedicated research efforts worldwide towards broadening the scope of all of these reactions. As a consequence, coupling reactions under milder conditions with lower Pd loadings were developed, using more efficient

catalytic systems by incorporating a plethora of ligands with different steric and electronic properties. These powerful ligands ultimately led to the discovery of new cross-coupling reactions generating other bonds. Researchers worldwide strove to extend, apply, and discover new variants of these powerful transformations and, indeed, such efforts continue at an ever increasing pace today. As depicted in Figure 1.2, substantial growth in this area has taken place during the last decade in terms of publications and patents with the Suzuki-Miyaura cross-coupling proving by far the most popular, followed by the Heck and Sonogashira coupling reactions.

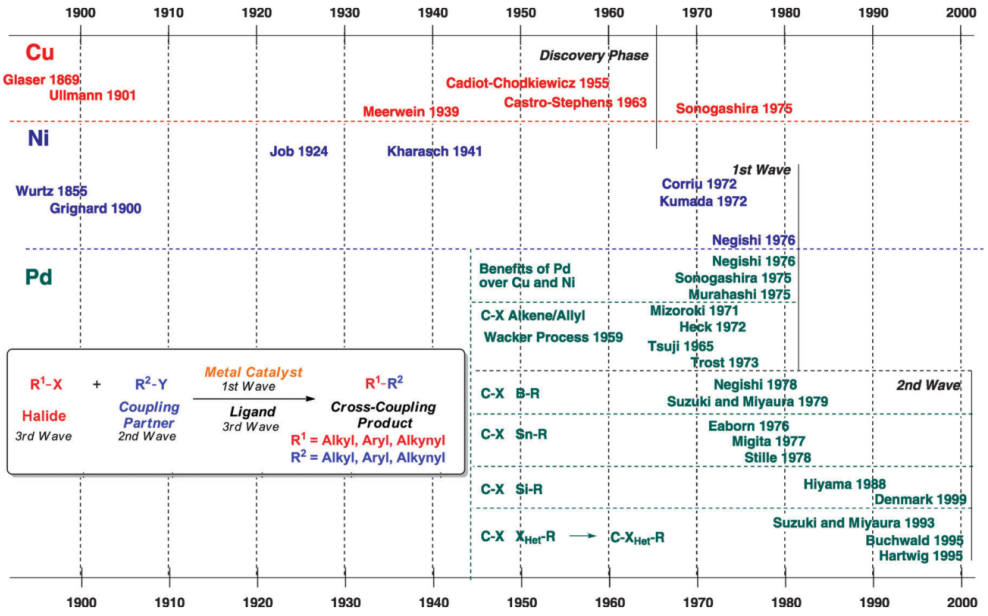

Figure 1.1: *Timeline of the discovery and development of metal-catalyzed cross-coupling reaction.*

In this chapter we present a brief overview of the palladium catalysis. We give first some historical information, explaining why this metal captured the attention of the chemists over the last decades and mentioning the most important discoveries in this field. Then we discuss the peculiarities of this kind of catalysis and the reasons for which the palladium is preferred to other coinage metals, although it is more expensive. In conclusion we present a brief discussion about the aid that the computational chemistry can give for a better understanding of such catalysis and, consequently, for its improvement.

1.2 Historical background

1.2.1 Copper mediated process

The development of metal-catalyzed cross-coupling reactions begins with some of the oldest known transformations in organic chemistry-stoichiometric metal-

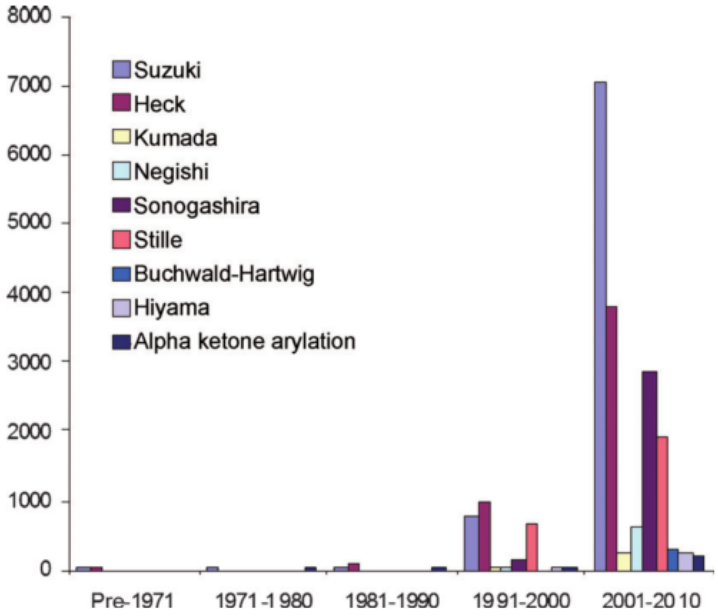

Figure 1.2: *Growth in the number of publications and patents on named metal-catalyzed cross coupling reactions.*

promoted homocouplings. The first examples of the use of metal salts to assemble carbon-carbon bonds between appropriately functionalized sp, sp^2 or sp^3 centers, are found in the late nineteenth century literature. Historically, in the field of coupling chemistry, copper was the first metal used. In 1869 Glaser reported the homocoupling of metallic acetylides (Figure 1.3).[6,7] Although the initial method involved the isolation of the potentially explosive copper acetylene intermediate,[8] the advantage of this new sp-sp bond forming reaction was appreciated by the synthetic community during the following decades.

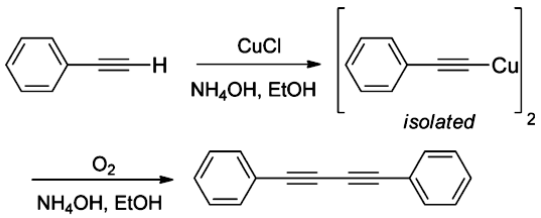

Figure 1.3: *The Glaser coupling (1869).*

Following the development of C(sp)-C(sp) homocoupling, the copper method was extended to C(sp^2)-C(sp^2) bond formation. In 1901, Ullmann reported the dimerization of 2-bromo and 2-chloronitrobenzene promoted by the use of super-stoichiometric copper sources (Figure 1.4).[9–11]

As is typical of the early copper-mediated reactions, the transformation required

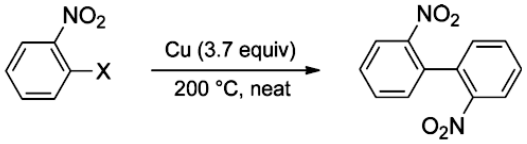

Figure 1.4: *The Ullmann reaction (1901).*

fairly forcing conditions. The Ullmann dimerization, although linked to the Glaser-type process, differed in one fundamental aspect: *the dimerization occurs between carbons bearing halogens rather than between simple unfunctionalized carbon systems*. Although catalytic quantities of copper had been shown to promote the C-O coupling reaction of phenols with aryl halides as early as 1905 by Ullmann,[12] the use of metals in catalytic amounts for the formation of C-C bonds somehow remained an elusive concept during the first part of the the 20^{th} century. The origin of catalysis for the construction of C-C bonds is shrouded by the fog of World War I.

In 1939, Meerwein reported the effects of catalytic copper(II) salts on the coupling of aryldiazonium salts with substituted alkenes (Figure 1.5).[13]

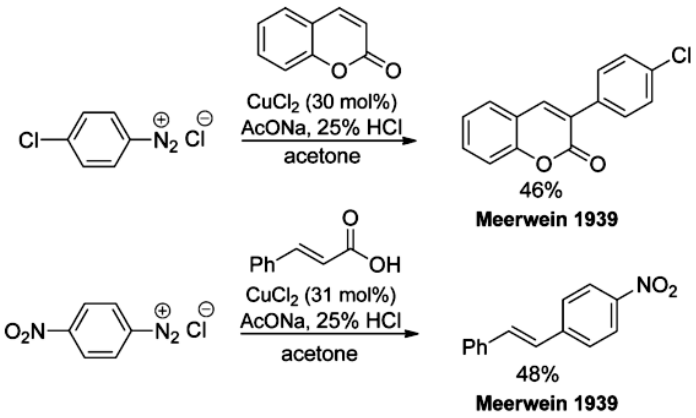

Figure 1.5: *Meerwein couplings.*

Although the reactions described were limited to coumarins and cinnamic acids, and would themselves be expanded in later years, the significance of Meerwein's observations in the field of cross-coupling, especially decarboxylative coupling, appears to have been lost.

The first systematic investigation of transition-metal-catalyzed C(sp^2)- C(sp^2) coupling is found in a publication by Kharasch in 1941 concerning the observation of homocoupling of Grignard reagents.[14] In 1943, this work was extended to the cross-coupling of vinyl bromide with aryl organomagnesium species using cobalt chloride (Figure 1.6).

Meerwein and Kharasch's works represent the earliest reports of a *cross-coupling product, i.e. the use of metals to connect two different coupling partners*.

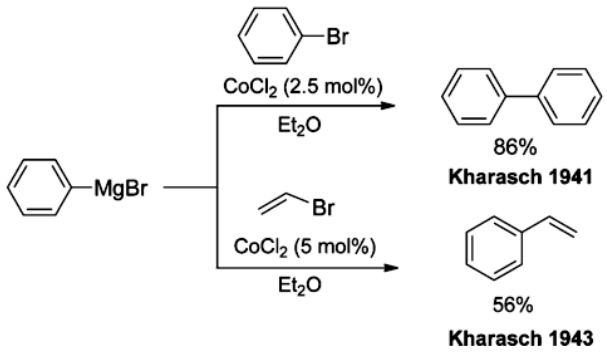

Figure 1.6: *Kharasch couplings.*

Although the early Meerwein and Kharasch-type couplings were extremely limited in substrate scope and functional-group compatibility, they had demonstrated a fundamental premise that would serve as the foundation for all the coupling chemistry to follow: *transition metal could be used in catalytic quantities to form carbon-carbon bonds*.

Unfortunately, many limitations rendered these conditions unsuitable for broad applications in synthesis. In particular, a fundamental problem of selectivity lays at the core of the cobalt and nickel promoted couplings, namely the ratio of the homocoupling to cross-coupling products observed was highly substrate specific, producing uncontrollably variable yields. Thus, advances in the field awaited discovery of conditions which increased selectivity in favor of the cross-coupling products.

Moreover, at this point in the history of coupling chemistry, a set of standard requirements for coupling processes became apparent. In the broadest sense, any coupling procedure required three components to achieve a selective cross-coupling event:

- an *organohalide*, usually aryl or alkynyl, as a coupling partner.
- a *stoichiometric organometallic partner* to prevent homocoupling of the halide coupling component.
- a *transition metal*, in stoichiometric or catalytic quantities, to effect the C-C bond forming event.

These components would prove to be the guiding principle in coupling chemistry throughout the following 50 years.

1.2.2 The rise of palladium: Heck and Suzuki-Miyaura coupling

Following Wollaston's discovery of palladium in 1802, later reported in 1805,[15] his attempts to reap financial benefit were ineffective. Without a useful function, the new element remained a mere chemical curiosity and, on his death, 97% of

the palladium he had extracted remained unsold.[16] For the next hundred years, the chemistry of palladium would be superseded by its more active cousins, platinum and nickel, as researchers investigated these metals reactivity in oxidations, reductions and hydrogenations of unsaturated hydrocarbons.

Post World War II Europe was being rebuilt, and to rebuild required materials. The economic boom was accompanied by surging demand for cheap sources of plastic and precursor fine chemicals.[17] As part of this effort, chemists led by Walter Hafner, began on a quest to synthesize ethylene oxide from ethylene. On exposure of a stream of ethylene and oxygen to a bed of palladium on charcoal, however, the distinctive pungent smell generated suggested the production of acetaldehyde. This fruitful observation, known as Wacker process (Figure 1.7) established the importance of palladium as a metal for the synthesis of organic compounds.[17]

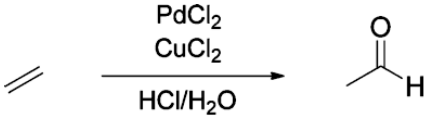

Wacker Chemie GmbH 1959

Figure 1.7: *The Wacker process.*

The work of Wacker would serve as the inspiration for one of the most important discoveries in organic synthesis during the 20^{th} century. In the late 1960s Heck discovered that the transmetalation of organomercury compounds provided arylpalladium salts that could be employed as substrates for several types of olefinic substitution reactions.[18–24] A few years later, Heck[25] and Mizoroki[26] independantly found that organic halides could be coupled with olefins in the presence of catalytic Pd and base. This versatile transformation, known as the Heck reaction (or Mizoroki-Heck reaction), creates new carbon-carbon bonds and has become widely used for the synthesis of pharmaceuticals and natural products, as well as for other industrial applications. Mechanistically, an initial oxidative addition of a vinyl or aryl halide to an unsaturated Pd(0) complex results in a Pd(II) intermediate, which then forms a π complex with the alkene substrate. The alkene undergoes migratory insertion into the palladium-carbon bond, followed by β-hydride elimination, to give a substituted alkene product. The catalyst is regenerated via base-assisted reductive elimination of HX (Figure 1.8).[27]

Together with the Heck reaction, the Suzuki-Miyaura reaction is one of the most widely used methods for the formation of carbon-carbon bonds.[28–30] Suzuki reaction is routinely used in pharmaceutical industry for the assembly of biaryl synthetic targets and this transformation is overwhelmingly the most common Pd-catalyzed coupling for the large scale drugs synthesis candidates.[31] This reactions consists of the coupling between an organoboron compound and an organic halide (or triflate), mediated by a palladium catalyst in the presence of a base (Figure 1.9).

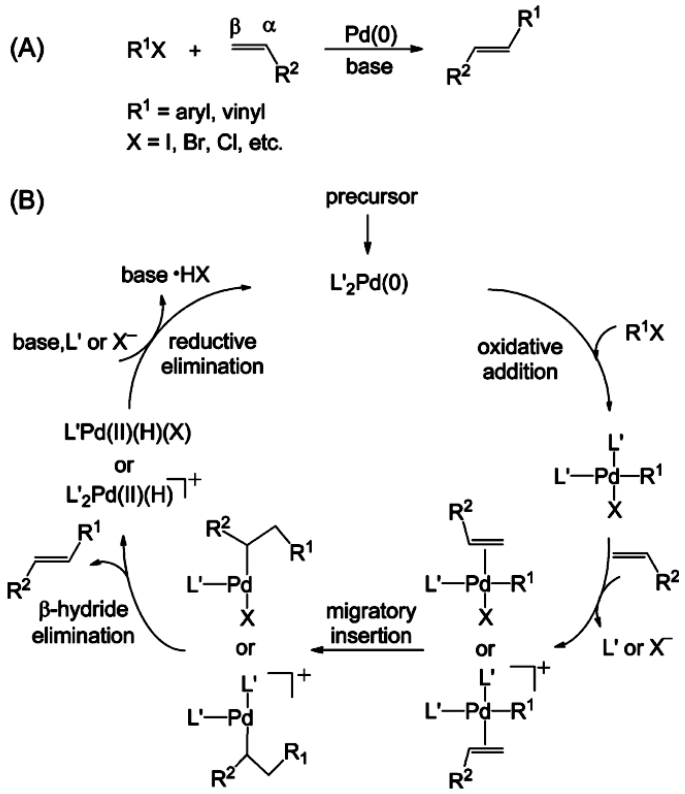

Figure 1.8: *The Heck reaction (A) and its mechanism (B).*

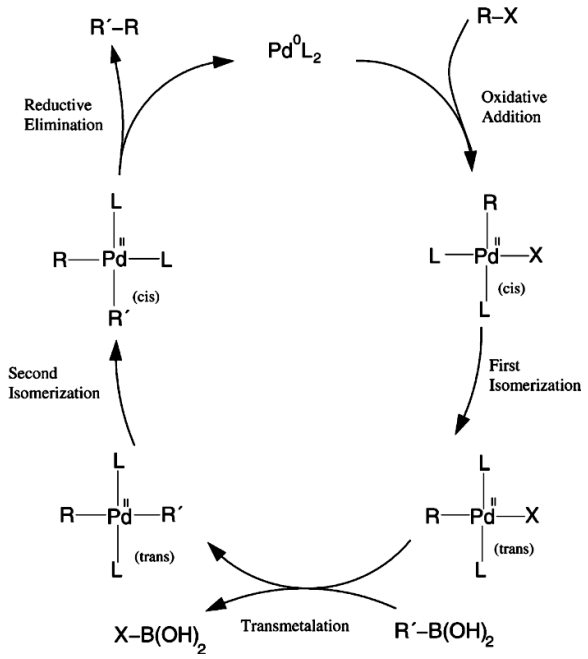

Figure 1.9: *Generally accepted mechanism for the Suzuki-Miyaura cross- coupling.*

Beside these recently awarded reaction types, many other cross-coupling reactions with palladium as catalytic metal exist. Figure 1.10 gives an overview of the typically applied Pd-catalyzed cross-coupling reactions.[1] Whereas the similarity of these reactions, apart from the catalyst, is the organo-halide (or pseudohalides), the second reactant varies.

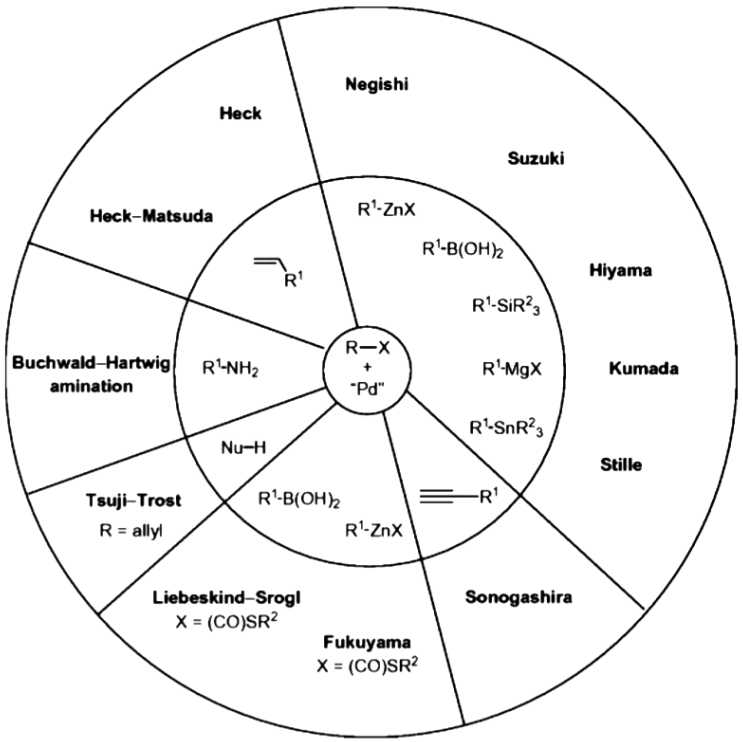

Figure 1.10: *Overview of well-established Pd-catalyzed cross-coupling reactions (R=organic group; X=halogen atom or pseudohalide such as triflate; 'Pd'= Pd catalyst; Nu=nucleophile such as enolate or amine.*

1.3 Features of palladium catalysis

Regarding cross-coupling reactions, palladium as catalyst competes with non precious metals such as copper,[32] nickel[33] and, more recently, iron.[34] Although these and some other d-block transition metals have been shown to be useful elements in C-C cross coupling, Pd proves to be clearly the most useful catalyst. Though nickel, copper, and iron are more cost effective, several advantages of palladium-catalyzed bond formations are decisive. In particular, palladium catalysts show clearly higher activity than their metal alternatives in most cases, enabling the conversion of less reactive substrate at relatively low temperature and providing high catalyst turnover numbers (TONs). In fact, the outstanding role and the particular properties of palladium in catalysis compared to other transition metals can be understood only in the context of the whole catalytic cycle. Of course palladium shares some important features with other transition metals, such as the ability to readily interact with non polar π-bonds, such as those in alkenes, alkynes and arenes. This interaction leads to facile, selective, and often reversible oxidative addition, transmetalation, and reductive elimination (Figure 1.11).

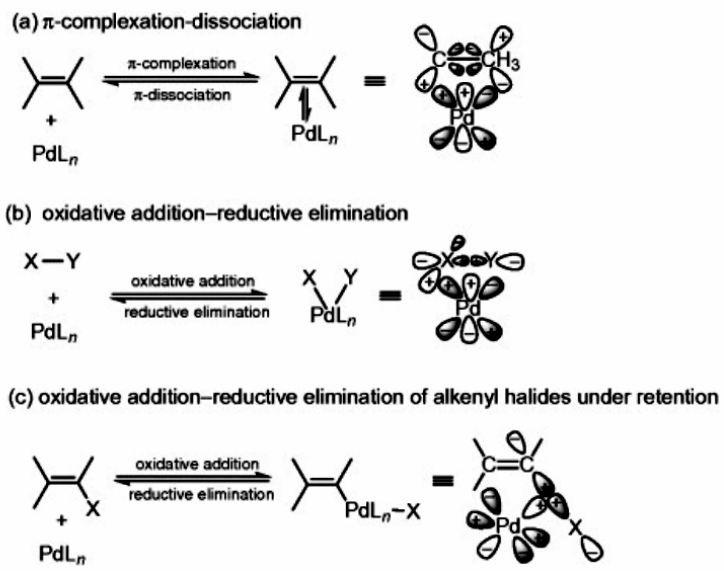

Figure 1.11: *Dewar-Chatt-Duncanson synergistic bonding schemes.*

In addition, palladium is the metal of first choice in the cross-coupling processes, for different reasons: In contrast to the high reactivity of organic halides, most of the traditionally important heteroatom-containing functional groups, such as various carbonyl derivatives, are much less reactive toward Pd and their presence is readily tolerated. The specific features of Pd are the facile coordination of π-electrons, the reversible two-electrons processes, and the facile reductive elimination. The metal needs to participate in redox processes in both directions under one set of reaction parameters and in one vessel. In comparison with the other members of the Ni group all of which fullfill the required frontier orbital condi-

tions, only Pd preferentially undergoes two-electrons redox reactions, being stable as Pd^0, Pd^{II} and Pd^{IV}. Oxidative addition and reductive elimination are two-electrons reactions. For Ni and Cu, one-electron processes are possible leading to highly reactive carbon radical intermediates and thus increasing the number of possible products resulting in lower selectivity. Ni-catalyzed cross-coupling reactions generally display lower TONs by a factor of 10^2 and lower stereo- and regioselectivity. For Pd-catalyzed cross-coupling reactions, often TONs of millions have been observed.[35] The higher activity of palladium allows conversion of less reactive substrate under milder conditions (especially low temperature) providing higher TONs. Of similar importance is the tolerance of functional groups when palladium is employed: group protection is not required. High stability of organopalladium compounds to water and air (except some phosphane complexes) enables easy processing and lower costs. General disadvantages of the Pd-mediated reactions are rooted in high noble metal prices and toxicity of the metal residue that can become problematic in pharmaceutical products. Thanks to excellent activities of palladium catalysts, these problems can be minimized, because only very small amounts are required for high conversion and yields. In addition to palladium complexes in homogeneous solution, a series of new, highly active, and effective heterogeneous (supported) palladium catalysts have been developed in recent years.[36] They can be repeatedly used and thus contribute to efficient and economic application of coupling reactions. Thus, this palladium-catalyzed approach has very often made possible the transfer from gram-scale synthesis in academic laboratories to large-scale production in the pharmaceutical, agrochemical, and fine chemical industries in the past two decades.

1.4 Development of new palladium-catalysis: the challenge of computations

A number of variables must be considered when studying the mechanism of a palladium-mediated reaction. The choice of ligand can have a dramatic effect on a reaction, as both steric and electronic factors have an impact. Also, the solvent used and the additives present in the reaction mixture are particularly important. These variables can influence which palladium species function as the active species in a reaction, as well as define the substrate scope and affect the selectivity in the various steps of the catalytic cycle.[37] Experiment can be used to some extent to investigate the mechanism; however the complexity of a catalytic cycle reaction and the fleeting nature of many intermediates can render the investigation of mechanistic pathways via experiment and spectroscopy alone challenging, if not impossible.

To prove a mechanism one may use experimental methods to detect the intermediates *in situ*. The history of mechanistic inorganic chemistry is full of attempts to isolate or detect more or less short-lived species hypothesized to be formed during a given reaction. However, some species are very hard or indeed impossible to

detect, and theory and computations have provided invaluable help in establishing which intermediates are likely to be formed. Crucially, computations can also predict features of these intermediates, such as their structure or their likely spectroscopic properties that can assist in their identification or at least provide support for their involvement in a given reaction.
Further, computations enable to examinate the elementary reaction steps linking these species. Indeed, computationally, finding transition states for individual steps is needed to characterize the mechanism. Although, with the development of improved computer power, the use of computational studies have become a powerful tool in chemistry, it faces its own challenges and limitations, particularly in the field of metal-based catalysis.
In catalysis several competiting reaction pathways of similar energy frequently exist, and small changes in terms of solvent, additive or ligand can therefore result in completely different pathways being favoured, which is computationally challenging to capture. Also, the relatively large ligands within palladium catalysis may result in various possible conformations of intermediates or transition states that require individual computational assessment. However, the study of one particular step of the catalytic cycle (e.g. oxidative addition or reductive elimination), and the focus on the relative energy differences (e.g. selectivity), rather than absolute energy barriers, may provide valuable insights, as one may benefit from error cancellations of structurally similar geometries. Moreover, this approach allows one to indirectly acquire mechanistic information about specific steps, and the computed differences in selectivity for the individual step of interest can be directly compared with experiments.

Indeed the present work is devoted to a better understanding of the cross-coupling reactions, mediated by Pd catalysts by using the tools of computational chemistry. Our main goal is to study in detail all the possible reaction paths and to clarify the electronic effect of different auxiliary ligands on such cycles.

In particular we divided this work in two main parts. In the first part (REAL SYSTEMS) we carry out a detailed mechanistic study, at the DFT level, on two experimental Pd-catalyzed processes:

- Hydrophosphonylation of alkenes with dialkyl-H-phosphonates (Chapter 3).
- Arylation of Fluorobenzenes (Chapter 4).

In these computational studies, our goal was to reproduce and rationalize experimental data, such as activation barriers and regioselectivity.

In the second part (MODEL SYSTEMS) we investigate in detail the electronic effect of different ligands on the most common steps of Pd-catalyzed processes:

- Oxidative addition (Chapter 5)
- Transmetalation (Chapter 6)
- Reductive elimination (Chapter 7)

The theoretical models we used to characterize the various reaction pathway and the electronic effect of the ligands are discussed in the Chapter 2.

Bibliography

[1] *Palladium-Catalyzed Coupling Reactions: Practical Aspects and Future Developments*; Wiley-VCH, 2012.

[2] Heck, R.; Nolley, J. *J. Org. Chem.* **1972**, *37*, 2320.

[3] Negishi, E.; King, A.; Okudado, N. *J. Org. Chem.* **1977**, *42*, 1821.

[4] Miyaura, N.; Yamada, K.; Suzuki, A. *Tetrahedron Lett.* **1979**, *20*, 3437.

[5] Seechurn, C.; Kitching, M.; Colacot, T.; Snieckus, V. *Angew. Chem. Int. Ed.* **2012**, *51*, 5062.

[6] Glaser, C. *Ber. Dtsch. Chem. Ges.* **1869**, *2*, 422.

[7] Glaser, C. *Ann. Chem. Pharm.* **1870**, *154*, 137.

[8] Walfer, J.; Londergan, T. *US patent* **1948**, *2*, 439.

[9] Ullmann, F.; Bielecki, J. *Ber. Dtsch. Chem. Ges.* **1901**, *34*, 2174.

[10] Hassan, J.; Sevignon, M.; Gozzi, C.; Schulz, E.; Lemaire, M. *Chem. Rev.* **2002**, *102*, 1359.

[11] Ley, S.; Thomas, A. *Angew. Chem. Int. Ed.* **2003**, *115*, 5558.

[12] Ullmann, F.; Sponagel, P. *Ber. Dtsch. Chem. Ges* **1905**, *38*, 2211.

[13] Meerwein, H.; Buchner, E.; van Emster, K. *J. Prakt. Chem.* **1939**, *152*, 237.

[14] Kharasch, M.; Fields, E. *J. Am. Chem. Soc.* **1941**, *63*, 2316.

[15] Wollaston, W. *Philos. Trans. R. Soc. London* **1805**, *95*, 316.

[16] Kronberg, C. L., B.I.; Usselman, M. *Ambix* **1981**, *28*, 20.

[17] Smidt, J.; Hafner, W.; Jira, R.; Sedlmeier, J.; Sieber, R.; Kojer, H.; Ruttinger, R. *Angew. Chem.* **1959**, *71*, 176.

[18] Heck, R. *J. Am. Chem. Soc.* **1968**, *90*, 5518.

[19] Heck, R. *J. Am. Chem. Soc.* **1968**, *90*, 5526.

[20] Heck, R. *J. Am. Chem. Soc.* **1968**, *90*, 5531.

[21] Heck, R. *J. Am. Chem. Soc.* **1968**, *90*, 5531.

[22] Heck, R. *J. Am. Chem. Soc.* **1968**, *90*, 5535.

[23] Heck, R. *J. Am. Chem. Soc.* **1968**, *90*, 5538.

[24] Heck, R. *J. Am. Chem. Soc.* **1968**, *90*, 5542.

[25] Heck, R.; Nolley, J. *J. Org. Chem.* **1972**, *37*, 2320.

[26] Mizoroki, T.; Mori, K.; Ozaki, A. *Bull. Chem. Soc. Jpn.* **1972**, *44*, 1505.

[27] Dang, Y.; Shuanglin, Q.; Wang, Z.; Wang, X. *J. Am. Chem. Soc.* **2014**, *136*, 986.

[28] Suzuki, A.; Miyaura, N. *Chem. Rev.* **1995**, *95*, 2457.

[29] Suzuki, A.; Miyaura, N.; Yamada, K. *Tetrahedron Lett.* **1979**, *20*, 3437.

[30] Suzuki, A.; Miyaura, N. *J. Am. Chem. Soc.* **1979**, *20*, 866.

[31] Magano, J.; Dunetz, J. *Chem. Rev.* **2011**, *111*, 2177.

[32] Tamura, M.; Kochi, J. *Synthesis* **1971**, 303.

[33] Corriu, R.; Masse, J. *J. Am. Chem. Soc.* **1972**, *144*.

[34] Tamura, M.; Kochi, J. *J. Am. Chem. Soc.* **1972**, 303.

[35] Negishi, E.; Wang, G.; Rao, H.; Xu, Z. *J. Org. Chem.* **2010**, *75*, 3151.

[36] Coperet, C.; Comas-Vives, A.; Conley, M.; Estes, D.; Fedorov, A.; Mougel, V.; Nagae, H.; Nunez-Zarur, F.; Zhizhko, P. *Chem. Rev.* **2016**, *116*, 323–421.

[37] Bonney, K.; F., S. *Chem. Soc. Rev.* **2014**, *43*, 6609.

Chapter 2

Theoretical Models for the Chemical Analysis

2.1 Synopsis

In this chapter, the theoretical models that we applied for the chemical analysis will be discussed. This general discussion includes a brief introduction to the DFT model for the characterization of the energetic pathways and the importance of calculating and including the dispersion correction in such paths. Then we introduce the two theories we used to investigate the chemical bond in the Pd-based catalysis: the *Natural Bond Orbitals Theory* (NBO) and the *Charge Displacement Analysis via Natural Orbitals for Chemical Valence* (CD-NOCV).

2.2 Density functional theory (DFT)

Density Functional Theory (DFT) has become very widely used to study the electronic structure and related properties of transition metal complexes. The development of DFT has led to a huge change in the field of transition metal chemistry.[1] Such development in the late 1980s and early 1990s of new, more accurate functionals and of efficient, user friendly computer codes led to an explosion in the number and the breadth of applications. DFT computations have become an accepted tool for analyzing structure, bonding, reactivity and properties. The reason of this remarkable development is that DFT is both relatively cheap and relatively accurate. This means that useful results can be obtained in a routine way for realistic models of the target molecule, or indeed for the molecule itself.

The basic idea of DFT is that the energy of a system composed of fixed nuclei (Born Oppenheimer approximation) and electrons can be expressed as a functional $E[\rho]$ of the electron density function.[2] This represents a considerable simplification over the *ab initio* traditional electronic structure theory, in which the central object is the electronic wavefunction Ψ, which depends simultaneously on the coordinates of all the electrons (3N variables). The electronic density function ρ only depends on three variables.

The foundations of DFT are the two Hohenberg-Kohn theorems,[3] which state that the external potential associated to the mutual position of the nuclei defines the density of the ground state of the system, and that the density can be derived from a variational procedure. However, the form of the exact functional is not clearly defined. In practice the energy is usually written as a sum of three well defined terms and one smaller, less well understood term, the exchange correlation term, in which the uncertainties concerning the form of the functional are collected (equation 2.1):

$$E[\rho] = T_0[\rho] + J[\rho] + \int \nu(r)\rho(r)dr + E_{XC}[\rho] \tag{2.1}$$

$T_0[\rho]$ is an approximation to the electronic kinetic energy. J[ρ] is the Coulomb energy, and represents the repulsion between the electron density and itself. This term is non-zero even for one-electron systems because it includes electron self interaction. $\int \nu(\mathrm{r})\rho(\mathrm{r})$ term represents the electromagnetic interaction of the electron density with the external potential, in most cases this simply corresponds to the Coulombic interactions between electrons and nuclei. The $E_{XC}[\rho]$ term, the exchange correlation functional, corrects the first three terms. First, it contains a term for electronic exchange to reflect the fermionic nature of the electrons. This term also serves to correct for the spurious self interaction introduced by the Coulomb energy. Next, it accounts for electron correlation. Finally, it could in principle correct for the approximate nature of the kinetic energy term, although common functionals do not usually contain a term explicitly aimed at correcting for this effect. The energy expression given in equation (2.1) leads to a set of equations defining the shape of the orbitals that are used to expand the density. These are the Kohn Sham equations that are the foundation of all modern DFT applications.[4]

$$\left[-\frac{1}{2}\nabla^2 + \nu_0(r) \right] \phi_i = \epsilon_i \phi_i \tag{2.2}$$

The Kohn Sham equation is defined by a local effective (fictitious) external potential in which the non-interacting particles move, typically denoted as $\nu_0(\mathrm{r})$, called the Kohn Sham potential. As the particles in the Kohn Sham system are non-interacting fermions, the Kohn Sham wavefunction is a single Slater determinant constructed from a set of orbitals that are the lowest energy solutions. Here, ϵ_i is the orbital energy of the corresponding Kohn Sham orbital, ϕ_i, and the density for an N-particle system is

$$\rho(r) = \sum_{i}^{N} |\phi_i(r)|^2 \tag{2.3}$$

Solving these equations leads in principle to the exact energy and density of the target system. The degree of accuracy obtained depends on the form given to the exchange correlation functional.

Over the years, many exchange correlation functionals have been developed. In the first generation of exchange correlation functionals, the energy was ob-

tained from a purely local integral over the density, *local density approximation, LDA* (equation 2.4). In this equation, separated local exchange and correlation terms ϵ_X and ϵ_C are introduced.

$$E_{XC}[\rho] = \int \epsilon_X[\rho(r)] + \epsilon_C[\rho(r)]\rho(r)dr \tag{2.4}$$

In the LDA approximation, ϵ_X and ϵ_C are functions which depend only on the scalar value of the electron density at a given point in the space. A simple exchange correlation functional is that due to Slater:[5]

$$\epsilon_X[\rho(r)] = -\frac{3}{2}\Big(\frac{3}{\pi}\rho(r)\Big)^{\frac{1}{3}} \tag{2.5}$$

The expressions used for local correlation functionals are more complicated. The local density approximation is a remarkably accurate method given the relative simplicity of the energy functional. It leads to very good predicted molecular geometries, and to a reasonable description of molecular electronic structure and thermochemistry. However, bond energies (and atomization energies) are almost always overestimated compared to experiment, with a quite large deviation.

A second generation of exchange correlation functionals includes not only functions of the scalar density, but also functions of the gradient of the density (*Generalized Gradient Approximation, GGA*). Whilst more fundamental theoretical reasons can be given for including the gradient terms, they can be justified in hand-waving terms based on the fact that the energy functional is expected to be different in regions such as those surrounding the nuclei (where the density varies rapidly) and those far from the nuclei (where it varies only slowly).

Many different GGA exchange and correlation functionals exist. Some are defined as corrections to the local exchange and correlation functionals mentioned above, whereas some include both local and non-local effects. For example, one of the most popular exchange functionals, proposed in 1988 by Becke, is written as a sum of the local exchange of equation 2.5 and a correction term that depends on the gradient of the density. (equation 2.6, the index σ refers to up and down spin, separately).[6] This functional was developed so as to reproduce the correct long-range behavior of the Coulomb potential:

$$\epsilon_X[\rho] = -\sum_\sigma {\rho_\sigma}^{1/3}\left(\frac{3}{2}\left(\frac{3}{4\pi}\right)^{1/3} + \frac{\beta{\chi_\sigma}^2}{1+6\beta\chi_\sigma sinh^{-1}\chi_\sigma}\right) \tag{2.6}$$

when $\chi_\sigma = \mid \bigtriangledown\rho_\sigma \mid / {\rho_\sigma}^{4/3}$

The use of local exchange and correlation functionals leads to significant overestimates of atomisations energies. Many GGAs also lead to the same type of overbonding, if to a lesser extent. However, the Hartree-Fock method substantially understimates these energies. This suggests that some combined treatment might yield improved thermochemical results, and this is indeed the case. It is also possible to put forward sophisticated theoretical arguments based on the adiabatic connection in favour of using the resulting functionals, which are referred to as

hybrid. In the first application of this approach, the exchange correlation energy was calculated using one half of the Hartree Fock type exchange energy of the Slater determinant formed from the Kohn Sham orbitals, and one half of the LDA exchange energy of the corresponding density, and this led to accurate results for a number of test cases.

More sophisticated hybrid functionals were then developed, including the very popular B3LYP functional. This was based on an earlier three-parameters functional in which the exchange correlation energy was expressed as a combination of the local exchange correlation energy, the HF exchange energy, and the gradient corrections to the exchange and correlation energies as shown in equation 2.7:[7]

$$E_{XC} = {E_{XC}}^{LSDA} + a_0({E_X}^{HF} - {E_X}^{LSDA}) + a_X\Delta{E_X}^{B88} + a_c\Delta{E_C}^{PW} \qquad (2.7)$$

In the original form of this functional, the non-local exchange and correlation terms were taken from the GGA exchange and correlation functionals of Becke[6] and Perdew,[8] respectively. The semi-empirical coefficients a_0, a_X and a_C were fitted to reproduce as well as possible a set of ca. 100 atomization energies, ionization energies, proton affinities and atomic energies.

The description above of the four types of functional suggests that there has been constant development of more and more accurate functionals, with the latest developments leading to methods that can be used as black-box tools yielding very high accuracy for all sorts of problems.

Despite the many successes obtained using modern functionals, care is still needed as quite large errors can occur. These can be best understood by taking into consideration how density functional theory works, and how well it performs for the simpler case of main-group compounds. This serves to highlight the critical role of the exchange functional, which describes such varied effects as electron self-interaction, static (or non-dynamic) correlation , and dynamic correlation. A poor balance between these effects can lead to significant errors even for main-group compounds. This is even truer for transition metal compounds.

Overall, DFT is already a tremendously useful method for studying structure, properties, and reactivity in metallic compounds, in such diverse areas as inorganic, organometallic and bioinorganic chemistry. Even non-expert users can easily predict geometries, binding energies, mechanisms and activation energies to a useful level of accuracy. It should however be realized that all currently used functionals are still liable to yield very inaccurate results, especially for energetic quantities. This type of problem occurs more often for transition metal compounds than for other species.

2.3 The dispersion correction

Dispersion interactions play an important role in physical organic chemistry.[9,10] For example, self assembly processes, ranging from small organic molecules cry-

stal formation, to protein folding, can be driven primarily by dispersion interactions.[11,12] These systems share many common features, including the fact that their properties arise from non-covalent interactions, especially dispersion, between monomer components. Computational modeling is critical for providing insight into these systems and to allow their unique features to be exploited. Theoretical techniques, to treat large organic systems with significant dispersion interactions, have been undergoing constant development over the last decade.

Dispersion interactions are generally described as the interactions between instantaneous dipole moments within the electron distributions of two atoms or molecules.[13] The dispersion energy, E_{disp} between two atoms or molecules at large separation takes the form of a series expansion:

$$E_{disp} = -\frac{C_6}{R^6} - \frac{C_8}{R^8} - \frac{C_{10}}{R^{10}} - ... \tag{2.8}$$

The dispersion coefficients can be determined experimentally[14] or theoretically.[15] There are several approximate methods to evaluate the dispersion coefficients, such as the London[16] and Slater-Kirkwood models.[17] In most of the cases, dispersion attraction is modeled only by the first term in the series. For example, in molecular mechanics (MM) force fields, a Lennard-Jones 6-12 potential is used to describe non-bonded interaction with the R^6 term accounting for dispersion attraction and the R^{12} term corresponding to Pauli repulsion.[18]

In the wavefunction approach of quantum chemistry, dispersion is a dynamical correlation effect. The Hartree-Fock method, which is the simplest wavefunction approach, does not include dynamical correlation. Therefore, the HF method cannot model dispersion interactions and produces entirely repulsive potential energy surface (PESs) for dispersion-bound complexes. Figure 2.1 shows this repulsion in the case of parallel structure of the benzene dimer, which serves as a good model for dispersion interactions.[10] HF-based wavefunction can be improved by expanding the wavefunctions with additonal electronic configurations. These methods, which create correlated wavefunction, usually provide more reasonable treatments of dispersion. A perturbative approach such as MP2 predicts the bonded nature of the benzene dimer, accurately. Accurate dispersion-binding is predicted by the computationally intensive coupled-cluster theory, provided that large basis sets are used. The time and resources required to perform such calculations quickly become very large as the size of the systems increase.

Dispersion-Correction DFT

All standard DFT methods predict repulsive interactions between nominally dispersion-bound complexes at large separation,[19] rather than the $-C_6/R^6$ behavior that is characteristic of dispersion attraction. This includes LDA, GGA and meta-GGA functionals. Ideally, the DFT exchange terms should reproduce the exact exchange of the system. Therefore, DFT exchange terms should predict completely repulsive in-

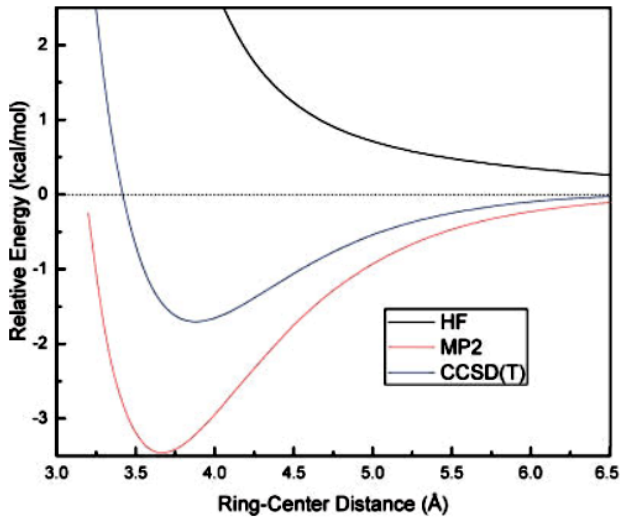

Figure 2.1: *Parallel benzene dimer (D_{6h} symmetry) PESs generated using the HF, and CCSD(T) methods at the estimated complete basis set limit.*

teractions in dispersion-bound systems. Likewise, since dispersion is a dynamical-correlation effect, the DFT correlation terms should ideally predict an attractive interaction in dispersion-bound systems. However, most of the popular correlation functionals do not predict the correct dispersion physics, and the dispersion-like binding of some functionals has been shown to originate from the exchange terms.[20]

A simple and intuitive approach for correcting conventional DFT methods for dispersion is to add explicit, attractive C_6/R^6 terms between all atomic pairs. The use of C_6/R^6 terms to correct DFT is termed *DFT-D*. Within the general set of DFT-D methods, several approaches have been used to obtain the empirical dispersion-coefficients, including use of the Slater-Kirkwood[21,22] model and London-type approximations.[23,24]

DFT-D methods, particularly the approaches of Grimme[22,24] and of Hobza,[25] have been successfully used in many applications. The technique does not add any computational cost over conventional DFT calculations, but generally requires the use of relative large basis sets to ensure reliable results. Therefore, the DFT-D methods implemented by Grimme may be quite time consuming essentially because large basis sets are required. Nevertheless, the DFT-D approach works quite well. For example, Grimme has shown that their BLYP-D/TZV(2d,2p) approach gives a MAPE of 10.1 % for the binding energies of the S22 set.[26] To illustrate the long-range behavior of DFT-D, in Figure (2.2) is reported the generated PES, using BLYP-D, for the benzene dimer potential.

The inclusion of dispersion corrections using a DFT-D approach can be easily performed in a posteriori fashion. That is, electronic energies of dispersion-bound complexes may be calculated using the DFT approach. Following this, dispersion energy corrections can be calculated with relatively little computational effort. The

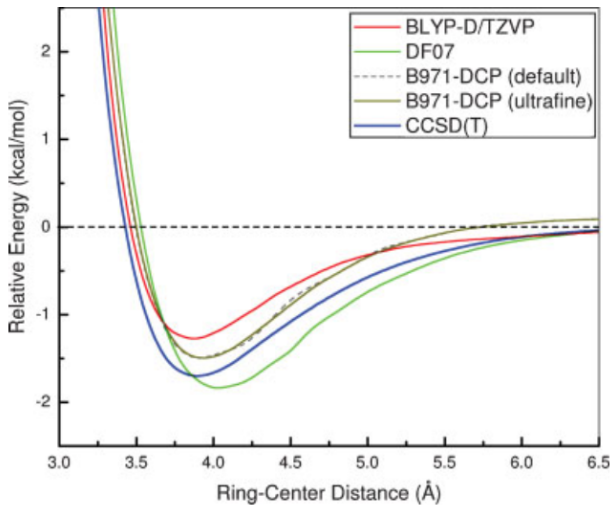

Figure 2.2: *Parallel benzene dimer (D_{6h} symmetry) PESs generated using BLYP-D/TZVP. The potentials generated with default potential and ultrafine integration grids with B971/6-31G(d,p)-DCP are also shown. The surface obtained using CCSD(T)/CBS is also shown.*

general form for the dispersion energy (which is simply added to the Kohn Sham energy) is:

$$E_{disp}^{DFT-D} = -\sum_{AB}\sum_{n=6,8,10,\ldots} s_n \frac{C_n^{AB}}{R_{AB}^n} f_{damp}(R_{AB}) \tag{2.9}$$

where, the sum is over all atom pairs (A,B) in the system, $C_n{}^{AB}$ denotes the averaged (isotropic) n^{th}-order dispersion coefficient (orders n = 6,8,10,...) for atom pair AB, and R_{AB} is the internuclear distance. S_n are scaling factors used to adjust the correction to the repulsive behavior of the chosen parametrized functional. In order to avoid near singularities for small R, and double counting effects of correlations at intermediate distances, damping functions f_{damp} are used, which determinate the range of the dispersion correction.[27] The contribution of the higher-ranked multipole terms n > 6 is important at short range and rather strongly interferes with the (short-ranged) description of electronic correlation.

In our computational investigations, we used the Grimme model to calculate the contribution of the dispersion correction to the molecular energy. In such model, the dispersion corrected total energy is given by:[22]

$$E_{disp} = -s_6 \sum_{i=1}^{N_{at}-1}\sum_{j=i+1}^{N_{at}} \frac{C_6^{ij}}{R_{ij}^6} f_{damp}(R_{ij}) \tag{2.10}$$

where N_{at} is the number of atoms in the system, $C^{ij}{}_6$ denotes the dispersion coefficient for atom pair (i,j), s_6 is a global scaling factor and R_{ij} is the interatomic distance. To avoid near singularities for small R, a damping function f_{damp} must be used which is given by

$$f_{damp}(R) = \frac{1}{1 + e^{-\alpha(R/R_0 - 1)}} \tag{2.11}$$

where R_0 is the sum of atomic van der Waals radii.

Different combination rules for the composed $C^{ij}{}_6$ coefficients have been carefully tested for many complexes. A simple average of the form

$$C_6^{ij} = 2\frac{C_6^i C_6^j}{C_6^i + C_6^j} \tag{2.12}$$

is used. The atomic coefficients are taken from the work of Wu and Yang.[21]

The DFT-D atomic dispersion coefficients are highly empirical molecular mechanics like parameters. They only depend on atom type and do not respond to changes in an atom electronic environment. This is a good approximation for organic systems because like atoms tend to have very similar C_6 values in neutral molecules. DFT-D methods tend to perform very well for dispersion interactions involving neutral, organic systems.

In general, because dispersion is an electronic correlation effect, it operates also intramolecularly (between atoms or functional groups that are not directly bonded). This contributes to the internal energy of (essentially larger) molecules and must be considered for accurate thermochemical computations.

2.4 Natural Bond Orbital (NBO) analysis

Natural Bond Orbital methodology (NBO) is based essentially on the wavefunction Ψ and its practical evaluation (to sufficient chemical accuracy) by modern computational methods.[28,29] Unlike conventional valence bond (VB) or molecular orbital (MO) viewpoints, NBO theory makes no assumption about the mathematical form of Ψ. Most essential to natural methods is the *reduced* form of Ψ given by the one-electron density operator $D^{(1)}$. This is derived by averaging over (integrating out) all but one of the N electronic space-spin coordinates, namely,

$$D^{(1)} = N \int |\Psi(1, 2, ..., N)|^2 dr_2 dr_3 ... dr_N \tag{2.13}$$

As originally introduced by Lowdin, natural orbitals $\{\theta_k\}$are the eigenfunctions of $D^{(1)}$ satisfying

$$D^{(1)}\chi_k = n_k\chi_k \tag{2.14}$$

where

$$n_k =< \chi_k|D^{(1)}|\chi_k >= \int \chi_k^* D^{(1)}\chi_k dr_1 \tag{2.15}$$

is the occupancy (electronic population) of χ_k subject to the usual Pauli exclusion principle ($0 \leq n_k \leq 1$ for the spin orbital and $0 \leq n_k \leq 2$ for the spatial orbital). Each θ_k represents a principal component of $D^{(1)}$ with extremal occupancy. Each χ_k could alternatively be defined as a *maximum occupancy* (or maximum density) orbital, contributing incremental electron density $\rho_k = n_k|\chi_k|^2$ that gives the most compact description of the total electron density ρ.

The key distinguishing feature of NBOs is their formulation in terms of *natural atomic orbitals* (NAOs), a complete orthonormal set for optimally describing the effective atom-like constituents within the molecule environment.[30] These NAOs $\{\chi^{(A)}\}$ of atom A are obtained by diagonalizing the matrix representing $D^{(1)}$ on the AO centered on A.

At large interatomic separations, the NAOs $\{\chi^{(A)}\}$ essentially reduce to the corresponding atomic natural orbitals of the isolated atoms.[31] However, in a given molecular environment, the NAOs reflect the chemical give and take of electronic interactions, with variations of shape and size, which distinguish them from free-atoms form. In contrast to Gaussian-type orbitals (GTOs), Slater-type orbitals (STOs), or other atomic orbital basis function in common usage, the NAOs are most strongly distinguished by their *strict maintenance of intra- and interatomic orthonormality*. Indeed such orthonormality

$$< \xi_i^{(A)}|\xi_j^{(B)} >= \delta_{ij}\delta_{AB} \tag{2.16}$$

is an elementary mathematic prerequisite for eigenorbitals of any physical Hermitian operator. Note that the NAO and, NBO, and associated occupancies are in principle uniquely determined by $D^{(1)}$, and thus by Ψ itself. In practice, the NBO-based quantities are found to converge rapidly to well-defined numerical limits, independently of the numerical basis set or other arbitrary details of approximating Ψ. Thus, these orbitals can be used to represent exactly any property of the system in localized terms. The NAOs divide naturally into a leading high-occupancy set (the natural minimal basis) and a residual low-occupancy set (the natural Rydberg basis), where the occupancies of the latter orbitals are usually quite negligible for chemical purposes.

In an isolated ionic or neutral species, each NAO retains the characteristic angular shape of the pure s and p hydrogenic orbitals. However, in the presence of another atom or ion this symmetry is broken, and the optimal valence orbitals acquire sp^λ hybrid form (assumed for simplicity to include only valence s and p orbitals), as represented mathematically by

$$h = \frac{1}{(1+\lambda)^{1/2}}(s + \lambda^{1/2}p) \tag{2.17}$$

In this expression, the hybridization parameter λ varies between 0 (pure s) and ∞ (pure p), with any integer or non-integer value in this range being physically allowed. The general relationships between λ and percentage s and p characters are given by

$$\%s = 100\frac{1}{1+\lambda} \tag{2.18}$$

$$\%p = 100\frac{\lambda}{1+\lambda} \tag{2.19}$$

or equivalently

$$\lambda = \frac{\%p}{\%s} \tag{2.20}$$

The N/2 Lewis-type NBOs of highest occupancy can be directly associated with the localized electron pairs of the chemists Lewis-structure diagram. Each Lewis-type NBO can be decomposed into constituent natural hybrid orbitals (NHOs) h_A and h_B on atoms A and B,

$$\theta_{AB} = c_A h_A + c_B h_B \tag{2.21}$$

with polarization coefficients c_A and c_B satisfying $|c_A|^2 + |c_B|^2 = 1$. The bonding hybrids h_A and h_B are constructed from NAOs on atoms A and B in a manner that closely resembles the classical Pauling hybridization picture, but all details of NHO hybridization and polarization are numerically optimized to give the best possible description of electron density. The two valence hybrids h_A and h_B give rise to two valence-shell NBOs: an in-phase Lewis-type NBO (equation 2.21) and a corresponding out-of-phase non-Lewis NBO ${\theta^*}_{AB}$,

$$\theta^*_{AB} = c_B h_B - c_A h_A \tag{2.22}$$

which is unoccupied in the Lewis-structure picture. The set of Lewis-type NBOs typically includes a one-center core (labeled CR in the NBO program output) and valence lone pair (LP) as well as two-centers bond (BD) orbitals. The non- Lewis set includes unoccupied valence nonbonding (LP*) and extra-valence-shell Rydberg (RY*) orbitals as well as the valence antibonds (BD*) (equation 2.22).

Thus, the NBOs form a chemist's basis set of Lewis-type (unstarred) and non-Lewis-type (starred) orbitals, each member being closely associated with some aspect of the localized Lewis structure diagram or its capacity for chemical change.

The localized wavefunction $\Psi^{(L)}$ formed from N/2 doubly occupied Lewis-type NBOs,

$$\Psi^{(L)} = \hat{A}[(\theta_{AB})^2(\theta_{CD})^2...] \tag{2.23}$$

corresponds to an idealized natural Lewis-structure picture. As usual, the wavefunction (2.23) can be associated with an Hamiltonian $\hat{H}^{(L)}$ and an energy $E^{(L)}$ of a strictly localized Lewis-structure model chemistry, with Schrodinger equation

$$\hat{H}^{(L)}\Psi^{(L)} = E^{(L)}\Psi^{(L)} \tag{2.24}$$

Let us consider the hydrogen fluoride as a simple example. The conventional Lewis structure diagram of this molecule corresponds to a sigma bond (σ_{HF}) and three fluorine lone pairs ($n^1{}_F$, $n^2{}_F$ and $n^3{}_F$), as well as the fluorine core pair (K_F). A portion of the NBO output is shown below:

```
NATURAL BOND ORBITAL ANALYSIS:
    (Occupancy)  Bond orbital/ Coefficients/ Hybrids
-------------------------------------------------------------------------------
 1. (2.00000) BD ( 1) H 1- F 2
              ( 22.39%)  0.4732* H 1 s( 99.89%)p 0.00 (  0.11%)
              ( 77.61%)  0.8810* F 2 s( 20.93%)p 3.77 ( 78.95%)d 0.01(  0.12%)
 2. (1.99994) CR ( 1) F 2            s (100.00%)
 3. (1.99940) LP ( 1) F 2            s ( 79.14%)p 0.26( 20.86%)d 0.00(  0.00%)
 4. (1.99791) LP ( 2) F 2            s (  0.00%)p 1.00( 99.97%)d 0.00(  0.03%)
 5. (1.99791) LP ( 3) F 2            s (  0.00%)p 1.00( 99.97%)d 0.00(  0.03%)
```

NBO 1 is the σ_{HF} bond (BD), which can be written in the form of equation 2.21 as

$$\sigma_{HF} = 0.88(sp^{3.77})_F + 0.47(1s)_H \tag{2.25}$$

The fluorine $sp^{3.77}$ hybrid with 78.95% p character also has weak d-orbital contributions (0.12%) that can usually be ignored. The polarization coefficients indicate that about 77.6% of the electron density is polarized toward the more electronegative F atom.

NBO 2 is the KF core (CR) orbital, of 100% s character. NBOs 3 to 5 are the three fluorine lone pairs (LP). As shown by the occupancies and hybrid composition, these lone pairs are inequivalent. LP(1) is the s rich σ-type $sp^{0.26}$ lone pair ($n_F{}^{(\sigma)}$; 79% s character), directed along the bond axis opposite to H. LP(2) and LP(3) are the p-rich π-type lone pairs ($n_F{}^{(\pi)}$ and $n'_F{}^{(\pi)}$; 99.97% p-character), perpendicular to the bond axis. The lone pairs have occupancies slightly less than 2 (due to weak delocalization into Rydberg orbitals of the adjacent H), but overall, the correspondence with the elementary Lewis-structure description is excellent.

The general object of NBO method is to translate accurate calculations into chemical insights. Such insights are formulated in terms of commonly bond concepts such as

- atomic charge
- Lewis structure
- bond type (covalent vs. dative vs. ionic; σ vs. π etc.)

- hybridization
- bond order
- charge transfer
- resonance weight
- sterics
- energy decomposition (EDA)
- spectroscopic description

Even through the NBO method provides several insight that are directly formulated in terms of bonding concepts, here we briefly discute the ones we have applied in the present thesis.

2.4.1 Second-Order Perturbative Analysis of Donor-Acceptor Interactions

The NBOs method provides the picture of the wavefunction in terms of Lewis-type NBOs ($\Psi^{(L)}$). Naturally the complete NBO basis set $\{\theta_i\}$ separates into Lewis and non-Lewis components.

$$\{\theta_i\} = \{\theta_i^{(L)}\} + \{\theta_i^{(NL)}\} \tag{2.26}$$

The total electron density (ρ) and the system energy (E) can be similarly divided into Lewis and non-Lewis contributions,

$$\rho = \rho_L + \rho_{NL} \tag{2.27}$$

$$E = E^L + E^{NL} \tag{2.28}$$

Equations (2.26), (2.27) and (2.28) form the starting point for a systematic *perturbation theory* analysis.

The unperturbed $\Psi^{(L)}$ corresponds to an idealized single-configuration picture, in which each Lewis-type NBO has exact double occupancy (or single occupancy in the open shell case). In this limit, the model N-electron Schrödinger equation leads to a corresponding Lewis-type one-electron eigenvalue equation,

$$h_{op}^{(0)}\theta_i^{(L)} = \epsilon_i^{(L)}\theta_i^{(L)} (i = 1, 2, ..., N) \tag{2.29}$$

where $h_{op}{}^{(0)}$ is the Lewis-type Hamiltonian operator. The first N eigenfunctions $\{\theta_i{}^{(L)}\}$ are the filled Lewis-type NBOs (σ_{AB},σ_{CD},...) with corresponding orbital energies $\epsilon_i{}^{(L)}$.

However the eigenfunctions of $h_{op}{}^{(0)}$ also include the remaining non-Lewis-type NBOs $\{\theta_i{}^{(NL)}\}$($\sigma_{AB}{}^*$,$\sigma_{CD}{}^*$,...)

$$h_{op}^{(0)}\theta_j^{(NL)} = \epsilon_j^{(NL)}\theta_j^{(NL)}(j = N+1, ...) \tag{2.30}$$

that are formally vacant. We refer to the filled (Lewis-type) NBOs of equation (2.29) as *donor* orbitals and the vacant (non-Lewis-type) of equation (2.31) as *acceptor* orbitals.

In the resonance free world, the donor-acceptor NBOs have no interaction (due to their mutual orthogonality)

$$\int \theta_i^{*(L)} h_{op}^{(0)} \theta_j^{(NL)} d\tau = 0 \quad \text{for all i,j} \tag{2.31}$$

However, the corresponding real-world effective Hamiltonian operator F_{op} (i.e. Fock, Kohn Sham) has non-vanishing donor-acceptor interactions,

$$F_{ij} = \int \theta_i^{*(L)} F_{op} \theta_j^{(NL)} d\tau \neq 0 \tag{2.32}$$

and hence will lead to real-world donor-acceptor *mixing* (delocalizations) that bring in contributions from non-Lewis NBOs.

The perturbation theory of NBO-donor acceptor interactions can be expressed quite simply in graphical or equation form for the leading (second-order) correction $\Delta E^{(2)}{}_{i \to j^*}$ for each ${\theta_i}^{(L)}$- ${\theta_j}^{(NL)}$ donor-acceptor pair. The schematic perturbation diagram for doubly occupied donor NBO ${\theta_i}^{(L)}$ interacting with vacant acceptor ${\theta_j}^{(NL)}$ is depicted in Figure (2.3).

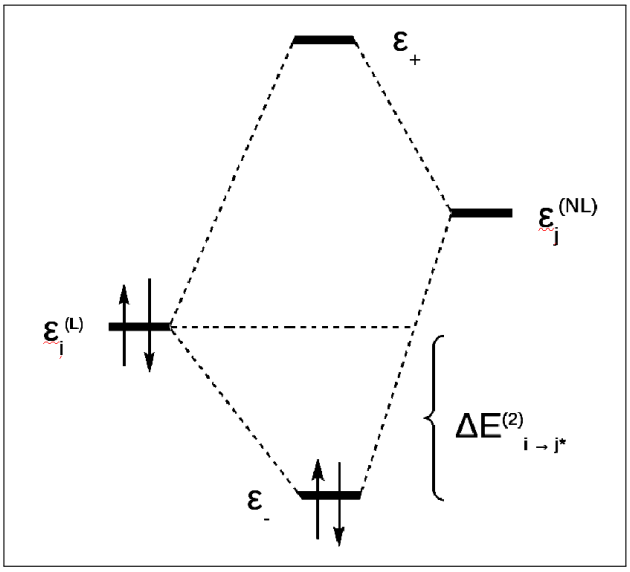

Figure 2.3: *2e-stabilizing interaction between a filled donor orbital ${\theta_i}^{(L)}$ and a vacant acceptor ${\theta_j}^{(NL)}$, leading to energy lowering $\Delta E^{(2)}{}_{i \to j^*}$.*

The unperturbed energy levels have respective NBO energies ${\epsilon_i}^{(L)}$, ${\epsilon_j}^{(NL)}$ on the vertical energy scale. However, in the presence of the perturbation, these levels mix (dashed line) and split to become the final perturbed levels (center), with

the lower level (marked ϵ_-) now below $\epsilon_i{}^{(L)}$ while the higher level (marked ϵ_+) rises above $\epsilon_j{}^{(NL)}$. Because only two electrons are involved in this interaction, they naturally occupy the lower ϵ_- level.

The net perturbative energy lowering $\Delta E^{(2)}{}_{i\to j^*}$ can be expressed by the following simple equation:

$$\Delta E^{(2)}_{i\to j^*} = \frac{-q_i|F_{ij}|^2}{\epsilon_j^{(NL)} - \epsilon_i^{(L)}} \tag{2.33}$$

where q_i is the occupancy of the donor orbital ($\sim$2), F_{ij} is given by equation (2.32) and $\epsilon_i{}^{(L)}$, $\epsilon_j{}^{(NL)}$ are the respective donor acceptor orbital energies.

Upon a general perturbation between a Lewis and non-Lewis type orbitals ($\theta_i{}^{(L)} \to \theta_j{}^{(NL)}$), the starting Lewis NBO orbital acquires a weak antibonding character in the final (doubly occupied) NLMO (*Natural Localized Molecular Orbital*) Ω_i orbital.

More generally, each occupied NLMO may be expressed as a parent L-type $\theta_i{}^{(L)}$ with weak NL-type delocalization tails (governed by coefficients c_{ij}) from each $\theta_j{}^{(NL)}$:

$$\Omega_i^{(L)} = c_{ii}\theta_i^{(L)} + \sum_j c_{ij}\theta_j^{(NL)}, \text{i = 1,2,....,N/2} \tag{2.34}$$

$$\sum_{i,j_{(i=j)}} c_{ij}^2 = 1 \tag{2.35}$$

The tails of the $\Omega_i{}^{(L)}$ NLMOs represent the intrinsic contribution (nonvanishing occupancy) of each NL-type $\theta_j{}^{(NL)}$ in delocalizing the parent L-type NBO in the molecular environment.

The magnitude of coefficients c_{ij} represents the contribution that each Non-Lewis NBO orbital $\theta_j{}^{(NL)}$ has in the formation of the NLMO Ω_i orbital.

2.5 Charge Displacement Analysis via Natural Orbitals for Chemical Valence (CD-NOCV)

The coordination between a transition metal (M) and an unsaturated substrate (S) is usually described in terms of the well known Dewar-Chatt-Duncanson (DCD) model[32,33] as a donor-acceptor interaction, involving the donation of π electrons from the substrate to empty orbitals of the metal (S→M) and the back-donation from filled d_π orbitals of the metal to empty substrate orbitals of appropriate symmetry (M→S). The DCD model was introduced to describe the η^2-coordination of ethene to a coinage-metal and has since enjoyed enormous popularity among the chemists. It is, in fact, the standard framework for analyzing the electronic properties of ligands and metal fragments, with the desirable aim of rationalizing coordination chemistry and/or controlling the outcome of metal catalyzed reactions. Nevertheless, the difficulty of finding rigorous relationship (of either empirical or theoretical nature) between experimental observables and the DCD bond components, makes the assessment of the relative importance of donation and back-donation a still ambiguous and controversial issue.[34–37] From a theoretical point of view, the problem stems from the very definition of the DCD (donation and back-donation) components, that are not very well defined quantum mechanical observables, and thus require the development of adequate quantum mechanical models.[38,39]

Recently a simple yet powerful method, for analyzing a chemical bond in terms of the charge rearrangement taking place upon formation of an adduct from two constituting fragments, has been proposed. This model is based on the so called Charge-Displacement (CD) function[40]

$$\Delta q(z) = \int_{-\infty}^{z} dz^{'} \int_{-\infty}^{+\infty} \int_{-\infty}^{+\infty} \Delta\rho(x, y, z^{'}) dx dy \tag{2.36}$$

defined as a progressive partial integration along a suitable z axis of the difference $\Delta\rho$(x,y,z$^{'}$) between the electron density of the adduct and that of its non-interacting fragments placed in the same position that they occupy in the adduct. The z axis is usually chosen to be the bond axis between the fragments. Accordingly, the CD function at a given point z quantifies the exact amount of electron charge that, upon formation of the bond, is transferred from right to left (the direction of decreasing z) across a plane perpendicular to the bond axis through z. Negative values of the CD function identify charge flow in the opposite direction.

The CD function was first introduced to study the chemical bond between gold and the noble gases.[40] It was later on successfully employed to study the charge transfer in hydrogen bonding[41–44] and halogen bonding[45] in weakly bound adducts, to characterize charge transfer effects on the conduction band of dye sensitized solar cells[46] and also to describe the charge rearrangement in excited states.[47] Above all, it proved to be extremely versatile in coordination chemistry.[48–51]

By studying the metal-substrate chemical bond in symmetric complexes, it has

been shown that the CD function can be decomposed into additive symmetry components providing a quantitative, spatially detailed picture of the DCD donation and back-donation charge flows.[48–51]

Furthermore the estimates of the donation and back-donation charge transfers in M-ethyne complexes were found to predict very accurately experimental observables such as ethyne distortion from linearity and C-C stretching frequency.[52] This proved the reliability of the CD analysis and suggests that the DCD components may, in principle, be measured through simple experiments.

It is clearly a severe limitation that such CD analysis, in its current formulation, can only be carried out if both the systems and its constituting fragments have suitable symmetry properties, which is of course not the case for most systems of interest in coordination chemistry. This limitation can be entirely eliminated by taking advantage of the recently proposed Natural Orbitals for Chemical Valence (NOCV).[53,54]

Theoretical Aspects

As already mentioned, the CD approach is based on the analysis of the electron density rearrangement ($\Delta\rho$ in equation 2.37) taking place upon the formation of an adduct AB from two molecular fragments A and B. This quantity is formulated as the difference between the electron density of AB and that of its two constituting fragments A and B frozen at their in-adduct geometries. Accordingly, in terms of occupied Kohn Sham (or Hartree-Fock) spin-orbitals (ψ_i) of the AB, A and B systems, $\Delta\rho$ can be written as[55]

$$\Delta\rho = \sum_i |\psi_i^{(AB)}|^2 - \sum_i |\psi_i^{(A)}|^2 - \sum_i |\psi_i^{(B)}|^2 \tag{2.37}$$

If both the adduct and its constituting fragments can be classified in the same symmetry group, the electron density difference can be partitioned into additive symmetry components according to the following equations

$$\Delta\rho = \sum_p \Delta\rho_p \tag{2.38}$$

$$\Delta\rho_p = \sum_{i\in p} |\psi_i^{(AB)}|^2 - \sum_{i\in p} |\psi_i^{(A)}|^2 - \sum_{i\in p} |\psi_i^{(B)}|^2 \tag{2.39}$$

where p labels are the different irreducible representations of the (unique) symmetry point group of AB, A and B. The overall CD function Δq (see equation 2.36) is similarly decomposed into additive symmetry components (defined as in equation 2.39 for each $\Delta\rho_p$) which, for suitable cases when the symmetry components correspond unambiguously to DCD components, give a quantitative picture of donation and back-donation charges.[48–51]

While the $\Delta(q)$ curves accurately depict charge displacement over the whole molecular region, one can obtain a reasonable measure of donation, back-donation, and net charge transfer (CT_{don}, CT_{back} and CT_{Tot}, respectively) between the fragments by taking the value of the corresponding CD function at a plausible inter-fragment boundary along z. Our standard choice is the z point where isodensities surfaces of the isolated fragments intersect.

As an example we report the CD analysis of the gold carbon coordination bond in $[Au(CO)]^+$.[56] In Figure (2.4) are shown the CD functions (CDF) for the overall density difference and its symmetry separated components. We recall here that, at a given point z, a positive CDF value corresponds to a charge flow from right to left (i.e., in the $Au^+ \leftarrow CO$) direction, while a negative value corresponds to a charge flow in the opposite ($Au^+ \rightarrow CO$) direction. The total CDF is positive over both the Au-C and C-O bond regions and also the oxygen far side of CO, indicating a continuous flow of electrons in the direction from CO towards gold.

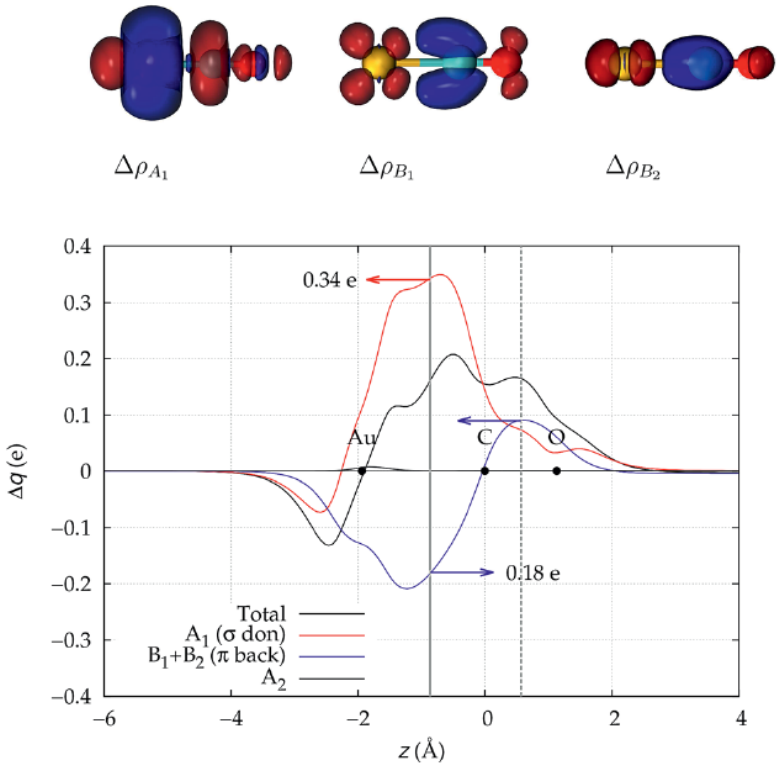

Figure 2.4: *Total CDF and its symmetry (C_{2v}) components for the Au-CO bond in the complex $[Au(CO)]^+$. Black dots indicate the z position of the atomic nuclei. A solid vertical line marks the boundary between the Au^+ and the CO fragments. The boundary between the two fragments is the z point in which isodensity surfaces of the isolated fragments intersect. At the top: isodensity surfaces (0.0025 e a.u.$^{-1}$) for the A_1, B_1, and B_2 components of $\Delta\rho(x,y,z)$. Red surfaces identify charge depletion areas, while blue surfaces identify charge accumulation areas.*

The negative values of the curve on the left side of Au^+ indicate a rearrange-

ment in the opposite direction. The total CDF results from an A_1 component which is large and positive in the Au-carbon region (identifying σ-donation) and B_1 + B_2 component which is negative in the same zone (identifying π-backdonation) plus a negligible A_2 component. These components are easily recognized in the isodensity plots of the respective density difference shown at the top of the figure.

The net charge transfer CT_{net} from CO to Au^+ (the CDF value at the boundary solid vertical line) amounts to 0.16e resulting from a donation component $CT^{\sigma}{}_{don}$ of 0.34e and a back-donation from a donation component $CT^{\pi}{}_{back}$ of 0.18e. The first important comment here is that the back-donation is actually a significant component of the interaction, estimated to be more than half as large as the donation.

However, when the system under study and its fragments do not satisfy the symmetry requirements recalled above (as happens for most cases of interest), the above decomposition cannot be applied. Therefore a different, more general, decomposition scheme has been proposed.[55] Such a scheme can still provide the desired identification of the donation and back-donation components of the interaction, using the properties of the *Natural Orbitals for Chemical Valence* (NOCVs). In the NOCV scheme, the charge rearrangement taking place upon the formation of AB from fragments A and B is defined with respect to a slightly different reference density, which is no longer the simple superposition of the densities of A and B. In other words, rather than two separate A and B wavefunctions, their antisymmetrized product $\Psi^{(0)}{}_i$ is taken as reference (the so called promolecule). The resulting density rearrangement,

$$\Delta\rho' = \sum_i |\psi_i^{(AB)}|^2 - \sum_i |\psi_i^{(0)}|^2 \tag{2.40}$$

can be brought into diagonal contributions of the *valence operator* of Nalewajski and Mrozek theory[57,58] that can be defined in terms of molecule ($\psi_i{}^{(AB)}$) and promolecule ($\psi_i{}^{(0)}$) occupied spin-orbitals, as

$$\hat{V} = \sum_i (|\psi_i^{(AB)} >< \psi_i^{(AB)}| - |\psi_i^0 >< \psi_i^0|). \tag{2.41}$$

NOCVs feature the peculiar property that they can be grouped in pairs of complementary orbitals (φ_k, φ_{-k}) corresponding to eigenvalues with same absolute value but opposite sign,[59]

$$\hat{V}\varphi_{\pm k} = \pm\nu_k\varphi_{\pm k}. \tag{2.42}$$

In terms of NOCV pairs, $\Delta\rho'$ reads

$$\Delta\rho^{'} = \sum_{k} \nu_k(|\varphi_k|^2 - |\varphi_{-k}|^2) = \sum_{k} \Delta\rho_k^{'}. \tag{2.43}$$

Equation 2.43 sheds light on the interpretation of the NOCVs: upon the formation of AB from promolecule, a fraction ν_k of electrons is transferred from the φ_{-k} to the φ_k orbitals. k ranges, as can be directly demonstrated from the definition of the operator $\hat{V}$ (equation 2.41), from 1 to the number of occupied spin-orbitals (total number of electrons). However, only a small subset of these NOCV pairs actually contributes to the overall charge rearrangement $\Delta\rho^{'}$ because a large part of them presents values of ν_k close to zero.[54,60] NOCVs proved all their usefulness in the qualitative analysis of donation and back-donation in transition metal complexes.

More recently, it was shown that a combined Extended Transition State (ETS)[61] NOCV approach permits to separate contributions ΔE_k (associated with different $\Delta\rho_k$ s) from σ and π bonding components to the interaction energy.[62]

$\Delta\rho$ and $\Delta\rho^{'}$ differ for a term, $\Delta\rho^{anti}$ ($\Delta\rho^{anti}$ = $\Delta\rho$ - $\Delta\rho^{'}$), which may be seen as the electron density rearrangement occurring upon going from the separated A and B fragments to the promolecule. This contribution, by removing the orbital overlap between the A and B fragments, shifts charge density from the inter-fragment region towards the fragments. In other words, $\Delta\rho$ presents a larger accumulation (or smaller depletion) of charge density in the bonding region than $\Delta\rho^{'}$ does.

Bibliography

[1] Harvey, J. *Annu. Rep. Prog. Chem. - Sect C* **2006**, *102*, 203.

[2] Cramer, C. *Essential of Computational Chemistry - Theories and Models*; Wiley, 2004.

[3] Hohenberg, P.; Kohn, W. *Phys. Rev. Sect. B.* **1964**, *136*, B864.

[4] Hohenberg, P.; Kohn, W. *Phys. Rev. Sect. A.* **1965**, *140*, A1133.

[5] Slater, J. *Phys. Rev.* **1951**, *81*, 385.

[6] Becke, A. *Phys. Rev. A* **1988**, *38*, 3098.

[7] Becke, A. *J. Chem. Phys.* **1993**, *98*, 5648.

[8] Perdew, J.; Chevary, J.; Vosko, S.; Jackson, K.; Pederson, M.; Singh, D.; Fiolhais, C. *Phys. Rev. B* **1992**, *46*, 6671.

[9] Wright, J.; Johnson, E.; DiLabio, G. *J. Am. Chem. Soc.* **2001**, *123*, 1173.

[10] Johnson, E.; Mackie, I.; DiLabio, G. *J. Phys. Org. Chem.* **2009**, *22*, 1127.

[11] Mackie, I.; DiLabio, G.; McClure, G. *J. Phys. Chem. A.* **2009**, *113*, 5476.

[12] Mackie, I.; DiLabio, G. *J. Phys. Chem. A.* **2008**, *112*, 10968.

[13] Stone.A.J., *The Theory of Intermolecular Forces*; Clarendon Press, Oxford, 1996.

[14] Zeiss, G.; Meath, W. *Mol. Phys.* **1977**, *33*, 1155.

[15] Casimir, H.; Polder, D. *Phys. Rev.* **1948**, *73*, 360.

[16] London, F. *Z. Phys. Chem.* **1930**, *11*, 222.

[17] Slater, J.; Kirkwood, J. *Phys. Rev.* **1931**, *37*, 682.

[18] Lennard-Jones, J. *Proc. Phys. Soc.* **1931**, *43*, 461.

[19] Johnson, E.; Wolkow, R.; DiLabio, G. *Chem. Phys. Lett.* **2004**, *394*, 334.

[20] Allen, M.; Tozer, D. *J. Chem. Phys.* **1997**, *117*, 11113.

[21] Wu, Q.; Yang, W. *J. Chem. Phys.* **2002**, *116*, 515.

[22] Grimme, S. *J. Compt. Chem.* **2004**, *25*, 1463.

[23] Wu, X.; Varga, M.; Nayak, S.; Lotrich, V.; Scoles, G. *J. Chem. Phys.* **2001**, *115*, 8748.

[24] Grimme, S. *J. Compt. Chem.* **2006**, *27*, 1787.

[25] Jurecka, P.; Cerny, J.; Hobza, P.; Salahub, D. *J. Compt. Chem.* **2007**, *28*, 555.

[26] Grimme, S.; Antony, J.; Schwabe, T.; Muck-Lichtenfeld, C. *Org. Biol. Chem.* **2007**, *5*, 741.

[27] Goddard, L. *Mat. Trans.* **2009**, *50*, 1664.

[28] Weinhold, F.; Landis, C. *Discovering Chemistry with Natural Bond Orbitals*; Wiley, 2012.

[29] Weinhold, F.; Landis, C. *Valence and Bonding. A Natural Bond Orbital Dono-Acceptor Perspective*; Cambridge, 2005.

[30] Glendening, E.; Landis, C.; Weinhold, F. *Wiley Interdisciplinary Reviews: Computational Molecular Science* **2011**, 1.

[31] Almolf, J. *Adv. Quant. Chem.* **1991**, *22*, 301.

[32] Dewar, M. *Bull. Soc. Chim. Fr.* **1951**, *18*, C71.

[33] Chatt, J.; Duncanson, A. *J. Chem. Soc.* **1953**, *18*, 2939.

[34] Echavarren, A. *Nat. Chem.* **2009**, *1*, 431.

[35] Furstner, A.; Morency, L. *Angew. Chem. Int. Ed.* **2008**, *120*, 5108.

[36] Benitez, D.; Shapiro, N.; Tkatchouk, E.; Wang, Y.; Goddard, W.; Toste, F. *Nat. Chem.* **2009**, *1*, 482.

[37] Hansmann, M.; Rominger, F.; Hashmi.A.S.K., *Chem. Sci.* **2013**, *4*, 1552.

[38] Frenking, G.; Frohlich, N. *Chem. Rev.* **2000**, *100*, 717.

[39] Frenking, G.; Shaik, S. *The Chemical Bond: Fundamental Aspects of Chemical Bonding*; Wiley-VCH Verlag GmbH & Co.. KGaA, 2014.

[40] Belpassi, L.; Infante, I.; Tarantelli, F.; Visscher, L. *J. Am. Chem. Soc.* **2008**, *130*, 1048.

[41] Cappelletti, D.; Ronca, E.; Belpassi, L.; Tarantelli, F.; Pirani, F. *Acc. Chem. Res.* **2012**, *45*, 1571.

[42] Belpassi, L.; Reca, M.; Tarantelli, F.; Roncaratti, L.; Pirani, F.; Cappelletti, D.; Faure, A.; Scribano, Y. *J. Am. Chem. Soc.* **2010**, *132*, 13046.

[43] Bartocci, A.; Cappelletti, D.; Pirani, F.; Tarantelli, F.; Belpassi, L. *J. Phys. Chem. A* **2014**, *118*, 6440.

[44] Bisotni, G.; Belpassi, L.; Tarantelli, F.; Pirani, F.; cappelletti, D. *J. Phys. Chem. A* **2011**, *115*, 14657.

[45] Cappelletti, D.; Candori, P.; Pirani, F.; Belpassi, L.; Tarantelli, F. *Cryst. Growth Des.* **2011**, *11*, 4279.

[46] Ronca, E.; Pastore, M.; Belpassi, L.; Tarantelli, F.; De Angelis, F. *Energy Environ Sci.* **2013**, *6*, 183.

[47] Ronca, E.; Pastore, M.; Belpassi, L.; De Angelis, F.; Angeli, C.; Cimiraglia, R.; Tarantelli, F. *J. Chem. Phys.* **2014**, *140*, 054110.

[48] Salvi, N.; Belpassi, L.; Tarantelli, F. *Chem. Eur. J.* **2010**, *16*, 7231.

[49] Zuccaccia, D.; Belpassi, L.; Macchioni, A.; Tarantelli, F. *Eur. J. Inorg. Chem.* **2013**, 4121.

[50] Marchione, D.; Belpassi, L.; Macchioni, A.; Tarantelli, F.; Zuccaccia, D. *Organometallics* **2014**, *33*, 4200.

[51] Ciancaleoni, G.; Scafuri, N.; Bistoni, G.; Macchioni, A.; Tarantelli, F.; Zuccaccia, D.; Belpassi, L. *Inorg. Chem.* **2014**, *53*, 9907.

[52] Bistoni, G.; Belpassi, L.; Tarantelli, F. *Angew. Chem. Int. Ed.* **2013**, *52*, 11599.

[53] Mitoraj, M.; Michalak, A. *J. Mol. Model* **2007**, *13*, 347.

[54] Michalak, A.; Mitoraj, M.; Ziegler, T. *J. Phys. Chem. A* **2008**, *112*, 1933.

[55] Bistoni, G.; Rampino, S.; Tarantelli, F.; Balpssi, L. *J. Chem. Phys.* **2015**, *142*, 084112.

[56] Bistoni, G.; Rampino, S.; Scafuri, N.; Ciancaleoni, G.; Zuccaccia, D.; Belpassi, L.; Tarantelli, F. *Chem. Sci.* **2016**, *7*, 1174.

[57] Nalewajski, R.; Koster, A.; Jug, K. *Theor. Chim. Acta* **1993**, *85*, 463.

[58] Nalewajski, R.; Mrozek, J. *Int. J. Quantum Chem.* **1994**, *51*, 187.

[59] Radon, M. *Theor. Chem. Acc.* **2008**, *120*, 337.

[60] Mitoraj, M.; Michalak, A.; Ziegler, T. *J. Chem. Theory Comput.* **2009**, *5*, 962.

[61] Ziegler, T.; Rauk, A. *Theor. Chim. Acta* **1977**, *46*, 1.

[62] Mitoraj, M.; Michalak, A.; Ziegler, T. *J. Chem. Theory Comput.* **2009**, *5*, 962.

Part I

REAL SYSTEMS

Chapter 3

Palladium-Catalyzed Hydrophosphonylation of Alkenes with Dialkyl H-Phosphonates

3.1 Synopsis

Organophosphorus compounds are highly useful building blocks in synthetic organic chemistry.[1–4] In recent years, transition metal-catalyzed reactions have emerged as highly efficient and selective tools for the preparation of carbon-phosphorus bonds.[5–9] In particular, the development of metal-catalyzed methods for the addition of H-P(O) bonds to alkynes and alkenes has become very attractive since these transformations are intrinsically atom-economical.[10–13]

The addition of H-P(O) bonds to alkynes has been well investigated, whereas the addition of H-P(0) bonds to the less reactive alkenes remains more problematic. Hydrophosphonylation processes have remained challenging and limited in scope. The group of Tanaka has enabled the addition of pinacol-derived H-phosphonate **1** to alkene under palladium catalysis (Figure 3.1).[14]

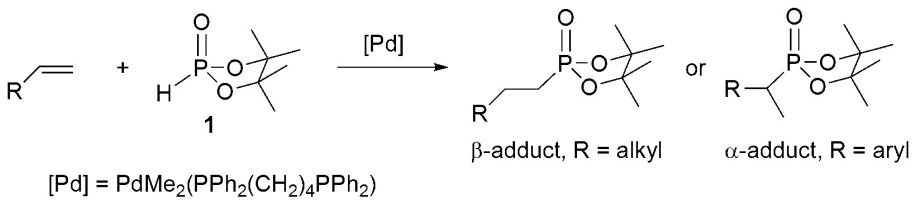

Figure 3.1: *Pd-catalyzed pinacol-derived H-phosphonylation of alkenes.*

Terminal aliphatic alkenes exclusively yield the anti-Markovnikov β-adduct and styrene derivatives provide the Markovnikov α-adduct with excellent selectivity (95:5). Mechanistic investigations by Tanaka suggest that the transformation proceeds through : i) oxidative addition of Pd(0) into the P-H bond, ii) reversible

hydropalladation of the alkene, and iii) reductive elimination. However, the reaction is essentially working with highly reactive pinacol-derived H-phosphonate **1**. Acyclic H-phosphonate derivatives have remained largely unreactive. The higher reactivity of **1** is supposed to be due to an easier reductive elimination, that is assumed to be the rate-determining step.

Inspired by these results, the group of Campagne has studied the Pd-catalyzed hydrophosphonylation of styrene using DavePhos as a ligand (DavePhos = 2-dicyclohexylphosphino-2'-(N,N-dimethylamino)biphenyl), as this ligand is known to facilitate reductive elimination process.[15] They could find conditions where both cyclic and acyclic H-phosphonate derivatives reacted with styrene (Figure 3.2).

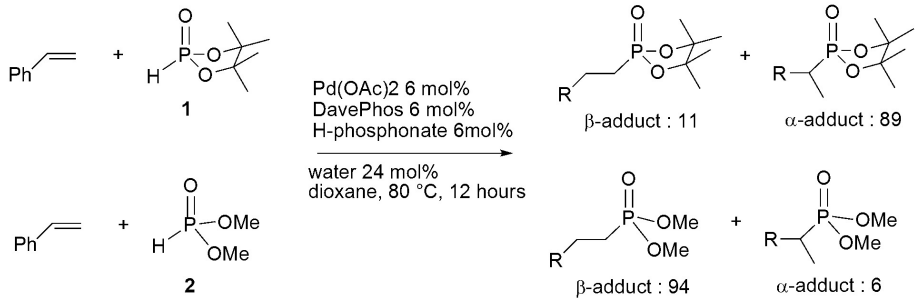

Figure 3.2: *Difference in regiochemistry in H-phosphonylation of styrene observed experimentally according to the nature of the H-phosphonate derivative.*

Interestingly, the regiochemistry of the reaction was highly dependent on the nature of the H-phosphonate derivative. With pinacol-derived **1**, the expected Markovnikov α-adduct was obtained with a selectivity of 89:11. In the case of the acyclic H-phosphonate **2**, the anti-Markovnikov β-adduct was obtained with a selectivity of 94:6. Within the same catalytic system, there is thus a dramatic influence of the nature of the H-phosphonate substrate. This is thus a perfect case study for computational chemistry, where theoretical investigation of the reaction mechanism may provide insights into the origin of the difference in regiochemistry.

3.2 Computational methodology

All the calculations have been performed with the Gaussian 09 package, at DFT level, using PBE0 functional.[16,17] The palladium atom was represented by the relativistic effective core potential (RECP) from the Stuttgart group and the associated basis sets,[18] augmented by an f polarization function.[19]

All the others atoms (C,H,P,O,N) were represented by a SVP basis set. The frequency analysis and the the Gibbs energy correction were carried out at 353 K (experimental temperature). Connection between reactants and products has been done through a given TS, altering his geometry along the two directions of the vector associated with the imaginary frequency.
For each geometry (TS and minima) a single point calculation has been carried out with the Orca package,[20] using an effective core potential for palladium, and a

QZVPP basis set for the other atoms. In this single point calculation, the influence of the solvent (1,4-dioxane, experimental solvent) was taken into consoderation through the COSMO model implemented in the ORCA package.[21] Influence of the dispersion forces was considered by adding to the COSMO energy the D3(BJ) corrections as described by Grimme.[22,23] All of the energies reported in the present work are Gibbs free energy obtained by summing the COSMO energy, the gas-phase Gibbs contribution at 353 K, and the D3(BJ)correction.

The kinetic simulation was carried out using COPASI package.[24–27] The rate constants were calculated using the Eyring equation with the computed $\Delta G^{\ddagger}$ values.

3.3 Nature of the active catalyst

The composition of the catalytic mixture is very complex with 6 mol% of $Pd(OAc)_2$, 6 mol% of DavePhos, 6 mol% of the H-phosphonate, 24 mol% of water in dioxane at 100 °C. This mixture of species is assumed to activate the palladium source to deliver the active catalyst usually considered to be a Pd(0) complex. As the reaction is also working when 15 mol% of DavePhos is used, a reasonable assumption is to consider that the Pd(0) complex formed is $Pd(DavePhos)_2$. Such kind of complexes have been observed and the X-ray structure of $Pd(SPhos)_2$ (SPhos = 2-Dicyclohexylphosphino-2',6'-dimethoxybiphenyl) has been obtained.[28]

The experimental structure of $Pd(SPhos)_2$ has been used to construct the guess geometry of $Pd(DavePhos)_2$. The resulting optimized structure **PdL$_2$** is shown in Figure 3.3. Both Pd-P bond distances are very similar (2.312 and 2.308 Å) and the geometry is almost linear (∠ P-Pd-P = 161.5°). The shorter Pd-P bond is associated to the DavePhos ligand presenting the NMe_2-substituted aromatic ring toward Pd. Such a geometry is assumed to provide extra stabilization. However, in the present case, both the nitrogen atom and the *ipso*-carbon atom are far from Pd (3.796 and 3.468 Å, respectively). Two different geometries were optimized for the Pd(DavePhos) mono-ligated complex (Figure 3.3).

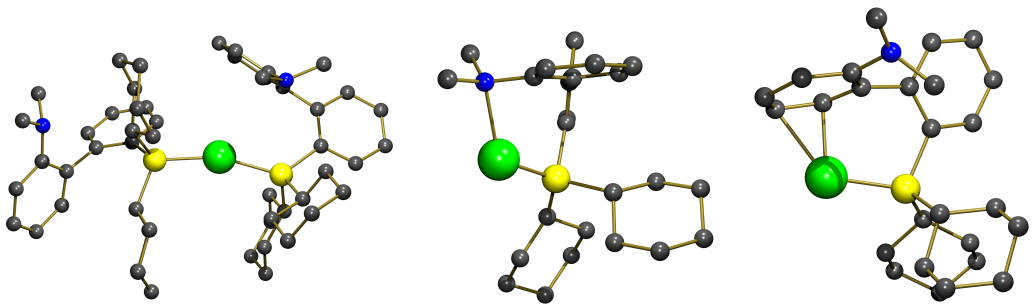

PdL$_2$ **PdL-1** **PdL-2**

Figure 3.3: *Optimized structures of **PdL$_2$**, **PdL-1**, **PdL-2**. H omitted for clarity.*

In **PdL-1**, there is a direct interaction between N and Pd as illustrated by the Pd-

N bond distance of 2.314 Å. This structure is computed to be less stable than **PdL$_2$** by $\Delta G = 27.5$ kcal mol^{-1}. An alternate geometry, **PdL-2**, where the interaction between the aromatic ring and Pd occurs essentially through asymmetric η^2-C=C coordination (2.109 and 2.377 Å) is computed to be slightly more stable at $\Delta G = 23.4$ kcal mol^{-1}. The calculations clearly indicate that the bis-ligated situation in **PdL$_2$** is thermodynamically prefered over the mono-ligated one in both **PdL-1** and **PdL-2**.

Without any specific proof, the mechanism is assumed to start with P-H oxidative addition on Pd(0). This would require formation of a mono-ligated Pd-L intermediate that would interact with the P-H bond of the H-phosphonate substrate to promote P-H bond cleavage. Despite many attempts, we were unable to located any transition state associated to such an oxidative addition reaction. Consequently, the mono-ligated Pd(0) complex is not an active species to induce P-H bond cleavage.

Styrene is a potential ligand to Pd(0) and complexes such as Pd(DavePhos)-(styrene) could be reactive in P-H bond cleavage. For a system like Pd(PCy$_3$), two different geometries for the η^2-styrene complex would have been expected (Figure 3.4). The situation is more complicated when one Cy group is substituted by an aromatic ring Ar. The asymmetry introduced leads to potentially four different styrene complexes (Figure 3.4).

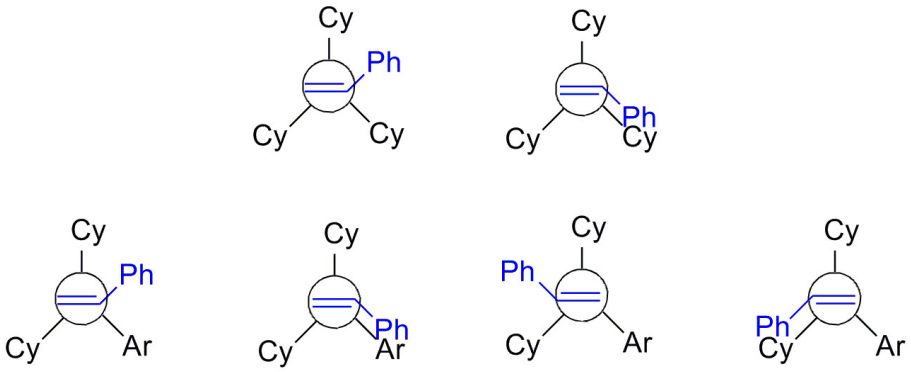

Figure 3.4: *Schematic representation of the expected geometries for styrene coordination to Pd(PCy$_3$) (top) or PdCy$_2$Ar (bottom).*

In addition, in the specific case of the DavePhos ligand, there is an extra stabilization originating from an interaction between the *ipso*-carbon on the aromatic ring and Pd. This distorts the geometry of styrene coordination that is more of a ML$_3$ type. As a result, and due to the asymmetry in the substitution of the aromatic ring by NMe$_2$, there are eight different styrene complexes to consider. The resulting optimized geometries are shown in Figure 3.5.

In Table 3.1 are given the Gibbs free energy of each complex relative to the bis-ligated complex **PdL$_2$**, together with selected bond distances. Inspection of the geometrical data in Table 3.1 does not allow to identify a specific trend that could be linked to the relative energies of the styrene complexes. Normally, at this stage, computational studies usually consider only the most stable complex

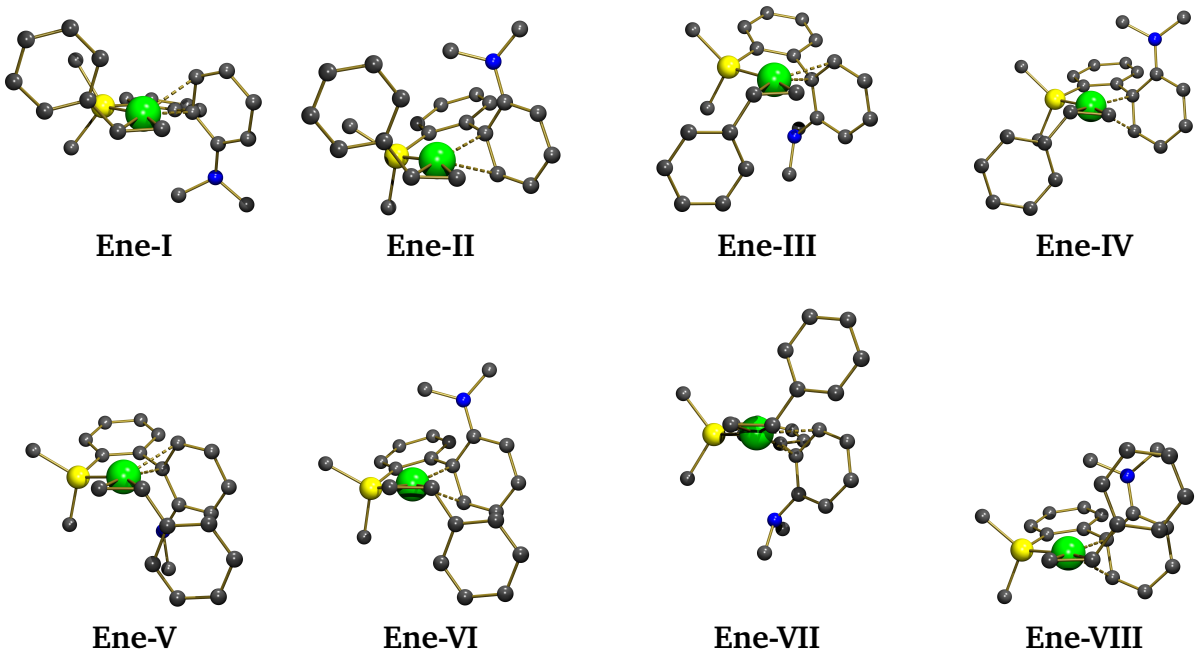

Figure 3.5: *Optimized geometries for the eight styrene complexes considered.H atoms and some C atoms on cyclohexyl groups have been omitted for clarity.*

and would discard the other alternatives. This would lead to retain only **Ene-IV** and **Ene-VIII** as starting reactants for the mechanistic study. However, we felt that the energy differences among the various complexes are not big enough to reject potential reactive trajectories that may reveal themselves as more productive when subsequent steps are considered. Therefore we have considered as active species the eight styrene complexes shown in Figure 3.5.

These complexes are formed from the more stable resting state **PdL$_2$**. As it was impossible to locate the transition state for styrene coordination, we assumed that the complex formation is dissociative through **PdL-2** and used the Gibbs free energy of this complex ($\Delta G = 23.4$ kcal mol^{-1}) as an estimate of the activation barrier. The relative energies of all the styrene complexes allowed to estimate the activation barriers of the reversed reactions.

3.4 P-H bond cleavage

In all the styrene complexes described above, the DavePhos ligand can be considered as hemilabile. The Pd...C$_{ipso}$ interaction can be lost in order to allow coordination of another substrate. For both H-phosphonate substrates **1** and **2**, the interaction with Pd is of the η^1-HP type as illustrated in Figure 3.6 for the complex between **2** and **Ene-I**. Table 3.2 collects selected geometrical parameters for these

	Pd-P	Pd...C_{ipso}	Pd-C_α	Pd-C_β	ΔG
Ene-I	2.335	2.341	2.164	2.114	9.7
Ene-II	2.341	2.312	2.174	2.111	9.8
Ene-III	2.346	2.319	2.161	2.119	10.6
Ene-IV	2.336	2.326	2.160	2.115	7.3
Ene-V	2.331	2.333	2.184	2.108	10.4
Ene-VI	2.326	2.340	2.174	2.103	9.1
Ene-VII	2.329	2.347	2.172	2.110	11.9
Ene-VIII	2.328	2.338	2.170	2.104	7.9

Table 3.1: *Selected bond distances (Å) and Gibbs energy (kcal mol^{-1}) of the styrene complexes.*

η^1-HP adducts together with their Gibbs energy relative to **PdL**$_2$.[1]

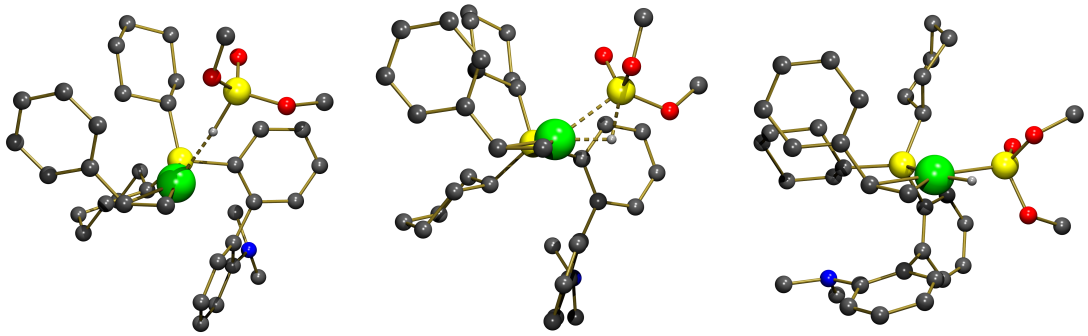

2PH-I **2PH-TS-I** **2PH-Prod-I**

Figure 3.6: *Optimized geometries for the η^1-HP complex between **Ene-I** and **2** and the subsequent TS for P-H bond cleavage and the resulting product of such cleavage.*

In both cases (**1** and **2**), the P-H bond gets slightly elongated upon coordination from its value in the free H-phosphonate (1.410 Å). The main difference between **1** and **2** lies in the H...Pd bond distance that is significantly shorter for **1**. This could be due to less steric bulk imparted by **1** compared to **2**, thus allowing shorter Pd...H contact. However, this does not translate into any significant energy difference as the ΔG values for coordination are sensibly identical for **1** and **2**. The average value for the Gibbs free energy of the η^1-adducts with **1** amounts to 20.0 kcal mol^{-1}, whereas the corresponding value for the adducts with **2** is 19.3 kcal mol^{-1}. Even though considering average value of Gibbs free energy of various isomers is not a rigourous way to describe reactivity, in the present case, it offers a quick estimate of the energy needed to achieve the various steps along the overall catalytic cycle. In a subsequent section, we will analyze in more details the in-

[1] In the case of the η^1-HP adduct with **1**, two styrene coordination **Ene-VII** and **Ene-VIII** did not lead to any minimum optimized for the η^1-HP adduct.

dependant behavior of the eight pathways considered for each H-phosphonate, in order to understand the regiochemistry observed experimentally.

	P-H	H...Pd	P...Pd	∠ Pd-H-P	ΔG
1PH-I	1.462	1.822	2.909	124.4	20.6
1PH-II	1.449	1.910	3.268	153.1	19.6
1PH-III	1.442	1.979	3.256	143.5	20.0
1PH-IV	1.443	1.943	3.320	157.1	20.0
1PH-V	1.452	1.841	3.020	132.6	21.0
1PH-VI	1.438	1.980	3.233	141.7	19.1
2PH-I	1.440	2.046	3.477	172.0	17.9
2PH-II	1.440	2.057	3.487	170.9	18.8
2PH-III	1.437	1.995	3.285	145.8	20.0
2PH-IV	1.437	1.932	3.150	137.9	19.4
2PH-V	1.431	2.036	3.202	134.2	19.0
2PH-VI	1.431	2.085	3.413	151.7	19.1
2PH-VII	1.435	2.007	3.212	137.2	20.0
2PH-VIII	1.441	1.899	3.149	140.7	20.0

Table 3.2: *Selected geometrical parameters (distances in Å and angle in degree) for the η^1-HP adduct of **1** (top) and **2** (bottom) to the various styrene complexes, and Gibbs free energy of these complexes (in kcal mol^{-1}) relative to **PdL**$_2$.*

For all the cases studied (including **Ene-VII** and **Ene-VIII** with **1**), the transition state for P-H bond cleavage could be located on the potential energy surface. Table 3.3 collects selected geometrical parameters and Gibbs free energy (relative to **PdL**$_2$) for the various TS and Figure 3.6 shows the geometry of **2PH-TS-I**, the transition state originating from **2PH-I**. The main geometrical aspect of the TS for P-H cleavage is a switch from η^1-HP coordination to η^2-HP coordination for the P-H bond. This is illustrated by a significant decrease of the Pd-H-P angle, but more substantially by a decrease in both the Pd...H and Pd...P bond distances. As expected the P-H bond gets elongated in the transition state with respect to its value in the η^1-HP adducts.

The Gibbs free energies of the transition states are rather similar for **1** and **2**. However, the average value of ΔG for the TS related to activation of **1** amounts to 24.7 kcal mol^{-1}, whereas that in the case of **2** is 26.6 kcal mol^{-1}. The PH oxidative addition to the styrene complexes is thus substantially more difficult for the non-cyclic H-phosphonate substrate **2** compared to the cyclic one **1**. All the geometrical parameters in Table 3.3 point to a more distorted geometry in the TS for the case of **2**: shorter H...Pd, short Pd...P, longer P-H and smaller Pd-H-P angle. This tends to indicate that the P-H bond in **2** is less reactive than the P-H bond in **1**, and thus needs to create stronger interaction with Pd to achieve P-H bond cleavage. This occurs with an increased energetic cost as exemplified by the ca. 2 kcal mol^{-1} energy difference between the average Gibbs free energy values of the TS.

	P-H	H...Pd	P...Pd	∠ Pd-H-P	ΔG
1PH-TS-I	1.498	1.724	2.659	111.0	22.6
1PH-TS-II	1.622	1.615	2.433	97.5	28.0
1PH-TS-III	1.496	1.727	2.667	111.5	22.9
1PH-TS-IV	1.537	1.665	2.578	107.2	27.9
1PH-TS-V	1.485	1.740	2.722	114.9	20.5
1PH-TS-VI	1.541	1.659	2.565	106.6	26.3
1PH-TS-VII	1.504	1.714	2.650	110.7	23.8
1PH-TS-VIII	1.575	1.642	2.476	100.6	25.4
2PH-TS-I	1.566	1.659	2.407	96.5	25.6
2PH-TS-II	1.570	1.652	2.394	96.0	26.1
2PH-TS-III	1.616	1.625	2.367	93.9	28.0
2PH-TS-IV	1.589	1.647	2.382	94.8	27.5
2PH-TS-V	1.684	1.609	2.317	89.4	28.7
2PH-TS-VI	1.579	1.649	2.373	94.6	27.4
2PH-TS-VII	1.541	1.662	2.518	103.6	24.9
2PH-TS-VIII	1.540	1.662	2.504	102.9	24.8

Table 3.3: *Selected geometrical parameters (distances in Å and angle in degree) for the transition states associated to P-H bond cleavage for **1** (top) and **2** (bottom) from the corresponding η^1-PH adducts, and Gibbs free energy of these TS (in kcal mol^{-1}) relative to **PdL**$_2$.*

The product of the P-H bond cleavage is a pseudo-square-planar Pd(II) complex with the hydride trans to the DavePhos phosphorus atom and the phosphonate trans to styrene. Such a product of P-H oxidative addition is shown in Figure 3.6. The transformation is essentially thermoneutral with respect to the η^1-HP addcut with the average value of the Gibbs free energy for the product of P-H oxidative addition amounting to 19.6 kcal mol^{-1} in the case of **1**, whereas an average value of 20.4 kcal mol^{-1} is obtained with **2**.

3.5 Styrene Insertion Into Pd-H

The product of the P-H oxidative addition (**nPH-Prod-X**; n=1,2; X=I-VIII) is a ML$_4$ hydrido-styrene complex with the hydrido and the olefin mutually cis. For each H-phosphonate cases **1** and **2**, the eight transition states **nTS-Ins-X** (n=1,2; X=I-VIII) of the insertion of the C=C double bond into the Pd-H bond have been located (Table 3.4). The average value of the Gibbs free energy of these 8 TSs in the case of n=1 (resp. n=2) amounts to 20.7 kcal mol^{-1} (resp. 21.1 kcal mol^{-1}), whereas the average value of the Gibbs free energy for the hydrido-styrene complexes is 19.6 kcal mol^{-1} (resp. 20.4 kcal mol^{-1}). This corresponds thus to an insertion with an activation barrier of ca. 1 kcal mol^{-1} on average, irrespective of the nature of the phosphonate substrate.

In all the cases, the product of the insertion is a Pd(II) alkyl complex featuring a β-CH interaction *trans* to the DavePhos phosphorus atom. The insertion reaction is exoergic as illustrated by the value of the average Gibbs free energy of **nIns-Prod-X** (n=1,2; X=I-VIII; see Table 3.4) of 15.4 kcal mol^{-1} (resp. 17.6 kcal mol^{-1}) for n=1 (resp. n=2). Among the eight different cases studied, positions I to IV correspond to the formation of a C_β-H bond, whereas positions V to VIII are associated to the formation of a C_α-H bond upon insertion.

	nPH-Prod-X	**nIns-TS-X**	**nIns-Prod-X**	**nIns-Isom-X**
n=1, X=I	18.7	19.8	14.5	2.6
n=1, X=II	19.1	19.0	12.9	11.4
n=1, X=III	21.4	22.1	16.4	3.1
n=1, X=IV	26.3	24.3	17.4	12.9
n=1, X=V	19.1	20.6	16.3	10.8
n=1, X=VI	16.9	21.2	16.9	16.4
n=1, X=VII	18.1	21.3	14.9	15.8
n=1, X=VIII	16.9	17.5	13.8	14.8
n=2, X=I	18.4	20.7	15.3	-2.4
n=2, X=II	18.2	19.4	14.5	7.2
n=2, X=III	22.5	22.9	19.5	-1.0
n=2, X=IV	23.3	23.7	18.2	0.6
n=2, X=V	23.5	23.0	18.1	7.2
n=2, X=VI	20.3	21.2	18.3	4.0
n=2, X=VII	18.6	19.6	19.4	7.1
n=2, X=VIII	18.1	18.5	17.2	16.6

Table 3.4: *Gibbs free energy (kcal mol^{-1}) of the extrema located along the pathway for styrene insertion into the Pd-H bond after P-H oxidative addition.*

The product of the styrene insertion into Pd-H (**nIns-Prod-X**;
n=1,2; X=I-VIII) are neither the more stable alkyl complexes for these ML_3 Pd(II) species, nor are they suited for the needed subsequent P-C bond formation as the carbon and phosphorus atoms are mutually *trans*. Despite many attempts, we could not locate any TS structure for the isomerization from the T-shaped ML_3 geometry with alkyl and phosphonate *trans* to that with both ligands mutually *cis*. However, in all the cases, the situation with the alkyl and the phosphonate *cis* is more stable energetically (see Table 3.4).

Figure 3.7 shows the geometry of the most stable ML_3 species **nIns-Isom-X** for each regioselectivity of insertion and each phosphonate case. Insertion to form C_β-H (position I to IV) delivers a secondary alkyl group bonded to Pd, whereas insertion to form C_α-H (positions V to VIII) forms a primary alkyl. Due to the expected larger BDE of the Pd-C bond to primary carbon, the products featuring C_α-H formation are expected to be more stable. Yet, the contrary is observed in Table 3.4. One possible explanation is the systematic presence of an interaction

between Pd and C_{ipso} of the aromatic ring on styrene in the complexes **nIns-Isom-X** (n=1,2; X=I-IV). The Pd...C_{ipso} distance is 2.346 Å in **1Ins-Isom-I** and 2.355 Å in **2ins-Isom-X**. For the complexes **nIns-Isom-X** (n=1,2; X=V-VIII), the only source of potential extra stabilization is a β-CH agostic interaction as illustrated in Figure 3.7, that does not provide enough stabilization.

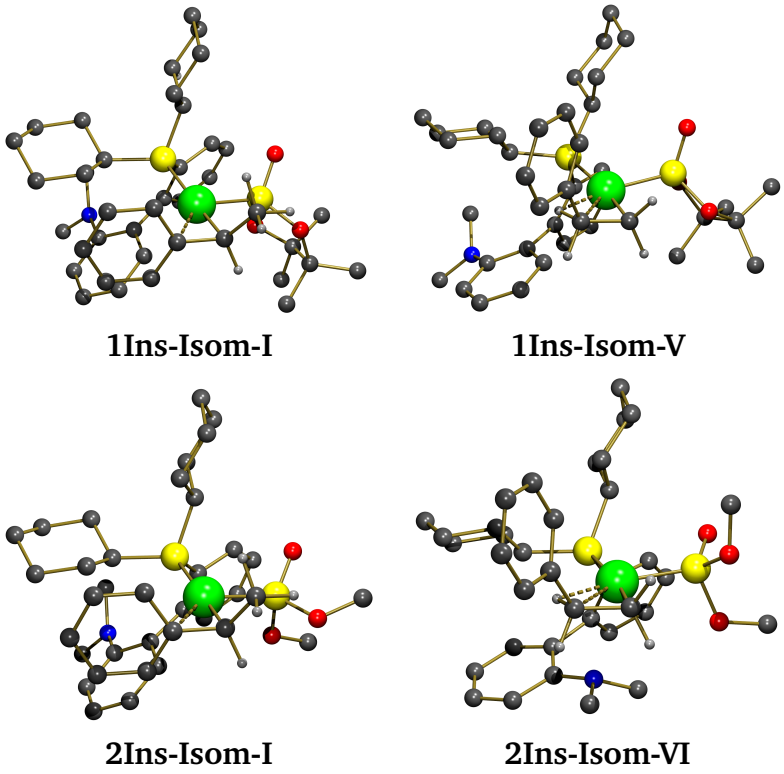

Figure 3.7: *Optimized geometry for the most stable ML_3 alkyl complexes resulting from the two regiochemistry of styrene insertion into Pd-H.*

3.6 P-C Bond Formation

The last step of the Pd-catalyzed styrene hydro-phosphonylation is the reductive elimination from **nIns-Isom-X** (n=1,2; X=I-VIII) forming the P-C bond through **nPC-TS-X** (n=1,2; X=I-VIII) and regenerating the Pd(0) active species. In Figure 3.8 are shown the TS obtained from the most stable isomers shown in Figure 3.7. Tables 3.5 and 3.6 collects selected geometrical parameters for both the reactant and the transition states, together with the Gibbs free energy relative to **PdL_2**.

Inspection of the geometrical parameters in Tables 3.5 and 3.6 indicates that the transition state structures are relatively late. The forming P-C bond distances vary between 1.986 Å and 2.204 Å but, in the vast majority of cases, the distance is ca. 2.10 Å. This is to be compared with the P-C bond distance in the products (**1-**α

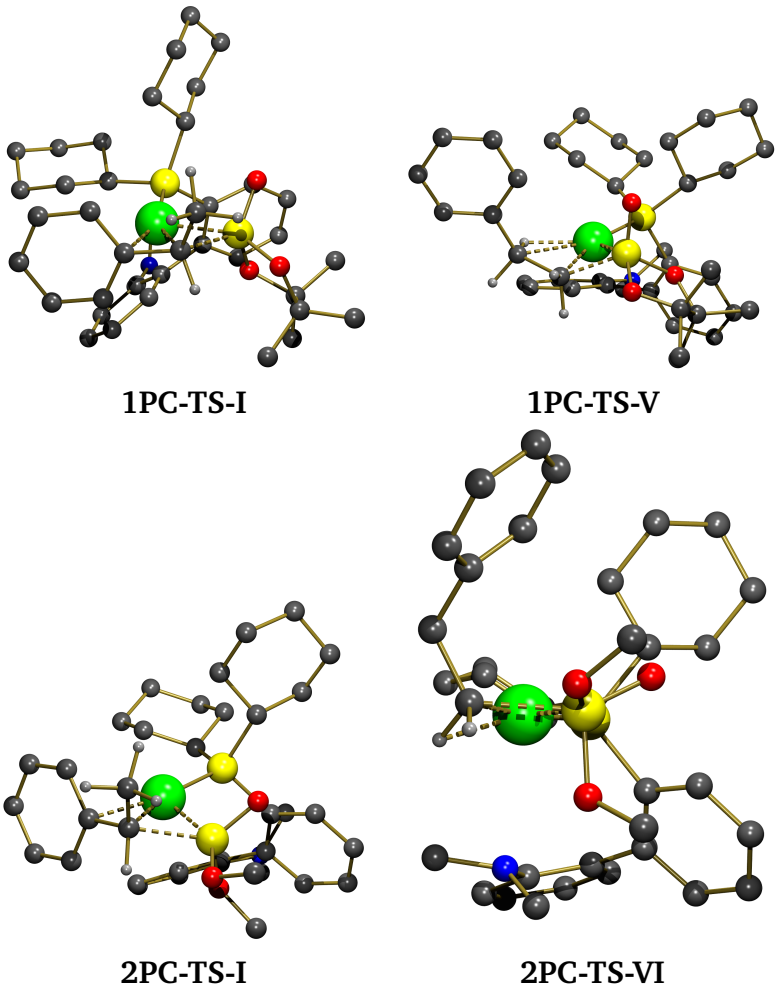

Figure 3.8: *Optimized geometry for the transition states originating from the most stable ML_3 alkyl complexes resulting from the two regiochemistry of styrene insertion into Pd-H.*

: 1.821 Å, **1-**β : 1.804 Å,**2-**α : 1.817 Å, **2-**β : 1.796 Å). This expected shortening of the P-C distance in the TS is accompanied by a lenghtening of both Pd-C and Pd-P bond distances. However, there is a clear difference of behavior between Pd-P and Pd-C where the latter bond distance experiences a significantly larger increas (ca. 0.3 Å for Pd-C compared to ca. 0.08 Å fo Pd-P). This is particularly evident in the TS originating from reactants showing a marked Pd...C_{ipso} interaction (positions I-IV, both phosphonates) or from some reactants associated to positions V-VIII featuring a β-CH agostic interaction.

As a matter of fact, the existing interaction in the reactant is somehow reinforced in the transition state. Thus the Pd...C_{ipso} distance of 2.346 Å (resp. 2.355 Å) in **1Ins-Isom-I** (resp. **2Ins-Isom-I**) is reduced to 2.196 Å (resp. 2.206 Å) in **1PC-TS-I** (resp. **2PC-TS-I**). This interaction does stabilize the developing Pd(O) caracter in the transition state. In the same vein, for the pathways forming β-

products, the β-CH agostic interaction present in **1Ins-Isom-V** (resp. **2Ins-Isom-VI**) is significant as illustrated by the C-H bond distance of 1.172 Å (resp. 1.170 Å) and the short H...Pd contact of 1.939 Å (resp. 1.952 Å). The corresponding values in **1PC-TS-V** (resp. **2PC-TS-VI** point to a still existing interaction between the CH bond and Pd as corroborated by the value of the C-H bond distance of 1.129 Å (resp. 1.122 Å) and of the H...Pd contact of 2.029 Å (resp. 2.076 Å). Here again, the interaction of the C-H bond with Pd does stabilize the developping Pd(O) caracter in the transition state.

	Pd-P	Pd-C	P-C	ΔG
1Ins-Isom-I	2.240	2.079	3.102	2.6
1PC-TS-I	2.317	2.368	2.138	22.2
1Ins-Isom-II	2.249	2.067	3.255	11.4
1PC-TS-II	2.322	2.375	2.087	34.1
1Ins-Isom-III	2.253	2.095	3.024	3.1
1PC-TS-III	2.350	2.391	2.054	21.6
1Ins-Isom-IV	2.208	2.070	3.152	12.9
1PC-TS-IV	2.257	2.241	2.204	25.1
1Ins-Isom-V	2.239	2.036	3.061	10.8
1PC-TS-V	2.348	2.354	1.986	31.0
1Ins-Isom-VI	2.209	2.041	2.883	16.4
1PC-TS-VI	2.265	2.183	2.149	26.7
1Ins-Isom-VII	2.210	2.057	2.794	15.8
1PC-TS-VII	2.260	2.200	2.112	24.5
1Ins-Isom-VIII	2.200	2.054	2.838	14.8
1PC-TS-VIII	2.274	2.203	2.051	23.3

Table 3.5: *Selected geometrical parameters (distance in Å) and Gibbs free energy (kcal mol^{-1}) relative to* ***PdL***$_2$ *for the reactants and transition states associated to P-C bond formation with the phosphonate* ***1****.*

There is thus a subbtle interplay of various contributions and crude examination of the data in Tables 3.5 and 3.6 is not helpfull in understanding the regiochemistry observed as a function of the nature of the phosphonate. A bold approach, as we already did for the other steps, is to consider a global view by using average Gibbs free energy values. For the reactants **1Ins-Isom-X** (resp. **2Ins-Isom-X**) prior to P-C bond formation, the corresponding ΔG value relative to **PdL**$_2$ is 11.0 kcal mol^{-1} (resp. 4.9 kcal mol^{-1}). For the transition states originating from these reactants, the average Gibbs free energy is $\Delta G = 26.1$ kcal mol^{-1} (resp. 23.3 kcal mol^{-1}). At this stage, it is interesting to comare the reactivity of **1** and **2** using the average Gibbs free energy values. Figure 3.9 shows a comparison between the average PES for both substrates **1** and **2**.

The first step is the formation of the styrene complexes after DavePhos dissociation. This step is independant of the nature of the phosphonate. Subsequently

	Pd-P	Pd-C	P-C	ΔG
2Ins-Isom-I	2.241	2.078	3.138	-2.4
2PC-TS-I	2.331	2.326	2.157	20.5
2Ins-Isom-II	2.249	2.073	3.021	7.2
2PC-TS-II	2.348	2.323	2.135	21.7
2Ins-Isom-III	2.262	2.097	3.083	-1.0
2PC-TS-III	2.367	2.334	2.114	23.5
2Ins-Isom-IV	2.247	2.078	3.042	0.6
2PC-TS-IV	2.344	2.350	2.118	21.7
2Ins-Isom-V	2.207	2.043	2.937	7.2
2PC-TS-V	2.287	2.165	2.108	25.2
2Ins-Isom-VI	2.246	2.032	3.096	4.0
2PC-TS-VI	2.281	2.166	2.143	25.7
2Ins-Isom-VII	2.212	2.044	2.919	7.1
2PC-TS-VII	2.300	2.160	2.113	23.8
2Ins-Isom-VIII	2.205	2.047	2.899	16.6
2PC-TS-VIII	2.281	2.168	2.106	24.0

Table 3.6: *Selected geometrical parameters (distance in Å) and Gibbs free energy (kcal mol^{-1}) relative to* ***PdL***$_2$ *for the reactants and transition states associated to P-C bond formation with the phosphonate* ***2****.*

there are three steps : P-H oxidative addition, olefine insertion, and P-C reductive elimination. The main qualitative conclusions that can be drawn from these PES are :

1. **1** is more reactive than **2** because the highest point to overcome is 0.5 kcal mol^{-1} lower;
2. the nature of the rate-limiting step depends on the nature of the phosphonate. With **1**, it is the reductive elimination, whereas with **2** it is the oxidative addition;
3. access to the reactive styrene complexes is kinetically competitive with the actual functionalization.

These general observations are obviously made using a very crude approach and do not aloow to reproduce nor explain the change in regiochemistry observed experimentally.

3.7 Kinetic Modeling of the Reaction

The calculations in parallel of eight reaction pathways for each phosphonate generated a lot of data difficult to analyze in details. In particular, by inspecting the

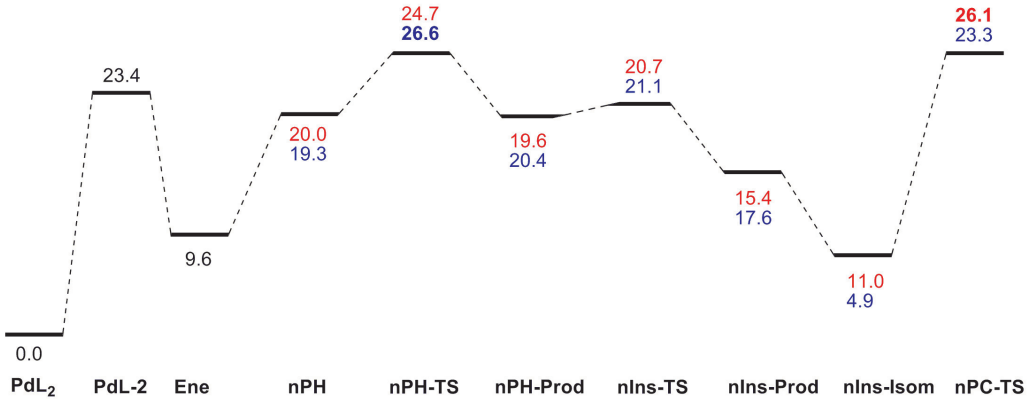

Figure 3.9: *Comparison of the PES for the reaction of **1** (red values) and **2** (blue values) with **PdL**$_2$ using the average Gibbs free energy of the eight computed extrema in each cases. Energies are in kcal mol*$^{-1}$.

value of the Gibbs free energies along each path, it is difficult to anticipate which regioisomer will be prefered. It is therefore interesting to devise a kinetic model, using the computed activation energies to determine the evolution with time of the concentration of all the species optimized.

The generic kinetic model we have considered is shown in Figure 3.10 for **1**. The only value assumed is that corresponding to the activation barrier to form the styrene complex **Ene-X**. The calculations have shown the among the Pd(0) starting materials, **PdL**$_2$ is the most stable. The mono-ligated complex is computed to be $\Delta G = 23.4$ kcal mol^{-1} less stable. The actual mechanism to form the styrene complex has not been caracterized but it is reasonable to assume that an associative displacement might occur and we considered that a barrier of $\Delta G^{\ddagger} = 23$ kcal mol^{-1} is a reasonable estimate. This sets a value for k_1 at a given temperature using the Eyring equation. We also considered that formation of the styrene complex is independant of the geometry of the styrene complex, hence k_1 is independant of X. However, in order to properly place energetically the various styrene complex **Ene-X**, the energy difference between the hypothetical TS at 23.0 kcal mol^{-1} and the actual Gibbs free energy of each styrene complex was used to evaluate $k_{1,X}$.

For the P-H oxidative addition, to evaluate $k_{2,X}$, the energy differences between **1PH-TS-X** and **Ene-X** + **1** was considered as the η^1-HP adduct **1PH-X** were all calculated less stable than the styrene complex. For the olefin insertion, in order to evaluate the kinetic of the back reaction ($k_{-3,X}$), the energy difference between **1Ins-TS-X** and **1Ins-Isom-X** was considered as the latter complex is calculated more stable than the actual product of insertion (**1Ins-Prod-X**). Finally, the last P-C reduction elimination step was considered to form irreversibly the product **1**-α (X = I-IV) or **1**-β (X = V-VIII). This step also regenerates the catalyst **PdL**$_2$. The same kinetic model was used for the reaction with the acyclic H-phosphonate **2**.

Figure 3.11 shows the time evolution of the concentration of the products **Prod-X** for the eight different chanels considered simultaneously at 353 K with the following initial concentrations : 0.06 for **PdL**$_2$, 1 for styrene and 1 for **1**. These are

the conditions used in the catalytic experiment. It is important to note that four products are in fact identical to **1-**α (**Prod-X** for X = I-IV), while the four remaining ones are **1-**β (**Prod-X** for X = V-VIII). From the curves in Figure 3.11, only two chanels (X = I and X = III) are producing significant amount of **1-**α for a final concentration of 0.9. There are also two chanels producing the other regioisomer **1-**β (X = VII and X = VIII) with a final concentration of 0.1. The final ratio between the α and β products is thus computed to be 90:10 in excellent agreement with the experimental observations.

The results of the kinetic modeling for the reaction with the acyclic phosphonate **2** are shown in Figure 3.12. For this case too, there are two chanels dominating the product formation for each regioisomers. For the formation of **2-**α, positions I and II are the productive ones, whereas for the formation of **2-**β the productive cases are X = VII and X = VIII. The main observation that can be made is a complete reversal of regiochemistry with now **2-**β prefered over **2-**α by a ratio of 75:25. This is qualitatively in good agreement with the experimental observations where the ratio was 96:4. The other observation reveled by the kinetic study is the longer reaction time needed to reach the plateau in the case of **2** compared to **1**.

This computational study of the Pd-catalyzed hydro-phosphonylation of styrene has revealed the complexity of describing a catalytic transformation where many different conformers can be potentially involved in the reaction. However, by performing a systematic study of all the potential pathways coupled with a kinetic study, it was possible to deconvoluate the various influences and thus to isolate the few productive pathways. The calculations did then reproduce the change in regiochemistry observed experimentally.

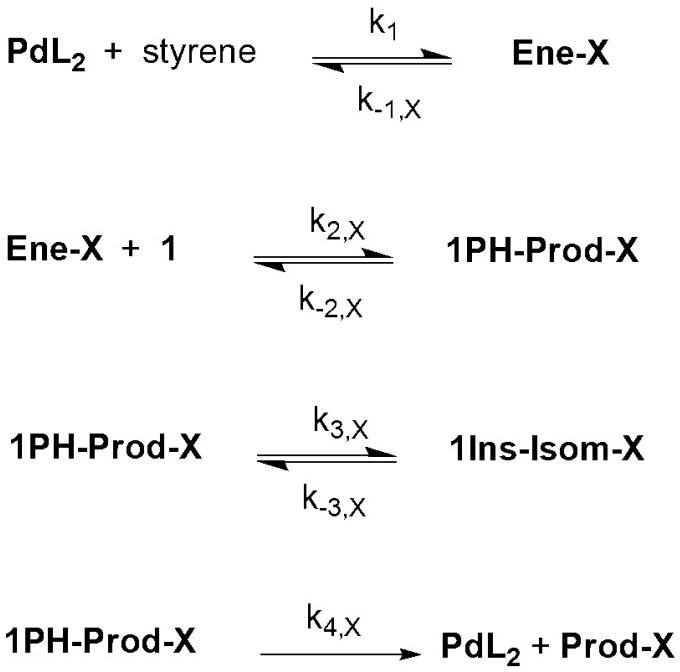

Figure 3.10: *Kinetic model used to described the pathway association to the the reaction of the styrene complexe* ***Ene-X*** *with* ***1***.

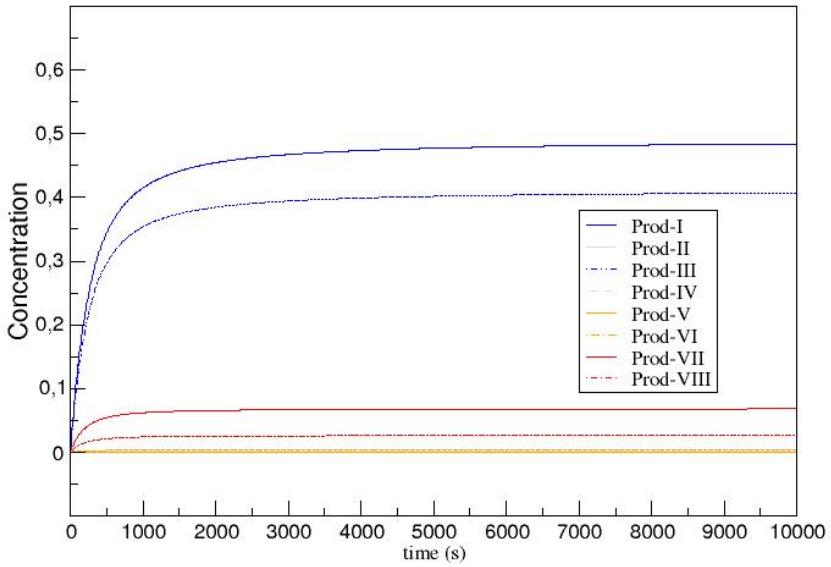

Figure 3.11: *Time evolution of the concentration of the various regioisomers.*

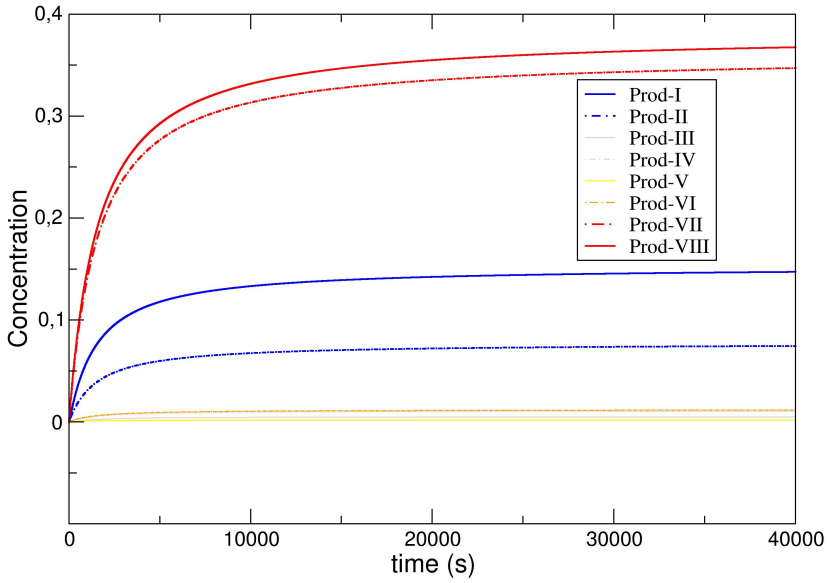

Figure 3.12: *Time evolution of the concentration of the various regioisomers.*

Bibliography

[1] Maryanoff, B. E.; Reitz, A. B. *Chem. Rev.* **1989**, *89*, 863.

[2] Byrne, P. A.; Gilheany, D. G. *Chem. Soc. Rev.* **2013**, *42*, 6670.

[3] Swamy, K. C. K.; Kumar, N. N. B.; Balaraman, E.; Kumar, K. V. P. P. *Chem. Rev.* **2009**, *109*, 2551.

[4] Methot, J. L.; Roush, W. R. *Adv. Synth. Catal.* **2004**, *346*, 1035.

[5] Beletskaya, I. P.; Kazankova, M. A. *Russ. J. Org. Chem.* **2002**, *38*, 1391.

[6] Schwan, A. L. *Chem. Soc. Rev.* **2004**, *33*, 218.

[7] Alonso, F.; Beletskaya, I. P.; Yus, M. *Chem. Rev.* **2004**, *104*, 3079.

[8] Glueck, D. S. *Synlett* **2007**, 2627.

[9] Tappe, F. M.; Trepohl, V. T.; Oestreich, M. *Synthesis* **2010**, 3037.

[10] Tanaka, M. *Top. Curr. Chem.* **2004**, *232*, 25.

[11] Coudray, L.; Montchamp, J.-L. *Eur. J. Org. Chem.* **2008**, 3601.

[12] Xu, Q.; Han, L. B. *J. Organomet. Chem.* **2011**, *696*, 130.

[13] Tanaka, M. *Top. Organomet. Chem.* **2013**, *43*, 167.

[14] Han, L.-B.; Mirzaei, F.; Zhao, C.-Q.; Tanaka, M. *J. Am. Chem. Soc.* **2000**, *122*, 5407.

[15] Candy, M.; Rousseaux, S. A. L.; Román, A. C. S.; Szymczyk, M.; Kafarski, P.; Leclerc, E.; Vrancken, E.; Campagne, J.-M. *Adv. Synth. Catal.* **2014**, *356*, 2703.

[16] Perdew, J.; Burke, K.; Ernzerhof, M. *Phys. Rev. Lett.* **1996**, *77*, 3865.

[17] Perdew, J.; Burke, K.; Ernzerhof, M. *Phys. Rev. Lett.* **1997**, *78*, 1396.

[18] Andrae, D.; Haubermann, U.; Dolg, M.; Stoll, H.; Preub, H. *Theor. Chim. Acta* **1990**, *77*, 123.

[19] Ehlers, A.; Bohme, M.; Dapprich, S.; Gobbi, A.; Hollwarth, A.; Jonas, V.; Kohler, K.; Stegmann, F.; Veldkamp, A.; Frenking, G. *Chem. Phys. Lett.* **1993**, *208*, 111.

[20] Neese, F. *Comput. Mol. Sci.* **2012**, *2*, 73.

[21] Klamt, A. *Comput. Mol. Sci.* **2009**, *1*, 699.

[22] Grimme, S.; Antony, J.; Ehrlich, S.; Krieg, H. *J. Chem. Phys.* **2010**, *132*, 1456.

[23] Grimme, S.; Ehrlich, S.; Goerigk, L. *J. Comput. Chem.* **2011**, *32*, 1456.

[24] Hoops, S.; Sahle, S.; Lee, C.; Pahle, J.; Simus, N.; Singhal, M.; Xu, L.; Mendes, P.; Kummer, U. *Bioinformatics* **2006**, *22*, 3067.

[25] Hoops, S.; Sahle, S.; Lee, C.; Gauges, R.; Pahle, J.; Simus, N.; Singhal, M.; Xu, L.; Mendes, P.; Kummer, U. *In WSC 2066: Proceedings of the 37th conference on Winter simuation* **2006**, *22*, 1698.

[26] Manninen, T.; Makairaatikka, E.; Ylippa, A.; Pettinen, A.; Leinonen, K.; Linne, M. *Engineering in Medicine and Biology Society, 2006. EMBS '06. 28th Annual International Conference of the IEEE In Engineering in Medicine and Biology Society, 2006. EMBS '06. 28th Annual International Conference of the IEEE* **2006**, 2013.

[27] Mendes, P.; Hoops, S.; Sahle, S.; Gauges, R.; Dada, J.; Kummer, U. *Methods in molecular biology (Clifton, N.J.)* **2009**, *500*, 17.

[28] Barder, T. E.; Walker, S. D.; Martinelli, J. R.; Buchwald, S. L. *J. Am. Chem. Soc.* **2005**, *127*, 4685.

Chapter 4

Arylation of Fluorobenzenes mediated by Pd(0) catalyst

4.1 Synopsis

The activation of inert C-H bond of organic molecule into useful functional group is an important and very active area research. An illustrative class of C-H bond functionalization is direct arylation. The most common mechanism of C-H bond cleavage is electrophilic substitution (S_EAr) involving reaction of an electrophilic metal catalyst with an electron-rich, nucleophilic aromatic ring.[1,2] This pathway is fundamentally limiting since the majority of aromatic compounds are not sufficiently nucleophilic.

A seminal discovery was made by Fagnou who found that haloarenes could be coupled to other unactivated aromatics with a palladium catalyst (Figure 4.1).[3–10]

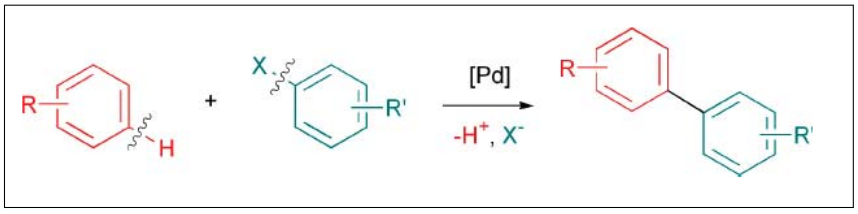

Figure 4.1: *Scheme of coupling reaction of haloarenes to unactivated aromatic systems in presence of a palladium catalyst.*

Underlying these transformations is a mechanism that actually favors reaction with electron-deficient, C-H acidic benzenes, constituting a complete inversion of reactivity compared to the S_EAr pathway.

Computational studies reveal the key C-H bond functionalization step occurs via a concerted arene metalation and carbon-hydrogen bond cleaving process, the accessibility of which depends directly on the acidity of the C-H bond being cleaved.[11]

These reactions are scalable and can employ a nearly equimolar ratio of the two benzene cross-coupling components, and produce perfluorobiphenyl products.

In this chapter we report the results of the computational study we carried out on the arylation reaction of fluorinated substrates, mediated by Pd(0) catalyst in presence of a base yielding fluorobiphenyl products. In particular we focused on a catalysis, experimentally developed with para-methyl-iodobenzene as aromatic substrate, pentafluorobenzene as fluorinated substrate, $Pd(PPh_3)_2$ as catalyst and silver carbonate as base.

The main goal of this computational study is to identify the active catalytic species involved in the energetic path and to reproduce the activation barrier of the whole process, experimentally measured.

4.2 Computational methodology

All the calculations have been performed with the Gaussian 09 package, at DFT level, using PBE0 functional.[12,13] The palladium, iodide and silver atoms were represented by the relativistic effective core potential (RECP) from the Stuttgart group and the associated basis sets,[14] augmented by an f polarization function.[15] All the others atoms (C,H,P,F,O) were represented by a SVP basis set. Full optimizations of the geometries were performed including the dispersion correction, in particular the Grimme dispersion model with the Becke-Johnson damping d3(bj).[16,17].

The frequency analysis and the the Gibbs energy correction were carried out at 298 K. Connection between reactants and products has been done through a given TS, altering his geometry along the two directions of the vector associated with the imaginary frequency.

For each geometry (TS and minima) a single point calculation has been carried out with the Orca package,[18] using an effective core potential for palladium, and a QZVPP basis set for the other atoms. In this single point calculation, the influence of the solvent (dimethylformammide, experimental solvent) was taken into consideration through the COSMO model implemented in the ORCA package.[19] Influence of the dispersion forces was considered by adding to the COSMO energy the D3(BJ) corrections as described by Grimme.[16,17] All of the energies reported in the present work are Gibbs free energy obtained by summing the COSMO energy, the gas-phase Gibbs contribution at 298 K, and the D3(BJ)correction.

4.3 Experimental results

In Figure 4.2 is reported the general scheme of the Pd-catalyzed reaction of arylation of pentafluorobenzene experimentally performed.

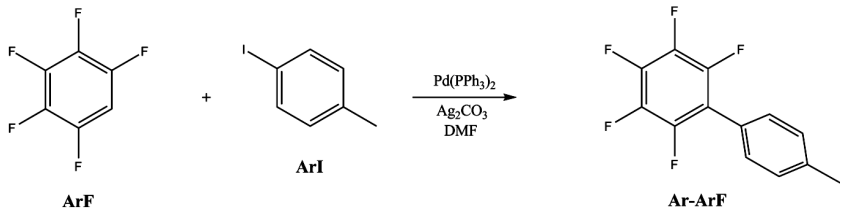

Figure 4.2: *General scheme of arylation of pentafluorobenzene mediated by Pd(0) catalyst.*

Results from a selected model reaction system indicate a first-order dependence on pentafluorobenzene and a half-order dependence on the Pd catalyst generated in situ.[20] IR spectroscopic analysis allowed the kinetic isotope effect and the activation parameters to be determined. These observation suggests that the AMLA-typr C-H activation (Figure 4.3) is the rate- determining step of the reaction presented in Figure 4.2.

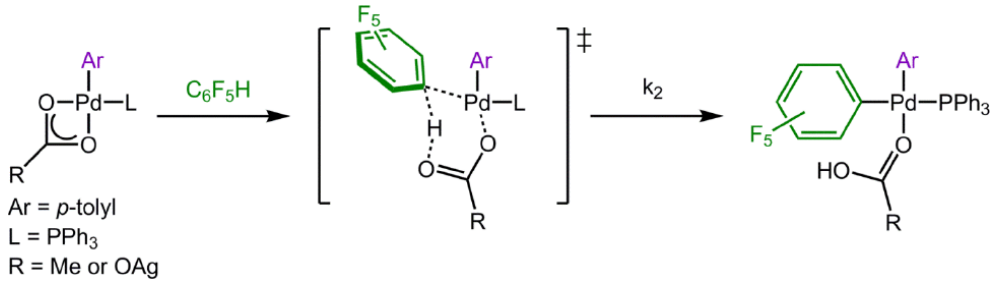

Figure 4.3: *C-H bond activation process associated to AMLA transition state.*

Kinetic model based on the Arrhenius and Eyring model allowed to determinate the activation parameters (E_a and $\Delta G^{\ddagger}$) relative to this step (Table 4.1).

Activation parameter	1	2
$\Delta G^{\ddagger}$ (kj mol^{-1})	98.9±5.6	98.9±16.8
E_a (kj mol^{-1})	72.4±2.9	64.2±8.7

Table 4.1: *Activation parameters for the C-H bond activation process. 1 and 2 are referred to different measures carried out with different initial concentrations of [p-$MeC_6H_4I]_0$ (0.18 M and 0.018 M respectively). The values of E_a were determined from Arrhenius plot, while $\Delta G^{\ddagger}$ from Eyring plot.*

Computational calculations using DFT methods have previously been used to propose a reaction mechanism involving a concerted metalation-deprotonation (CMD), also referred to as ambiphilic metal ligand activation (AMLA).[21,22]

4.4 Catalytic cycle

The reaction mechanism can be discussed as the succession of three steps (Figure 4.4):

- Oxidative addition
- Proton abstraction
- Reductive elimination

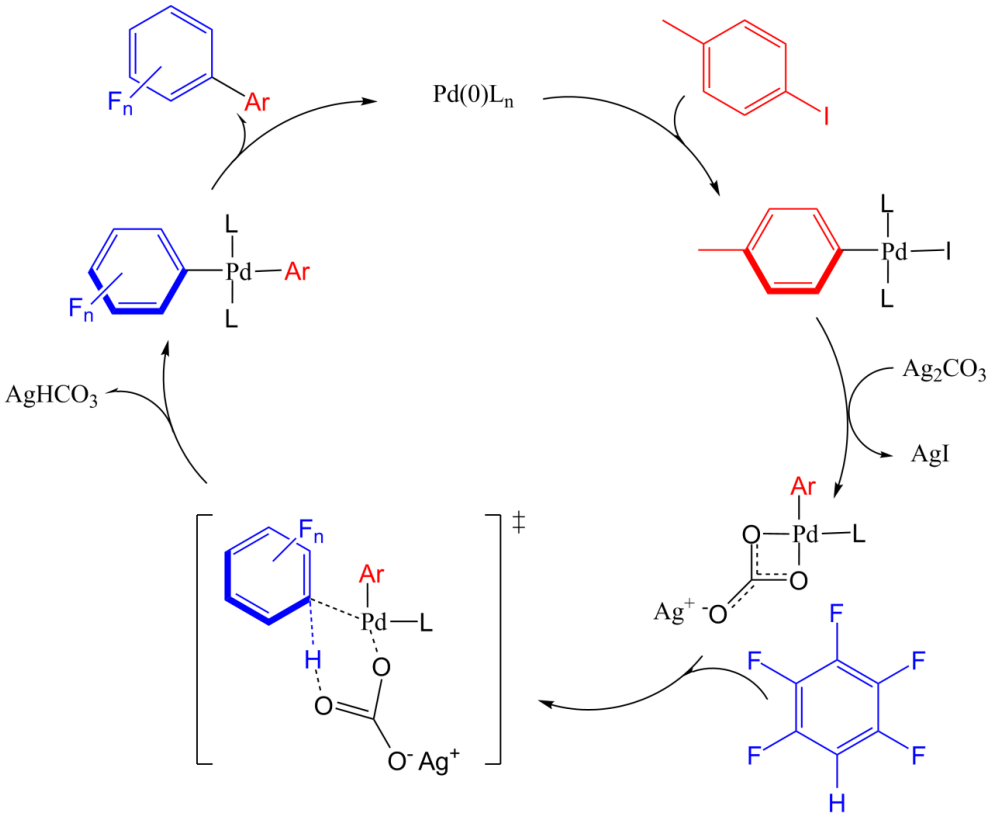

Figure 4.4: *General scheme of arylation of pentafluorobenzene mediated by Pd(0) catalyst*

Oxidative addition

In the oxidative addition step, the para-methyl-iodobenzene (ArI) approaches to $Pd(PPh_3)_n$ catalyst through an η^2 interaction between the C-I bond and the palladium center, forming the $(PPh_3)_n$-Pd(Ar)(I) species. This approach can occur both on $(PPh_3)Pd$ (Figure 4.5) or $(PPh_3)_2Pd$ (Figure 4.6), leading respectively to the formation of React-oxadd-L and React-oxadd-L2 adducts. The cleavage of the C-I

bond is effective through TS-oxadd-L or TS-oxadd-L2 transition states. Unfortunately, TS-oxadd-L can not be located on the potential energy surface. In Figure 4.7 is reported the structure of TS-oxadd-L2.

In TS-oxadd-L2 transition state, the formation of the Pd-C bond is well advanced (2.112 Å) as well as the cleavage of the C-I bond (2.319 Å), if compared with the same bond distance in the free ArI (2.111 Å). In order to favor the approach of ArI, $(PPh_3)_2Pd$ needs to distort its geometry, in particular changing the P-Pd-P angle (from 135° to 111°).

Upon the cleavage of the C-I bond and the formation of the Pd-C and Pd-I bonds, several isomers of $(PPh_3)_nPd(Ar)(I)$ can be obtained. In particular, from TS-oxadd-L2, can be obtained Prod-oxadd-L2-cis, which can isomerize to form Prod-oxadd-L2-trans (Figure 4.6). No transition state for such isomerization could be located on the potential energy surface. Three isomers of $(PPh_3)Pd(Ar)(I)$ can be obtained from TS-oxadd-L: Prod-cis-L, Prod-cis-bis-L and Prod-trans-L (Figure 4.5).

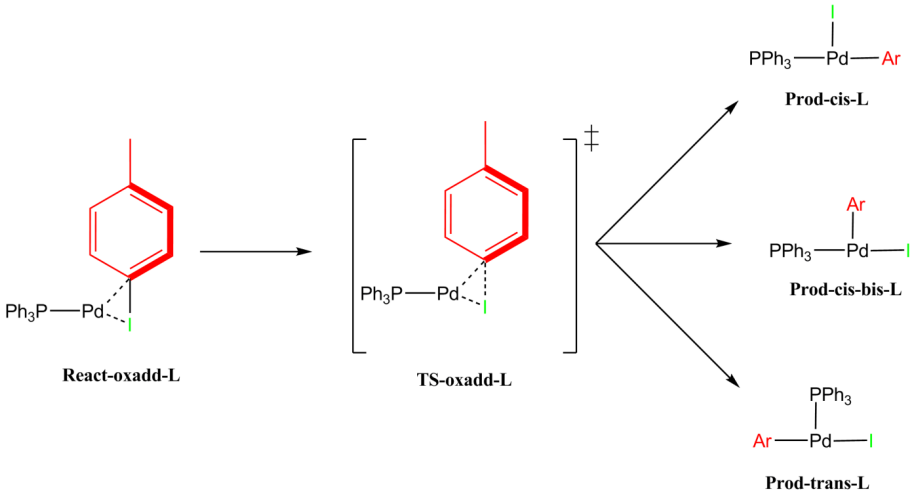

Figure 4.5: *Oxidative addition of p-methyl-iodobenzene to Pd(PPh_3) complex.*

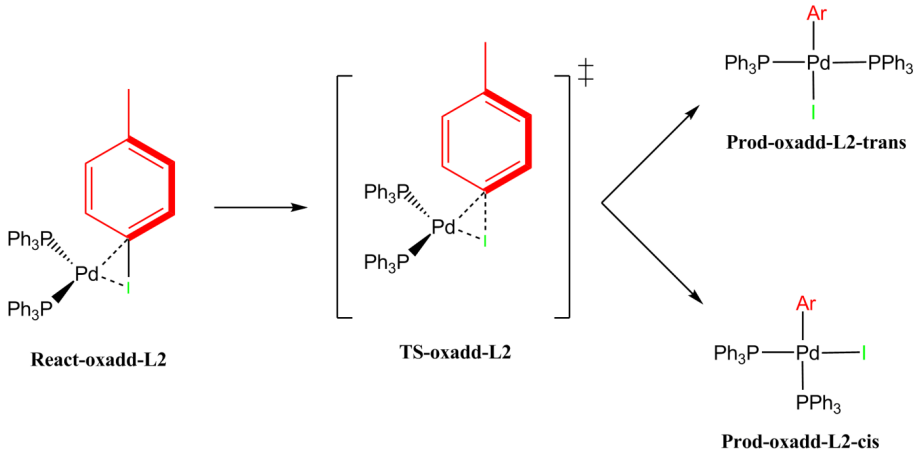

Figure 4.6: *Oxidative addition of p-methyl-iodobenzene to $Pd(PPh_3)_2$ complex.*

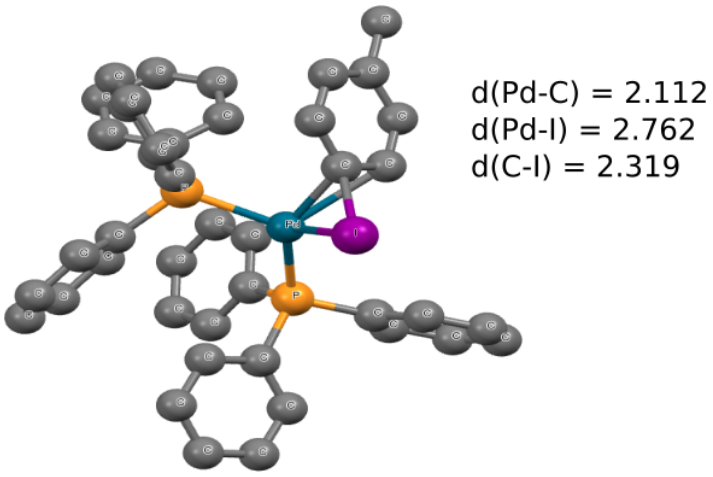

Figure 4.7: *Structure of the TS-oxadd-L2 transition state. Hydrogen atoms have been omitted for clarity. The bond distances are reported in Å.*

Proton Abstraction

The proton abstraction involves first the coordination of Ag_2CO_3 on the product of the oxidative addition, through an O-Pd-O three center interaction, leading to the formation of K2AgCO$_3$-PdLAr species (see Figure 4.8), upon the elimination of AgI. No transition state could be located on the potential energy surface for such process. If the coordination occurs on $(PPh_3)_2Pd(Ar)(I)$, then the formation of K2AgCO$_3$-PdLAr requires the loss of a PPh_3 ligand from the palladium center. Then the C-H bond of ArF is activated upon the coordination of ArF on K2AgCO$_3$-PdLAr, which leads to the formation of React-AMLA-alpha and React-AMLA-beta. These two species differ among them by the relative position of approach of ArF on palladium (*cis* and *trans* respectively with respect to PPh_3). The C-H bond activation is effective through two possible transition states: TS-AMLA-alpha and TS-AMLA-beta (see Figure 4.9). These two transition states arise from the two different reactants (React-AMLA-alpha and React-AMLA-beta). TS-AMLA-alpha exhibits a longer Pd-C bond distance with respect to TS-AMLA-beta (2.429 Å and 2.295 Å respectively). This is due to the steric bulk of $P(Ph)_3$ in *cis* that prevents an optimal approach of ArF on the palladium. The cleavage of the C-H bond is more advanced in TS-AMLA-alpha (1.248 Å) with respect to TS-AMLA-beta (1.230 Å), confirmed by the shorter O-H bond distance (1.402 Å versus 1.412 Å respectively).

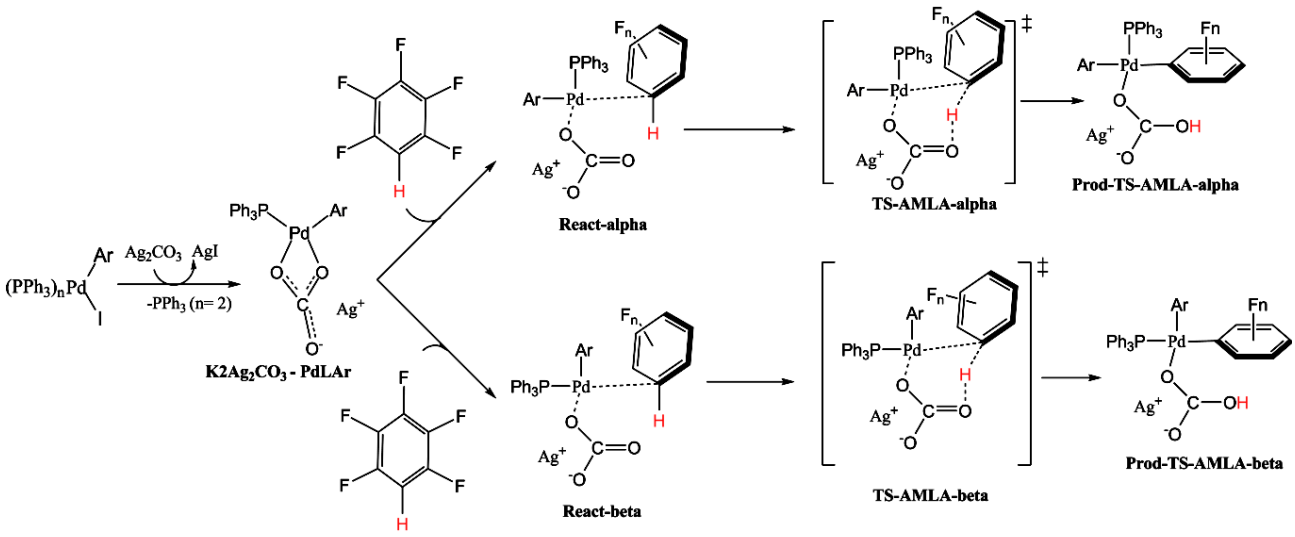

Figure 4.8: *Coordination of Ag_2CO_3 to Pd(II) complexes and activation of C-H bond*

The products arising from TS-AMLA-alpha and TS-AMLA-beta are respectively Prod-TS-AMLA-alpha and Prod-TS-AMLA-beta, in which Ar and ArF are respectively in *cis* and in *trans* position. $AgHCO_3$ is still coordinated to palladium. For the last step of the catalytic cycle, the dissociation of $AgHCO_3$ with the formation of $(PPh_3Pd(Ar)(ArF)$ and $AgHCO_3$, is required. No transition state for such process could be located on the potential energy surface.

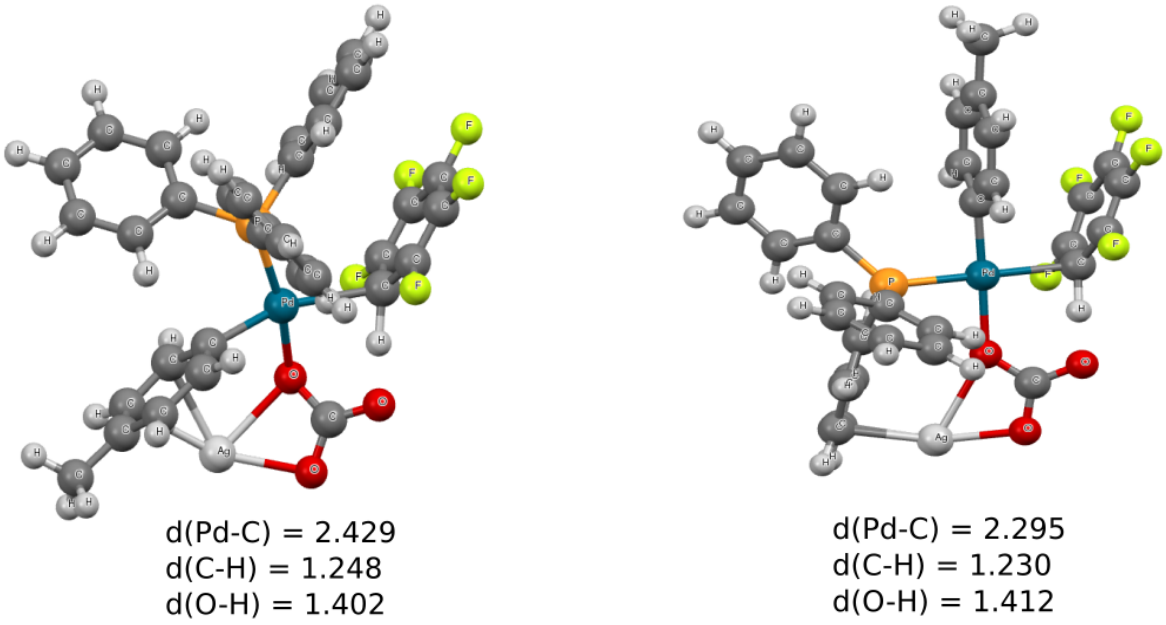

(a) TS-AMLA-alpha

(b) TS-AMLA-beta

Figure 4.9: *Structures of TS-AMLA-alpha (a) and TS-AMLA-beta (b).*

Reductive elimination

The reductive elimination involves the formation of the C-C bond between Ar and ArF, the dissociative of Ar-ArF and the regeneration of the catalyst. When $(PPh_3)Pd(Ar)(ArF)$ is formed, two pathways can be followed: (i) direct reductive elimination through TS-RedElim-L-cis and TS-RedElim-L-cisbis transition states (Figure 4.10) (ii) coordination of a second ligand to palladium to form PdL2-Ar-ArF-cis or PdL2-Ar-ArF-trans species, followed by the reductive elimination through TS-RedElim-L2 transition state (Figure 4.11). In the direct pathway, three possible isomers of $(PPh_3)Pd(Ar)(ArF)$ can undergo the reductive elimination, while, in the case of $(PPh_3)_2Pd(Ar)(ArF)$, only the *cis* isomer can lead to TS-RedElim-L2. In Figure 4.12 are reported the structure of the three possible transition states.

In TS-RedElim-L2, the formation of the C-C bond is more advanced (1.861 Å) with respect to TS-RedElim-L-cis (1.984 Å) and TS-RedElim-L-cisbis (2.049 Å). TS-RedElim-L-cisbis could be less favored in energy with respect to TS-RedElim-L-cis, because of the C-C bond distance much higher than the one in the free Ar-ArF (1.479 Å). For such reason, TS-RedElim-L-cis can be seen as the only possible transition state arising from $(PPh_3)Pd(Ar)(ArF)$.

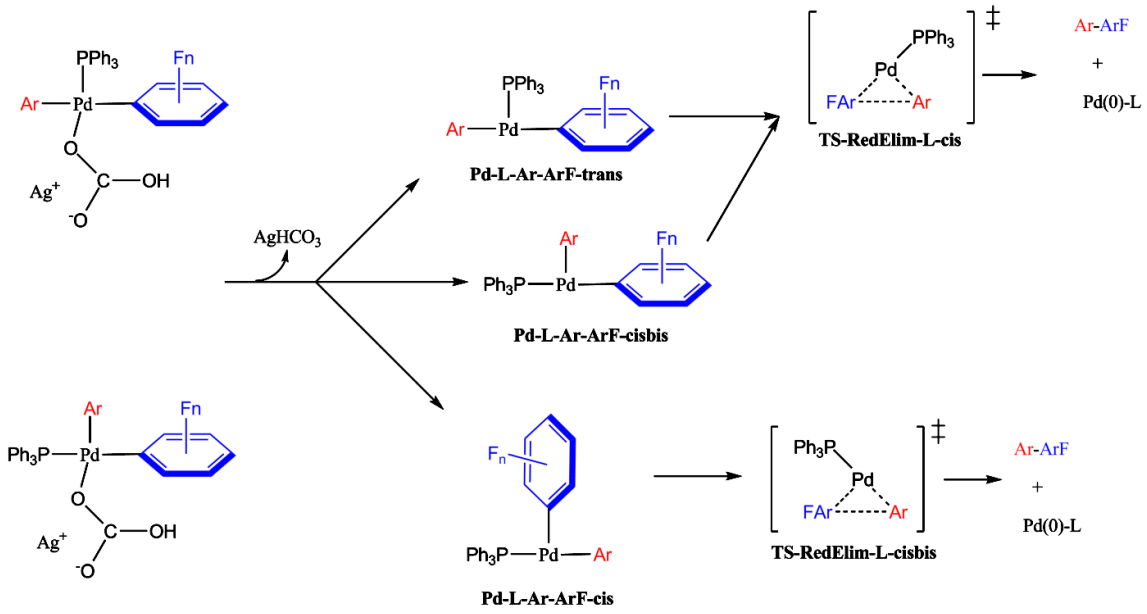

Figure 4.10: *Reductive elimination from $(PPh_3)Pd(Ar)(ArF)$.*

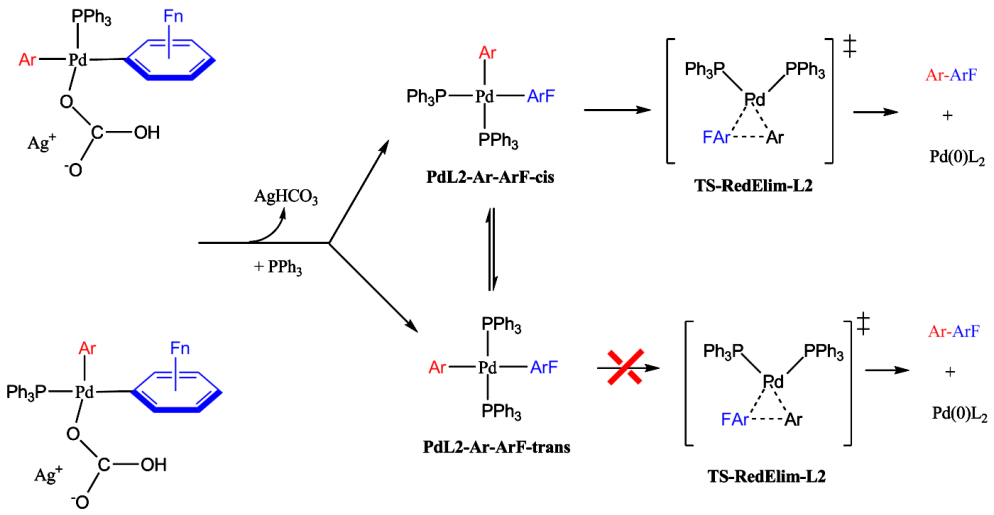

Figure 4.11: *Reductive elimination from $(PPh_3)_2Pd(Ar)(ArF)$.*

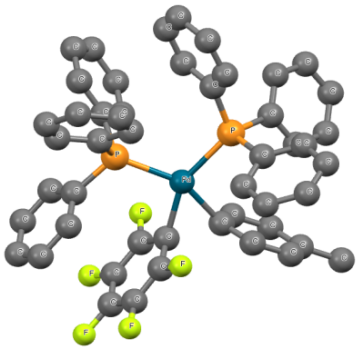

(a) TS-RedElim-L2

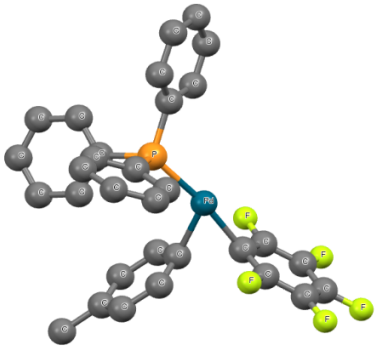

(b) TS-RedElim-L-cis

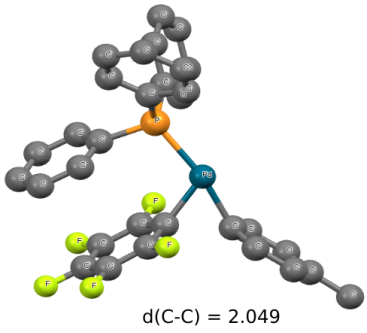

(c) TS-RedElim-cisbis

Figure 4.12: *Structures of TS-RedElim-L2 (a) TS-RedElim-L-cis (b) and TS-RedElim-L-cisbis (c) transition states. The distance are reported in Angstrom. Hydrogen atoms have been omitted for clarity.*

4.5 Energetic paths

In the present section we report the energetic paths for the reaction including $(PPh_3)Pd$ and $(PPh_3)_2Pd$ species as catalysts. In addition, in order to visualize the effect of the dispersion corrections, we show the energetic values of the points along the paths not including such corrections. Since palladium complexes are able to form stable dimers,[23] which can alterate the kinetics studies of the catalysis, and since experimentally the formation of dimers of Pd(II) were supposed, we included in the study the research of stable palladium dimers, evaluating their impact on the energetic paths. The two most stable dimers (labeled as Dimer-I and Dimer-II) are shown in Figure 4.13. Dimer-I arises from the coordination of $(PPh_3Pd(I)(Ar)$ species, through a binding coordination of iodide between two Pd centers. Dimer-II arises from the coordination of two K2AgCO$_3$-PdLAr species.

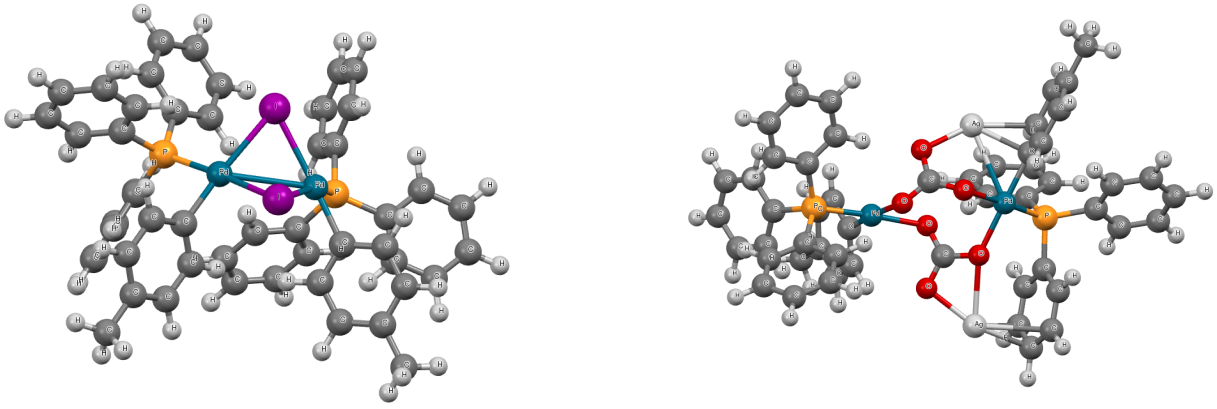

(a) Dimer-I

(b) Dimer-II

Figure 4.13: *Structures of Dimer-I (a) and Dimer-II (b).*

In Figure 4.14 are reported the energetic paths relative to the arylation of C_6F_5H catalyzed by $Pd(PPh_3)_2$ (blue path) and $Pd(PPh_3)$ (red path).

The approach of Ar-I on $(PPh_3)_2Pd$ is a slightly endothermic process (ΔG= 0.9 kcal mol^{-1}), and the cleavage of the C-I bond and the formation of Pd-I and Pd-C bonds, effective through Ts-oxadd-L2, is associated to an energetic barrier of $\Delta G^{\ddagger}$ = 4.9 kcal mol^{-1}. The approach of Ar-I on $(PPh_3)Pd$ is much more endothermic (ΔG= 14.3 kcal mol^{-1}), and, even if was not not possible to locate TS-L-oxadd-L, it is clear that $(PPh_3)Pd$ is inactive in catalyzing the oxidative addition. The oxidative addition on $(PPh_3)_2Pd$ yields first Prod-oxadd-L2-cis as product (ΔG= -22.6 kcal mol^{-1}), which can isomerize to yield the more stable Prod-oxadd-L2-trans (ΔG= -23.6 kcal mol^{-1}). Among the three possible products arising from the oxidative addition on $(PPh_3)Pd$, Prod-oxadd-L-cisbis is the most stable (ΔG= -5.4 kcal mol^{-1}), while Prod-oxadd-L-cis and Prod-oxadd-L-trans exhibit relative energies of ΔG= 6.5 kcal mol^{-1}and ΔG= -3.3 kcal mol^{-1}respectively. Prod-oxadd-L-cisbis can follow several paths: (i) upon the addition of a second ligand, it can yield Prod-oxadd-L2-cis; (ii) upon the coordination of a second Prod-oxadd-L-cisbis species,

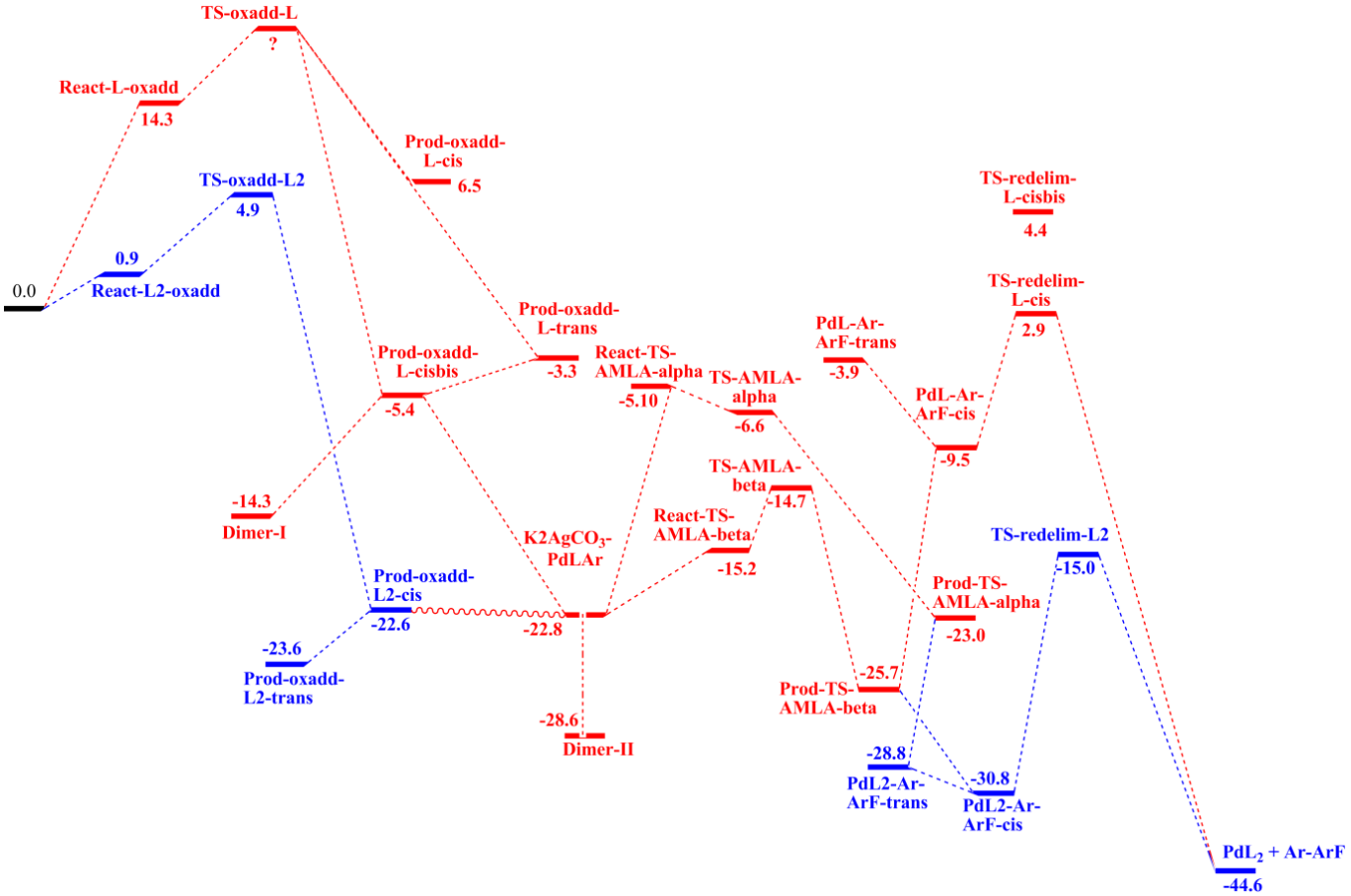

Figure 4.14: *Energetic paths relative to the arylation of C_6F_5H catalyzed by $Pd(PPh_3)_n$,including the dispersion correction. In blue is indicated the path catalyzed by $Pd(PPh_3)_2$, while in red the path catalyzed by $Pd(PPh_3)$. The energetic values are reported in kcal mol^{-1}.*

Dimer-I can be formed (ΔG= -14.3 kcal mol^{-1}); (iii) upon the coordination of Ag_2CO_3, K2AgCO$_3$-PdLAr can be formed with dissociation of AgI. The formation of Prod-oxadd-L2-cis and K2AgCO$_3$-PdLAr exhibit the same relative energies (ΔG= -22.6 and ΔG= -22.8 kcal mol^{-1}respectively). The formation of K2AgCO$_3$-PdLAr can also occur from Prod-oxadd-L2-cis, upon the loss of a ligand. The formation of the stable Dimer-II (ΔG= -28.6 kcal mol^{-1}) arises from the approach of two K2AgCO$_3$-PdLAr species. Conversely, the approach of Ar-F to K2AgCO$_3$-PdLAr in *cis* to Ar substituent leads to the isomerization and the formation of React-TS-AMLA-beta (ΔG= -15.2 kcal mol^{-1}). The cleavage of the C-H bond and the formation of Pd-ArF bond is effective through TS-AMLA-beta ($\Delta G^{\ddagger}$ = 8.1 kcal mol^{-1}).The same activation barrier, if calculated with respect to Dimer-II, exhibits a value of $\Delta G^{\ddagger}$ = 13.9 kcal mol^{-1}. TS-AMLA-alpha is higher in energy (ΔG= -6.6 kcal mol^{-1}), suggesting that the path passes only through TS-AMLA-beta. The product arising from the C-H bond activation, Prod-TS-AMLA-beta, upon the cleavage of the Pd-O bond and the formation of AgHCO$_3$, leads to PdL2-Ar-ArF-cis (ΔG= -30.8 kcal

mol^{-1}), upon the insertion of an additional ligand on palladium. PdLAr-ArF-cis is much more destabilized (ΔG = -9.5 kcal mol^{-1}), as well as PdLAr-ArF-trans (ΔG= -3.9 kcal mol^{-1}), suggesting that the PdL2-Ar-ArF-cis is the only possible species. The reductive elimination from PdL2-Ar-ArF-cis is effective through TS-redelim-L2 ($\Delta G^{\ddagger}$ = 15.8 kcal mol^{-1}), while the same process from PdL-Ar-ArF-cis through TS-redelim-L-cis, even if exhibiting a lower barrier of $\Delta G^{\ddagger}$ = 12.4 kcal mol^{-1}, is not energetically favored. Oxidative addition and reductive elimination processes are effective only with $(PPh_3)_2Pd$, while C-H bond activation can occur only through (PPh_3Pd) species. The same path is energetically different if the dispersion correction is not included. In Figure 4.15 are reported the energetic paths for the arylation process of C_6F_5H catalyzed by $Pd(PPh_3)_2$ (blue path) and $Pd(PPh_3)$ (red path), not including the dispersion corrections to the energy.

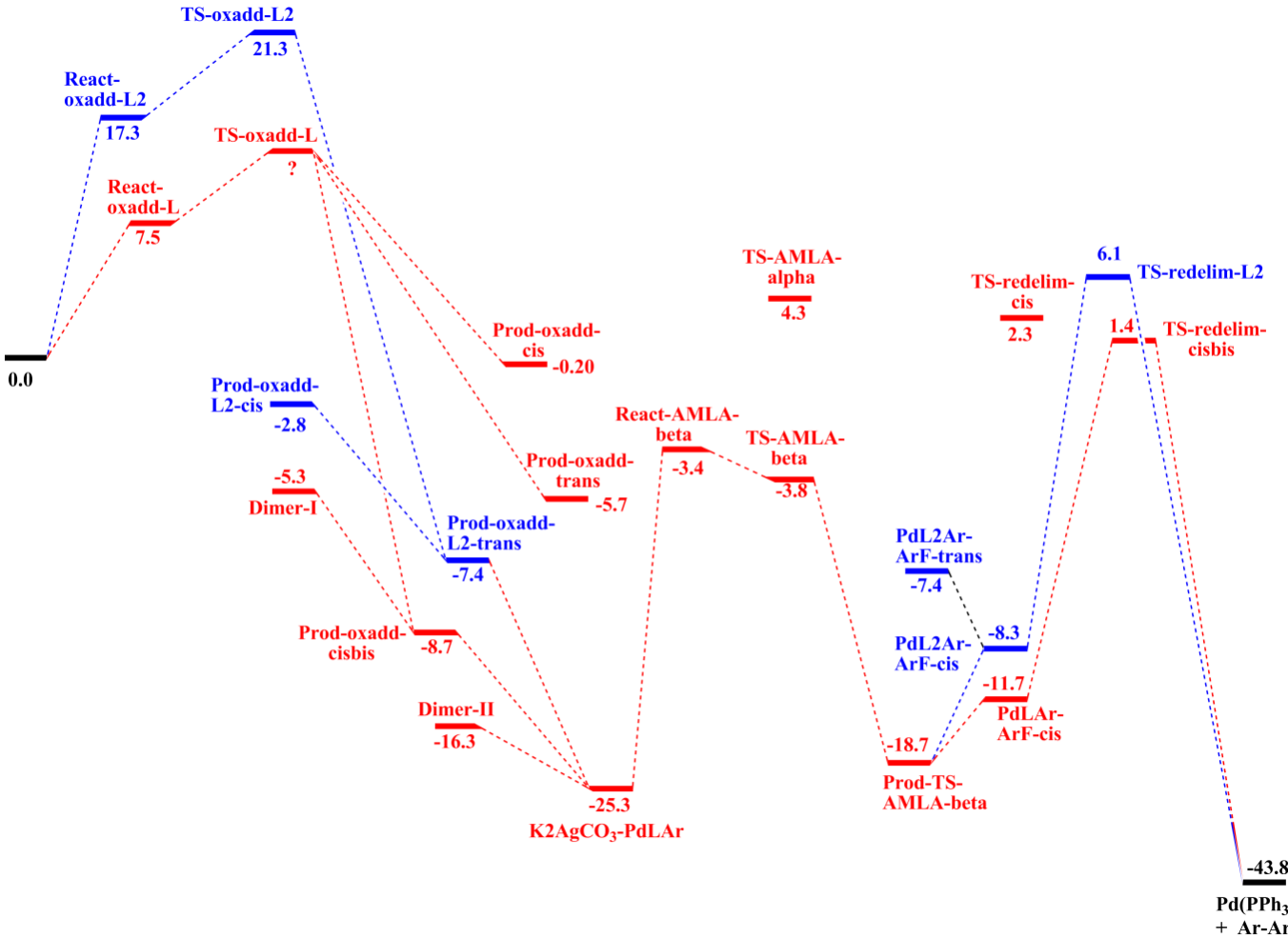

Figure 4.15: *Energetic paths relative to the arylation of C_6F_5H catalyzed by $Pd(PPh_3)_n$, not including the dispersion correction. In blue is indicated the path catalyzed by $Pd(PPh_3)_2$, while in red the path catalyzed by $Pd(PPh_3)$. The energetic values are reported in kcal mol^{-1}.*

When the dispersion corrections are not included in the calculations of the en-

ergetic paths, remarkably differences in such path can be observed. First of all, the approach of ArI on $Pd(PPh_3)$ is much more favored (ΔG = 7.5 kcal mol^{-1}) with respect to the approach on $Pd(PPh_3)_2$ (ΔG = 17.3 kcal mol^{-1}), and the global barrier for the oxidative addition on $Pd(PPh_3)_2$ exhibit a value of $\Delta G^{\ddagger}$ = 21.3 kcal mol^{-1}. The activation barrier for $Pd(PPh_3)$, even if it can not be located on the PES, is supposed to be lower in energy. The higher values of ΔG for React-oxadd-L2 and TS-oxadd-L2 on the path are due to the fact that, in absence of the dispersion corrections to the energy, the large number of pairwise interactions between non-bonded atoms, with mutual distance typical of Van der Waals attraction, are lost and, consequently, these system are much more destabilized with respect to the reactants. Conversely, React-oxadd-L and TS-oxadd-L are more stabilized when no dispersion corrections are included with respect to the reactants, making the oxidative addition on $Pd(PPh_3)$ more accessible in energy. Also the three possible products arising from TS-oxadd-L, are more stabilized. Prod-oxadd-cisbis is the most stable (ΔG = -8.7 kcal mol^{-1}) among the three products. Conversely, the products arising from TS-oxadd-L2 are destabilized by *ca* 16-18 kcal mol^{-1}. Prod-oxadd-L2-trans (ΔG = -7.4) is more stable than Prod-oxadd-L2-cis (ΔG = -2.8). However, the addition of a second PPh_3 ligand on Prod-oxadd-L to form Prod-oxadd-L2 is still favored in energy. The formation of Dimer-I becomes less favored (ΔG = -5.3 kcal mol^{-1}) in absence of the dispersion corrections, suggesting that such species could not play a crucial role in the catalytic cycle. The formation of K2Ag2CO3-PdLAr, upon the coordination of Ag_2CO_3 on $(PPh_3)_nPd(Ar)(I)$ and the elimination of AgI, is more favored in energy (ΔG = -25.3 kcal mol^{-1}). The formation of Dimer-II arising from the approach ow two K2Ag2CO3-PdLAr fragments, is not favored (ΔG = -16.3 kcal mol^{-1}) and, as already seen for Dimer-I, it would not play a crucial role in the catalytic cycle. The approach of ArF on the palladium, in *trans* to PPh_3, and the cleavage of the Pd-O bond to form React-AMLA-beta (ΔG = -3.4 kcal mol^{-1}) is higher in energy, with a barrier of ΔG = 21.9 kcal mol^{-1}. The approach of ArF alterates the geometry of K2Ag2CO3-PdLAr, and, in absence of any pairwise stabilizing interactions between non bonded atoms, this process is sensibly energetically disfavored.

The approach of ArF in *cis* to PPh_3 leads to an energetic barrier of $\Delta G^{\ddagger}$ = 29.6 kcal mol^{-1}. The elimination of $AgHCO_3$ from Prod-TS-AMLA-beta is an endoergonic process (ΔG = 7 kcal mol^{-1}) and the addition of a PPh_3 ligand leads to a more destabilized PdL2-Ar-ArF-cis (ΔG = -8.3 kcal mol^{-1}) and PdL2-Ar-ArF-trans (ΔG = -7.4 kcal mol^{-1}). The reductive elimination from these species is more disfavored when no dispersion corrections are considered. In particular, the reductive elimination through TS-redelim-cisbis exhibits an activation barrier of $\Delta G^{\ddagger}$ = 13.1 kcal mol^{-1}), while the reductive elimination through TS-redelim-L2 exhibits a barrier of $\Delta G^{\ddagger}$ = 14.4 kcal mol^{-1}.

In Table 4.2 are given the energetic values of the different steps (oxidative addition, C-H bond activation and reductive elimination) relative to the process catalyzed by $Pd(PPh_3)_2$ and $Pd(PPh_3)$ species. The energetic paths shown in Figure 4.14 and 4.15, as well as the data collected in Table 4.2, give a general picture on the crucial role that the dispersion corrections play in the calculation of the ener-

$Pd(PPh_3)_2$ catalyst				
	Ox. Add.	C-H activ.(alpha)	C-H activ.(beta)	Red. Elim.
Dispersion	4.9	23.5	13.9	15.8
No Dispersion	21.3	29.6	21.9	24.8
$Pd(PPh_3)$ catalyst				
	Ox. Add.	C-H activ.(alpha)	C-H activ.(beta)	Red. Elim.
Dispersion	-	23.5	13.9	28.6
No Dispersion	-	29.6	21.9	20.1

Table 4.2: *Energetic values of the different steps (oxidative addition, C-H bond activation and reductive elimination) relative to the process catalyzed by $Pd(PPh_3)$ and $Pd(PPh_3)_2$ species in presence of Ag_2CO_3. The energetic values are reported in kcal mol^{-1}.*

getic paths. The activation barrier for the oxidative addition on $Pd(PPh_3)_2$ shows a remarkable difference when calculated without such corrections ($\Delta G^{\ddagger}$ = 4.9 kcal $mol^{-1}$and $\Delta G^{\ddagger}$ = 21.3 kcal mol^{-1}). The activation barrier for C-H activation process, catalyzed only by $(PPh_3)Pd$ species, passes from $\Delta G^{\ddagger}$ = 13.9 kcal $mol^{-1}$to $\Delta G^{\ddagger}$ = 21.9 kcal mol^{-1}. The reductive elimination from $(PPh_3)Pd(Ar)(ArF)$ passes from $\Delta G^{\ddagger}$ = 15.8 kcal mol^{-1} to $\Delta G^{\ddagger}$ = 24.8 kcal mol^{-1}. No transition state for the oxidative addition on $(PPh_3)Pd$ species could be located, and the activation barrier for the reductive elimination from $(PPh_3)Pd(Ar)(ArF)$ passes from $\Delta G^{\ddagger}$ = 28.6 kcal mol^{-1} to $\Delta G^{\ddagger}$ = 20.1 kcal mol^{-1}. In all the cases, the rate determining step of the process is the reductive elimination, to which are associated the higher activation barriers.

The rate determining step of the process is reductive elimination ($\Delta G^{\ddagger}$ = 15.8 kcal $mol^{-1}$and $\Delta G^{\ddagger}$ = 28.8 kcal $mol^{-1}$with $Pd(Ph_3)_2$ and $Pd(Ph_3)$ respectively). The C-H bond activation is effective through two transition states, TS-AMLA-alpha and TS-AMLA-beta, which exhibit different relative energies (ΔG = -6.6 kcal $mol^{-1}$and ΔG = -14.7 kcal mol^{-1}). The activation barriers associated with these two transition states are $\Delta G^{\ddagger}$ = 22.0 kcal mol^{-1}, and $\Delta G^{\ddagger}$ = 13.9 kcal mol^{-1}The activation barriers for the C-H bond activation are calculated with respect to Dimer-II (in the case of the path including the dispersion correction), and with respect to $K2AgCO_3$-PdLAr (in the case of the path not including the dispersion correction). In the first energetic path, although TS-AMLA-beta is more accessible in energy, the activation barrier associated to it is not in agreement with the experimental results. This could suggest that, even if TS-AMLA-alpha is higher in energy, the process passes through the latter transition state, because of the structure of Dimer-II. Indeed, in order to reach TS-AMLA, the cleavage of one Pd-O bond in Dimer-II is required. Depending on which Pd-O is cleaved, both React-TS-AMLA-alpha and React-TS-AMLA-beta can be formed, and an isomerization between them is not possible because of the presence of $AgCO_3$ species coordinated to palladium. A preference in the formation of React-AMLA-alpha, with a consequent C-H bond activation through TS-AMLA-alpha, could be supposed.

Reaction path without silver

In this section we present the energetic path for the arylation of C_6F_5H with [p-$MeC_6H_4I]_0$, catalyzed by $Pd(PPh_3)_n$, including $AgCO_3^-$ as base instead of Ag_2CO_3. The inclusion of $AgCO_3^-$ species as reactant does not affect the oxidative addition, since the Ag salt is not involved in such step. Therefore the energetic values for the oxidative addition are the same seen for the paths including Ag_2CO_3 and they are not shown in the energetic paths.

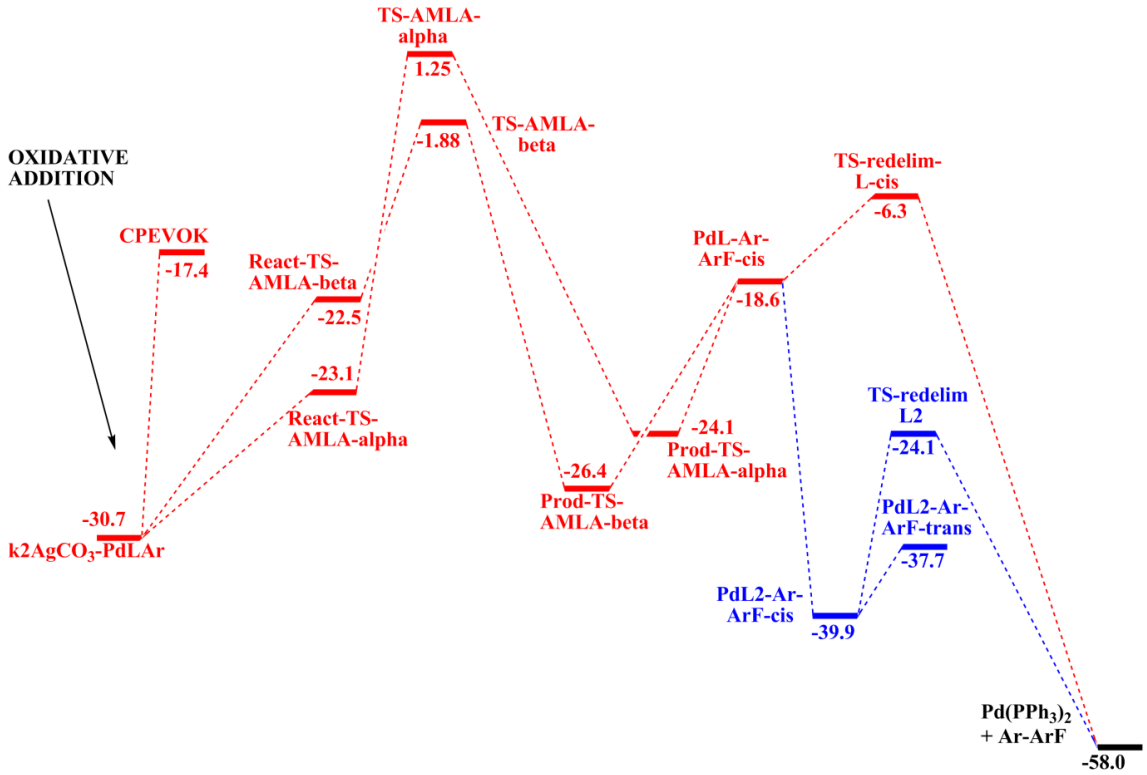

Figure 4.16: *Reaction path mediated by $Pd(PPh_3)_2$ (blue path) and $Pd(PPh_3)$ (red path) catalyst not including the silver in the C-H bond activation step, including the dispersion correction. The energetic values are reported in Kcal/mol.*

Conversely, the C-H bond activation step is affected by the different nature of the Ag salt, since the coordination of $AgCO_3^-$ to the products of the oxidative addition and the elimination of AgI leads to the formation of K2$AgCO_3$-PdLAr, React-TS-AMLA, TS-AMLA and Prod-TS-AMLA species with a formal negative charge. In addition, in order to have the reductive elimination, the elimination of HCO_3^- anion, and not $AgHCO_3^-$, is required. In order to individuate a possible stable dimer along the path, without silver atoms and with a formal charge of -2, we consulted the *Cambridge Structural Database* (CSD)[24] and we found the structure of the so labeled CPEVOK structure (Figure 4.17).

In Figure 4.16 is shown the energetic path with $AgHCO_3^-$ as base, including the dispersion corrections to the energy. As already mentioned, the energetic of the

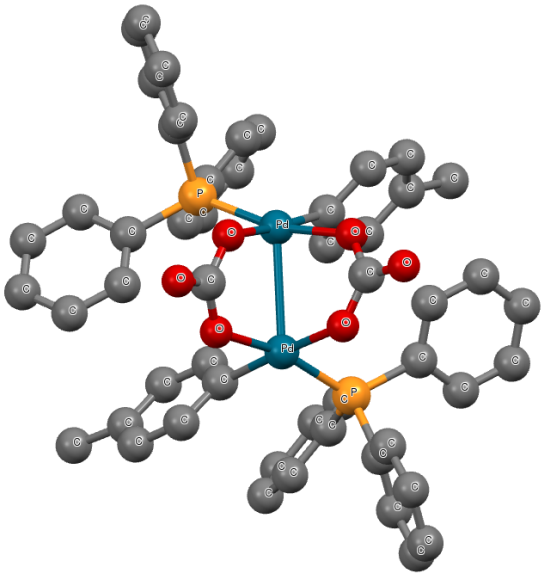

Figure 4.17: *Optimized structure of CPEVOK dimer. The formal charge of the system -2.*

oxidative addition is not affected by the different Ag salt, and, therefore, this step is not shown in Figure 4.16. The formation of K2AgCO$_3$-PdLAr and the elimination of AgI is more favored in energy (ΔG = -30.7 kcal mol^{-1}) when AgHCO$_3^-$ is involved. The formation of CPEVOK from K2AgCO$_3$-PdLAr is disfavored (ΔG = -17.4 kcal mol^{-1}), therefore such species does not play a crucial role in the path. Differently from the case involving Ag$_2$CO$_3$, the approach of ArF (in *cis* or *trans* to PPh$_3$) and the cleavage of Pd-O bond leads respectively to the formation of React-TS-AMLA-alpha and React-TS-AMLA-beta, which are very close in energy (ΔG = -23.1 kcal mol^{-1}and ΔG = -22.5 kcal mol^{-1}respectively). The C-H bond activation is effective through TS-AMLA-alpha (ΔG = 1.25 kcal mol^{-1}) and TS-AMLA-beta (ΔG = -1.88 kcal mol^{-1}), to which are associated energetic barriers of ΔG‡ = 32.0 kcal mol^{-1}and ΔG‡ = 28.8 kcal mol^{-1}respectively. The higher relative stability of K2AgCO$_3$-PdLAr increases the energetic barriers for the C-H bond activation. Also Prod-TS-AMLA-alpha and Prod-TS-AMLA-beta are very close in energy (ΔG = -24.1 kcal mol^{-1}and ΔG = -26.4 kcal mol^{-1}). These species can follow two different path: (i) upon the loss of HCO$_3^-$ they can form PdL-Ar-ArF-cis species (ΔG = -18.6 kcal mol^{-1}) or (ii) upon the loss of HCO$_3^-$ and the addition of a second PPh$_3$ on palladium they can form PdL$_2$-Ar-ArF-cis (ΔG = -39.9 kcal mol^{-1}) or PdL$_2$-Ar-ArF-trans (ΔG = -37.7 kcal mol^{-1}). The second process is much more favored in energy, and from PdL$_2$-Ar-ArF-cis , the reductive elimination is effective through TS-redelim-L2 (ΔG‡ = 15.8 kcal mol^{-1}). Conversely, from PdL-Ar-ArF-cis, the reductive elimination is effective through TS-redelim-L-cis (ΔG‡ = 12.3 kcal mol^{-1}). Even if this latter process exhibits a lower energetic barrier, it is less favored because of the lower stability of PdL-Ar-ArF-cis with respect to PdL$_2$-Ar-ArF-cis. In general, the reaction path involving AgCO$_3^-$ sensibly influences the C-H

bond activation. Even if the approach of ArF to palladium is possible both in *cis* and in *trans* position to PPh_3 (alpha and beta), the energetic barriers are much higher in energy, due to the higher stability of $K2AgCO_3$-PdLAr. The reductive elimination is not sensibly affected, and the path passing through $PdL_2(Ar)(ArF)$ is favored.

In Figure 4.18 is reported the same energetic path not including the dispersion corrections to the energy.

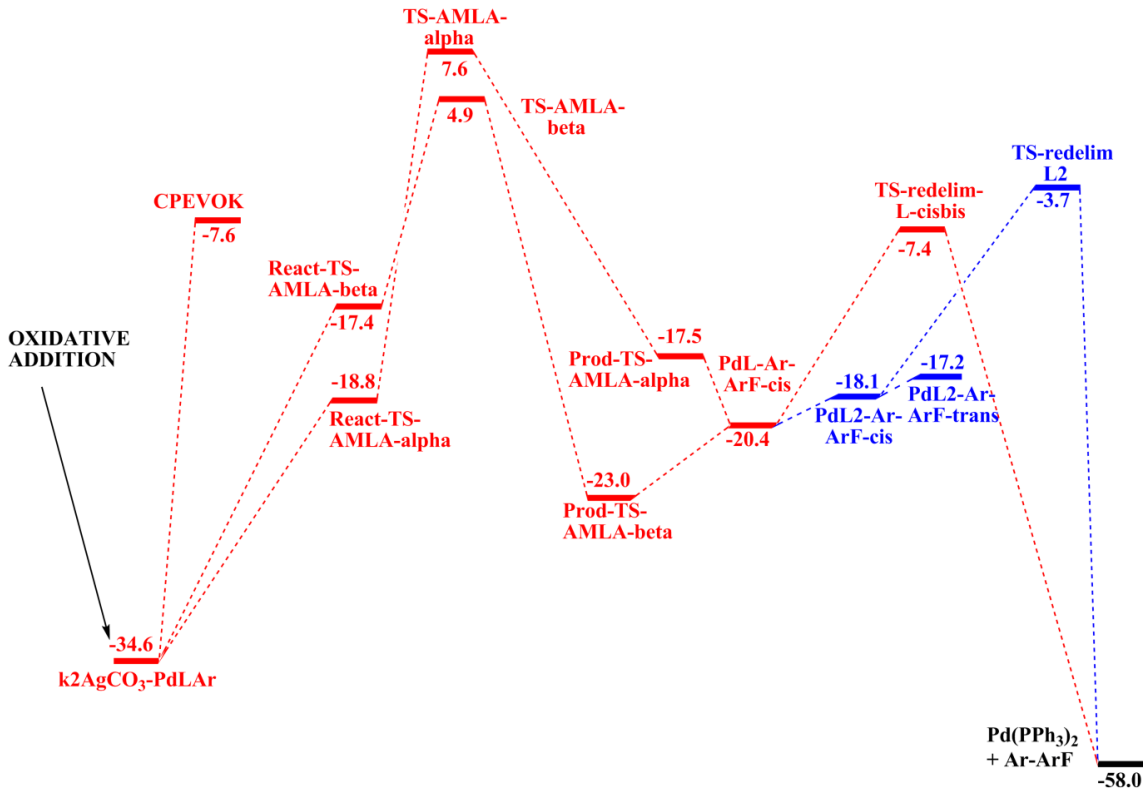

Figure 4.18: *Reaction path mediated by $Pd(PPh_3)_2$ (blue path) and $Pd(PPh_3)$ (red path) catalyst not including the silver in the C-H bond activation step, not including the dispersion correction. The energetic values are reported in kcal mol^{-1}.*

When no dispersion corrections are included in the calculations of the energetic path, the C-H bond activation becomes less favored in energy. In particular, $K2AgCO_3$-PdLAr is more stabilized (ΔG = -34.6 kcal mol^{-1}), while the two transition states TS-AMLA-alpha and TS-AMLA-beta are more destabilized (ΔG = 7.6 kcal $mol^{-1}$and ΔG = 4.9 kcal mol^{-1}respectively), with relative activation barriers of $\Delta G^{\ddagger}$ = 42.2 kcal $mol^{-1}$and $\Delta G^{\ddagger}$ = 39.5 kcal mol^{-1}respectively. The formation of Prod-TS-AMLA-alpha and Prod-TS-AMLA-beta is less exoergonic (ΔG = -17.5 kcal $mol^{-1}$and ΔG = -23.0 kcal mol^{-1}respectively), while the addition to a second PPh_3 ligand to form $PdL_2(Ar)(ArF)$ species is disfavored (ΔG = -18.1 for PdL2-Ar-ArF-cis and ΔG = -17.2 for PdL2-Ar-ArF-trans). The reductive elimination through TS-redelim-L2 is associated to an energetic barrier of $\Delta G^{\ddagger}$ = 14.4 kcal mol^{-1}, while reductive elimination through TS-redelim-L-cisbis is associated with an energetic barrier of $\Delta G^{\ddagger}$ = 13.0 kcal mol^{-1}. The absence of the dispersion corrections makes

less favored the reductive elimination from PdL2-Ar-ArF-cis, while the same process from PdL-Ar-ArF-cis remains unalterated in energy.

$Pd(PPh_3)_2$ catalyst				
	Ox. Add.	C-H activ.(alpha)	C-H activ.(beta)	Red. Elim.
Dispersion	4.9	32.0	20.6	15.8
No Dispersion	21.3	42.2	39.5	14.4
$Pd(PPh_3)$ catalyst				
	Ox. Add.	C-H activ.(alpha)	C-H activ.(beta)	Red. Elim.
Dispersion	-	32.0	20.6	12.3
No Dispersion	-	42.2	39.5	13.0

Table 4.3: *Energetic values of the different steps (oxidative addition, C-H bond activation and reductive elimination) relative to the process catalyzed by $Pd(PPh_3)$ and $Pd(PPh_3)_2$ species in presence of $AgCO_3^-$. The energetic values are reported in kcal mol^{-1}.*

In Table 4.3 are resumed the activations barriers, relative to the three main steps of the process, relative to $Pd(PPh_3)_2$ and $Pd(PPh_3)$ catalysts, calculated including and not including the dispersion corrections. While the oxidative addition barriers are not altered by the different base involved, the C-H bond activation barriers undergo a sensible increase in energy.

4.6 Comparison with experimental results

In the reaction path involving Ag_2CO_3 as base, the rate determining step of the whole process is the reductive elimination ($\Delta G^{\ddagger}$ = 15.8 kcal $mol^{-1}$and $\Delta G^{\ddagger}$ = 28.8 kcal $mol^{-1}$with $Pd(Ph_3)_2$ and $Pd(Ph_3)$ respectively). This is not in agreement with the experimental results, which clearly show that the rate determining step is the C-H bond activation. Conversely, the mechanistic study involving $AgCO_3^-$ as base indicates that the rate determining step is the C-H bond activation. In particular, this process is effective through TS-AMLA-beta, to which is associated an activation barrier of $\Delta G^{\ddagger}$ = 20.6 kcal mol^{-1}(86.1 kj mol^{-1}). This value is very close in energy to the experimental one ($\Delta G^{\ddagger}$ = 98.9 $\pm$ 5.6 kj mol^{-1}). This barrier is calculated as difference in energy between TS-AMLA-beta and K2$AgCO_3$-PdLAr.

Bibliography

[1] Campeau, L.; Fagnou, K. *Chem. Comm.* **2006**, 1253.

[2] Hassan, J.; Sevignon, M.; Gozzi, C.; Schulz, E.; Lemaire, M. *Chem. Rev.* **2002**, *102*, 1359.

[3] Campeau, L.; Rooseaux, S.; Fagnou, K. *J. Am. Chem. Soc.* **2005**, *127*, 18020.

[4] Lafrance, M.; Fagnou, K. *J. Am. Chem. Soc.* **2006**, *128*, 16496.

[5] Lafrnce, M.; Shore, D.; Fagnou, K. *Org. Lett.* **2006**, *8*, 5097.

[6] Campeau, L.; Parisien, M.; Jean, A.; Fagnou, K. *J. Am. Chem. Soc.* **2006**, *128*, 581.

[7] Leclerc, J.; Fagnou, K. *Angew. Chem. Int. Ed.* **2006**, *45*, 7781.

[8] Caron, L.; Campeau, L.; Fagnou, K. *Org. Lett.* **2008**, *10*, 4533.

[9] Liegault, B.; Lapointe, D.; Caron, L.; Vlassova, A.; Fagnou, K. *J. Org. Chem.* **2009**, *74*, 1826.

[10] Liegault, B.; Petrov, I.; Gorelsky, S.; Fagnou, K. *J. Org. Chem.* **2010**, *75*, 1047.

[11] Lafrance, M.; Rowley, C.; Woo, T.; Fagnou, K. *J. Am. Chem. Soc.* **2006**, *128*, 8754.

[12] Perdew, J.; Burke, K.; Ernzerhof, M. *Phys. Rev. Lett.* **1996**, *77*, 3865.

[13] Perdew, J.; Burke, K.; Ernzerhof, M. *Phys. Rev. Lett.* **1997**, *78*, 1396.

[14] Andrae, D.; Haubermann, U.; Dolg, M.; Stoll, H.; Preub, H. *Theor. Chim. Acta* **1990**, *77*, 123.

[15] Ehlers, A.; Bohme, M.; Dapprich, S.; Gobbi, A.; Hollwarth, A.; Jonas, V.; Kohler, K.; Stegmann, F.; Veldkamp, A.; Frenking, G. *Chem. Phys. Lett.* **1993**, *208*, 111.

[16] Grimme, S.; Antony, J.; Ehrlich, S.; Krieg, H. *J. Chem. Phys.* **2010**, *132*, 1456.

[17] Grimme, S.; Ehrlich, S.; Goerigk, L. *J. Comput. Chem.* **2011**, *32*, 1456.

[18] Neese, F. *Comput. Mol. Sci.* **2012**, *2*, 73.

[19] Klamt, A. *Comput. Mol. Sci.* **2009**, *1*, 699.

[20] Perutz, R. *unpublished results*

[21] Gorelsky, S.; Lapointe, D.; Fagnou, K. *J. Org. Chem.* **2012**, *77*, 658.

[22] Boutalda, Y.; Davies, D. L.; Macgregor, S.; Poblador-Bahamonde, A. *Dalt. Trans.* **2009**, 5587.

[23] Derat, E.; Maestri, G. *WIREs Comp. Mol. Sc. - doi: 10.1002/wcms.1137* **2013**,

[24] Groom, C.; Bruno, I.; Lightfott, M.; Ward, S. *Acta Cryst.* **2016**, *B72*, 171.

Part II

MODEL SYSTEMS

Chapter 5

Oxidative Addition

5.1 Synopsis

The oxidative addition of an aryl halide, or aryl triflate, to a palladium metal is in general the first step in the catalytic cycle. This process involves the cleavage of C-X bond, the formation of the Pd-X and Pd-aryl bonds, followed by the increase of oxidation state of the palladium from 0 to $+2$.[1] This step, if irreversible, can have a crucial impact in terms of selectivity of the reaction. A detailed understanding of the corresponding mechanism is crucial for the improvement of the catalytic performance. In this chapter we carried out a computational analysis on the oxidative addition of phenyl bromide (PhBr) to L_2Pd complexes with different ligands (L = tertiary phosphines (PR_3) or N-heterocyclic carbenes (NHC). Our goal was to investigate how the energetic barriers of the process ($\Delta E^{\ddagger}$) were influenced by the different electronic properties of each ligand. Such electronic effects were studied by applying the innovative CD-NOCV (*Charge Displacement by Natural Orbitals for Chemical Valence*) analysis on the L-Pd bond. The CD-NOCV method provides a description of a chemical bond in terms of charge transfer between two chemical fragments in different symmetries (σ-donation and π-backdonation). In particular we were interested to investigate how such bond components change going from the L_2Pd catalyst to the $[LPd(PhBr]^{\ddagger}$ transition state and how they influence the energetic barriers. Furthermore we correlated the bond components also with the alteration of L-Pd and C-Br bond distances along the path. In addition, in order to understand how the Pd–PhBr interaction is influenced by the ligand effect in the process, we carried out an NBO (Natural Bond Orbitals) analysis on such bond, in particular by using the perturbative analysis, which provides a description of the chemical interaction in a donor-acceptor orbitals point of view .

5.2 Computational methodolgy

As already mentioned in Chapter 2, the *Charge Displacement via Natural Orbitals for Chemical Valence* (CD-NOCV) analysis is based on the so called Charge-Displacement (CD) function[2]

$$\Delta q(z) = \int_{-\infty}^{z} dz^{'} \int_{-\infty}^{+\infty} \int_{-\infty}^{+\infty} \Delta\rho(x, y, z^{'})dxdy \tag{5.1}$$

defined as a progressive partial integration along a suitable z axis of the difference $\Delta\rho$(x,y,z$^{'}$) between the electron density of the adduct and that of its non-interacting fragments placed in the same position that they occupy in the adduct. The z axis is usually chosen to be the bond axis between the fragments. Accordingly, the CD function at a given point z quantifies the exact amount of electron charge that, upon formation of the bond, is transferred from right to left (the direction of decreasing z) across a plane perpendicular to the bond axis through z. Negative values of the CD function identify charge flow in the opposite direction.

Recently, a general methodology to decompose the CD function in different symmetries components has been proposed.[3] Such scheme can still provide the desired identification of the donation and back-donation components of the interaction, using the properties of the *Natural Orbitals for Chemical Valence* (NOCVs) (see Chapter 2 for more details).

As an example of application of the CD-NOCV analysis of donation and back-donation, we chose one of the simplest case we investigated: the phosphorus-palladium bond in the (Me_3P)-Pd complex. The relevant fragments here are the phosphine PMe_3 and the palladium atom, and the integration (z) axis is the one joining the phosphorus and palladium atoms. We label the NOCV orbital pairs, and the associated $\Delta\rho^{'}$ components, by an integer k=1,2,... in order of decreasing eigenvalue. In the case of (Me_3P)-Pd complex, only the first 5 $\Delta\rho^{'}$ components have $CT_k \geq 0.001$.

The three main charge rearrangements occurring upon the formation of the Pd-P bond are shown in figure 5.1: a (largely dominating) donation component ($\Delta{\rho_1}^{'}$) and two smaller components of back-donation ($\Delta{\rho_2}^{'}$ and $\Delta{\rho_3}^{'}$).

Visual inspection of the first three $\Delta\rho^{'}$ isodensity surfaces shown in Figure 5.1 indicates that (i) $\Delta{\rho_1}^{'}$ correlates to the σ donation from the phosphorus lone-pair to palladium d_{z^2} orbital (note that blue surface identifies charge accumulation on the palladium) (ii) $\Delta{\rho_2}^{'}$ correlates to π back-donation from palladium to the out-of-plane σ^* antibonding orbitals of the phosphine; (iii) $\Delta{\rho_3}^{'}$ correlates to donation from palladium to the in plane σ^* orbitals of the phosphine.

In Figure 5.2 are shown the CD functions associated with the first three components $\Delta{\rho_k}^{'}$. Note that, since the system presented is a symmetric one (C_{3v} symmetry), the components relative to the back-donation ($\Delta{\rho_2}^{'}$ and $\Delta{\rho_3}^{'}$), are degenerate and, therefore, the CD curves associated to these two components are identical (Figure 5.2).

While the Δ(q) curves accurately depict charge displacement over the whole molecular region, one can obtain a reasonable measure of donation, back-donation, and net charge transfer (CT_{don}, CT_{back} and CT_{tot},respectively) between the fragments by taking the value of the corresponding CD function at a plausible inter-fragment boundary along z. Our standard choice is the point z where the densities of each separated fragment do intersect. (see Figure 5.3).

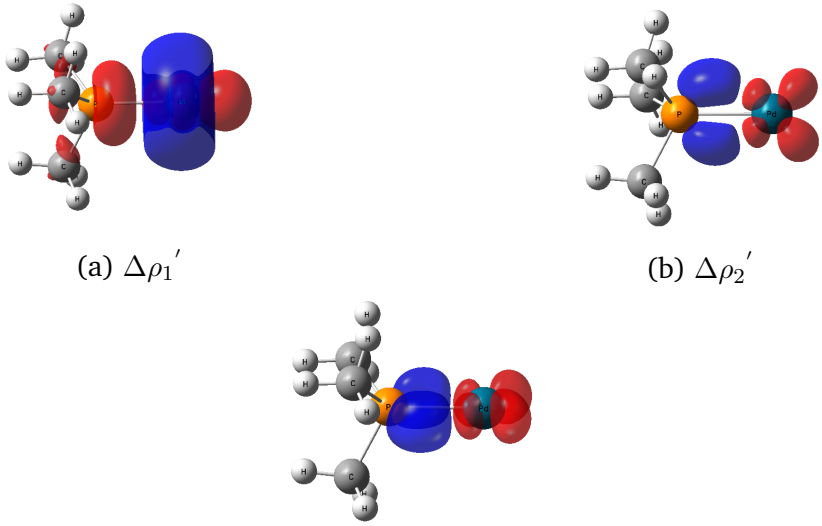

(a) $\Delta\rho_1{}'$ (b) $\Delta\rho_2{}'$

(c) $\Delta\rho_3{}'$

Figure 5.1: *Isodensity surfaces ($\pm$0.002 e/a.u.^{3}) for $\Delta\rho_1{}'$, $\Delta\rho_2{}'$ and $\Delta\rho_3{}'$ superimposed to the molecular structure of the (Me_3P)-Pd complex. Red surfaces (negative values) identify charge depletion areas, and blue surfaces (positive values) identify charge accumulation areas.*

Geometry optimizations and frequencies analysis have been performed with the Gaussian 09 package, at DFT level, using the hybrid Perdew, Burke and Ernzerhof exchange correlation functional (PBE0).[4,5] The palladium atom was represented by the relativistic effective core potential (RECP) from the Stuttgart group and the associated basis sets,[6] augmented by an f polarization function.[7] All the other atoms (C,H,P,O,N) were represented by a SVP basis set. For each geometry (TS and minima) a single point calculation has been carried out with the Orca package,[8] using an effective core potential for palladium, and a QZVPP basis set for the other atoms. Influence of the dispersion forces was considered by adding to the SCF energy the D3(BJ) corrections as described by Grimme.[9,10] All of the energies reported in the present work are obtained by summing SCF energies, Gibbs correction at 298 K and the D3(BJ) dispersion correction.

NBO analysis was performed with the Gaussian 09 package, using the Perdew, Burke and Ernzerhof exchange correlation functional (PBE0).[4,5] The palladium atom was represented by the relativistic effective core potential (RECP) from the Stuttgart group and the associated basis sets,[6] augmented by an f polarization function.[7] All the others atoms (C,H,P,O,N) were represented by a TZVP basis set.

The CD-NOCV analysis was performed by means of Density Functional Theory (DFT) with the Amsterdam Density Functional (ADF) package[11,12] using the Perdew, Burke and Ernzerhof (PBE0) exchange-correlation functional and all electron triple-ζ basis set with two polarization functions (TZ2P) for all atoms. Relativistic effect were included by means of the zeroth-order regular approximation (ZORA) Hamiltonian.[13–15] The NOCV orbitals and ETS-NOCV analysis have been worked

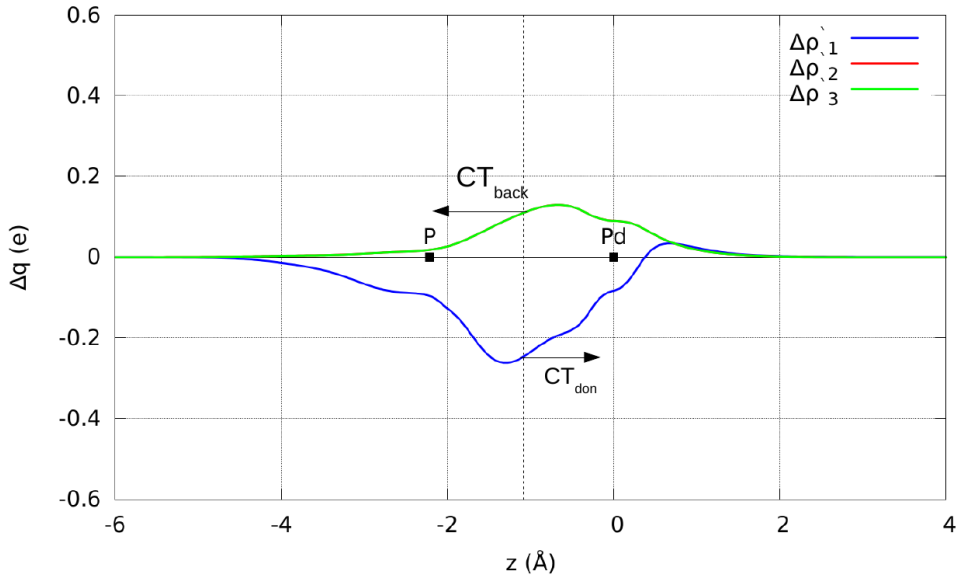

Figure 5.2: *CD functions associated with the first three $\Delta\rho_k{}'$ components for (Me)$_3$P-Pd complex. The blue line represent the donation L→Pd, while the green and red curves (degenerate) represent the back-donation L←Pd. The black dots represent the position of the atoms on the integration axis (z in this case), while the vertical dashed line represents the z value in which the charge transfers are taken (the so called isoboundary).*

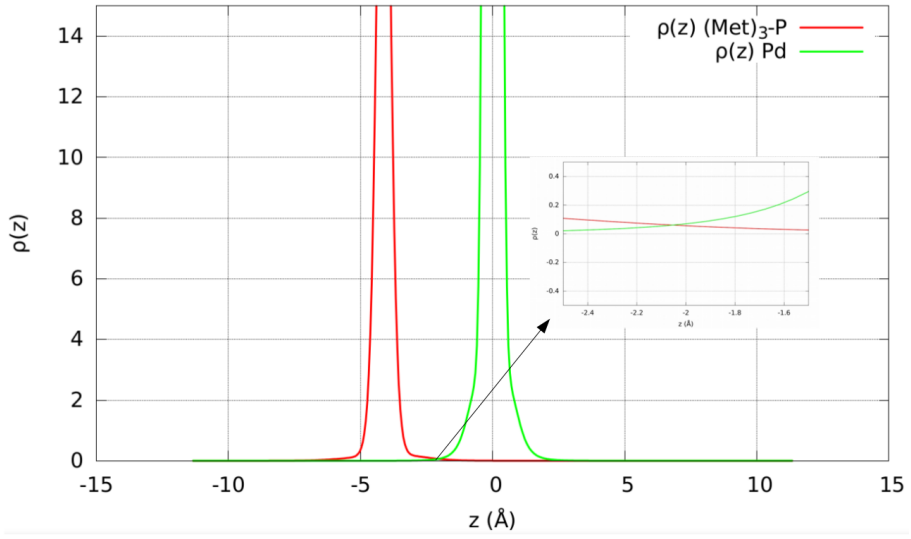

Figure 5.3: *Density functions $\rho(z)$ of the (Me$_3$)P and Pd fragments, non interacting but placed at the same position they assume in the (Me$_3$)-Pd complex, plotted along z. The z point in which the two functions intersect is (our standard choice) the inter-fragment boundary in which the measure of donation and back-donation (CT_{don}, CT_{back}) are taken.*

out using the keyword ETSLOWDIN in the ADF program suite.

5.3 Pathways Manifold

Once the catalyst L_2Pd is activated, several pathways for L_2Pd + PhBr oxidative addition are possible (Figure 5.7). The *bisphosphine pathway* (P2) involves the direct coordination of PhBr on palladium to form the adduct **AD2**. The cleavage of the C-Br bond is effective through the transition state (TS) [$\mathbf{C}^{\ddagger}$], (see Figure 5.4) leading to the tetra-coordinated isomer **L2C** with Pd and Br cis. **L2C** can isomerize to the more stable trans isomer **L2T**. These *cis* and *trans* isomers have been observed crystallographically with PPh_3.[16,17]

A second possible pathway, the *Dissociative Pathway (P1)*, involves initial loss of one ligand to yield LPd, followed by the coordination of PhBr to form adduct **AD1**. Then the oxidative addition can take place through TS [$\mathbf{A}^{\ddagger}$] (L and Br in trans), or through TS [$\mathbf{B}^{\ddagger}$] (L and phenyl in trans, see Figure 5.5). These pathways yield three different T-shaped isomers [LPd(Ph)(Br)] (**LB**,**L0** and **LA**). The isomer **LB** is directly connected to TS [$\mathbf{B}^{\ddagger}$] while **LA** is connected to TS [$\mathbf{A}^{\ddagger}$]. The third isomer, **L0**, can only be obtained from an isomerization of **LA** and **LB**.

Furthermore, other possible pathways, involving loss of one ligand from the adduct **AD2** or anionic specie L_2PdX^- have been proposed,[18–20] but cannot be characterized in the gas-phase simulation.[1]

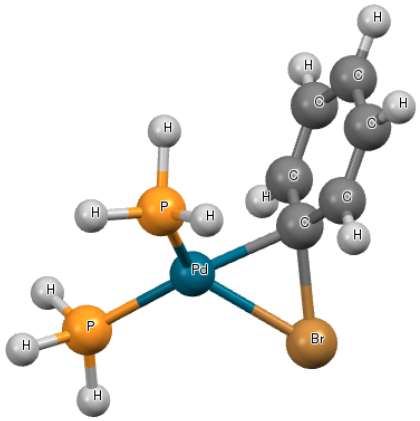

Figure 5.4: *Structure of transition state [C]‡ , with PH_3 as ligand.*

The energetic preferred pathway, between *P1* and *P2*, strongly depends on the size and the electron donor power of the ligand.

5.4 Energetic aspects

In Figure 5.7 is reported the energetic schematic representation of the P1 and P2 pathways (red and blue dashed lines for dissociative and associative pathways

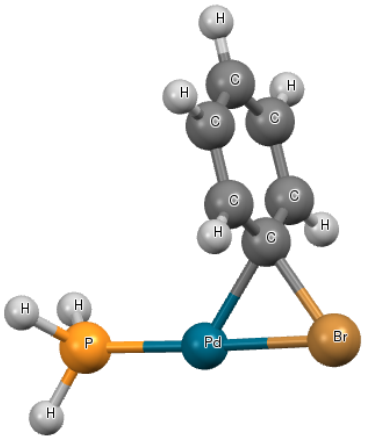

(a) TS [A]‡

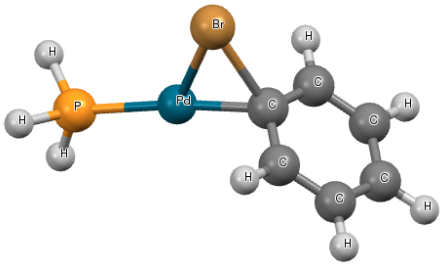

(b) TS [B]‡

Figure 5.5: *Structures of the transition states, with PH_3 as ligand, for the dissociative pathway of the oxidative addition.*

respectively) we analyzed for all the chosen ligands (Figure 5.6).

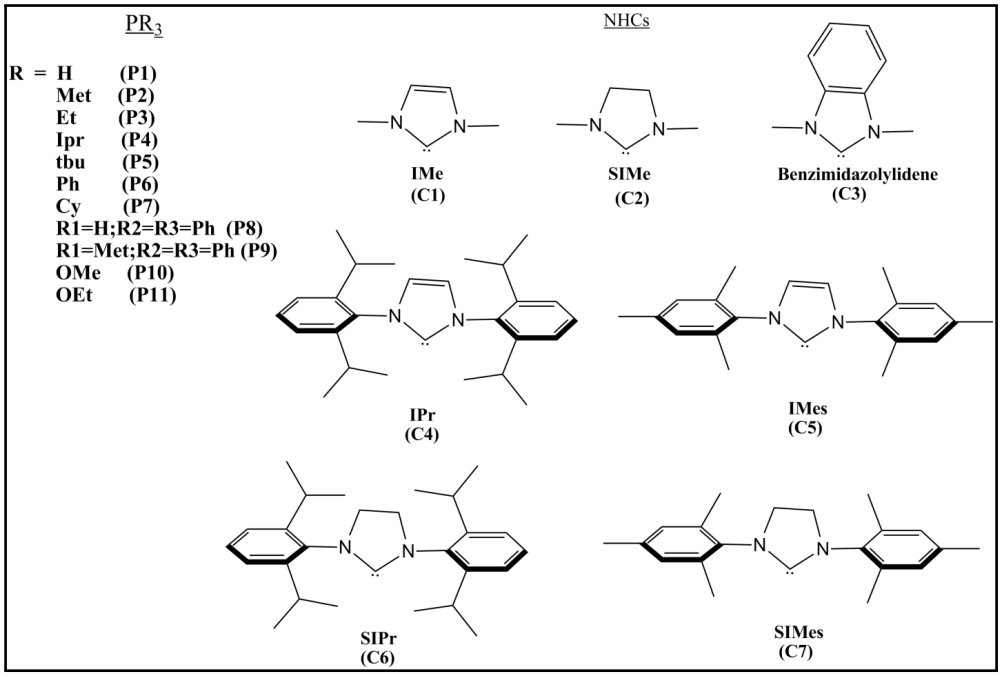

Figure 5.6: *List and abbreviations for the ligands (L) considered in the present work.*

In theory, when PhBr coordinates to L_nPd to form [(LPd-PhBr)], there are several possible isomers for the resulting η^2 complexes, depending on which sp^2-carbons in the aromatic ring are involved in the coordination. Our calculations suggest that the *ortho*-interaction (AD1 and AD2 adducts, Figure 5.8) are energetically preferred for all the ligands.

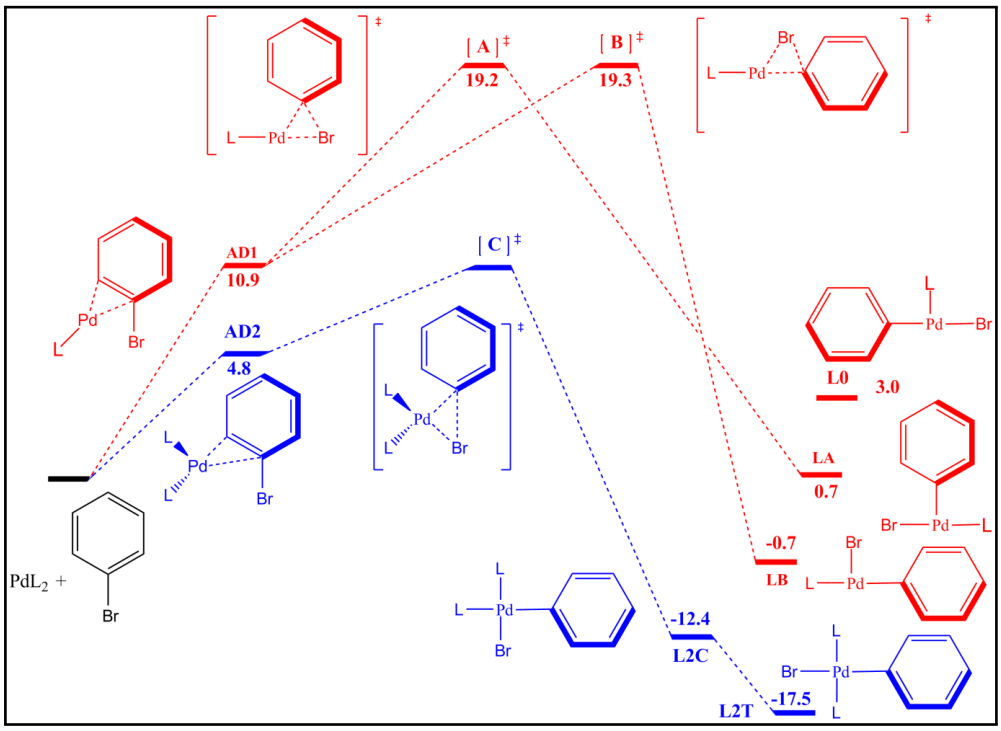

Figure 5.7: *Schematic representation of the associative (blue dashed line) and dissociative (red dashed line) pathways for the oxidative addition of PhBr on L_nPd ($L = PH_3$) catalysts ($n=1,2$).*

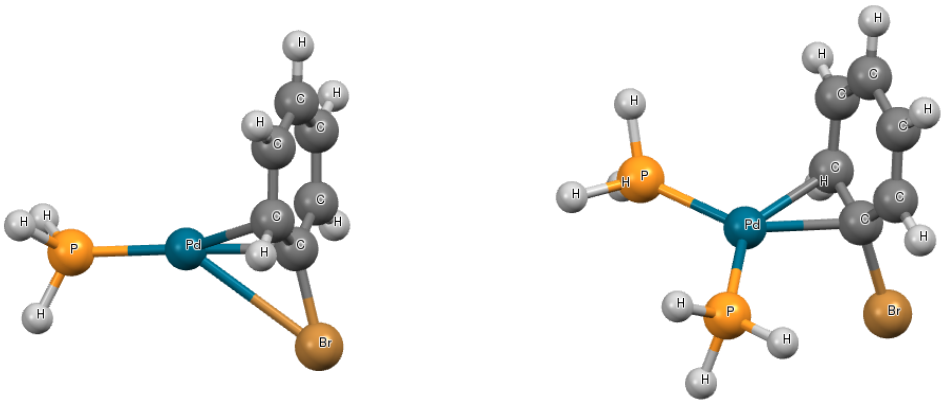

(a) AD1

(b) AD2

Figure 5.8: *Structures of the adducts AD1 and AD2, with PH_3 as ligand, relative respectively to the dissociative and associative pathways of the oxidative addition.*

5.4.1 Associative Pathway

We start by considering the associative mechanism, which involves the direct coordination of PhBr to L_2Pd. In Table 5.1 are reported the calculated relative Gibbs free energies for the different species involved in such pathway. The analysis in-

volves different ligands, in particular tertiary phosphines and NHCs carbenes (Figure 7.3).

Associative Pathway (L_2Pd)				
Ligand(PR_3)	**AD2**	**[C]‡**	**L2C**	**L2T**
P1	4.8 (10.9)	15.9(22.0)	-12.4(-6.1)	-17.5(-11.3)
P2	4.9(14.2)	15.0(24.1)	-21.8(-11.7)	-33.7(-23.3)
P3	3.4(14.4)	14.6(25.1)	-19.0(-6.9)	-31.9(-20.2)
P4	13.5(28.2)	20.1(33.6)	-8.4(7.3)	-21.9(-6.8)
P5	-	-	-	17.3(32.4)
P6	-0.1(17.5)	8.8(26.4)	-18.1(3.0)	-24.4(6.6)
P7	9.8(28.8)	21.8(41.1)	3.1(22.5)	-20.1(-0.7)
P8	1.6(15.5)	11.4(24.0)	-21.2(-8.6)	-26.2(-13.8)
P9	2.3(17.4)	10.7(24.9)	-21.1(-5.1)	-28.5(-13.5)
P10	16.6(26.5)	29.9(39.4)	-4.3(6.5)	-6.3(4.3)
P11	0.4(13.1)	14.7(27.6)	-20.7(-6.9)	-25.9(-13.1)
Ligand(NHCs)	**AD2**	**[C]‡**	**L2C**	**L2T**
C1	-	-	-26.8(-16.8)	-35.8(-26.0)
C2	-	-	-28.1(-17.9)	-37.9(-27.9)
C3	-	-	-24.1(13.7)	-34.7(-24.5)
C4	-	-	-	-
C5	-	-	-	-28.6(-9.8)
C6	-	-	-	-
C7	-	-	-	-26.7(-7.0)

Table 5.1: *Calculated relative Gibbs free energies (ΔG) in kcal mol^{-1}for different species involved in the associative mechanism for the oxidative addition of PhBr to L_2Pd. The Gibbs energy correction was carried out at 298K. The energetic values are calculated with respect to PdL_2 + PhBr. In parenthesis are shown the same values calculated without including the dispersion correction to the energy.*

- **PR_3 Ligands**

  The data collected in Table 5.1 show that for all the PR_3 ligands but $P(tbu)_3$, all the points could be located on the potential energy surface. In the case of $P(tbu)_3$, the steric bulk of the ligand prevents the optimization of TS [C]‡, and only the trans isomer L2C could be located. Compared to the other PR_3 cases, this isomer is thermodynamically significantly destabilized.

  For all the phosphine series, the formation of the adduct AD2 is an endoergonic process (or isoergonic in the case of PPh_3 and $P(OEt)_3$). The lowest ΔG values for the aromatic ring coordination are associated to phosphine bearing at least one aromatic ring. Apart from the two bulky ligands P4 and P7 (and surprisingly P10) the reactive energy for coordination are all below ΔG = 5

kcal mol^{-1}, thus showing that adding an extra ligand to PdL_2 is not costly energetically. This situation is drastically different when the dispersion corrections are not included. The coordination energy is then ca 10 to 20 kcal mol^{-1}more endoergonic. The least sterically hindered ligand PH_3 does show the lowest increase (6.1), whereas the bulky phosphines P4 and P7 are associated to significant destabilization of the adduct (14.7 and 19 kcal mol^{-1}, respectively). Upon formation of an adduct between two fragments, there is action of a large number of pairwise interactions between non-bonded atoms with mutual distance typical of Van der Waals attraction. Inclusion of the dispersion corrections according to the scheme of Grimme introduce many stabilizing interactions. The bigger the two fragments, the more important these corrections will be, leading to significantly different values for reacting energies computed without dispersion corrections.

From the adducts AD2, the actual C-Br bond cleavage through $[C]^{\ddagger}$ transition state is associated to activation barriers ranging from $\Delta G^{\ddagger}$ = 6.6 kcal mol^{-1}(P4) to $\Delta G^{\ddagger}$ = 14.3 kcal mol^{-1}(P11). The phosphine ligands bearing aromatic rings have smallest activation barriers then the aliphatic ones. The phosphite ligands exhibit the highest barriers for the series. The values of these activation barriers are not significantly affected when the dispersion corrections are not included. Relative to PdL_2 + PhBr, the high energy of $[C]^{\ddagger}$ when no dispersion corrections are considered is essentially due to the destabilization of adduct AD2 upon bringing together two molecules without considering the many stabilizing interactions between non-bonded atoms.

The transformation from Pd(0) in AD2 to Pd(II) in L2C is an exoergonic process with reaction energies ranging from ΔG = -17.8 kcal mol^{-1}(P1) to ΔG = -26.7 kcal mol^{-1}(P2). In the case of P7, the reaction energy is less exoergonic (ΔG = -6.7 kcal mol^{-1}) because of the steric bulk in L2C with two *cis*-PCy_3 ligands. As expected the reaction energies are not significantly altered when no dispersion corrections are considered with values ranging from -14.5 kcal mol^{-1}(P6) to -25.9 kcal mol^{-1}(P2).

The product of the C-Br bond cleavage by PdL_2 has the two phosphine ligands mutually *cis*. However it is shown that the *trans* isomer L2T is energetically preferred as illustrated in Table 5.1. There are clearly two distinct classes of ligands: for the aliphatic phosphines (P2, P4, P7) L2T is ca 12-13 kcal mol^{-1}more stable than L2C, whereas for the other cases the stabilization is ca 5-7 kcal mol^{-1}. The aliphatic phosphines favor energetically the path where the two phosphines ligands are mutually *trans*.

The overall pathway for oxidative addition of PhBr to PdL_2 (L = phosphines) can be described qualitatively as a one-step forming the *trans* isomer L2T through the transition state $[C]^{\ddagger}$. From the values in Table 5.1 the most active system is with PPh_3. The substitution of one phenyl group by either H (P8) or Me (P5) increases the activation barrier by ca 2-3 kcal mol^{-1}. An increase of 2 kcal mol^{-1} for an activation barrier corresponds to a reaction

that is ca 30 times slower.

The activation barriers are even larger for the aliphatic phosphines with values in the range 14.6 - 21.8 kcal mol^{-1}. For the small phosphines P1-P3 the behavior in reactivity is PEt_3 > PMe_3 > PH_3 following the donating phosphines. The situation for P4 and P7 is complicated by the influence of the steric bulky, resulting in significantly higher activation barrier. The difference between the activation barrier for PCy_3 (21.8 kcal mol^{-1}) and PPh_3 (8.8 kcal mol^{-1}) of $\Delta\Delta G^{\ddagger}$ = 21 kcal mol^{-1}leads to a difference in the rates of 9 orders of magnitude. This clearly shows the large impact that ligands have on the catalytic activity.

- **NHC Ligands**

  In the case of NHC ligands, the steric bulk prevented the characterization of the reaction pathway with PdL_2. Only for the smallest NHC (C1-C3) could both the *cis* and *trans* oxidative addition products L2C and L2T be located.

  Similarly to the phosphines case, the *trans* isomer L2T is always more stable than the *cis* one by 10 kcal mol^{-1}. Interestingly, the overall reaction PdL_2 + PhBr $\rightarrow$ L2T significantly more exoergonic with the NHC ligands, in agreement with their strong donating power stabilizing the Pd(II) product.

5.4.2 Dissociative Pathway

The dissociative pathway initially involves the loss of a ligand from L_2Pd, followed by the coordination of PhBr to the resulting LPd species. In Table 5.2 are reported the calculated relative Gibbs free energies for the different species ,involved in such pathway, including all the ligands chosen.

- **PR_3 Ligands**

  The energy of the adduct AD1, where PhBr is η^2-coordinated to Pd, reflects the energetic associated to substitution of L by PhBr. The fact that all the values are positive in Table 5.2 indicates that PhBr is a weaker ligand to Pd than any phosphine. The reaction energies vary between ΔG = 15 kcal mol^{-1}and ΔG = 25 kcal mol^{-1}, with a slightly easier substitution for P1 (ΔG = 10.9 kcal mol^{-1}) and P3 (ΔG = 9.6 kcal mol^{-1}). Interestingly, the values of the reaction energy when no dispersion correction are included are slightly lower. The reaction energy lowering is important for bulky ligand P4 (-2 kcal mol^{-1}), P5 (-3.9 kcal mol^{-1}) and P7 (-3.2 kcal mol^{-1}). This is explained by the loss of many stabilizing interactions between the two ligands L in PdL_2 that are lost when L is substituted by PhBr. When dispersion corrections are considered this introduces an energy penalty that is absent in the calculations without dispersion.

  The transition states for C-Br bond cleavage has a distorted Y-shaped geometry with one atom X (X=Br, $[A]^{\ddagger}$; X=C, $[B]^{\ddagger}$, see Figure 5.5) pseudo-trans

to Pd. The two different TS are thus possible and both were located on the potential energy surface (except $[A]^{\ddagger}$ for $Ptbu_3$).

The actual C-Br bond cleavage is easier from AD1 than it is for AD2 when an extra ligand is present. The activation energies from AD1 to $[A]^{\ddagger}$ range from 6 kcal mol^{-1} to 9.1 kcal mol^{-1}. The lowering of the activation barriers is significant for the aliphatic phosphines with $\Delta G^{\ddagger}$ = 12 kcal mol^{-1} for PCy_3 from AD2, whereas it is only $\Delta G^{\ddagger}$ = 6 kcal $mol^{-1}$from AD1. Contrary to what was observed in the associative pathway, the aliphatic phosphines correspond to more active species for the C-Br bond cleavage in the dissociative pathway. The situation is similar for the TS $[B]^{\ddagger}$ where the aromatic ring is trans to Pd in the TS. The energy difference between $[A]^{\ddagger}$ and $[B]^{\ddagger}$ is relatively small (except for P3) but $[B]^{\ddagger}$ is sensibly more stable than $[A]^{\ddagger}$.

The formation of LA from AD1 through $[A]^{\ddagger}$ and the formation of LB from AD1 through $[B]^{\ddagger}$ are both exoergonic. Even through the two TS $[A]^{\ddagger}$ and $[B]^{\ddagger}$ are close in energy, the respective products LA and LB have significantly different stabilities. LB, with a phenyl group trans to L, is significantly (except for P1) less stable than LA by 10-15 kcal mol^{-1}. The former is thus able to isomerize to the latter through the isomer L0 with the phenyl group in *trans* to Br (Figure **??**). Ideally, L0 should have an energy intermediate between that of LB and LA to function as an intermediate in the isomerization process. But for almost all the phosphine ligands L0 is the most stable tri-coordinated Pd(II) oxidative addition product.

Here again there is a trend among the aliphatic phosphines favoring L0, whereas PPh_3 tends to favor LA. Coordination of L to L0 will form L2T, the most stable Pd(II) complex resulting from PhBr oxidative addition. Overall the dissociative pathway starts by the substitution of L by PhBr to form the adduct AD1. The less efficient bonding of PhBr to Pd compared to PR_3 shifts the energy of the system up. From this adduct the actual C-Br bond cleavage is easy, through either $[A]^{\ddagger}$ or $[B]^{\ddagger}$. The isomer with L in trans to the vacant site is generally the most stable isomer. A comparison between the associative and dissociative pathways for $L{=}P(Ipr)_3$ is shown in Figure 5.9. The comparison between the two different pathways is sensibly alterated depending on the dispersion corrections. When such corrections are not included in the calculation of the energetic paths, the dissociative pathway is more favored than the associative one , with energetic barriers of $\Delta G^{\ddagger}$ = 23.0 kcal $mol^{-1}$and $\Delta G^{\ddagger}$ = 33.6 kcal mol^{-1}. Conversely, including the dispersion corrections, the associative pathway becomes more favored ($\Delta G^{\ddagger}$ = 20.1 kcal mol^{-1}) than the dissociative one ($\Delta G^{\ddagger}$ = 25.0 kcal mol^{-1}). The disperion corrections influence much more the associative pathway, in terms of activation barrier and relative stability of L2T, while the dissociative pathway remains generally unalterated.

- **NHC Ligands**

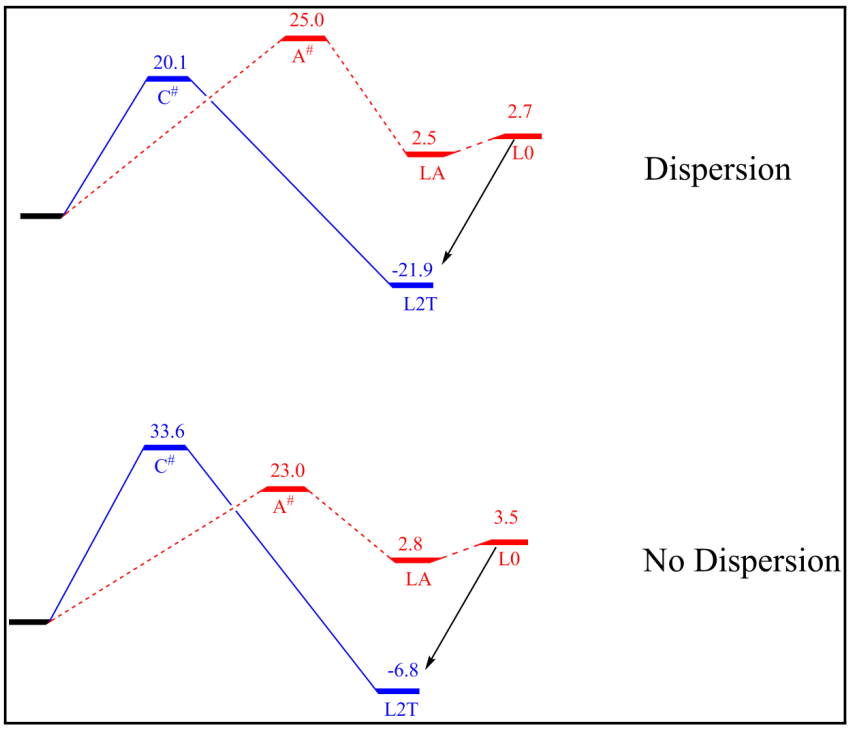

Figure 5.9: *Comparison between the associative (blue solid line) and dissociative (red dashed line) pathways for L= P(Ipr)$_3$ including and not including the dispersion corrections. The energetic values are reported in kcal mol^{-1}.*

For the NHC ligands, because of the strong donating power of the carbenes, the substitution reaction forming AD1 is more endoergonic than in the case of the phosphines. This energy of reaction is also influenced by the inclusion or not of the dispersion correction. The latter destabilize AD1 relative to PdL_2 because many pairwise interactions are lost. From AD1, owing to the donating power of the NHCs, the actual C-Br bond cleavage is very easy with activation barriers $\Delta G^{\ddagger}$ essentially between 5 and 7 kcal mol^{-1}. However the energy penalty introduced by the substitution reaction sets the energy of $\Delta G^{\ddagger}$ too high for significant catalytic activity to be observed at RT. The result without dispersion correction does not modify drastically the pathway except for the very bulky ligands SIpr (C6) and Ipr (C4). For Ipr the calculation without dispersion indicate an easy transformation with a significant exothermicity.

There is no comparison possible between the associative and dissociative pathway for the NHC series.

Dissociative Pathway (LPd)						
Ligand(PR_3)	**AD1**	**[A]‡**	**[B]‡**	**LA**	**LB**	**L0**
P1	10.9(13.1)	19.2(21.4)	19.3(21.1)	0.7(3.3)	-0.7(2.0)	3.0(5.3)
P2	17.2(18.2)	24.3(25.6)	24.3(24.9)	-0.2(2.3)	15.6(16.7)	-2.1(0.7)
P3	9.6(9.0)	16.0(15.8)	12.0(11.3)	-8.9(-7.5)	3.9(3.7)	-11.5(-9.9)
P4	16.3(14.3)	25.0(23.0)	27.7(25.2)	2.9(2.8)	18.1(15.9)	2.7(3.5)
P5	22.6(18.7)	-	28.3(23.8)	8.7(6.8)	18.5(14.6)	-
P6	15.8(14.5)	24.9(24.7)	23.5(21.8)	0.4(2.1)	15.9(14.4)	1.8(4.2)
P7	28.3(25.1)	34.3(32.5)	33.5(29.6)	13.3(13.0)	26.9(23.6)	8.1(9.6)
P8	16.1(16.3)	22.4(24.0)	23.5(23.3)	1.5(4.7)	16.2(16.3)	-0.9(0.6)
P9	17.6(17.1)	23.9(23.7)	23.7(22.9)	-0.2(1.6)	16.1(15.6)	0.0(2.4)
P10	24.5(24.8)	32.4(33.5)	29.3(29.2)	11.4(13.2)	22.7(22.9)	6.5(8.1)
P11	16.8(17.1)	25.8(27.5)	25.1(24.9)	4.1(6.8)	17.7(18.0)	0.8(2.7)
Ligand(NHCs)	**AD1**	**[A]‡**	**[B]‡**	**LA**	**LB**	**L0**
C1	21.1(22.2)	-	27.4(28.3)	2.2(3.1)	17.5(18.4)	2.7(3.7)
C2	20.8(21.7)	-	27.1(27.6)	1.0(3.2)	26.7(27.4)	0.0(2.0)
C3	23.1(24.9)	-	29.3(29.8)	4.6(6.7)	20.0(20.6)	4.9(7.0)
C4	27.4(14.9)	-	33.2(19.8)	9.3(-0.8)	22.5(10.2)	-
C5	27.4(19.2)	-	32.5(24.0)	5.9(1.1)	22.8(14.6)	-
C6	21.4(7.7)	-	26.2(11.5)	4.0(-6.9)	18.4(5.3)	-
C7	30.9(22.7)	-	35.6(26.8)	9.9(5.1)	25.6(17.1)	-

Table 5.2: *Calculated relative Gibbs free energies (ΔG) in kcal $mol^{-1}$for different species involved in the dissociative mechanism for the oxidative addition of PhBr to LPd. The Gibbs energy correction was carried out at 298K. The energetic values are calculated with respect to PdL_2 + PhBr. In the parenthesis are shown the same values calculated without including the dispersion correction to the energy.*

5.5 CD-NOCV and NBO Analysis

In this section, we investigate the electronic effect of seven different ligands (Figure 5.10), on the oxidative addition of phenyl-bromide (PhBr) to PdL_2. Despite different pathways for such process are possible we describe only the dissociative one, since it allows to identify a specific axis between the ligand and the palladium along the reaction path.

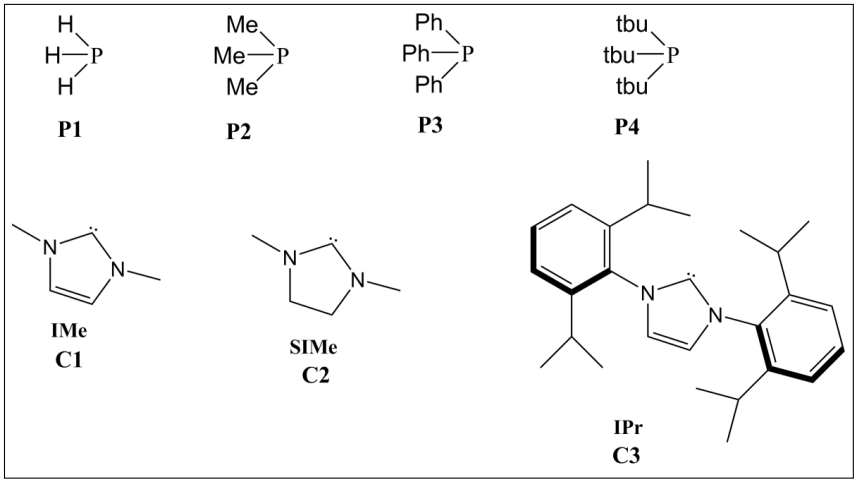

Figure 5.10: *List and abbreviations for the ligands (L) considered for the CD-NOCV analysis.*

Our goal was to investigate how the energetic barriers of the process ($\Delta E^{\ddagger}$) were influenced by the electronic properties of each ligand. Such electronic effects were studied by applying the innovative CD-NOCV (*Charge Displacement by Natural Orbitals for Chemical Valence*) analysis on the L-Pd bond, which provides a description of a chemical bond in terms of charge transfer between two chemical fragments in different symmetries (σ-donation and π-backdonation). In particular we were interested in examinating how such bond components change upon going from L_2Pd to the [LPd(PhBr)]‡ transition state and how they influence the energetic barriers. Furthermore we correlated the bond components also with the alteration of L-Pd and C-Br bond distances along the path. In addition, in order to understand how the Pd–PhBr interaction is influenced by the ligand effect in the process, we carried out an NBO (*Natural Bond Orbitals*) analysis on such bond, in particular by using the perturbative analysis, which provides a description of the chemical interaction in a donor-acceptor point of view. In particular we investigated the relations between $\Delta E^{\ddagger}$ values and Δr_{L-Pd} and the charge displacements variations, in σ and π symmetry between L and Pd, in the transformation from L_2Pd to the transition state [L-Pd(PhBr)]‡.

In order to compare the properties of the various ligands, we defined relative quantities, ω^{σ}, ω^{π}, K_{L-Pd} and K_{C-Br} as shown in the equation 5.2 - 5.5. These quantities express the variation of some value from PdL_2 to the TS relative to the value in PdL_2. For the C-Br bond distance the reference is the C-Br bond distance

in free PhBr ($d^{(0)}$(C-Br) = 1.889 Å).

$$\omega^{\sigma} = \frac{CT_{\sigma}^{(\mathrm{TS})} - CT_{\sigma}^{(0)}}{CT_{\sigma}^{(0)}} = \frac{\Delta CT_{\sigma}}{CT_{\sigma}^{(0)}} \tag{5.2}$$

$$\omega^{\pi} = \frac{CT_{\pi}^{(\mathrm{TS})} - CT_{\pi}^{(0)}}{CT_{\pi}^{(0)}} = \frac{\Delta CT_{\pi}}{CT_{\pi}^{(0)}} \tag{5.3}$$

$$K_{L-Pd} = \frac{d_{\text{L-Pd}}^{(\mathrm{TS})} - d_{\text{L-Pd}}^{(0)}}{d_{\text{L-Pd}}^{(0)}} = \frac{\Delta d_{L-Pd}}{d_{\text{L-Pd}}^{(0)}} \tag{5.4}$$

$$K_{C-Br} = \frac{d_{\text{C-Br}}^{(\mathrm{TS})} - d_{\text{C-Br}}^{(0)}}{d_{\text{C-Br}}^{(0)}} = \frac{\Delta d_{C-Br}}{d_{\text{C-Br}}^{(0)}} \tag{5.5}$$

$CT_{\sigma}^{(\mathrm{TS})}$, $CT_{\pi}^{(\mathrm{TS})}$, $d_{\text{L-Pd}}^{(\mathrm{TS})}$ and $d_{\text{C-Br}}^{(\mathrm{TS})}$ are the charge transfer between the ligand and the palladium, in the two different symmetries, and the L-Pd and C-Br bond distances calculated for [L-Pd(PhBr)]‡. $CT_{\sigma}^{(0)}$, and $CT_{\pi}^{(0)}$ are calculated for L_2Pd. $d_{\text{C-Br}}^{(0)}$ is the carbon-bromide bond distance in the free phenyl-bromide (1.889 Å). The magnitudes ω^{σ}, ω^{π}, K_{L-Pd} and K_{C-Br} represent, respectively, the variations in percentage in the process of oxidative addition of the σ-donation, the π backdonation, the ligand-palladium and carbon-bromide bond distances. Positive values of these magnitudes suggest their increase in the process. In other words, going from L_2Pd to [LPd(PhBr)]‡ the donor and acceptor abilities of the ligand grow, as well as the distances between the ligand and the palladium or carbon and bromide. Similarly, negative values, suggest their decrease.

In Table (5.3) are shown the activation energies ($\Delta E^{\ddagger}$), the ligand-Palladium bond distances (in Angstrom) and charge transfers results (e) obtained from the CD-NOCV analysis relative to either L_2Pd or [L-Pd(PhBr)]‡.

In addition, in Table 5.4 are reported the values of ω^{σ}, ω^{π}, K_{L-Pd} and K_{C-Br}.

As Table 5.3 shows, the values of the activation energies ($\Delta E^{\ddagger}$) are quite differ-

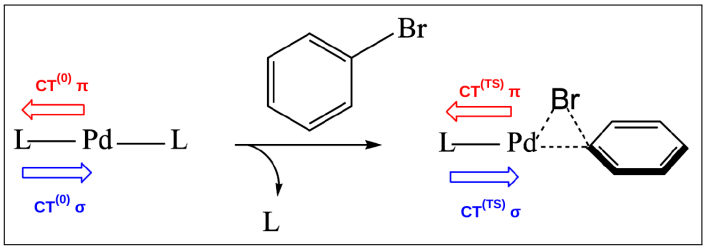

Figure 5.11: *Scheme of the oxidative addition (dissociative pathway) reaction and relative DCD (Dewar-Chatt-Duncanson) components ligand-palladium analyzed in the present work.*

ent along the ligand series: from 20.5 kcal $mol^{-1}$for L = P1 to 36.0 kcal $mol^{-1}$for L = C3. In particular the tertiary phosphines favor the process, showing lower values of $\Delta E^{\ddagger}$ with respect to NHCs.

L_2Pd complexes

The complexes bearing tertiary phosphines as ligands have longer ligand- palladium bond distances. In particular P4 [L=$P(tbu)_3$] shows the longest distance (2.316 Å), while the two carbenes C1 and C2 show the shortest distances (2.018 Å). This suggests that carbenes form stronger bonds with the palladium. Analyzing the DCD bond components in Table 5.3 for L_2Pd, the π-backdonation L $\leftarrow$ Pd is the more tunable component of the bond. Indeed, the values of $CT_{\pi}^{(0)}$ along the ligand series are quite different among them: from 0.199 e for P4 system, to 0.225 e for P1. As expected, $P(tbu)_3$ (P4) has the lower π- acceptor capacity among the phosphines. Indeed it is the only system that has a $CT_{net}^{(0)}$ negative (total charge transfer from palladium to the ligand). P1 shows the highest values of electrons transferred in π symmetry (0.225 e). NHCs ligands show a lower donor power along the series (0.161 e for C3 ligand), but the π-acceptor ability is comparable with that of the phosphines. All the ligands (except for P4) have a positive net charge transfer(the sum of $CT_{\sigma}^{(TS)}$ and $CT_{\pi}^{(TS)}$): this suggests that, in the L_2Pd systems, the ligand π-acceptor ability is stronger that their σ-donor ability.

[LPd(PhBr)]‡ TS

The [LPd(PhBr)]‡ systems are the transition states arising from the coordination of phenyl-bromide (PhBr) to the palladium centre, upon the loss of a ligand from L_2Pd, leading to the cleavage of the C-Br bond and the formation of Pd-C and Pd-Br bonds. We showed that two transition states are possible for the dissociative pathway of the oxidative addition, depending on the different direction of coordination of PhBr ([A]‡ and [B]‡). In this analysis we only consider the one with the phenyl in trans to the ligand ([B]‡, see Figure 6.6), since it is more accessible in energy. The coordination of PhBr alterates the L-Pd bond distances and, therefore, the bond components between them.

In [LPd(PhBr)]‡ the charge transfer $CT_{\sigma}^{(TS)}$ has a smaller range of variation, from -0.180 e (P1) to -0.210 e (P4), while $CT_{\pi}^{(TS)}$ shows a larger variation between the ligands from 0.128 e (C1) to 0.168 e (P1). In general, upon the exchange of L with PhBr the remaining L ligand increases its donor ability toward the palladium and lose its π-acceptor capacity. Between the two bond components, the π-backdonation is the more tunable one, since the variations of charge transfer in such symmetry is more remarkable.

The L-Pd bond distances increase in all the systems, and the K_{L-Pd} magnitude gives an indication about such alteration. Ligands with a remarkable steric hindrance (P4 and C3) show lower values of K_{L-Pd} (0.0203 and 0.0143 respectively). The

highest alteration of L-Pd bond is shown by P1 (K_{L-Pd} = 0.0252). As well as the L-Pd bond distances, also a variation in percentage of the bond components ($CT_{\sigma}^{(TS)}$ and $CT_{\pi}^{(TS)}$) can be calculated. Such bond components alterations are provided by ω^{σ} and ω^{π}. Positive values of these magnitudes suggest an increase of the relative bond components, as well as negative values suggest their decrease along the reaction path.

The bond component that show a remarkable variation in the process is σ-donation L $\rightarrow$ Pd. Indeed the ω^{σ} values range from -0.027 (P1) to 0.267 (C3). All the ligands (except P1) in the process increase their ability to donate charge to the Pd center, since the relative values of ω^{σ} are positive. In particular this effect is stronger for the NHCs ligands. Conversely, P1 loses its donor ability ($\omega^{\sigma} < 0$).

The ω^{π} values range from -0.250 (P1) to -0.380 (C3). All the values are negative and, therefore, all the ligands lose their capacity to accept charge from the Pd center in the TS.

Once again this effect is stronger for the NHC ligands. It is important to note that ω^{σ} and ω^{π} are directly correlated. The correlation shown in Figure 5.12 indicates that, during the process, the two charge transfers between the ligand and the palladium are inversely correlated. Going from L_2Pd to $[LPd(PhBr)]^{\ddagger}$, higher is the ability of a ligand to increase its donor power, lower will be the capacity to increase its π acceptor capacity.

These results can be rationalized as follows: when the L_2Pd system loses a ligand, it is substituted by the PhBr fragment, which is more able to accept electronic density from the palladium center. Therefore the ligand, in order to stabilize the palladium center, is forced to increase its donor ability. Furthermore, since the palladium increases its donor ability to the PhBr fragment, it loses the ability to transfer electronic density toward the ligand in π-symmetry.

These electronic rearrangements are more remarkable for the NHC ligands.

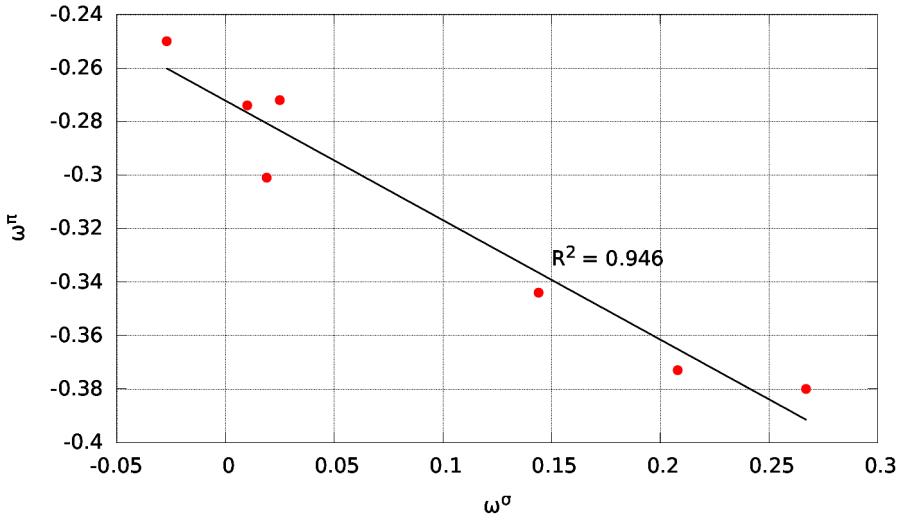

Figure 5.12: *Correlations between ω^{σ} and ω^{π} for the considered series of ligands in the process of oxidative addition of PhBr to L_2Pd.*

5.5.1 How Ligand-Palladium bond influences the energetic barriers ($\Delta E^{\ddagger}$)

In the previous section we have shown how different ligands, in the process of oxidative addition of phenyl bromide to L_2Pd, change their donor-acceptor abilities. In particular we analyzed the nature of these variations in terms of charge transfers toward the palladium (σ-donation) and from the palladium (π-backdonation) finding a correlation between these two bond components.

We now extend the analysis to the energetic barriers for the process ($\Delta E^{\ddagger}$). The values of $\Delta E^{\ddagger}$ are reported in Table 5.3. The range of variation is 15.5 kcal mol^{-1}(from 20.5 kcal mol^{-1} for P1 to 36.9 kcal mol^{-1} for C3). In general the phosphines show lower values with respect to the NHCs ligands. C1 and C2 ligands have the same $\Delta E^{\ddagger}$ values (29.7 kcal mol^{-1}), despite they show a different electronic structure. This suggests that the energetic barriers cannot be explained without a detailed analysis of the ligand-palladium chemical bond. In this section we analyze the $\Delta E^{\ddagger}$ values on the basis of CD-NOCV analysis of L-Pd bonds. In the Figures 5.13 and 5.14 are shown the $\Delta E^{\ddagger}$ values versus the ω^{σ} and ω^{π} values.

Focusing first on Figure 5.13, a weak correlation ($R^2 = 0.791$) can be seen between $\Delta E^{\ddagger}$ and ω^{σ}. $\Delta E^{\ddagger}$ values are correlated with the capacity of the ligand to increase its donor power. Higher is the power of a ligand to increase its donor ability (as NHCs ligands), higher will be the activation barrier. The ligands that have low ω^{σ} values (tertiary phosphines) show lower values of $\Delta E^{\ddagger}$.

Another correlation, between $\Delta E^{\ddagger}$ and ω^{π}, can be seen in Figure 5.14. Not surprisingly, all these quantities are all directly correlated. All the ligands lose their π-acceptor capacity during the process in a different measure.

The higher the loss of accepting capacity (ω^{π} negative), such as NHCs, the higher the activation energy will be. More generally, the ligands that exhibit the

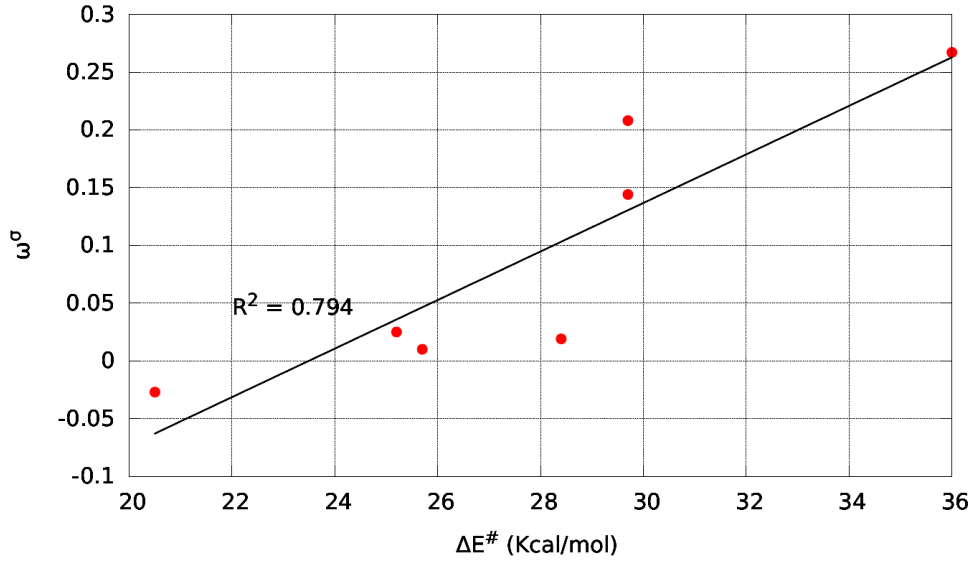

Figure 5.13: *Correlation between $\Delta E^{\ddagger}$ (kcal mol^{-1}) and ω^{σ} values for each ligand analyzed.*

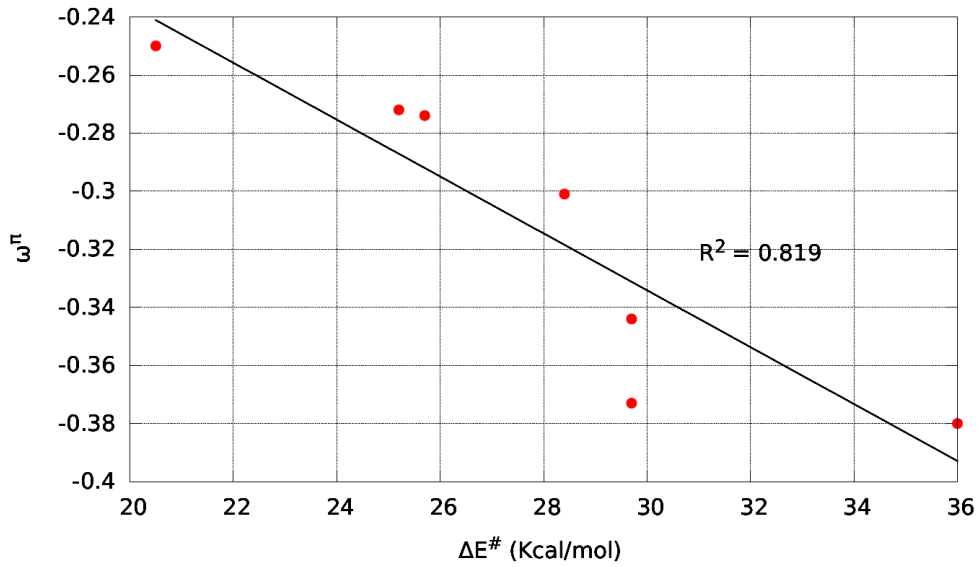

Figure 5.14: *Correlation between $\Delta E^{\ddagger}$ (kcal mol^{-1}) and ω^{π} values for each ligand analyzed.*

larger change in their electronic influences (NHC) are associated with larger activation energies.

	$\Delta E^{\ddagger}$	r(L-Pd) (Å)	$CT_{\sigma}^{(0)}$ (e)	$CT_{\pi}^{(0)}$ (e)	$CT_{net}^{(0)}$ (e)	
L_2Pd						
P1	-	2.264	-0.185	0.225	0.0395	
P2	-	2.282	-0.210	0.210	0.0091	
P3	-	2.285	-0.202	0.220	0.0175	
P4	-	2.316	-0.206	0.199	-0.0067	
C1	-	2.018	-0.173	0.204	0.0309	
C2	-	2.018	-0.180	0.218	0.0378	
C3	-	2.033	-0.161	0.209	0.0478	
	$\Delta E^{\ddagger}$	r(L-Pd) (Å)	r(C-Br) (Å)	$CT_{\sigma}^{(TS)}$ (e)	$CT_{\pi}^{(TS)}$ (e)	$CT_{net}^{(TS)}$ (e)
[LPd(PhBr)]‡						
P1	20.5	2.321	2.289	-0.180	0.168	-0.012
P2	25.2	2.332	2.243	-0.206	0.153	-0.053
P3	25.7	2.335	2.248	-0.204	0.159	-0.045
P4	28.4	2.363	2.209	-0.210	0.139	-0.071
C1	29.7	2.068	2.162	-0.209	0.128	-0.081
C2	29.7	2.066	2.175	-0.206	0.143	-0.063
C3	36.0	2.062	2.175	-0.204	0.129	-0.075

Table 5.3: *Activation energies ($\Delta E^{\ddagger}$), ligand-Palladium bond distances (in Angstrom) and charge transfers results (e) obtained from the CD-NOCV analysis for the considered series of L_2Pd and [L-Pd(PhBr)]‡ systems.*

	$\Delta E^{\ddagger}$	ω^{σ}	ω^{π}	K_{L-Pd}	K_{C-Br}
P1	20.5	-0.027	-0.250	0.0252	0.212
P2	25.2	0.025	-0.272	0.0219	0.187
P3	25.7	0.010	-0.274	0.0219	0.190
P4	28.4	0.019	-0.301	0.0203	0.169
C1	29.7	0.208	-0.373	0.0248	0.145
C2	29.7	0.144	-0.344	0.0238	0.151
C3	36.0	0.267	-0.380	0.0143	0.151

Table 5.4: *Activation energies ($\Delta E^{\ddagger}$), ω^{σ}, ω^{π}, K_{L-Pd} and K_{C-Br} values obtained from the CD-NOCV analysis. The values of K_{C-Br} are calculated with respect to the C-Br bond distance in the free phenyl bromide (1.889 Å)*

5.5.2 Natural Bond Orbitals analysis of Pd-PhBr interaction

In order to rationalize the results about the energetic barriers and the electronic rearrangement of the ligand, a parallel analysis on the palladium and phenyl-bromide bond is needed. However, in this case, it is not easy to carry out a CD-NOCV analysis since it is not possible to find a specific axis between the two fragments unambiguously. Indeed, when phenyl bromide approaches, an η^2-coordination between the palladium and the aromatic ring occurs, followed by the cleavage of the carbon-bromide bond in the [LPd(PhBr)]‡ transition state.

For such reason we analyzed the Pd-PhBr interaction, in the [LPd(PhBr)]‡ transition states, using the second-order perturbative analysis of donor-acceptor interactions with the NBO method.

In the calculations, it was necessary to specify the reference Lewis structure for [LPd(PhBr)]‡, in order to obtain a constant reference and hence a meaningful comparison among the various sytems.

L-Pd and PhBr were described as two interacting fragments not bounded each other. Palladium was described as a d^{10} system (5 lone pairs) forming a bond with the ligand through the lone pair of the latter. In the PhBr fragment, the bromide was considered as forming a bond with the carbon. The two strongest donor-acceptor interactions, which are mostly responsible of the energy interaction of the two fragments, are

- The interaction between the filled (C-Br) σ orbital and the empty (L-Pd) σ^* orbital. (σ-donation LPd $\leftarrow$ PhBr).
- The interaction between the d_{z^2}-lone pair of the palladium and the (C-Br) σ^* empty orbital (π-backdonation LPd $\rightarrow$ PhBr).

For simplicity, we will refer to the first interaction as $\Delta E^{(2)}{}_A$, and $\Delta E^{(2)}{}_B$ for the second one.

As mentioned, such interactions between filled Lewis type orbitals and empty non-Lewis type orbitals, and in particular their linear combination, lead to the formation of NLMO orbitals (doubly occupied). The weight of each non-Lewis type orbital in delocalizing the parent Lewis type orbital in the molecular environment is governed by the expansion coefficient relative to that non-Lewis type orbitals. (c_{ij}).

In our case, in order to analyze the two interactions, we focused on the two coefficients relative to (L-Pd) σ^* orbital and (C-Br) σ^* empty orbital in the NLMO linear combinations. In particular, the square of these coefficients gives a measure of the electronic density transferred upon the interactions.

In Table 5.5 are reported the perturbative energies lowering ($\Delta E^{(2)}$) due to such donor-acceptor interactions for all the [LPd(PhBr)]‡ systems, as well as the square of the two coefficients of linear expansion relative to the two non-Lewis orbitals.

The data in Table 5.5 show that the π-backdonation LPd $\rightarrow$ PhBr is weaker than the σ-donation LPd $\leftarrow$ PhBr along all the ligand series.

	$\Delta E^{(2)}{}_A$	$\Delta E^{(2)}{}_B$	c^2 ($\Delta E^{(2)}{}_A$)	c^2 ($\Delta E^{(2)}{}_B$)
[LPd(PhBr)]‡				
P1	51.4	59.9	0.0332	0.160
P2	44.3	53.8	0.0291	0.153
P3	41.7	52.5	0.0285	0.151
P4	38.2	46.7	0.0245	0.141
C1	32.9	40.9	0.0237	0.133
C2	34.7	42.6	0.0247	0.137
C3	33.4	43.4	0.0239	0.140

Table 5.5: *Main second order perturbative interactions ($\Delta E^{(2)}$) in the [LPd(PhBr)]‡ systems. $\Delta E^{(2)}{}_A$ refers to [$d_{z^2} \rightarrow$ (C-Br) σ^*] interaction, while $\Delta E^{(2)}{}_B$ to [(L-Pd) $\sigma^* \leftarrow$ (C-Br) σ] interaction. c^2 ($\Delta E^{(2)}{}_A$) and c^2 ($\Delta E^{(2)}{}_B$) are the coefficients of expansion, relative to the two interactions, of the non-Lewis type orbitals in the NLMO formation. The values of $\Delta E^{(2)}$ are reported in kcal mol^{-1}. The c^2 coefficients are adimensional.*

In particular the systems bearing phosphines ligands present higher energy stabilization for both interactions with respect to the ones bearing NHC as ligands. The P1 system shows the highest values of $\Delta E^{(2)}{}_A$ (51.4 kcal mol^{-1}) and $\Delta E^{(2)}{}_B$ (59.9 kcal mol^{-1}). Conversely C1 system shows the lowest values (32.9 and 40.9 kcal mol^{-1}respectively).

These two donor-acceptor interactions are directly correlated, as is shown in Figure 5.15.

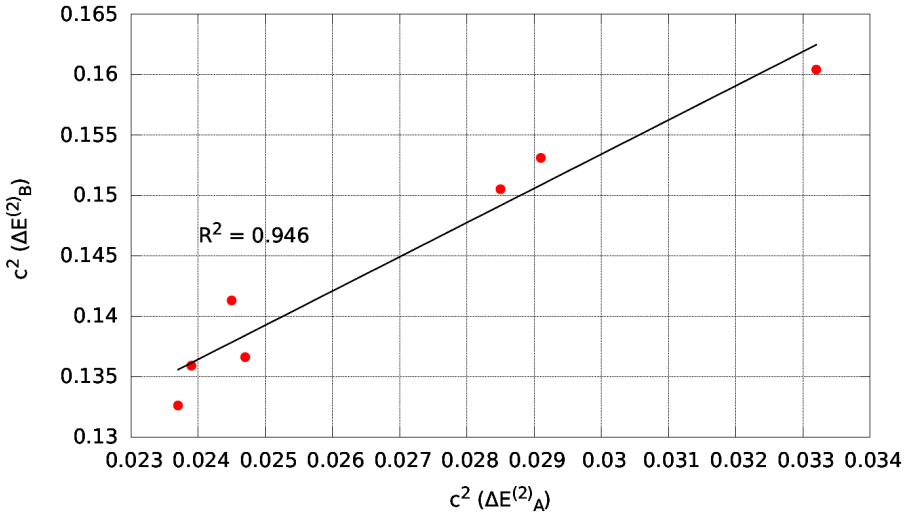

Figure 5.15: *Correlation between c^2 ($\Delta E^{(2)}{}_A$) and c^2 ($\Delta E^{(2)}{}_B$) coefficients.*

Furthermore, the donor-acceptor interactions are strongly correlated to the c^2 coefficients. Indeed, the stronger the $\sigma_i \rightarrow \sigma^*{}_j$ interaction is, the larger the weight of the non Lewis type orbital is (larger coefficients of NLMO expansion).

In this section, we will refer to the strength of the two interactions through the relative square coefficients relative to the non-Lewis type orbitals (c^2 ($\Delta E^{(2)}{}_A$)

and c^2 ($\Delta E^{(2)}{}_B$)). Since the (c^2 ($\Delta E^{(2)}{}_A$) and c^2 ($\Delta E^{(2)}{}_B$)) are directly correlated and since the c^2 ($\Delta E^{(2)}{}_B$) values are more remarkable, we will focus only on this interaction.

First of all we are interested on how these interactions are correlated with the geometrical parameters, in particular with the K_{C-Br} values. Indeed such values indicate how the PhBr fragment is approached to the Pd center in the [LPd(PhBr)]‡ transition states.

The correlation shown in Figure (5.16) indicates a clear correlation between the c^2 ($\Delta E^{(2)}{}_B$) coefficients and the K_{C-Br} values. Physically it suggests that, at higher values of K_{C-Br} (and therefore short distances between Pd and PhBr), the interaction is stronger. Since the two interactions are strictly correlated (Figure 5.15), at short values of K_{C-Br} also the interaction [(L-Pd) $\sigma^* \leftarrow$ (C-Br) σ] will be strong.

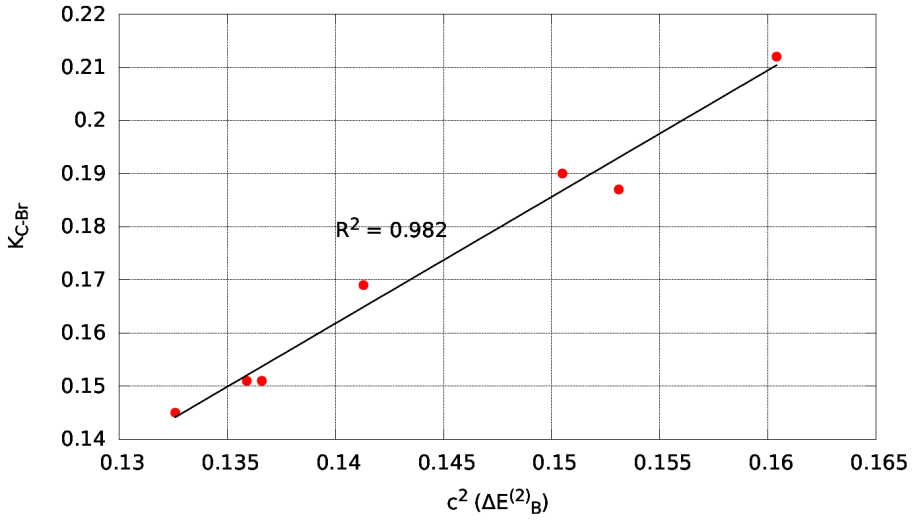

Figure 5.16: *Correlation between the coefficients c^2 ($\Delta E^{(2)}{}_B$) and the K_{C-Br}.*

In Figure 5.17 and 5.18 are reported the correlations between the c^2 ($\Delta E^{(2)}{}_B$) values and the electronic rearrangements of the ligands in the oxidative addition process (ω^{σ} and ω^{π} values respectively).

Such correlations show how the two electronic changes occurring in the process, ligand-palladium and palladium-PhBr interactions, are related. The NHCs ligands, increasing their donor power toward the palladium more than PR_3 ligands (higher values of ω^{σ}) make the palladium center more rich in electron density and, therefore, the interaction between LPd and PhBr is more disfavored (Figure 5.17).

Conversely, in the [LPd(PhBr)]‡ systems bearing phosphines as ligands, the interaction Pd-PhBr is favored, since these ligands do not increase the donor ability in the same measure of the NHC ligands.

In Figure 5.18 is reported the correlation between the c^2 ($\Delta E^{(2)}{}_B$) coefficients and ω^{π} values.

The PR_3 ligands are more able to accept electronic density from the palladium in the [LPd(PhBr)]‡ transition states (higher ω^{π} values). This effect favors the Pd-

PhBr interaction, since the phosphines are able to accept electronic density arising from PhBr. The synergy between the electronic rearrangement of the ligands and the Pd-PhBr interaction has a crucial impact on the energetic barriers of the process. Indeed the NHC carbenes, because of their capacity to transfer more electron density on the palladium and the loss of π acceptor capacity, more remarkable than the one of the phosphines, disfavor the whole process, increasing the energetic barriers.

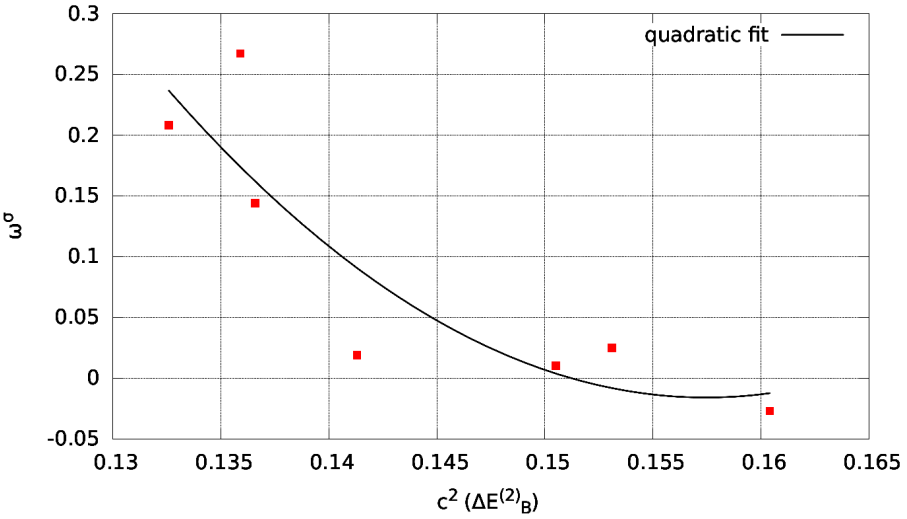

Figure 5.17: *Correlation between the coefficients* c^2 $(\Delta E^{(2)}{}_B)$ *and* ω^σ.

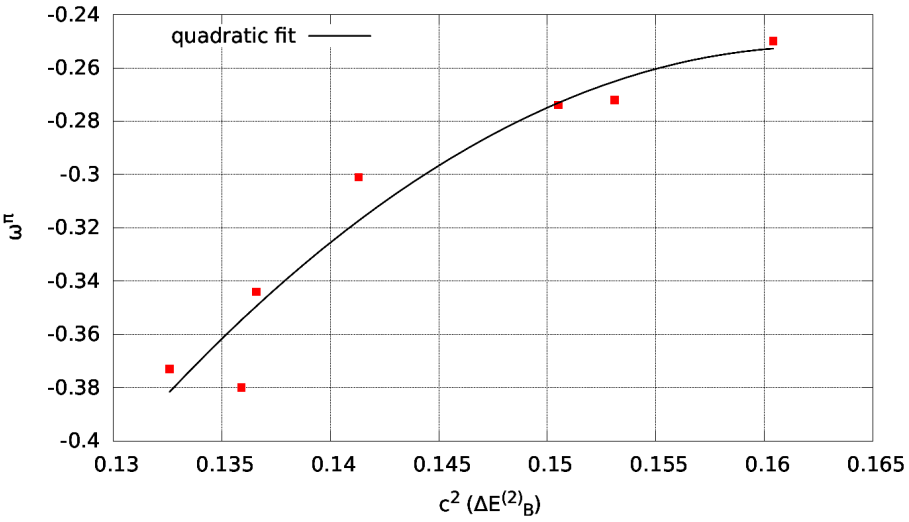

Figure 5.18: *Correlation between the coefficients* c^2 $(\Delta E^{(2)}{}_B)$ *and* ω^π.

5.6 Conclusions

In this chapter, we have carried out a computational analysis on the oxidative addition of phenylbromide (PhBr) to L_2Pd complexes with different ligands. The associative pathway, involving the direct coordination of PhBr on L_2Pd, is possible only for the phosphine series and, in addition, could not be characterized for the bulky phosphines (as tbu_3P). The coordination of PhBr on the palladium leads to a deformation of the geometry of L_2Pd. Therefore the process is endothermic for all the phosphines, in particular for the bulky ones (as $PIPr_3$ and PCy_3). The aromatic systems (Ph_3P and Ph_2HP) favor such process. The aromatic systems exhibit also lower energetic barriers for the process than the aliphatic ones, while the phosphites show the highest barriers of all the series. Among the two possible products, the one with phenyl and bromide in *trans* each other is more stable than the *cis* one (except for $Ptbu_3$). The dissociative pathway involves the loss of a ligand from L_2Pd and the coordination of PhBr to the resulting LPd species. The substutution of a ligand by PhBr is an endothermic process, suggesting that PhBr is a weaker ligand than any other phosphine. The cleavage of the C-Br bond is effective through two possible transition states, in which carbon or bromide can be in pseudo *trans* with the ligand. The transition state with carbon and ligand mutually *trans* is more stable for all the systems. The lowering of the activation barriers is significant for the aliphatic phosphines and, contrary to what observed in the associative pathway, the aliphatic phosphines correspond to more active species for the C-Br bond cleavage. This study shows that it is not possible to predict *a priori* which kind of ligand favors the oxidative addition without a detailed analysis of the L-Pd bond. We have carried out such an analysis, for seven representative ligands, on the basis of NOCV-CD analysis. The purpose of this study was to show that the donor-acceptor power of a ligand can not be rationalized only on the basis of the nature of the ligand. Many other factors should be considered (the metal center, the oxidative state of the metal, the species surrounding the ligand, *etc.*). For example, differently to what can be found in the literature, we have shown that, in L_2Pd, the phosphine ligands have an higher donor power toward the palladium center and an higher acceptor power compared to the carbenes (except for $Ptbu_3$). The same analysis in $[LPd(PhBr)]^{\ddagger}$ shows that the two classes of ligands have the same donor power. This suggests that, more than focusing on the analysis of one species in a process, one should analyze the electronic rearrangement of a ligand going from a reactant to a transition state. In the case of the oxidative addition from L_2Pd to $[LPd(PhBr)]^{\ddagger}$, we have shown that the ligands are forced to increase their donor ability toward the palladium to stabilize the system, and in addition they lose their acceptor capacity from the palladium. These electronic rearrangements are more remarkable for the carbenes, to which are associated the highest electronic barriers (calculated without dispersion corrections and Gibbs corrections). There are weaker correlations between these rearrangements (ω^{σ} and ω^{π}) and the electronic barriers. These preminary results are also confirmed by the perturabtive theory, carried out within the NBO framework. L-Pd and PhBr were described as two interacting fragments not bounded each other. The two strongest donor-acceptor

interactions between the two fragments are (i) the interaction between the filled (C-Br) σ orbital and the empty (L-Pd) σ^* orbital (σ-donation LPd $\leftarrow$ PhBr), and (ii) the interaction between the d_{z^2} lone pair of the palladium and the (C-Br) σ^* empty orbital (π-backdonation LPd $\rightarrow$ PhBr). The magnitude of these interactions were associated to the expansions coefficient of non-Lewis orbitals in the NLMO orbitals formation. In particular, the square of these coefficients gives a measure of the electronic density transfered upon the interactions. The stronger the interactions, the higher the expansion coefficients will be. These interactions are directly correlated with the C-Br bond distance (longer the bond distance, stronger the interactions will be) and, in addition, weak correlations between the square expansion coefficient relative to the π-backdonation LPd $\rightarrow$ PhBr and ω^σ and ω^π magnitudes. This suggests that the electronic rearrangements between L-Pd and Pd-PhBr are directly correlated. In particular, PR_3 ligands are more able to accept electronic density from the palladium in the transformation, thus favoring the Pd-PhBr interaction. Conversely, NHC ligands are more able to transfer electronic density toward the palladium during the process, disfavoring the PhBr approach and thus increasing the activation barriers. Beyond these preliminary results, we have shown that the CD-NOCV methodology can quantitatively quantify the electronic rearrangements occuring in the formation of chemical species and, if coupled to other methodologies (Natural Bond Orbital theory in our case), it can represent a considerable tool to rationalize the nature of the chemical bond, which can support the design of new ligand in the chemical catalysis.

Bibliography

[1] McMullin, C.; Jover, J.; Harvey, J.; Fey, N. *Dalt. Trans.* **2010**, *39*, 10833.

[2] Belpassi, L.; Infante, I.; Tarantelli, F.; Visscher, L. *J. Am. Chem. Soc.* **2008**, *130*, 1048.

[3] Bistoni, G.; Rampino, S.; Tarantelli, F.; Balpssi, L. *J. Chem. Phys.* **2015**, *142*, 084112.

[4] Perdew, J.; Burke, K.; Ernzerhof, M. *Phys. Rev. Lett.* **1996**, *77*, 3865–3868.

[5] Perdew, J.; Burke, K.; Ernzerhof, M. *Phys. Rev. Lett.* **1997**, *78*, 1396.

[6] Andrae, D.; Haubermann, U.; Dolg, M.; Stoll, H.; Preub, H. *Theor. Chim. Acta* **1990**, *77*, 123.

[7] Ehlers, A.; Bohme, M.; Dapprich, S.; Gobbi, A.; Hollwarth, A.; Jonas, V.; Kohler, K.; Stegmann, F.; Veldkamp, A.; Frenking, G. *Chem.Phys.Lett.* **1993**, *208*, 111.

[8] Neese, F. *Comput. Mol. Sci.* **2012**, *2*, 73.

[9] Grimme, S.; Antony, J.; Ehrlich, S.; Krieg, H. *J. Chem. Phys.* **2010**, *132*, 1456.

[10] Grimme, S.; Ehrlich, S.; Goerigk, L. *J.Comput.Chem.* **2011**, *32*, 1456.

[11] Fonseca Guerra, C.; Snijders, J.; de Velde, G.; Baerends, E. *Theor. Chem. Acc.* **1998**, *99*, 391.

[12] te Velde, G.; Bickelhaupt, F.; Baerends, C., E.J. Fonseca Guerra; van Gisbergen, J., S.J.A. Snijders; Ziegler, T. *J. Comp. Chem.* **2001**, *22*, 931.

[13] Van Lenthe, E.; Baerends, E.; Snijders, J. *J. Chem. Phys.* **1993**, *99*, 4597.

[14] Van Lenthe, E.; Baerends, E.; Snijders, J. *J. Chem. Phys.* **1994**, *101*, 9783.

[15] Van Lenthe, E.; Ehlers, A.; Baerends, E. *J. Chem. Phys.* **1999**, *110*, 8943.

[16] Aoki, T.; Ishii, Y. .; Mizobe, Y.; Hidai, M. *Chem.Lett.* **1991**, *20*, 615–618.

[17] Flemming, J.; Pilon, M.; Borbulevitich, O.; Antipin, M.; Grushin, V. *Inorg.Chim.Acta* **1998**, *280*, 87–98.

[18] Amatore, C.; Jutand, A. *Acc. Chem. Res.* **2000**, *33*, 314–321.

[19] Kozuch, S.; Amatore, C.; Jutand, A.; Shaik, S. *Organometallics* **2005**, *24*, 2319–2330.

[20] Kozuch, S.; Jutand, A.; Shaik, S.; Amatore, C. *Chem.Eur.J.* **2004**, *10*, 3072–3080.

Chapter 6

Transmetalation

6.1 Synopsis

In a typical palladium catalytic cycle, oxidative addition of an aryl halide or pseudohalide to a Pd(0) complex results in the formation of Pd(II) species. Transmetalation with an organometallic reagent subsequently takes place, resulting in a second Pd(II) complex.[1–4] Finally, this Pd(II) complex typically undergoes reductive elimination, forming the cross-coupled product, with the regeneration of Pd(0) species. The transmetalation step is expected to show differences depending on the corresponding nucleophile used and is less known. In the Negishi cross-coupling process the transmetalation step is carried out by using ZnR_2 or ZnXR organometallic species, and the more accessible reagent is usually chosen.[5–7]

In this chapter we present a computational analysis on the transmetalation step in the Negishi cross-coupling reaction, considering ZnPhBr as the organometallic nucleophile. The Pd(II) complex reacting with ZnPhBr in the transmetalation step is $L_nPd(Ph)(Br)$ (n=1,2), the products of the oxidative addition. Different ligands (L) have been taken into account, among tertiary phosphines (PR_3) and N-heterocyclic carbenes (NHC). Our goal is to investigate how the different energetic paths of the process are influenced by the different electronic properties of the ligand.

6.2 Computational methodology

Geometry optimizations and frequencies analysis have been performed with the Gaussian 09 package, at DFT level, using the Perdew, Burke and Ernzerhof exchange correlation functional (PBE0).[8,9] The palladium atom was represented by the relativistic effective core potential (RECP) from the Stuttgart group and the associated basis sets,[10] augmented by an f polarization function.[11]

All the other atoms (C,H,P,O,N) were represented by a SVP basis set. For each geometry (TS and minima) a single point calculation has been carried out with the Orca package,[12] using an effective core potential for palladium, and a QZVPP basis set for the other atoms. Influence of the dispersion forces was considered

by adding to the SCF energy the D3(BJ) corrections as described by Grimme.[13,14] All of the energies reported in the present work are obtained by summing SCF energies, Gibbs correction at 298 K and the D3(BJ) dispersion correction.

6.3 Pathways Manifold

In contrast with the other parts of the catalytic cycle, the transmetalation step is specific to cross-coupling reactions. In the Negishi reaction, the transmetalation is the stage where the migration of an organic group from the zinc organometallic species (ZnR_2 or ZnXR) to the palladium complex takes place, leading to the formation of new Pd(II) complexes ($L_nPd(II)R_1R_2$) and the elimination of zinc salt (ZnXR or ZnX_2). Since in the previous chapter we analyzed the oxidative addition of PhBr to L_nPd complexes (n=1,2) and the subsequent formation of $L_nPd(Ph)(Br)$ species, in the present chapter we analyze the transmetalation including $L_nPd(II)$-(Ph)(Br) complexes and ZnPhBr as nucleophilic species. The ligands considered are the same as in the study on oxidative addition.

Similarly to the oxidative addition, the transmetalation can take place with one or two ligands L coordinated to the palladium, and in addition all the isomers of $L_nPd(Ph)(Br)$ species have to be considered in the reaction paths (Figure 6.1).

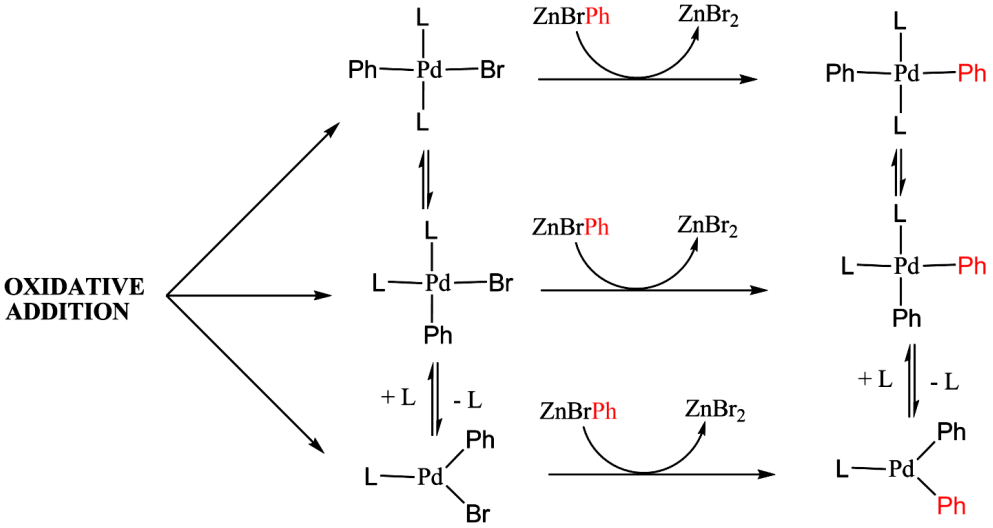

Figure 6.1: *Transmetalation between the isomers of $L_nPd(Ph)(Br)$ species arising from the oxidative addition product and ZnPhBr organozinc compound.*

In 2011, Espinet and co-workers reported their studies on the transmetalation step of the Negishi cross-coupling reaction, in which organozinc reagents are used as coupling partners.[15] It was found that a concerted mechanism on the neutral $(PPh_2Me)Pd(Me)(Cl)$ complex is possible, with the inclusion of ZnMeCl and $ZnMe_2$ species, in presence of THF as solvent. Although an ionic mechanism *via* the cationic intermediate $[PdR(L)_2(THF)^+]$ was found (THF = tetrahydrofuran),

we describe only the concerted mechanism taking into account a series of ligands among tertiary phosphines (PR_3) and N-heterocyclic carbenes (NHC) (Figure 6.2).

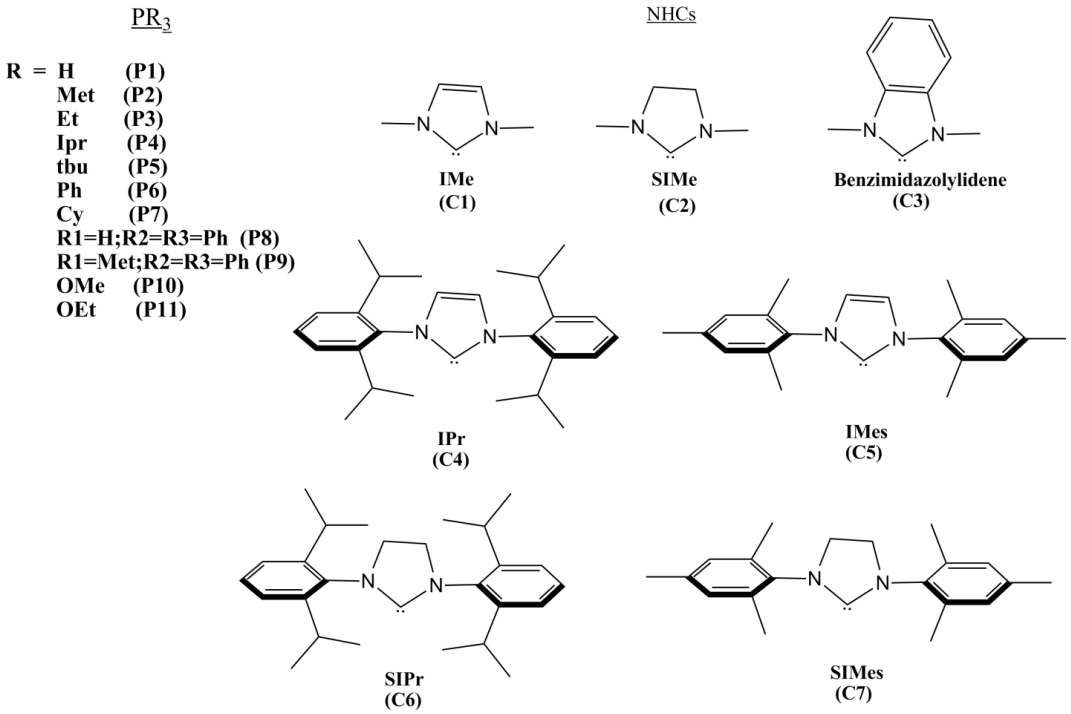

Figure 6.2: *List and abbreviations for the ligands (L) considered.*

Since the L_nPd(Ph)(Br) complexes, arising from the oxidative addition, undergo the transmetalation, it is important to consider which conformations of these species have to be taken into account. Indeed, different isomers of [L_nPd(PhBr)] complexes can be obtained from the oxidative addition. In particular, the L_2Pd(Ph)(Br) complexes can exist in two different conformations, *cis* or *trans*, whereas the [LPd(PhBr)] complexes can exist in three conformations. Since the L_2Pd(Ph)(Br) complexes are much more stable, we have considered their *cis* and *trans* conformations, as reference in analyzing the energetic pathways for the transmetalation process

As already mentioned, for the transmetalation process involving the L_2Pd(Ph)(Br) complexes and the ZnPhBr organozinc compound, two conformations of Pd(II) complex, *cis* and *trans* can be considered. In Figures 6.4 and 6.3 are reported the schematic representations of the two pathways involving respectively the *cis* and *trans* conformations.

Coordination of ZnPhBr to *trans*-L_2Pd(Ph)(Br) leads to the formation of the CT1-TRANS adduct (see Figure 6.5). This step takes place upon the interaction between Pd, acting as Lewis base, and Zn, acting as Lewis acid, with Br' of the palladium complex acting as a bridge between them. In this passage, the Pd-Br' bond distance increases (from 2.508 Å to 2.565 Å), as well as the Zn-Br bond distance (from 2.249 Å to 2.347 Å). This step is exoergonic (ΔG = -11.5 kcal mol^{-1}).

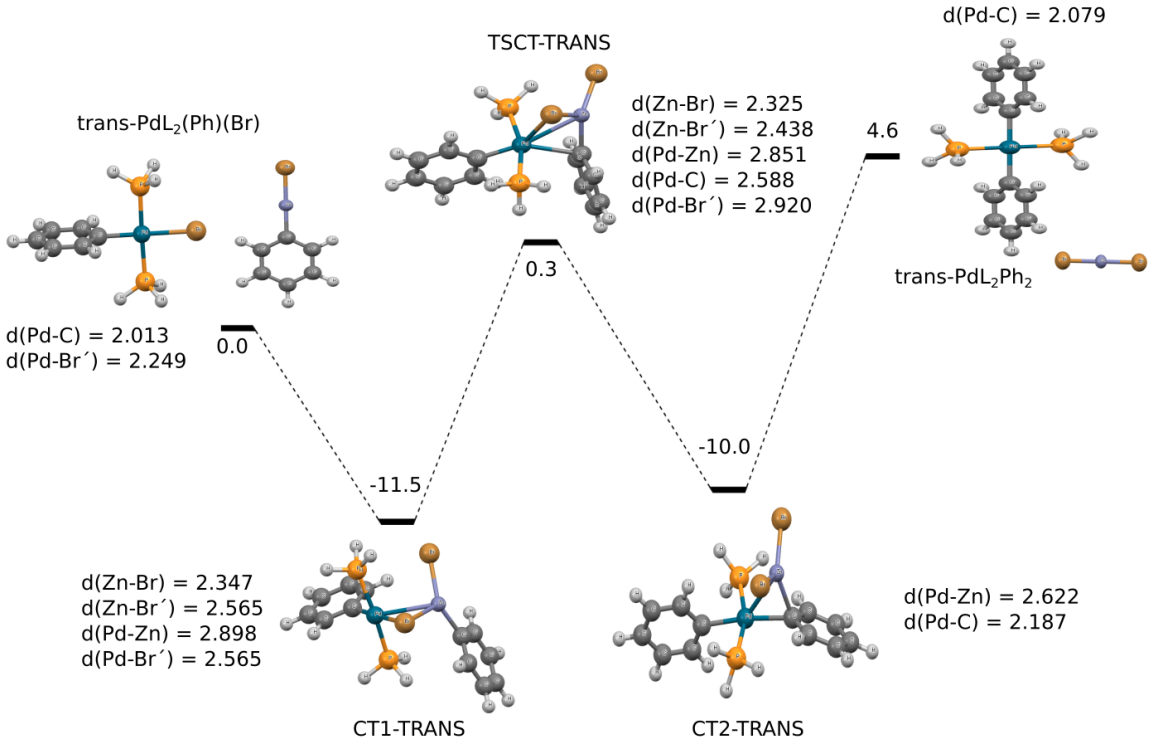

Figure 6.3: *Schematic representation of the pathway for the transmetalation between ZnPhBr and trans- $L_2Pd(Ph)(Br)$ for L=PH_3. Br' is referred to the bromide bonded to palladium. The energetic values are reported in kcal mol^{-1}, whereas the bond distances in Angstrom.*

The cleavage of the Pd-Br' bond is effective through the transition state TSCT-TRANS (see Figure 6.6), associated to an activation barrier of $\Delta G^{\ddagger}$ = 11.8 kcal mol^{-1}. In such transition state, the Pd-Br' bond distance is significantly elongated (2.920 Å), while Pd-Zn bond distance decreases (2.851 Å), allowing the coordination of the *ipso* carbon of the phenyl ring to palladium (Pd-C bond distance = 2.588 Å). The formation of Zn-Br' bond is well-advanced (2.438 Å). The formation of CT2-TRANS complex (ΔG = -10.0 kcal mol^{-1}, see Figure 6.7) is associated with the cleavage of Pd-Br' bond, while the formation of the Pd-C bond is well advanced (2.187 Å).

The decoordination of $ZnBr_2$ to form PdL_2Ph_2 + $ZnBr_2$, in absence of species that can favor this process, is a significantly endoergonic process (ΔG= 14.6 kcal mol^{-1}) and represents the slowest step of the whole process. No transition state relative to this step could be located on the potential energy surface. In the process, the Pd-C bond decreases to 2.079 Å.

In Figure 6.4 is reported the same transmetalation mechanism, but relative to the *cis*-$L_2Pd(Ph)(Br)$ complex, with PH_3 as ligand.

Similarly, the coordination of ZnPhBr to *cis*-$L_2Pd(Ph)(Br)$ leads to the formation of the CT1-CIS adduct (see Figure 6.5). In this passage, the Pd-Br' bond distance increases (from 2.463 Å to 2.508 Å), as well as the Zn-Br bond distance (from

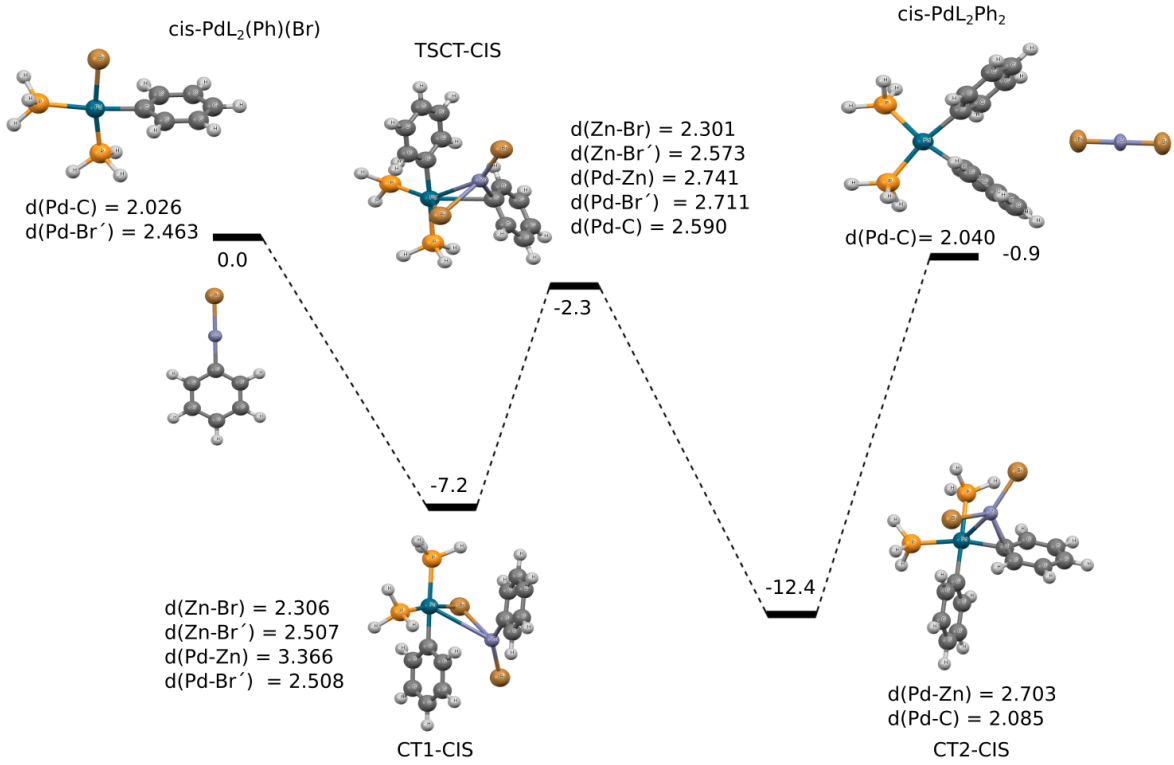

Figure 6.4: *Schematic representation of the pathway for the transmetalation between ZnPhBr and the cis-L_2Pd(Ph)(Br) for L=PH_3. Br is referred to the bromide bonded to palladium. The energetic values are reported in kcal mol^{-1}, whereas the bond distances in Angstrom.*

2.249 Å to 2.306 Å). The high Pd-Zn bond distance (3.366 Å), if compared with the one in the CT1-TRANS complex (2.989 Å), suggests that the coordination of ZnPhBr to palladium is less favored and is associated to a less exoergonic reaction energy (ΔG = - 7.2 kcal mol^{-1}).

The cleavage of the Pd-Br' bond is effective through the transition states TSCT-TRANS (see Figure 6.6), associated to an activation barrier of 4.9 kcal mol^{-1}. In such transition state, the Pd-Br' bond distance is significantly elongated (2.711 Å), while Pd-Zn bond distance decreases (2.741 Å), allowing the coordination of the *ipso* carbon of the phenyl ring to palladium (Pd-C bon distance = 2.590 Å). These bond distances, except for Pd-C bond distance, if compared with the ones in the TSCT-TRANS, are shorter by *ca* 0.12 - 0.20 Å, suggesting that TSCT-CIS is more accessible in energy ($\Delta G^{\ddagger}$ = 4.9 kcal mol^{-1}), and the formation of Zn-Br' bond is well-advanced (2.301 Å).

The formation of CT2-TRANS complex (ΔG = -12.4 kcal mol^{-1}, see Figure 6.7) is associated with the cleavage of Pd-Br' bond, while the formation of the Pd-C bond is well advanced (2.085 Å).

The decoordination of $ZnBr_2$ to form *cis*-PdL_2Ph_2 + $ZnBr_2$, in absence of species that can favor this process, is a significantly endoergonic process (ΔG = 11.5 kcal mol^{-1}) and represents the slowest step of the whole process. This energetic values

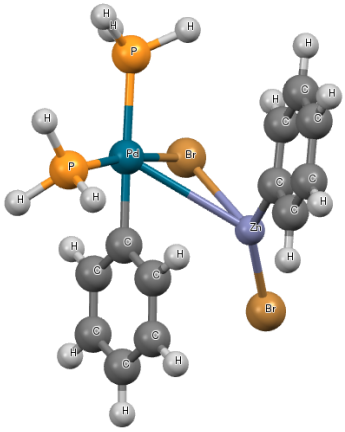

(a) CT1-CIS

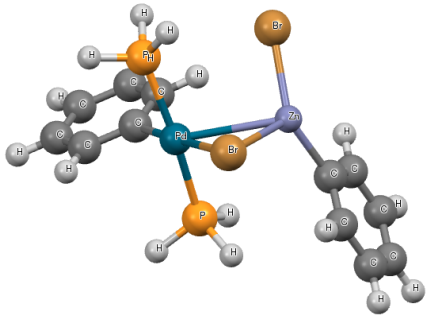

(b) CT1-TRANS

Figure 6.5: *Cis and trans isomers of CT1 adducts, with PH_3 as ligand. for the transmetalation on $[L_2Pd(PhBr)]$ complexes*

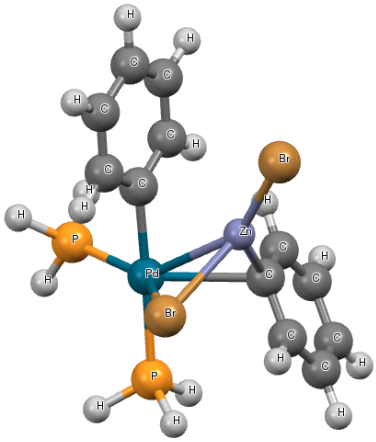

(a) TSCT-CIS

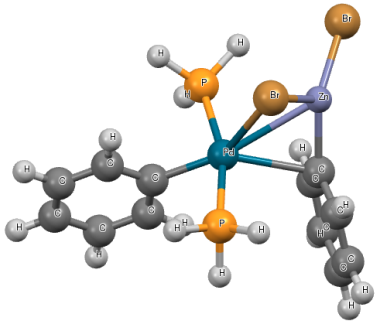

(b) TSCT-TRANS

Figure 6.6: *Structures of the transition states, with PH_3 as ligand, for the transmetalation on $[L_2Pd(PhBr)]$ complexes.*

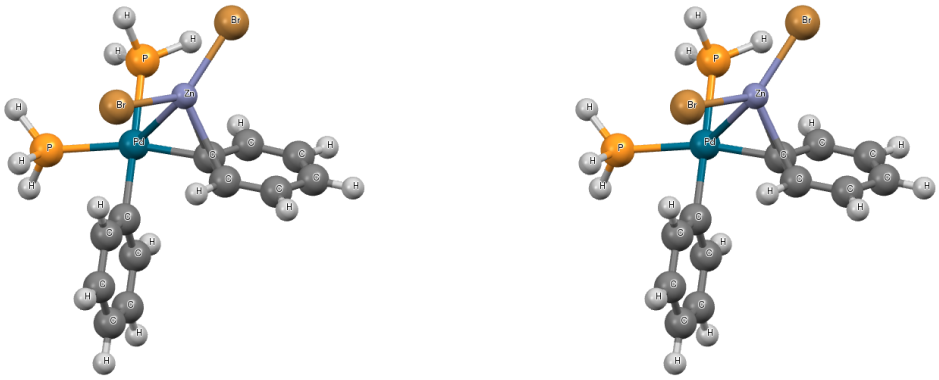

(a) CT2-CIS (b) CT2-TRANS

5

Figure 6.7: *Cis and trans isomers of CT2 complexes, with PH_3 as ligand, for the transmetalation on [L_2Pd(PhBr)] complexes.*

is lower with respect to the one for *trans*-L_2Pd(Ph)(Br) (ΔG = 14.6 kcal mol^{-1}). No transition state relative to this step could be located on the potential energy surface. In the process, the Pd-C bond decreases to 2.040 Å, a shorter distance if compared with the one of *cis*-PdL_2Ph_2 (2.079 Å). Comparing the two processes, the path involving *cis*-L_2Pd(Ph)(Br) is more favored in energy.

In Figure 6.8 is reported the schematic representation of the pathway for the transmetalation between ZnPhBr organozinc compound and the LPd(Ph)(Br) complex with PH_3 as ligand. This pathway involves the initial loss of one ligand from *trans*-[L_2Pd(PhBr)] complex to yield LPd(Ph)(Br), followed by the coordination of ZnPhBr to yield CT1 complex (see Figure 6.9). This process, as expected, is endoergonic (ΔG = 24.9 kcal mol^{-1}). The presence of only one ligand bonded to palladium, leads to have a coordination between the latter and the *ipso* carbon already in this species with a Pd-C bond distance of 2.501 Å. The Zn-Br' bond distance is already sensibly elongated (2.700 Å).

The cleavage of the Pd-Br' bond is effective through the transition states TSCT (see Figure 6.9), associated to an activation barrier of $\Delta G^{\ddagger}$ = 27.7 kcal mol^{-1}. In such transition state, the Pd-Br' bond distance is significantly elongated (2.637 Å), while Pd-Zn bond distance decreases (2.650 Å), while the Pd-C bond distance decreases to 2.303 Å. The absence of a ligand bonded to palladium allows the phenyl ring to approach much more to the palladium.

The formation of CT2 (ΔG = -5.8 kcal mol^{-1}, see Figure 6.9) is associated with the cleavage of Pd-Br', while the formation of the Pd-C bond is well advanced (2.116 Å). The decoordination of $ZnBr_2$ to form *cis*-PdLPh_2 + $ZnBr_2$, in absence of species that can favor this process, is a significantly endoergonic process (ΔG= 26.6 kcal mol^{-1}),

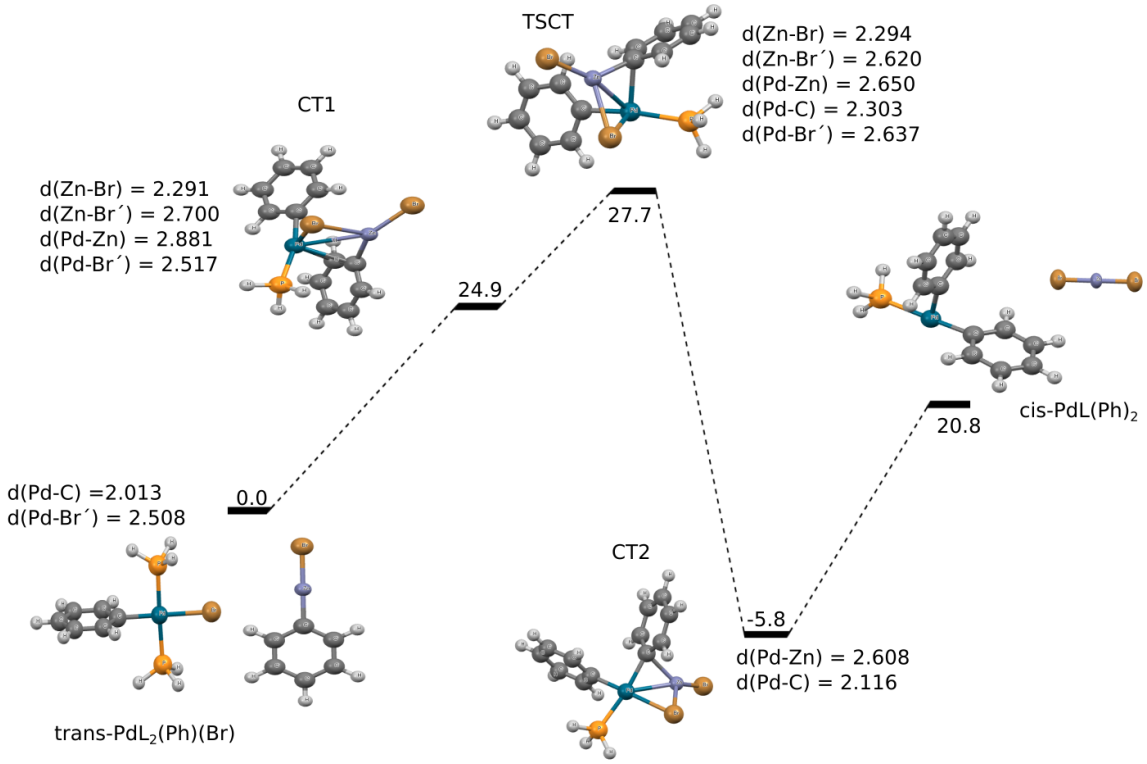

Figure 6.8: *Schematic representation of the pathway for the transmetalation between ZnPhBr organozinc compound and the [LPd(PhBr)] complex bearing PH_3 as ligand. Br´ is referred to the bromide bonded to palladium. The energetic values are reported in kcal mol^{-1}, whereas the bond distances in Angstrom.*

6.4 Energetic aspects

6.4.1 Transmetalation on trans-L_2Pd(Ph)(Br) complexes

We start by considering the transmetalation on *trans*-L_2Pd(Ph)(Br) complexes, which involves the direct coordination of ZnPhBr to such complexes. In Table 6.1 are reported the calculated relative free energies for the different species involved in such pathway. The analysis involves 13 different ligands, in particular tertiary phosphines and NHCs carbenes (Figure 6.2).

- **PR_3 Ligands**

  The data collected in Table 6.1 show that for all the PR_3 ligands, but $P(tbu)_3$ (P5), all the points could be located on the potential energy surface. In the case of P5, the steric bulk of the ligand prevents the optimization of all the points along the pathway.

  For all the phosphines, the formation of the adduct CT1-TRANS is an exoergonic process (except for P7, ΔG = 18.8 kcal mol^{-1}). In general, all the phosphines present the same energetic trend, ranging from ΔG = -10 kcal mol^{-1}(P4) to ΔG = -20 kcal mol^{-1}(P3). This situation is drastically different

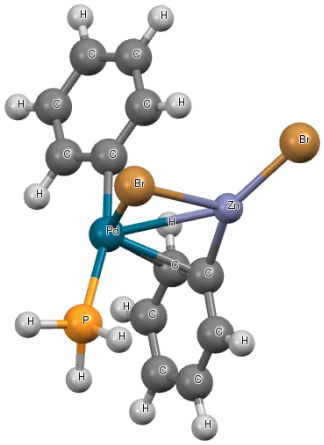

(a) CT1

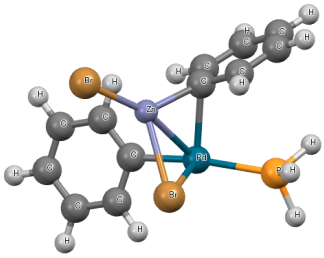

(b) TSCT

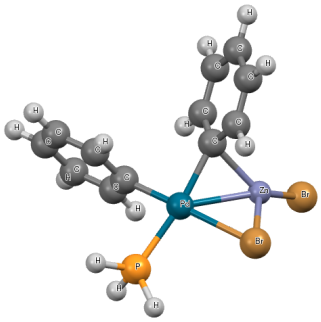

(c) CT2

Figure 6.9: *Structures of the CT1, TSCT and CT2 species, with PH_3 as ligand, for the transmetalation on [LPd(PhBr)] complexes.*

when the dispersion corrections are not included. The coordination energy is then *ca* 10 to 15 kcal mol^{-1}higher, making endoergonic the process for the systems P2, P4, P6 and P11. The least sterically hindered ligand, PH_3, shows the lowest increase ($\Delta\Delta G = +9.8$ kcal mol^{-1}), whereas the bulky phosphine P7 is associated to a significant destabilization of the CT1-TRANS adduct ($\Delta\Delta G = +20$ kcal mol^{-1}). Upon formation of an adduct between two fragments, there is action of a large number of pairwise interactions between non-bonded atoms with mutual distance typical of Van der Waals attraction. Inclusion of the dispersion corrections according to the scheme of Grimme introduce many stabilizing interactions. The bigger the two fragments, the more important these corrections will be, leading to significantly different values for reacting energies computed without dispersion corrections.

From the CT1-TRANS adduct, the Pd-Br bond cleavage through TSCT-TRANS transition state is associated to activation barriers ranging from $\Delta G^{\ddagger} = 1.9$ kcal mol^{-1}(P7) to $\Delta G^{\ddagger} = 23.1$ kcal mol^{-1}(P4).

These barriers are not significantly altered when no dispersion corrections

are considered, with values ranging from $\Delta G^{\ddagger}$ = 2 kcal mol^{-1}(P7) to $\Delta G^{\ddagger}$ = 29.7 kcal mol^{-1}(P4).

The formation of the product of the Pd-Br bond cleavage, CT2-TRANS, has an energetic range from $\Delta G^{\ddagger}$ = -9.7 kcal mol^{-1}(P1) to ΔG = -4.9 kcal mol^{-1}(P6).

The decoordination of $ZnBr_2$ yields PdL_2Ph_2 where the two phosphines are mutually *trans*. No transition state can be located on the potential energy surface. The formation of such complex is an endoergonic process for all the phosphines, except for P4 (ΔG = -3.0 kcal mol^{-1}) and P7 (ΔG = -12.0 kcal mol^{-1}). For the other systems, the energies range from ΔG = 9.2 kcal mol^{-1}(P3) to ΔG = 15.8 kcal mol^{-1}(P11).

These energetic values are significantly affected when no dispersion corrections are included. In general the absence of such corrections makes more accessible in energy this step. The values range from ΔG = -15.9 kcal mol^{-1}(P6) to ΔG = 9.6 kcal mol^{-1}(P1). These significant alteration are associated with a destabilization of the CT2-complexes, because in absence of dispersion corrections all the pairwise interactions between atoms non bonded are lost.

- **NHC Ligands**

  In the case of the NHC ligands, the steric bulk prevented the characterization of the reaction path. Only for the smallest NHC (C1-C3) all the points could be located. The formation of CT1-TRANS has the same energetic trend to the one observed for the phosphines, whereas the lowest $\Delta G^{\ddagger}$ values is associated to C3 carbene ($\Delta G^{\ddagger}$ = 8.2 kcal mol^{-1}). The CT2-TRANS complexes are more stabilized than the ones bearing the phosphines as ligands, in agreement with their strong donating power (ΔG values close to 0 for the process CT1-TRANS $\rightarrow$ CT2-TRANS).

  Because of such higher stabilization, NHCs ligands present values of ΔG relative to the formation of PdL_2Ph_2(*trans*) + $ZnBr_2$ much higher (ΔG = 21.7 kcal $mol^{-1}$for C1 and C2). This shows that, in absence of additional species that could favor this process, the NHC carbenes does not show high catalytic activity for the transmetalation of *trans*-$L_2Pd(Ph)_2$ complexes.

6.4.2 Transmetalation on cis-L_2Pd(Ph)(Br) complexes

In Table 6.2 are reported the relative free energies for the different species involved in the transmetalation on *cis*-L_2Pd(Ph)(Br) complexes (Figure 6.3).

- **PR_3 Ligands**

  The data collected in Table 6.2 show that for all the PR_3 ligands, but $P(tbu)_3$ (P5), all the point could be located on the potential energy surface. In the

case of $P(tbu)_3$, the steric bulk prevents the optimization of all the structures along the reaction path.

For all the phosphine series, the formation of the adduct CT1-CIS is an exoergonic process. The least exoergonic ΔG value for the coordination of ZnPhBr on Pd is associated with the system with P11 as ligand (ΔG = -2.8 kcal mol^{-1}), whereas the most exoergonic value is obtained with P3 as ligand (ΔG = -20.2 kcal mol^{-1}).

The situation is drastically different when the dispersion corrections are not included. The coordination energy is ca 10 to 15 kcal mol^{-1} more endoergonic. The less sterically hindered ligands show the lowest increase. The lowest sterically hindered ligand, PH_3, shows the lowest increase (10.4 kcal mol^{-1}), whereas the bulky phosphine P8 is associated with the highest destabilization of the CT1-CIS adduct (15.3 kcal mol^{-1}).

From the adducts CT1-CIS, the Pd-Br bond cleavage through TSCT-CIS transition state is associated to activation barriers ranging from $\Delta G^{\ddagger}$ = 4.9 kcal mol^{-1}(P1) to $\Delta G^{\ddagger}$ = 26.8 kcal mol^{-1}(P7). The phosphines ligands bearing aromatic systems, such as P8 and P9, exhibit the lowest barriers. The inclusion of dispersion corrections does not affect significantly the values of these activation barriers. The highest energies of $\Delta G^{\ddagger}$, when the dispersion corrections are not included, are associated to a destabilization of the TSCT-CIS transition state. This destabilization is due to the loss of many stabilizing interactions between non bonded atoms. The values of such destabilization's range from 2.3 kcal mol^{-1}(P1) to 7.6 kcal mol^{-1}(P7).

The formation of CT2-CIS, through the transition state TSCT-CIS, is an exoergonic process for all the phosphine series, with reaction energies ranging from ΔG = -10.1 kcal mol^{-1}(P1) to ΔG = -13.2 kcal mol^{-1}(P3). The reaction energies for the formation of CT2-CIS complexes are not sensibly altered when no dispersion corrections are considered, with values ranging from ΔG = -11.4 kcal mol^{-1}(P1) to ΔG = -26.8 kcal mol^{-1}(P7).

The decoordination of $ZnBr_2$ yields PdL_2Ph_2 where the two phosphines are mutually *cis*. No transition state could be located on the potential energy surface. Such process is endoergonic for all the phosphines, with energetic values ranging from ΔG = 6.5 kcal mol^{-1}(P11) to 18.8 kcal mol^{-1}(P6). These values are sensibly altered when the dispersion corrections are not considered. In particular, for certain ligands (P4, P7, P9 and P11), not considering such corrections makes the step exoergonic (ΔG = -3.7, -4.4, -0.5 and -6.3 kcal mol^{-1} respectively). Such alterations are due to the destabilization of the CT2-CIS complexes, because all the pairwise stabilizing interactions are lost.

- **NHC Ligands**

  In the case of NHC ligands, the steric bulk prevents the characterization of the reaction pathway. Only for the smallest NHC (C1-C3) could all the points

along the path be located on the potential energy surface.

Similarly to the phosphine case, the formation of CT1-CIS complexes is an exoergonic process, with values ranging from ΔG = -13.7 kcal mol^{-1} (C3) to ΔG = -12.7 kcal mol^{-1} (C2). These systems are sensibly destabilized when the dispersion corrections are not considered, making the process isoergonic (from ΔG = -0.1 kcal mol^{-1} for C2 to -1.0 kcal mol^{-1} for C3). The activation barriers $\Delta G^{\ddagger}$, through TSCT-CIS transition state, are very similar in energy to the ones seen for the phosphines ($\Delta G^{\ddagger}$ = 11.7, 10.4, 11.6 kcal mol^{-1} for C1, C2 and C3 respectively). These values are not sensibly affected when the dispersion corrections are not included, with increases of ca 2-3 kcal mol^{-1}. The formation of CT2-CIS complexes is much more exoergonic compared to the phosphine series, in agreement with the high donor power of the carbenes, with values ranging from ΔG = -17.4 kcal mol^{-1}(C1) to ΔG = -19.0 kcal mol^{-1}(C2). Such values are not affected if the dispersion corrections are not included. The decoordination of $ZnBr_2$ from Pd, leading to PdL_2Ph_2 + ZnPhBr, is a process much more endoergonic than the one seen for the phosphines. No transition state could be located on the potential energy surface. The energetic values for such process range from ΔG = 21.4 kcal mol^{-1}(C3) to ΔG = 23.8 kcal mol^{-1}(C2).

In order to visualize how the dispersion corrections alterate the energetic paths for the transmetalation of [L_2Pd(PhBr)] complexes, in Figure 6.10 and 6.11 are respectively shown the paths for the process involving *cis* and *trans* isomer of [P(Ipr)$_3$Pd(Ph)(Br) complex.

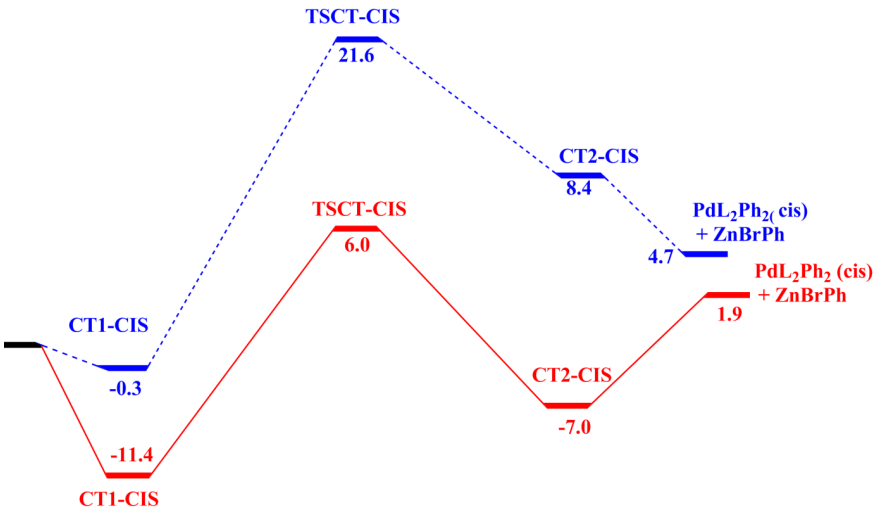

Figure 6.10: *Reaction path for the transmetalation of the cis isomer of cis-(PIpr$_3$)$_2$Pd(Ph)(Br), including (red solid lines) and not including (blue dashed line) the dispersion corrections.*

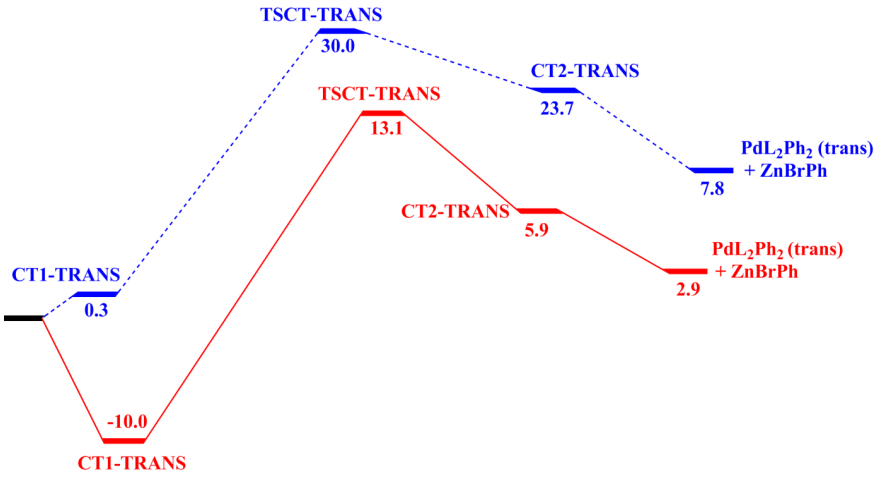

Figure 6.11: *Reaction path for the transmetalation of the trans isomer of trans-$(PIpr_3)_2Pd(Ph)(Br)$, including (red solid lines) and not including (blue dashed line) the dispersion corrections.*

[L_2Pd(PhBr)] Trans complex.						
Ligand	**CT1-TRANS**	**TSCT-TRANS**	**CT2-TRANS**	**PdL_2Ph_2(tr.)+ZnBr_2**	$\Delta G^{\ddagger}_{TSCT}$	$\Delta G_{PdL2Ph2}$
P1	-11.5(-1.7)	0.3(11.1)	-10.0(1.1)	4.6(6.1)	11.8(12.8)	14.6(5.0)
P2	-10.3(1.2)	3.9(18.2)	-3.0(11.4)	8.2(11.1)	14.2(17.0)	11.2(-0.3)
P3	-20.0(-7.8)	-0.8(16.5)	-8.2(8.8)	1.0(5.3)	19.2(24.3)	9.2(-3.5)
P4	-10.0(0.3)	13.1(30.0)	5.9(23.7)	2.9(7.8)	23.1(29.7)	-3.0(-15.9)
P5	-	-	-	-	-	-
P6	-11.3(5.0)	2.8(23.6)	-2.1(20.2)	7.9(14.9)	14.1(18.6)	10.0(-5.3)
P7	18.8(38.8)	20.7(40.8)	18.8(38.8)	6.8(13.8)	1.9(2.0)	-12.0(-25.0)
P8	-11.0(0.6)	-0.9(16.2)	-11.9(5.8)	5.9(9.4)	10.1(15.6)	17.8(3.6)
P9	-16.3(-3.8)	0.8(18.4)	-7.6(11.3)	5.8(10.3)	17.1(22.2)	13.4(-1.0)
P10	-16.7(-4.7)	-6.3(8.9)	-13.7(0.8)	1.9(4.8)	10.4(13.6)	15.6(4.0)
P11	-12.3(1.2)	2.5(18.7)	-6.5(10.3)	9.3(12.2)	14.8(17.5)	15.8(1.9)
C1	-13.7(-3.8)	-3.9(10.1)	-13.0(1.2)	8.7(11.4)	9.8(13.9)	21.7(10.2)
C2	-15.3(-5.8)	-4.7(9.9)	-14.2(0.6)	7.5(10.3)	10.6(15.7)	21.7(9.7)
C3	-11.0(-0.8)	-2.8(12.2)	-11.7(3.2)	7.9(10.9)	8.2(13.0)	19.6(7.7)
C4	-	-	-	-	-	-
C5	-	-	-	-	-	-
C6	-	-	-	-	-	-
C7	-	-	-	-	-	-

Table 6.1: *Calculated relative Gibbs free energies ,the activation barrier ($\Delta G^{\ddagger}_{TSCT}$) and the Gibbs free energy difference for the formation of PdL_2Ph_2 species ($\Delta G_{PdL2Ph2}$) in kcal mol^{-1}for the mechanism for the transmetalation between the trans-L_2Pd(Ph)(Br) and ZnPhBr. The values are calculated with respect to trans-L_2Pd(Ph)(Br) + ZnPhBr separated systems. The Gibbs energy correction was carried out at 298K. In parenthesis are shown the same values calculated without including the dispersion corrections to the energy.*

	[L_2Pd(PhBr)] Cis complex.					
Ligand	**CT1-CIS**	**TSCT-CIS**	**CT2-CIS**	**PdL$_2$Ph$_2$(cis)+ZnBr$_2$**	$\Delta G^{\ddagger}_{TSCT}$	$\Delta G_{PdL2Ph2}$
P1	-7.2(3.2)	-2.3(10.4)	-12.4(-1.0)	-0.9(1.0)	4.9(7.2)	11.5(2.0)
P2	-7.7(3.5)	-0.9(10.4)	-11.5(-0.2)	2.2(13.5)	6.8(6.9)	13.7(13.7)
P3	-20.2(-5.9)	-8.7(8.2)	-21.9(-5.6)	-6.7(-3.2)	11.5(14.1)	15.2(2.4)
P4	-11.4(-0.3)	6.0(21.6)	-7.0(8.4)	1.9(4.7)	17.4(21.9)	8.9(-3.7)
P5	-	-	-	-	-	-
P6	-8.3(3.8)	1.1(20.6)	-11.6(6.4)	7.2(10.2)	9.4(16.8)	18.8(3.8)
P7	-17.4(-5.1)	9.4(29.3)	-13.7(2.5)	-6.5(-1.9)	26.8(34.4)	7.2(-4.4)
P8	-12.4(2.9)	-4.5(13.2)	-16.5(-0.2)	0.9(5.4)	7.9(10.3)	17.4(5.6)
P9	-8.1(5.7)	-0.6(17.3)	-14.3(3.4)	-1.6(2.9)	7.5(11.6)	12.7(-0.5)
P10	-9.6(2.7)	2.4(17.4)	-10.7(3.5)	2.8(4.9)	12.0(14.7)	13.5(1.4)
P11	-2.8(8.5)	5.2(20.3)	-4.6(10.3)	1.9(4.0)	8.0(11.8)	6.5(-6.3)
C1	-13.4(-0.7)	-1.7(12.4)	-19.1(-5.5)	3.7(6.2)	11.7(13.1)	22.8(11.7)
C2	-12.7(-0.1)	-2.3(12.2)	-21.3(-7.4)	2.5(5.1)	10.4(12.3)	23.8(12.5)
C3	-13.7(-1.0)	-2.1(12.5)	-20.1(-6.2)	1.3(4.0)	11.6(13.5)	21.4(10.2)
C4	-	-	-	-	-	-
C5	-	-	-	-	-	-
C6	-	-	-	-	-	-
C7	-	-	-	-	-	-

Table 6.2: *Calculated relative Gibbs free energies ,the activation barrier ($\Delta G^{\ddagger}_{TSCT}$) and the Gibbs free energy difference for the formation of PdL$_2$Ph$_2$ species ($\Delta G_{PdL2Ph2}$) in kcal mol^{-1}for the mechanism for the transmetalation between the cis-L$_2$Pd(Ph)(Br) and ZnPhBr. The values are calculated with respect to cis-L$_2$Pd(Ph)(Br) + ZnPhBr separated systems. The Gibbs energy correction was carried out at 298K. In parenthesis are shown the same values calculated without including the dispersion correction to the energy.*

6.4.3 Transmetalation on LPd(Ph)(Br) complexes

As already mentioned, the transmetalation between ZnPhBr nucleophilic species and L_2Pd(Ph)(Br) can occur also through another pathway, which involves initial loss of one ligand to yield LPd(Ph)(Br), followed by the coordination of ZnPhBr to form the adduct CT1. The pathway is qualitatively similar to the one seen for the process involving L_2Pd(Ph)(Br). We have shown that three isomers of LPd(Ph)(Br) can exist, depending on the relative positions of the three substituents. Nevertheless, these species, arising from the oxidative addition, are largely unstable if compared with L_2Pd(Ph)(Br). For such reason, we assumed that *trans*-L_2Pd(Ph)(Br) is the only species that can exist after the oxidative addition, and also for the transmetalation of LPd(Ph)(Br) we considered the former as reactants.

In Table 6.3 are reported the relative free energies for the different species involved in such pathway, taking *trans*-[L_2Pd(Ph)(Br) + ZnPhBr as reference.

- **PR_3 Ligands**

  The data collected in Table 6.3 show that not all the points could be located on the potential energy surface. In particular, only for 5 phosphines (P1,P4,P5,P6,P8) the reaction path could be characterized. The energy of the adduct CT1 reflects the energetic associated to substitution of L by ZnPhBr. All the values are positive, except for $P(tbu)_3$ (P5), thus showing that the steric bulk of P5, the loss of a ligand is energetically favored. The fact that all the other values are positive indicates that ZnPhBr is a weaker ligand to Pd. The reaction energies for the formation of CT1 range from ΔG = -4.1 kcal mol^{-1}(P5) to 24.9 kcal mol^{-1}(P1). These values are not sensibly affected when no dispersion corrections are included. In particular, when no dispersion corrections are included, the process is slightly more favored, except for P1, which shows an increase of 6.7 kcal mol^{-1}.

  The most significant variation is shown by P5 (-8.2 kcal mol^{-1}).

  The activation energies are significant for the aromatic systems, $\Delta G^{\ddagger}$ = 23.5 kcal mol^{-1}(P8) and $\Delta G^{\ddagger}$ = 22.5 kcal mol^{-1}(P6), whereas $\Delta G^{\ddagger}$ = 2.2 kcal $mol^{-1}$for P4. The increases of the activation barriers in absence of the dispersion corrections are lower for all the systems: from + 2.1 kcal mol^{-1}(P4) to + 2.5 kcal mol^{-1}(P5). Conversely, P1 does not show any increase with respect to the separate reactants.

  The formation of CT2 is an exoergonic process for P1 and P5 (ΔG = -5.8 kcal $mol^{-1}$and ΔG = -22.0 kcal mol^{-1}), while it is endoergonic for the other systems, ΔG = 4.1 kcal mol^{-1}(P4). When the dispersion corrections are not included, the formation of CT2 is slightly more favored, except for P1, $\Delta\Delta G$ = + 6.7 kcal mol^{-1}. For the other systems, the values of $\Delta\Delta G$ range from -4.9 kcal mol^{-1}(P5) to 0.6 kcal mol^{-1}(P8).

  The decoordination of $ZnBr_2$ from *cis*-[$LPdPh_2$] is endoergonic for all the systems, with energetic values ranging from ΔG = 15.1 kcal mol^{-1}(P5) to ΔG = 28.7 kcal mol^{-1}. No transition state could be located on the potential energy

surface. When no dispersion corrections are included, such process is more favored for all the systems, except for P1. The values of $\Delta\Delta G$ range from -9.1 kcal mol^{-1}(P8) to -11.5 kcal mol^{-1}(P5). This can be explained by the loss of many stabilizing interactions in the CT2 adduct, which leads to a its destabilization and to a less endoergonic decoordination.

- **NHCs Ligands**

  For the NHC ligands, because of the strong donating power of the carbenes, the substitution reaction forming CT1 is considerably more endoergonic than in the case of the phosphines. The energetic values for such process range from ΔG = 11.9 kcal mol^{-1}(C4) to ΔG = 46.9 kcal mol^{-1}(C3). This energy of reaction is also influenced if the dispersion corrections are not included. In the case of C4 and C6 the process becomes exoergonic (ΔG = -3.6 kcal $mol^{-1}$and ΔG = -4.3 respectively). The energy decreases for the other systems is *ca* 3 - 11 kcal mol^{-1}.

  The values of the activation barriers range from $\Delta G^{\ddagger}$ = 2.3 kcal mol^{-1}(C1) to 26.0 kcal mol^{-1}(C4). The increase of such values, due to the dispersion corrections, are not significative, and range from $\Delta\Delta G$ = 0.1 kcal mol^{-1}(C1) to $\Delta\Delta G$ = 3.3 kcal mol^{-1}(C6).

  The formation of CT2 is an endoergonic process for all the carbenes, except for C6, for which is isoergonic (ΔG = 0.1 kcal mol^{-1}). The ΔG values range from 3.8 kcal mol^{-1}(C4) to ΔG = 26.2 kcal mol^{-1}(C3). The inclusion of the dispersion corrections making this process more energetically favored, except for C2 and C3 ($\Delta\Delta G$ = 2.5 kcal $mol^{-1}$and ($\Delta\Delta G$ = 2.3 kcal mol^{-1}respectively).

  The decoordination of $ZnBr_2$ from *cis*-[$LPdPh_2$] is endoergonic for all the systems, with energetic values ranging from ΔG = 13.2 kcal mol^{-1}(C6) to ΔG = 23.2 kcal mol^{-1}(C4). No transition state could be located on the potential energy surface. The inclusion of the dispersion corrections makes this process more energetically favored, except for C3 ($\Delta\Delta G$ = 0). The energy lowering range from $\Delta\Delta G$ = -12.2 kcal mol^{-1}(C7) to $\Delta\Delta G$ = -9.4 kcal mol^{-1}(C2).

In order to visualize the different possible pathways for the transmetalation, starting from *trans*-L_2Pd(Ph)(Br), in Figures 6.12 and 6.13 are shown the energetic pathways for the transmetalation on *trans*-$(PH_3)_2$Pd(Ph)(Br) and *trans*-$(PIpr_3)_2$Pd(Ph)(Br).

In both the cases, the associative pathway, involving L_2Pd(Ph)(Br), is the more accessible one in energy. In the case of L=PH_3, the direct transmetalation on L_2Pd(Ph)(Br) is favored, with either *trans*- L_2Pd(Ph)(Br) ($\Delta G^{\ddagger}$ = 11.2 kcal mol^{-1}) and *cis*-L_2Pd(Ph)(Br) ($\Delta G^{\ddagger}$ = 4.8 kcal mol^{-1}). However, the energetic cost for the isomerization from *trans*-L_2Pd(Ph)(Br) to *trans*-L_2Pd(Ph)(Br) has an energetic cost of ΔG = 5.1 kcal mol^{-1}, makes the transmetalation of *trans*-L_2Pd(Ph)(Br) the preferred pathway. The dissociative pathway, which involves the loss of a ligand from L_2Pd(Ph)(Br), is energetically disfavored ($\Delta G^{\ddagger}$ = 27.7 kcal mol^{-1}) because

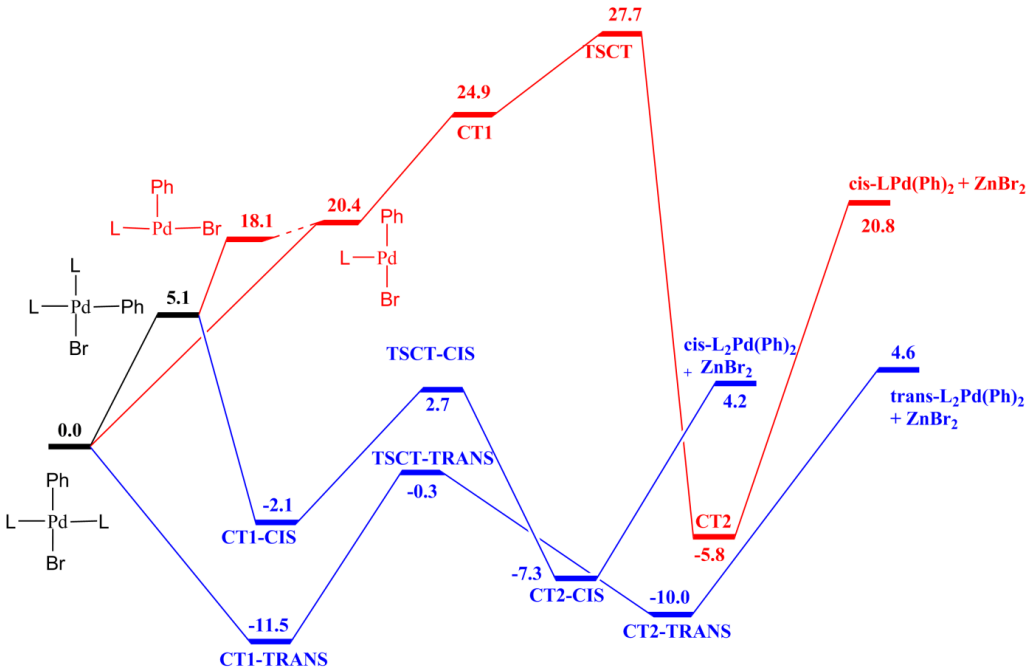

Figure 6.12: *Reaction paths for the transmetalation of trans-$(PH_3)_2$Pd(Ph)(Br). In red is highlighted the dissociative pathway, involving LPd(Ph)(Br), while in blue the associative one, involving L_2Pd(Ph)(Br).*

of the energy required to cleave the L-Pd bond. Among the three possible isomers of LPd(Ph)(Br), the one with ligand and bromide in *trans* is the most stable (ΔG = 18.1 kcal mol^{-1}), but is not suitable for the process and then an isomerization to the LPd(Ph)(Br) with phenyl and bromide in trans is required.

For L=P(Ipr)$_3$, the dissociative pathway is shifted higher in energy ($\Delta G^{\ddagger}$ = 36.1 kcal mol^{-1}) because of the high donor power of the ligand that makes more difficult the loss of one ligand from L_2Pd(Ph)(Br). Furthermore, the loss of a ligand from *trans*-L_2Pd(Ph)(Br) yielding LPd(Ph)(Br) with phenyl and bromide in *trans* is higher in energy (ΔG = 24.6 kcal mol^{-1}). Therefore, the associative pathway involving *cis*-L_2Pd(Ph)(Br) has an higher energetical cost ($\Delta G^{\ddagger}$ = 17.3 kcal mol^{-1}).

The isomerization from *trans*-L_2Pd(Ph)(Br) to *cis*-L_2Pd(Ph)(Br) is higher in energy (ΔG = 13.5 kcal mol^{-1}). Therefore, the associative pathway involving *cis*-L_2Pd(Ph)(Br) has an higher energetical cost. This suggests that, for L=P(Ipr)$_3$, the only possible pathway is the associative one involving *trans*-L_2Pd(Ph)(Br), even if it exhibits an activation barrier of $\Delta G^{\ddagger}$ = 23.1 kcal mol^{-1}.

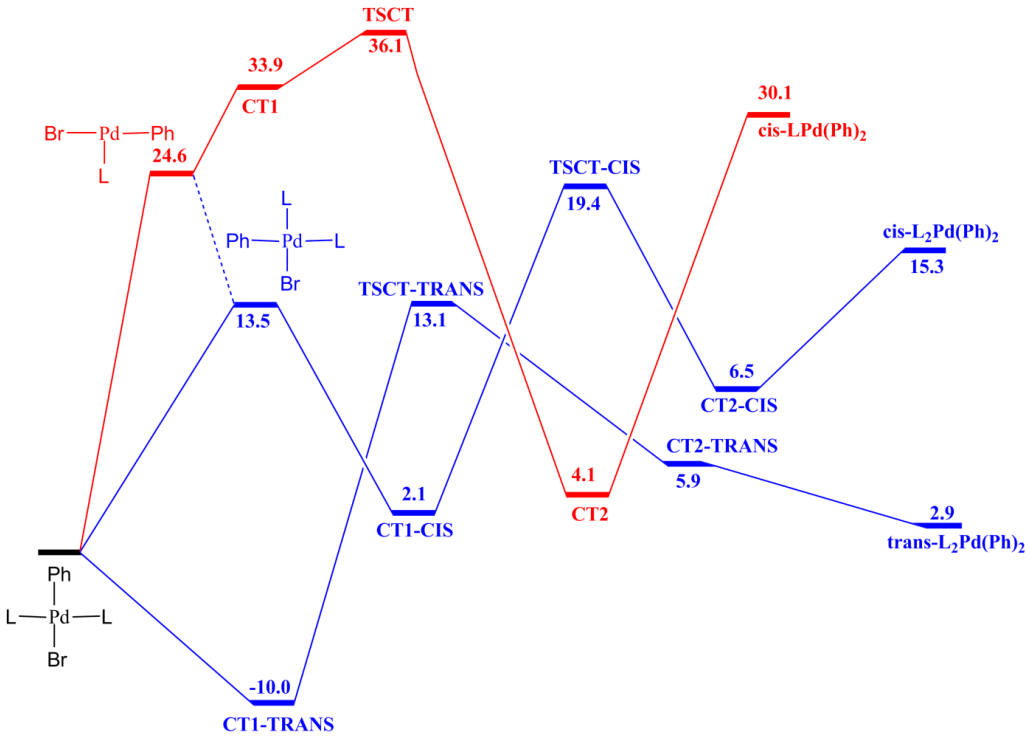

Figure 6.13: *Reaction paths for the transmetalation of trans-$(PIpr_3)_2Pd(Ph)(Br)$. In red is highlighted the dissociative pathway, involving LPd(Ph)(Br), while in blue the associative one, involving $L_2Pd(Ph)(Br)$.*

	[LPd(PhBr)] complexes					
Ligand	**CT1**	**TSCT**	**CT2**	**PdLPh$_2$(cis)+ZnBr$_2$**	Δ**G**$^{\ddagger}_{TSCT}$	Δ**G**$_{PdLPh2}$
P1	24.9(31.6)	27.7(34.4)	-5.8(0.9)	20.8(27.6)	2.8(2.8)	26.6(26.7)
P2	-	-	-	-	-	-
P3	-	-	-	-	-	-
P4	33.9(28.9)	36.1(33.2)	4.1(-0.1)	30.1(15.7)	2.2(4.3)	26.0(15.8)
P5	-4.1(-12.3)	0.4(-5.3)	-22.0(-26.9)	-6.9(-23.3)	4.5(7.0)	15.1(3.6)
P6	16.0(11.5)	38.5(35.3)	2.2(-2.3)	28.7(12.8)	22.5(23.8)	26.5(15.1)
P7	-	-	-	-	-	-
P8	13.1(12.4)	36.6(37.5)	2.6(2.0)	31.3(21.4)	23.5(25.1)	28.7(19.4)
P9	-	-	-	-	-	-
P10	-	-	-	-	-	-
P11	-	-	-	-	-	-
C1	44.9(40.6)	47.2(43.1)	24.5(20.4)	43.3(29.7)	2.3(2.5)	18.8(9.3)
C2	46.7(48.9)	50.0(52.4)	26.0(28.5)	44.7(37.8)	3.3(3.5)	18.7(9.3)
C3	46.9(49.1)	49.6(51.9)	26.2(28.5)	44.6(46.9)	2.7(2.8)	18.4(18.4)
C4	11.9(-3.6)	37.9(23.3)	3.8(-10.8)	27.0(1.5)	26.0(26.9)	23.2(12.3)
C5	40.9(30.1)	44.9(34.2)	21.5(11.3)	39.9(17.6)	4.0(4.1)	18.4(6.3)
C6	13.5(-4.3)	21.5(7.0)	0.1(-14.3)	13.3(-13.1)	8.0(11.3)	13.2(1.2)
C7	42.1(30.1)	46.6(35.1)	24.8(13.8)	40.7(17.5)	4.5(5.0)	15.9(3.7)

Table 6.3: *Calculated relative Gibbs free energies ,the activation barrier ($\Delta G^{\ddagger}_{TSCT}$) and the Gibbs free energy difference for the formation of PdLPh$_2$ species (ΔG_{PdLPh2}) in Kcal mol^{-1} for the mechanism for the transmetalation between [PdLPhBr] complexes and ZnPhBr. The values are calculated respect to PdL$_2$PhBr (trans) + ZnPhBr separated systems. The Gibbs energy correction was carried out at 298K. In the parenthesis are shown the same values calculated without including the dispersion correction to the energy.*

6.5 Conclusions

In this chapter, we have carried out a computational analysis on the transmetalation step from $L_nPd(Ph)(Br)$, with different ligands among tertiary phosphine and N-heterocylic carbenes, and ZnPhBr as the nucleophile species. The general mechanism involves the approach of ZnPhBr on the palladium, through a Pd-Zn-Br three centers coordination, to form CT1 species. Then the cleavage of the Pd-Br bond and the formation of the Pd-C bond is effective through TSCT, leading to CT2. The decoordination of $ZnBr_2$ to form $L_nPd(Ph)_2$, in absence of additional species that can favor it, is the most expensive step in terms of energy. Different isomers of $L_nPd(Ph)(Br)$, arising from the oxidative addition, can undergo the transmetalation. In particular, $L_nPd(Ph)(Br)$ can exist in two conformations, *cis* and *trans*, whereas, LPd(Ph)(Br) can exist in three conformations. We have always considered *trans*-$L_2Pd(Ph)(Br)$ and *cis*-$L_2Pd(Ph)(Br)$ as reference, since they are the most stable complexes. In the path involving *trans*-$L_2Pd(Ph)(Br)$, the stationary points relative to bulky systems, such as $P(tbu)_3$ and the biggest carbenes, could not be located on the potential energy surface. In the formation of CT1-TRANS and in the Pd-C bond formation, through TSCT-TRANS, no remarkable difference can be observed for the phosphines and the carbenes. In all the cases, except for $P(Cy)_3$, the formation of CT1-TRANS is an exoergonic process, and the energetic barriers for the Pd-C bond formation are not so different among the phosphines. The difference between phosphine and the smallest carbenes is in the different relative stability of CT2-TRANS, more stable for the carbenes. Because of such stabilization, carbenes exhibit higher ΔG values relative to the formation *trans*-$PdL_2(Ph)_2$. The same trend can be seen in the mechanism involving *cis*-$L_2Pd(Ph)(Br)$: for the bulky systems no stationary point could be located on the potential energy surface, the formation of CT1-CIS is an exoergonic process for all the ligands, and no remarkable difference can be observed between phosphines and carbenes in the activation barriers. Also in the case of the carbenes, the formation of CT2-CIS is much more exoergonic than the same process relative to the phosphine and, therefore, the process that leads to the *cis*-$PdL_2(Ph)_2$ is much more endoergonic for the carbenes. In the case of the path involving LPd(Ph)(Br), the reactions path for several phosphines could not be characterized. The formation of CT1 is an endoergonic process for all the systems, except for $P(tbu)_3$, and, in particular, much more expensive in terms of energy for the carbenes. The systems bearing aliphatic ligands and carbenes exhibit the lowest activation barriers. The formation of CT2 is an endoergonic process for all the systems, except for PH_3 and $P(tbu)_3$. The formation of LPd(Ph)(Br) + $ZnBr_2$ is more favored for the carbenes systems. In brief, we have shown that the energetic path involving *trans*-$PdL_2(Ph)(Br)$ and *cis*-$PdL_2(Ph)(Br)$ are much more favored for the phosphines, while carbenes ligand are not suitable for such transformation. The energetic path involving LPd(Ph)(Br) is more favored for the aliphatic systems and for the carbene ligands.

Bibliography

[1] Garcia-Melchor, M.; Braga, A.; Lledos, A.; Ujaque, G.; Maseras, F. *Acc. Chem. Res.* **2013**, *46*, 2626.

[2] Espinet, P.; Echavarren, A. *Angew. Chem. Int. Ed.* **2004**, *43*, 4704.

[3] Suzaki, Y.; Yagyu, T.; Osakada, K. *J. Organomet. Chem.* **2007**, *692*, 326.

[4] He, C.; Ke, J.; Xu, H.; Lei, A. *Angew. Chem. Int. Ed.* **2013**, *52*, 1527.

[5] Negishi, E. *Bull. Chem. Soc. Jpn.* **2007**, *80*, 233.

[6] Negishi, E.; Hu, Q.; Huang, Z.; Qian, M.; Wang, G. *Aldrichimica Acta* **2005**, *38*, 71.

[7] Phapale, V.; Cardenas, D. *Chem. Soc. Rev.* **2009**, *38*, 1598.

[8] Perdew, J.; Burke, K.; Ernzerhof, M. *Phys. Rev. Lett.* **1996**, *77*, 3865–3868.

[9] Perdew, J.; Burke, K.; Ernzerhof, M. *Phys. Rev. Lett.* **1997**, *78*, 1396.

[10] Andrae, D.; Haubermann, U.; Dolg, M.; Stoll, H.; Preub, H. *Theor. Chim. Acta* **1990**, *77*, 123.

[11] Ehlers, A.; Bohme, M.; Dapprich, S.; Gobbi, A.; Hollwarth, A.; Jonas, V.; Kohler, K.; Stegmann, F.; Veldkamp, A.; Frenking, G. *Chem.Phys.Lett.* **1993**, *208*, 111.

[12] Neese, F. *Comput. Mol. Sci.* **2012**, *2*, 73.

[13] Grimme, S.; Antony, J.; Ehrlich, S.; Krieg, H. *J. Chem. Phys.* **2010**, *132*, 1456.

[14] Grimme, S.; Ehrlich, S.; Goerigk, L. *J.Comput.Chem.* **2011**, *32*, 1456.

[15] Garcia-Melchor, M.; Fuentes, B.; Lledos, A.; Casares, J.; Ujaque, G.; Espinet, P. *J. Am. Chem. Soc.* **2011**, *133*, 13519.

Chapter 7

Reductive Elimination

7.1 Synopsis

In general, the final step in a catalytic cycle is reductive elimination from Pd(II), to form the C-C or C-X bond in the product, with simultaneous regeneration of the Pd(0) catalyst.[1] As well in the oxidative addition (see chapter 5), in this step there could be questions of selectivity. Also the reaction conditions, such as solvent, the temperature and ligands properties, can have a crucial impact on such step.

In this chapter we carried out a computational analysis on the reductive elimination of biphenyl (Ph-Ph) from L_2PdPh_2 complexes with different ligands (tertiary phosphines (PR_3) and N-heterocyclic carbenes (NHC)). (see Figure 7.3). Our goal was to investigate how the energetic barriers of the process ($\Delta E^{\ddagger}$) were influenced by the different electronic properties of each ligand. Such electronic effects were studied by applying the innovative CD-NOCV (*Charge Displacement by Natural Orbitals for Chemical Valence*) analysis on the L-Pd bond, which provides a description of a chemical bond in terms of charge tranfsers between two chemical fragments in different symmetries (σ-donation and π-backdonation). In particular we are interested to examinate how such bond components change going from $L_2Pd(Ph)_2$ catalyst to the $[L_2Pd(Ph_2)]^{\ddagger}$ transition states and how they influence the energetic barriers.

7.2 Computational methodology

Geometry optimizations and the frequency analysis have been performed with the Gaussian 09 package, at DFT level, using the Perdew, Burke and Ernzerhof exchange correlation functional (PBE0).[2,3] The palladium atom was represented by the relativistic effective core potential (RECP) from the Stuttgart group and the associated basis set,[4] augmented by an f polarization function.[5]

All the other atoms (C,H,P,O,N) were represented by a SVP basis set. For each geometry (TS and minima) a single point calculation has been carried out with the Orca package,[6] using an effective core potential for palladium, and a QZVPP basis set for the other atoms. Influence of the dispersion interactions was considered by

adding to the SCF energy the D3(BJ) corrections as described by Grimme.[7,8] All of the energies reported in the present work are obtained by summing SCF energies, the Gibbs correction at 298 K and the D3(BJ) dispersion correction.

NBO analysis was performed with the Gaussian 09 package, using the Perdew, Burke and Ernzerhof exchange correlation functional (PBE0).[2,3] The palladium atom was represented by the relativistic effective core potential (RECP) from the Stuttgart group and the associated basis sets,[4] augmented by an f polarization function.[5] All the others atoms (C,H,P,O,N) were represented by a TZVP basis set.

The CD-NOCV analysis was performed by means of Density Functional Theory (DFT) with the Amsterdam Density Functional (ADF) package[9,10] using the Perdew, Burke and Ernzerhof (PBE0) exchange-correlation functional and all electron triple-ζ basis set with two polarization functions (TZ2P) for all atoms. Relativistic effect were included by means of the zeroth-order regular approximation (ZORA) Hamiltonian.[11–13]

The NOCV orbitals and ETS-NOCV analysis have been worked out using the keyword ETSLOWDIN in the ADF program suite.

As an example of application of the CD-NOCV analysis of donation and back-donation we report the case of Trans-Pd$(PH_3)_2(Ph)_2$. The relevant fragments here are one ligand PH_3 and Pd$(PH_3)(Ph)_2$, and the integration (z) axis is the one joining the phosphorus of the former ligand and the palladium atom. We label the NOCV orbital pairs, and the associated $\Delta\rho'$ components by an integer k=1,2,... in order of decreasing eigenvalue. The four main charge rearrangments occurring upon the formation of the Pd-P bond are shown in Figure 7.1: a (largely dominating) donating component ($\Delta\rho_1{}'$) and three smallest components of back-donation ($\Delta\rho_2{}'$, $\Delta\rho_3{}'$ and $\Delta\rho_4{}'$).

Visual inspection of the first three $\Delta\rho'$ isodensity surface shown in Figure 7.1 indicates that (i) $\Delta\rho_1{}'$ correlates with the σ-donation from the phosphorus lone pair to the d_{z^2} orbital of palladium (note that blue surface identifies charge accumulation on the palladium) (ii) $\Delta\rho_2{}'$ correlates with the π back-donation from palladium to σ^* antibonding orbitals of the phosphines (note that red surface suggest also a charge depletion from the two aromatic rings) (iii) $\Delta\rho_3{}'$ correlates with the donation from palladium to the out-of-plane σ^* orbitals of the phosphine (iiii) $\Delta\rho_4{}'$ correlates with the in-plane σ^* orbitals of the phosphine.

In Figure 7.2 are shown the CD functions associated with the first four components $\Delta\rho_k{}'$. While Δ(q) curves accurately depict charge displacement over the whole molecular region, one can obtain a resonable measure of donation, back-donation and net charge transfer (CT_{don} CT_{back} and CT_{net}) respectively between the fragments by taking the value of the corresponding CD function at a plausible interfragment boundary along z. Our standard choice is the z point where the densities of each separated fragment do intersect.

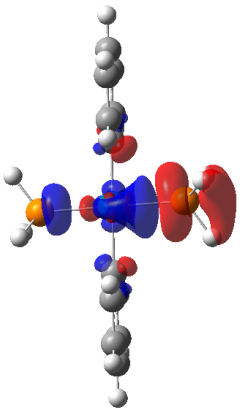

(a) $\Delta\rho_1{}'$

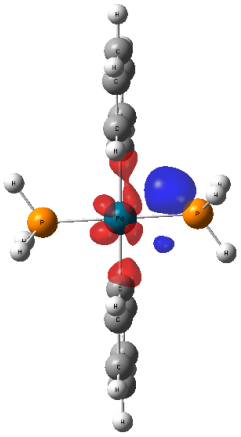

(b) $\Delta\rho_2{}'$

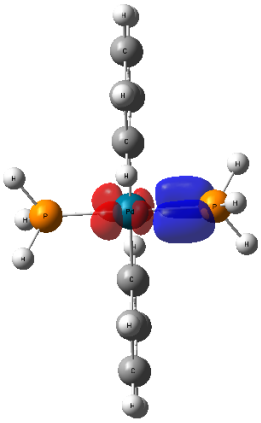

(c) $\Delta\rho_3{}'$

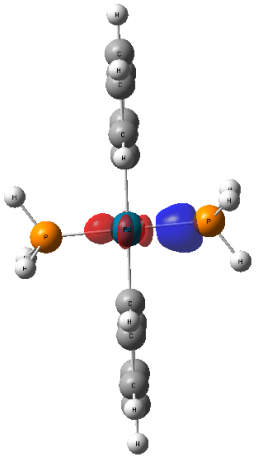

(d) $\Delta\rho_4{}'$

Figure 7.1: *Isodensity surfaces ($\pm$0.002 e/a.u.^{3}) for $\Delta\rho_1{}'$ (a) , $\Delta\rho_2{}'$ (b), $\Delta\rho_3{}'$ (c) and $\Delta\rho_4{}'$ (d) superimposed to the molecular structure of the Trans-Pd(PH$_3$)$_2$(Ph)$_2$. Red surfaces (negative values) identify charge depletion areas, and blue surfaces (positive values) identify charge accumulation areas.*

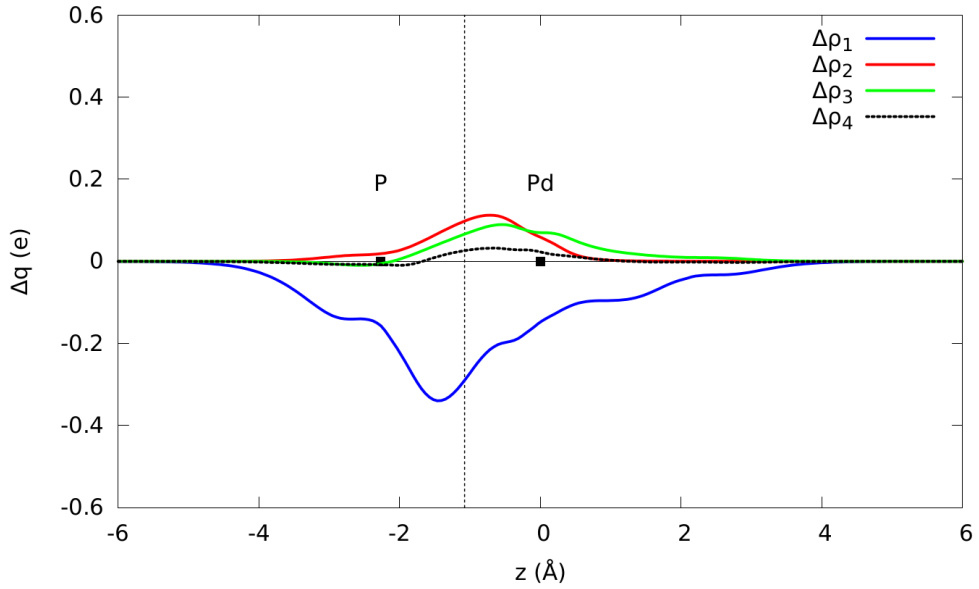

Figure 7.2: *CD functions associated with the first four $\Delta\rho_k{}'$ components for Trans-Pd(PH$_3$)$_2$(Ph)$_2$. The blue line represents the donation L→Pd, while the green, red and dashed black curves represent the back-donation L←Pd. The black dots represent the position of the atoms on the integration axis (z in this case), while the vertical dashed line represents the z value in which the charge transfers are taken (the so called isoboundary).*

7.3 Pathways Manifold

As already mentioned, in this chapter we carried out a computational analysis on the reductive elimination of biphenyl (Ph-Ph) from L$_2$Pd(Ph)$_2$ complexes with different ligands (L), among tertiary phosphines (PR$_3$) and N-heterocyclic carbenes (NHC). (see Figure 7.3).

The reductive elimination of biphenyl (Ph-Ph) from [L$_2$Pd(Ph)$_2$] complexes involves the formation of a new C-C bond between the two phenyl rings and the regeneration of the initial Pd(0) catalyst. There are several pathways for this process (see Figure 7.4).

The [L$_n$Pd(Ph)$_2$] (n=1,2) complexes, which undergo the reductive elimination, are formed in the transmetallation process (see Chapter 6). The latter process can occurs with different isomers of palladium complexes, depending on the relative positions (*cis* or *trans*) and the number (n=1,2) of the ligands bonded to palladium. In particular, for [L$_2$Pd(Ph)$_2$] species, both isomers can be obtained from the transmetalation process, and, in addition, an isomerization between these two species is possible. No transition state for such isomerization could be located on the potential energy surface. However, a direct elimination from [L$_2$Pd(Ph)$_2$] complexes is possible only from the *cis* isomer, through the TSL$_2$ transition state (see Figure 7.6).

Also in the case of the [LPd(Ph)$_2$] complexes, only the *cis* isomer can be ob-

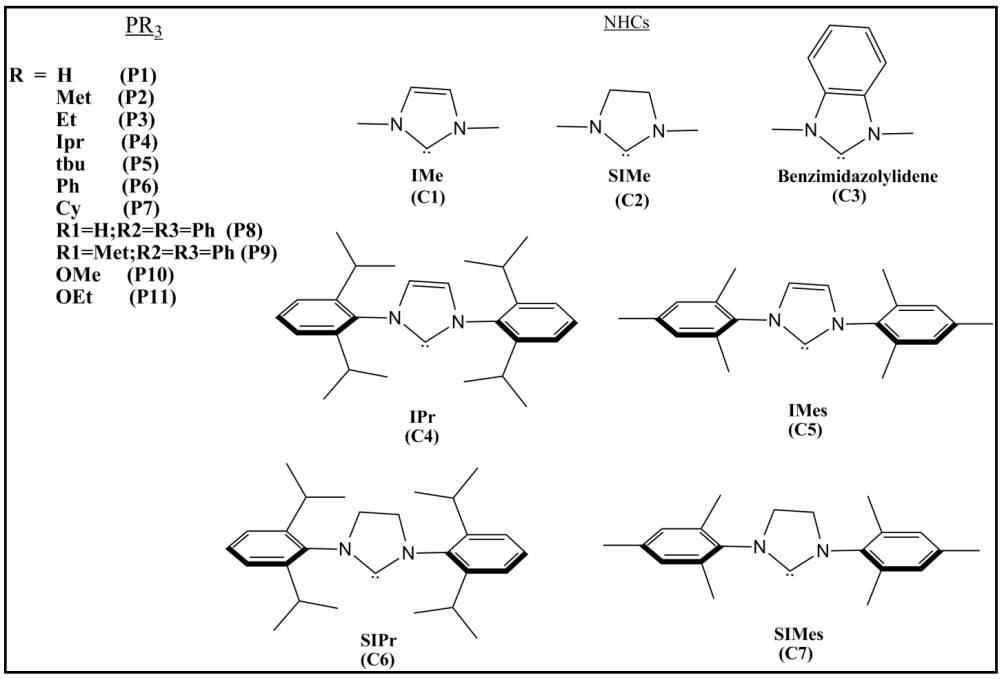

Figure 7.3: *List and abreaviations for the ligands (L) considered in the present work.*

tained. Once formed, such species can undergo two different process: the addition of a second ligand to form $[L_2Pd(Ph)_2]$, or the reductive elimination through the transition state TSL-Cis

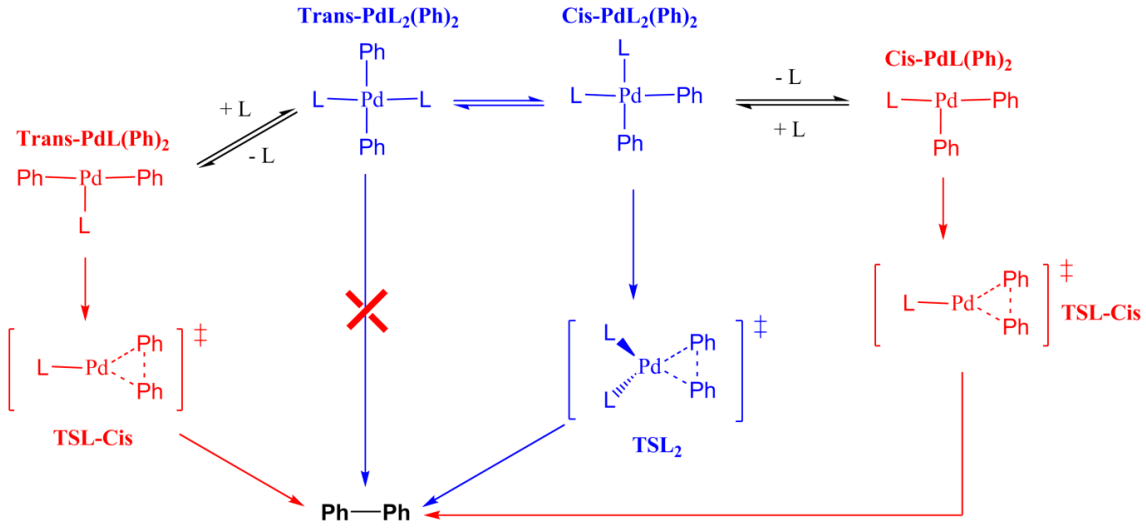

Figure 7.4: *Different pathways for the reductive elimination of Ph-Ph from $[L_nPd(Ph)_2]$ complexes (n=1,2). In blue is highlighted the direct elimination from $[L_2Pd(Ph)_2]$ complexes, while in red the dissociative pathway.*

Once $L_2Pd(Ph_2)$ is formed upon the transmetalation, it can undergo different processes. (i) The direct reductive elimination through TSL_2, yielding PdL_2 catalyst and Ph_2 species (blue path in Figure 7.5). In this case, only Cis-$PdL_2(Ph_2)$

can undergo the direct reductive elimination, because of the more stable isomer Trans-$PdL_2(Ph)_2$. (ii) The isomerization yielding Trans-$PdL_2(Ph)_2$, more stable with respect to the *cis* one, and then, upon the loss of a ligand and the formation of [$LPd(Ph)_2$] species, the reductive elimination through TSL-Cis transition state. [$LPd(Ph)_2$] species can exist in two different conformations (Cis-$PdLPh_2$ and Trans-$PdLPh_2$) with the two phenyl groups *cis* and *trans* to each other respectively. In general, LPh_2-Trans is much more destabilized with respect LPh_2-Cis, therefore the isomerization process from the former to the latter is thermodynamically favored. (iii) The dissociative pathway, which involves the loss of a ligand from [$L_2Pd(Ph)_2$] to form [$LPd(Ph)_2$], followed by the reductive elimination through the TSL-Cis transition state.

The competition between these three possible pathways , as well as the activation barriers, significantly depends on the size and the electronics of the ligand.

7.4 Energetic aspects

As an example, we report in Figure 7.5 the general energetic pathway for the reductive elimination of Ph_2 from *cis*-[$(PH_3)_2Pd(Ph_2)$]. Among the two $L_2Pd(Ph)_2$ complexes, the *cis* one is more stable than the *trans* by 0.4 kcal mol^{-1}. The direct reductive elimination from *cis*-[$(PH_3)_2Pd(Ph_2)$], through TSL_2 (Figure 7.6), exhibits a barrier of $\Delta G^{\ddagger}$ = 9.4 kcal mol^{-1}. The dissociative pathway, involves the loss of a ligand to form *cis*-$PdL_2(Ph)_2$ (ΔG= 3.4 kcal mol^{-1}) and the formation of C-C bond through TSL-Cis (Figure 7.6). The two possible transition states, TSL_2 and TSL-Cis, show different bond distance between the carbons of the phenyl rings (1.983 Åand 2.173 Årespectively). This suggest that in TSL_2 the formation of Ph-Ph is well advanced, and, in theory, this species is higher in energy. The pathway that involves the isomerization from *cis*-[$(PH_3)_2Pd(Ph_2)$] to *trans*-[$(PH_3)_2Pd(Ph_2)$] (ΔG= 0.4 kcal mol^{-1}), followed by the loss of a ligand to form *trans*-$PdL(Ph)_2$ (ΔG= 10.9 kcal mol^{-1}) and the formation of Ph-Ph throug TSL-Cis is not energetically favored. Indeed, over the isomerization to form *trans*-$PdL_2(Ph)_2$, in order to have the reductive elimination, a further isomerization to form *cis*-$PdL(Ph)_2$ is required. In theory, this latter step passes through a transition state, which could be not located on the potential energy surface.

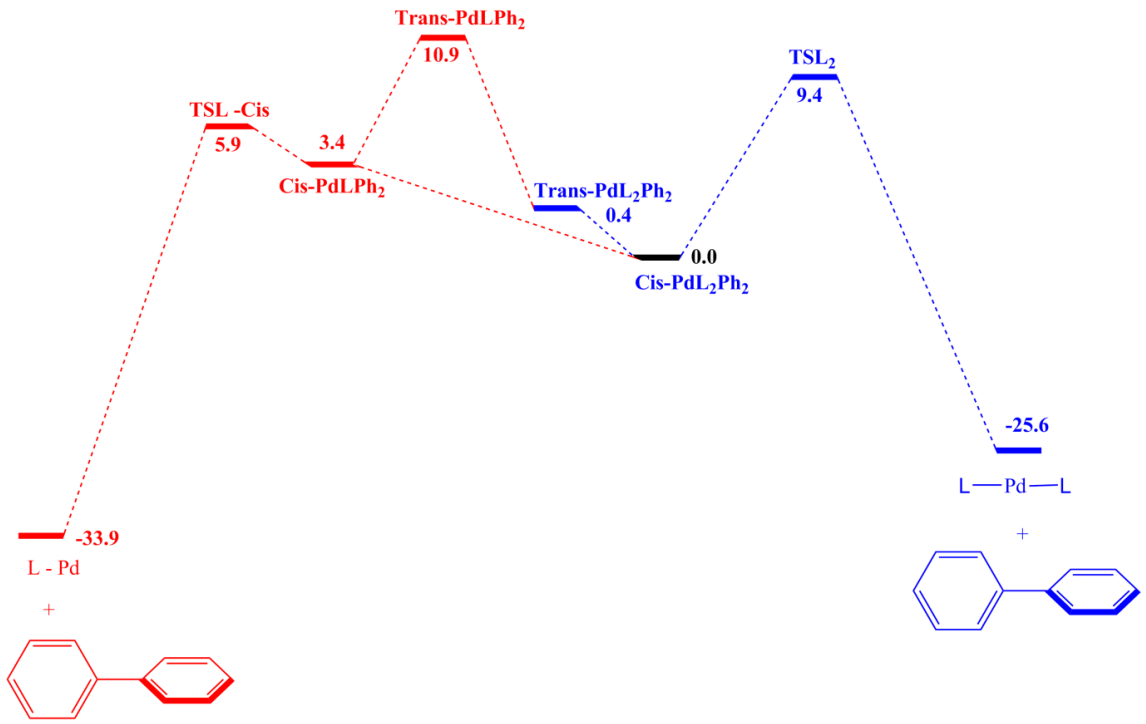

Figure 7.5: *Different pathways for the reductive elimination of Ph-Ph starting from cis [$L_2Pd(Ph)_2$] complexes. In blue is highlighted the direct elimination from [$L_2Pd(Ph)_2$] complexes, while in red the dissociative pathway.*

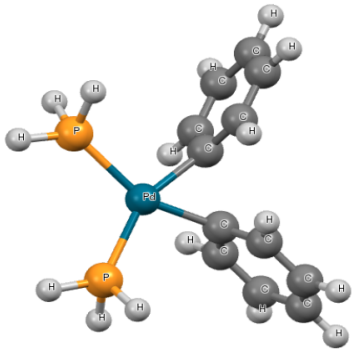

(a) TSL_2

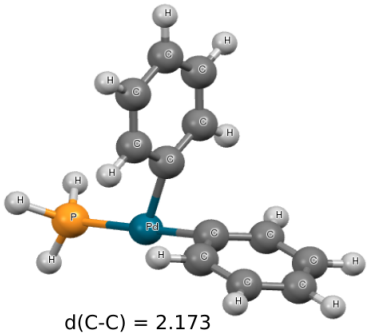

(b) TSL-Cis

Figure 7.6: *Structures of the transition states, bearing PH_3 as ligand, relative to the two pathways considered: direct (TSL_2) and dissociative (TSL-Cis).*

7.4.1 Direct Pathway from L_2PdPh_2-Cis

In Table 7.1 are reported the relative free energies for the different species involved in the direct reductive elimination from from the *cis* isomer of $[L_2Pd(Ph)_2]$

Ligand	*trans*-$PdL_2(Ph)_2$	TSL_2	L_2Pd + Ph-Ph
P1	0.4(-0.1)	9.4(9.3)	-25.6(-27.3)
P2	-6.0(-5.5)	12.9(12.3)	-23.4(-28.3)
P3	-5.3(-4.8)	12.4(11.8)	-21.1(-27.4)
P4	-12.5(-10.9)	8.3(7.4)	-32.0(-40.4)
P5	-	-	-
P6	-5.5(-4.9)	3.6(3.3)	-35.6(-37.3)
P7	-10.0(-8.4)	7.8(7.1)	-36.2(-50.3)
P8	0.0(-1.2)	13.8(12.1)	-26.0(-27.7)
P9	-0.1(-1.0)	13.2(11.4)	-20.3(-24.7)
P10	-2.9(-2.3)	13.0(12.1)	-29.7(-28.9)
P11	2.3(2.0)	17.1(15.0)	-21.1(-22.8)
C1	-4.0(-4.0)	22.7(22.0)	-17.5(-24.5)
C2	-4.7(-4.8)	23.6(22.2)	-17.0(-21.9)
C3	-4.0(-4.0)	22.8(21.7)	-12.3(-12.4)
C4	-	-	-
C5	-	-	-
C6	-	-	-
C7	-	-	-

Table 7.1: *Relative free energies (ΔG) for the direct reductive elimination from Cis-$PdPdL_2(Ph)_2$ and the isomerization to its trans conformation. The energetic values, reported in kcal mol^{-1}, are calculated relatively to Cis-$PdL_2(Ph)_2$. In the parenthesis are shown the values calculated without including the dispersion correction to the energy.*

- **PR_3 Ligands**

  The data collected in Table 7.1 show that for all the PR_3 ligands, but P5, all the points could be located on the potential energy surface. In the case of P5, the steric bulk of the ligand prevents the optimization of all the points.

  For all the phosphine series, except for P1, P8 and P11, the isomerization to Trans-$PdL_2(Ph)_2$ is thermodynamically favored, suggesting that the latter isomer is more stable than cis-$PdL_2(Ph)_2$. Unfortunately, no transition state associated with this isomerization process could be located on the potential energy surface. The phosphines bearing aliphatic R groups (P2, P4, P7) are associated with the most stable trans-$PdL_2(Ph)_2$ species (ΔG = -6.0 kcal mol^{-1}, -12.5 kcal $mol^{-1}$and -10.0 kcal mol^{-1}). These values are not sensibily affected when the dispersion corrections are not included. The values of $\Delta\Delta G$ range from 1.6 kcal mol^{-1}(P4 and P7) to -0.5 kcal mol^{-1}(P1). As expected, the most important corrections due to the dispersion corrections are associated with the most bulky ligands (P4 and P7) since there is a large number of pairwise interactions between non-bonded atoms with mutual distance typical of Van der Waals attraction.

  From cis-$PdL_2(Ph)_2$, the C-C bond formation through TSL_2 is associated to

activation barriers ranging from $\Delta G^{\ddagger}$ = 3.6 kcal mol^{-1}(P6) to $\Delta G^{\ddagger}$ = 17.1 kcal mol^{-1}(P11). The phosphite ligands exhibit the highest barriers for the series. The values of these activation barriers are not significantly affected when the dispersion corrections are not included. The $\Delta\Delta G$ values range from -2.1 kcal mol^{-1}(P11) to -0.1 kcal mol^{-1}(P1). The formation of PdL_2 + Ph_2 species is an exoergonic process.

The reaction energies are more affected when no dispersion are considered, with $\Delta\Delta G$ values ranging from -14.1 kcal mol^{-1}(P7) to -1.7 kcal mol^{-1}(P1, P8 and P11). This is due to the fact that, upon the formation of the two fragments PdL_2 and Ph_2, many pairwiese interactions between non-bonded atoms are lost. This destabilizes cis-$PdL_2(Ph)_2$ species much more than thw two separated fragments.

- **NHCs Ligands**

  In the case of the NHC ligands, the steric bulk prevents the characterization of the reaction pathway for C4-C7. Only for the smallest NHC (C1-C3) the points could be located.

  Similarly to the phosphine case, the isomerization yielding trans-$PdL_2(Ph)_2$ is an exoergonic process, with a reaction energy of *ca* -4 kcal mol^{-1}. These values are not altered when the dispersion corrections are not included.

  The activation barriers associated to TSL_2 are higher than the barriers for the phosphine series, with values of ca 22-23 kcal mol^{-1}.

  Similarly to the phosphine series, the formation of L_2Pd + Ph_2 is an exoergonic process, with reaction energies ranging from ΔG = -12.3 kcal mol^{-1}(C3) to ΔG = -17.5 kcal mol^{-1}. The inclusion of the dispersion corrections make more stable the systems bearing C1 and C2 carbenes as ligands ($\Delta\Delta G$ = -7 kcal mol^{-1}and $\Delta\Delta G$ = -4.9 kcal mol^{-1}respectively), whereas C3 is not affected by these corrections.

7.4.2 Dissociative Pathway from L_2PdPh_2-Cis

The dissociative pathway involves the loss of a ligand from L_2PdPh_2 to form cos-$PdL(Ph)_2$ or trans-$PdL(Ph)_2$ (see Figure 7.7) , followed by the formation of the C-C bond through TSL-Cis with the formation of LPd + Ph_2 species.

cis-$PdL_2(Ph)_2$ species can also isomerize to yield L_2PdPh_2-Tr complex, (see Figure 7.7) followed by the loss of a ligand and the formation of LPd + Ph_2 species through TSL-Cis. Starting from L_2PdPh_2, the preference to follow one path with respect to another depends on the size and the elctronics of the ligand.

In Table 7.2 are reported the relative free energies for the different species involved in the dissociatie pathway.

- **PR_3 Ligands**

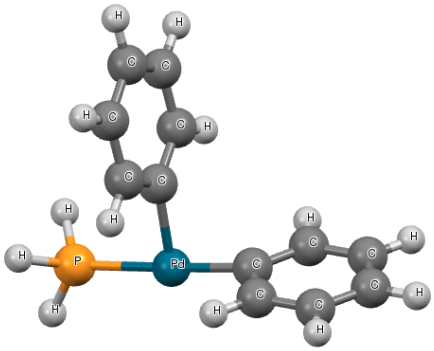

(a) cis-$PdLPh_2$

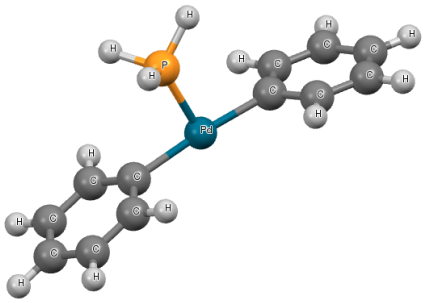

(b) trans-$PdLPh_2$

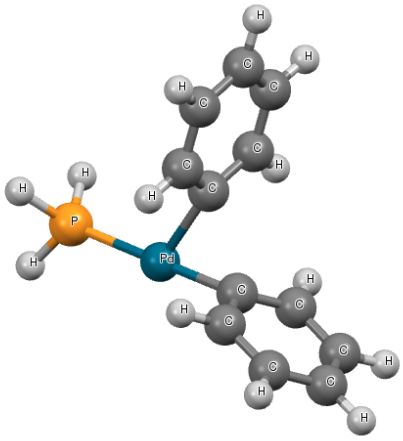

(c) TSL-Cis

Figure 7.7: *Structures of $LPdPh_2$-Cis, $LPdPh_2$-Tr and TSL-Cis , bearing PH_3 as ligand.*

Ligand	trans-PdL_2Ph_2	cis-$PdLPh_2$	trans-$PdLPh_2$	TSL-Cis	LPd + Ph_2	$\Delta G^{\ddagger}$
P1	0.4(-0.1)	3.4(12.2)	10.9(19.1)	5.9(15.0)	-25.6(-27.3)	2.5(2.8)
P2	-6.0(-5.5)	23.9(14.6)	27.5(18.7)	29.6(20.1)	-23.4(-28.3)	5.7(5.5)
P3	-5.3(-4.8)	26.3(13.0)	25.6(13.5)	31.8(18.3)	-5.1(-19.3)	5.5(5.3)
P4	-12.5(-10.9)	14.7(-3.0)	19.7(3.8)	19.9(1.8)	-17.0(-35.7)	5.2(4.8)
P5	0.0	-20.6(-43.2)	-4.9(-25.7)	-16.8(-39.6)	-39.5(-70.0)	3.8(3.6)
P6	-5.5(-4.9)	15.2(-7.0)	22.9(3.2)	19.5(-2.9)	-18.8(-41.9)	4.3(4.1)
P7	-10.0(-8.4)	20.9(-3.9)	22.5(1.0)	26.0(0.7)	-9.5(-35.5)	5.1(4.6)
P8	0.0(-1.2)	25.5(10.8)	32.1(18.7)	28.8(14.7)	-9.3(-23.8)	3.3(3.9)
P9	-0.1(-1.0)	28.0(9.4)	33.4(17.0)	32.3(13.6)	-4.9(-23.9)	4.3(4.2)
P10	-2.9(-2.3)	20.6(10.5)	24.7(15.0)	23.8(13.8)	-15.0(-25.9)	3.2(3.3)
P11	2.3(2.0)	3.4(5.0)	9.0(11.8)	7.0(8.5)	-19.0(-24.6)	3.6(3.5)
C1	-4.0(-4.0)	30.6(21.1)	36.2(27.0)	35.1(25.5)	16.9(1.6)	4.5(4.4)
C2	-4.7(-4.8)	32.5(22.8)	35.8(26.2)	37.3(27.3)	19.1(3.3)	4.8(4.5)
C3	-4.0(-4.0)	32.7(22.7)	37.5(27.7)	37.1(26.9)	17.7(1.7)	4.4(4.2)
C4	0.0	-12.3(-47.3)	-	-8.7(-45.4)	-25.2(-72.9)	3.6(1.9)
C5	0.0	21.9(-7.2)	-	26.5(-4.1)	10.9(-28.2)	4.6(3.1)
C6	0.0	-25.5(-63.0)	-	-19.9(-58.7)	-37.3(-87.5)	5.6(4.3)
C7	0.0	20.6(-9.8)	-	26.7(-4.8)	10.6(-30.3)	6.1(5.0)

Table 7.2: *Relative free energies (ΔG) for the dissociative pathway from cis-$PdL_2(Ph)_2$ and the isomerization to its trans conformation. In red are the values of relative free energies calculated relative to trans-$PdL_2(Ph)_2$. The energetic values, reported in kcal mol^{-1}, are calculated relative to cis-$PdL_2(Ph)_2$. $\Delta G^{\ddagger}$ values are calculated as difference between the relative free energies of TSL-Cis and $LPdPh_2$-Cis. In the parenthesis are shown the same values calculated without including the dispersion correction to the energy.*

For all the PR_3 ligands, but P5, all the points could be located on the potential energy surface. In the case of P5, the steric bulk of the ligand prevents the optimization of cis-$PdL_2(Ph)_2$. This suggests that for this system, upon the transmetalation process, only trans-$PdL_2(Ph)_2$ can be formed and, consequently, only the latter species can take place in the dissociative pathway. In the case of the system bearing P5 as ligand, the dissociative pathway was considered taking trans-$PdL_2(Ph)_2$ as reference, since is the only stable L_2PdPh_2 species arising from the transmetalation process. In Table 7.2, the energetic values calculated reltive to trans-$PdL_2(Ph)_2$ are indicated in red. It was already shown in the previous section that trans-$PdL_2(Ph)_2$ is more stable than L_2PdPh_2-Cis, and then the isomerization from cis-$PdL_2(Ph)_2$ to trans-$PdL_2(Ph)_2$ is thermodynamically favored for all the species, except for P1, P8 and P11.

Conversely, the loss of a ligand from cis-$PdL_2(Ph)_2$ to form cis-$LPd(Ph)_2$ is an endoergonic process, with energetic values ranging from ΔG = 3.4 kcal mol^{-1}(P1 and P11) to ΔG = 28.0 kcal mol^{-1}(P9). In the case of P5, cis-

$PdLPh_2$ is more stable by ΔG = -20.6 kcal $mol^{-1}$with respect trans-$PdL_2(Ph)_2$. When the dispersion corrections to the energy are not included, these values are sensibly altered, leading to an higher stabilization of cis-$PdL(Ph)_2$ of *cis*ca 10-20 kcal mol^{-1}, except for P1 and P11 that exhibit a destabilization of 8.8 and 1.6 kcal mol^{-1}respectively. Once formed, cis-$PdL(Ph)_2$ can also isomerize to yield trans-$PdL(Ph)_2$. Nevertheless, this isomer is much more destabilized than the *cis* one, with energetic values ranging from ΔG = 9.0 kcal mol^{-1}(P11) to ΔG = 33.4 kcal mol^{-1}(P9). In the case of P5, trans-$PdL(Ph)_2$ is destabilized by ΔG = 15.7 kcal mol^{-1}.

In absence of the dispersion corrections, such complexes are more stabilized by *ca* 3-16 kcal mol^{-1}. The bigger the ligand, the more important this corrections will be, leading to significantly different values of reacting energies computed without dispersion corrections. Conversely, because of its destabilization, when trans-$PdL(Ph)_2$ species is formed by the loss of a ligand from L_2PdPh_2-Tr, it fast isomerizes to form cis-$PdLPh_2$. For such reasons, it can be assumed that trans-$PdL(Ph)_2$ species do not partecipate in the dissociative pathway of the reductive elimination. Therefore, the activation barriers $\Delta G^{\ddagger}$ for such pathway are calculated as difference between TSL-Cis and $LPdPh_2$-Cis.

These barriers are quite low, with values ranging from $\Delta G^{\ddagger}$ = 2.5 kcal mol^{-1}(P1) to $\Delta G^{\ddagger}$ = 5.1 kcal mol^{-1}(P7). The absence of the dispersion corrections does not modify these values, with $\Delta\Delta G$ values of *ca* 0.2 - 0.4 kcal mol^{-1}. Despite the lower values of $\Delta G^{\ddagger}$, the dissociative pathway is not energetically favored for the phosphines ligands, since the loss of a ligand from L_2PdPh_2-Cis is a more endoergonic process with respect to the associative one, as shown in the previous section.

- **NHC Ligands**

  In the case of the NHC ligands, the steric bulk of C4-C7 prevents the optimization of trans-$PdL_2(Ph)_2$ and trans-$PdL(Ph)_2$. Consequntly, as well as P5, for the systems bearing such ligands the enrgetic pathway was calculated with cis-$PdL_2(Ph)_2$ as reference (energetic values in red).

  C1-C3

  For the smallest carbenes (C1-C3), the isomerization of cis-$PdL_2(Ph)_2$-Cis to form trans-$PdL_2(Ph)_2$ is an exoergonic process, with ΔG values of *ca* -4 kcal mol^{-1}. The absence of the dispersion corrections does not influence these values. Conversely, the loss of a ligand from trans-$PdL_2(Ph)_2$ to form trans-$PdL(Ph)_2$ exhibits high energy values (ca 32-34 kcal mol^{-1}), as well as the transformation from L_2PdPh_2-Cis to form $LPdPh_2$-Cis (ca 36-37 kcal mol^{-1}).

  The activation barriers $\Delta G^{\ddagger}$ are calculated as difference between TSL-Cis and $LPdPh_2$-Cis. Similarly to the phosphine series, these values are quite low (ca 4 kcal mol^{-1}), and the dispersion corrections do not show any influence on such values.

The formation of LPd + Ph_2 is an endoergonic process, with ΔG values by *ca* 16-19 kcal mol^{-1}. The absence of the dispersion corrections in such case, decrease such ΔG values of ca 15-16 kcal mol^{-1}.

C4-C7

For the biggest carbenes (C4-C7), cis-$PdL_2(Ph)_2$ can not be located on the potential energy surface, and trans-$PdL_2(Ph)_2$ is taken as reference for the calculations of the energetic pathway. In addition, for C4-C7, the steric bulk also prevents the optimization of trans-$PdL(Ph)_2$. The loss of a ligand from trans-$PdL_2(Ph)_2$ to form cis-$PdL(Ph)_2$ is an endoergonic process for C5 and C7 (ΔG = 21.9 kcal $mol^{-1}$and 20.6 kcal mol^{-1}respectively), whereas it is exoergonic for C4 and C6 (ΔG = -12.3 kcal $mol^{-1}$and -25.5 kcal mol^{-1}respectively). When the dispersion corrections are not included, the energetic values for such process are lower, and, in the case of C5 and C7, become negative (-7.2 kcal $mol^{-1}$and -9.8 kcal mol^{-1}respectively). The activation barriers $\Delta G^{\ddagger}$, as well as for the smallest carbenes, exhibit low values, from $\Delta G^{\ddagger}$ = 3.6 kcal mol^{-1}(C4) to $\Delta G^{\ddagger}$ = 6.1 kcal mol^{-1}(C7).

The formation of LPd + Ph_2 is endoergonic for C5 and C7 (ΔG = 10.9 kcal $mol^{-1}$and 10.6 kcal mol^{-1}respectively), whereas is exoergonic for C4 and C6 (ΔG = -25.2 kcal $mol^{-1}$and -37.3 kcal mol^{-1}respectively).

When no dispersion corrections are included, such values are drastically affected. In particular, for C5 and C7, the process becomes exoergonic (ΔG = -28.2 kcal $mol^{-1}$and ΔG = -30.3 kcal mol^{-1}respectively), whereas, for C4 and C6, the $\Delta\Delta G$ values are as high as 47-50 kcal mol^{-1}.

7.5 CD-NOCV Analysis

In this section, we investigate the electronic effect of seven different ligands (Figure 7.8), on the reductive elimination of Ph-Ph from $PdL_2(Ph)_2$. Despite different pathways for such processes are possible, we describe only the dissociative one. In particular, we focused on the dissociative involving trans-PdL_2Ph_2 as a reactant and TSL-Cis as transition state. This is due either to the fact that it allows to identify a specific axis between the ligand and the palladium along the reaction path and the energetic barriers ($\Delta E^{\ddagger}$) are quite different along the ligand series.

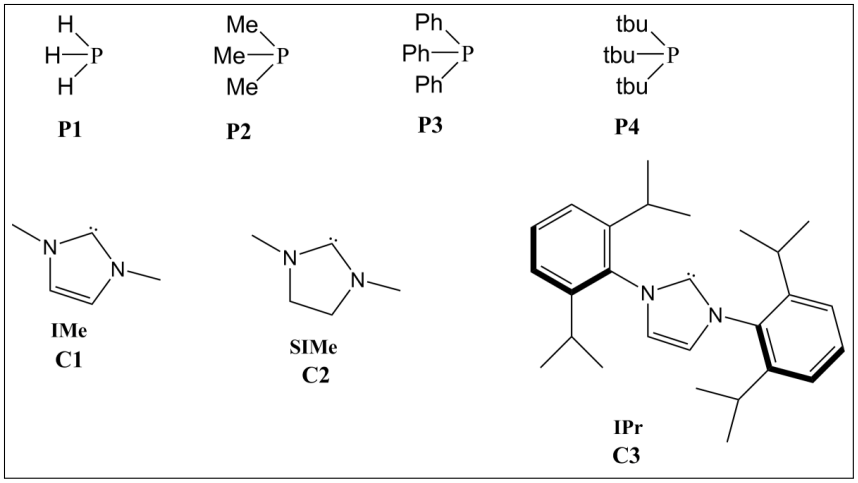

Figure 7.8: *List and abreviations for the ligands (L) considered for the CD-NOCV analysis.*

Our goal was to investigate how the energetic barriers of the process ($\Delta E^{\ddagger}$) were influenced by the electronic properties of each ligand. Such electronic effects were studied by applying the innovative CD-NOCV (*Charge Displacement by Natural Orbitals for Chemical Valence*) analysis on the L-Pd bond, which provides a description of a chemical bond in terms of charge transfer between two chemical fragments in different symmetries (σ-donation and π-backdonation). In particular we were interested to examinate how such bond components change going from L_2PdPh_2 to TSL-Cis transition state and how they influence the energetic barriers. Furthemore we correlated the bond components also with the alteration of L-Pd and C-C bond distances along the path.

In order to compare the properties of the various ligands, we defined relative quantities, ω^{σ}, ω^{π} and K_{L-Pd} as shown in the equation 7.1 - 7.3. These quantities express the variation of some values from L_2PdPh_2 to TSL-Cis.

$$\omega^{\sigma} = \frac{CT_{\sigma}^{(\mathrm{TS})} - CT_{\sigma}^{(0)}}{CT_{\sigma}^{(0)}} = \frac{\Delta CT_{\sigma}}{CT_{\sigma}^{(0)}} \tag{7.1}$$

$$\omega^{\pi} = \frac{CT_{\pi}^{(\mathrm{TS})} - CT_{\pi}^{(0)}}{CT_{\pi}^{(0)}} = \frac{\Delta CT_{\pi}}{CT_{\pi}^{(0)}} \tag{7.2}$$

$$K_{L-Pd} = \frac{d_{\text{L-Pd}}^{(\mathrm{TS})} - d_{\text{L-Pd}}^{(0)}}{d_{\text{L-Pd}}^{(0)}} = \frac{\Delta d_{L-Pd}}{d_{\text{L-Pd}}^{(0)}} \tag{7.3}$$

$CT_{\sigma}^{(\mathrm{TS})}$, $CT_{\pi}^{(\mathrm{TS})}$, $d_{\text{L-Pd}}^{(\mathrm{TS})}$ are the charge transfer between the ligand and the palladium, in the two different symmetries, and the L-Pd bond distance calculated for TSL-Cis.

$CT_{\sigma}^{(0)}$, $CT_{\pi}^{(0)}$ and $d_{\text{L-Pd}}^{(0)}$ are the corresponding values calculated for trans-$PdL_2(Ph)_2$-Tr systems.

The magnitudes ω^{σ}, ω^{π}, K_{L-Pd} represent, respectively, the variations in percentage in the process of reductive elimination of the σ-donation, the π backdonation, and the ligand-palladium bond distance. Positive values of these magnitudes suggest their increase in the process, as well as negative values suggest their decrease.

In Table (7.3) are shown the activation energies ($\Delta E^{\ddagger}$), the ligand-Palladium bond distances (in Angstrom) and charge transfers results (e) obtained from the CD-NOCV analysis relative to either trans-$PdL_2(Ph)_2$ or TSL-Cis.

L_2PdPh_2-Tr complexes

The complexes associated with tertiary phosphines as ligands have longer ligand-palladium bond distances. In particular, P4, because of its steric bulk, shows the longest distance (2.316 Å), whereas the two carbenes C1 and C2 the shortest ones (2.018 Å). Analyzing the DCD components in Table 7.3, in the L_2PdPh_2-Tr systems, $CT_{\sigma}^{(\mathrm{TS})}$ is the more tunable component of the bond, with values ranging from -0.161 e (C3) to -0.206 e (P4). P4 shows the highest σ-donation value toward palladium, and, in general the tertiary phosphines exhibit a higher donor ability with respect the carbenes. P4 exhibits also the lower acceptor ability, with $CT_{\pi}^{(\mathrm{TS})}$ = 0.199 e, whereas P1 the higher $CT_{\pi}^{(\mathrm{TS})}$ value (0.225 e). In general, there is not so much difference in the acceptor capacity between phosphines and carbenes. P4 is the only system that shows a negative value of $CT_{\text{net}}^{(\mathrm{TS})}$ (net charge transfer from ligand to palladium), whereas for the other systems the net charge transfer is toward the ligand.

TSL-Cis complexes

TSL-Cis is the transition state relative to the reductive elimination of Ph_2 from $PdL_2(Ph)_2$ complexes, upon the loss of a ligand. The process that leads to TSL-Cis alterates the L-Pd bond distances and, therefore, the bond components between them.

In TSL-Cis, the $CT_{\sigma}^{(TS)}$ values have a smaller range of variation, from $CT_{\sigma}^{(TS)}$ = -0.177 e (P1) to $CT_{\sigma}^{(TS)}$ = -0.215 e (P4). In general, except for P1, the phosphines exhibit a higher donor power with respect the carbenes. Analyzing the $CT_{\pi}^{(TS)}$ component, once again the phosphines show the higher acceptor power (0.179 e for P1), whereas carbenes and P4 the lowest values, from 0.133 e (P4,C1 and C3) to 0.143 e (C2). Also in TSL-Cis, $CT_{\sigma}^{(TS)}$ is the more tunable component of the L-Pd bond.

Analyzing the values reported in Table 7.4, in the process from L_2PdPh_2-Tr to TSL-Cis, the L-Pd bond distances increase in all the system, and the values of K_{L-Pd} give an indication about such alteration. The systems associated with P4, C1 and C2 ligands show the highest increases of the bond distance (K_{L-Pd} = 0.034, 0.035 and 0.034 respectively). The smallest phosphines (P1 and P2) show the lowest increases (K_{L-Pd} =0.029 and 0.025 respectively). Analyzing the activation barriers $\Delta E^{\ddagger}$, their values range from $\Delta E^{\ddagger}$= 51.7 kcal mol^{-1}(P1) to $\Delta E^{\ddagger}$= 64.0 kcal mol^{-1}(C3). The systems with tertiary phosphines are associated with the lower $\Delta E^{\ddagger}$values.

Analyzing the variations of the bond components (ω^{σ} and ω^{π}), for all the systems, except for P1, the ω^{σ} values are positive, suggesting that the ligands in the process increase their donor power to the palladium. In particular, the carbenes exhibit the highest values of ω^{σ} (0.137 for C3), whereas P1 loses its donor ability in the process (ω^{σ} = -0.043). Futhermore, the ω^{π} values are negative for all the systems, suggesting a loss of acceptor capacity of all of them. In particular, this loss is more important for the carbenes, with values of ω^{π} of *ca* (-0.340) to (0.360). Among the phosphines series, P5 exhibit the most pronunced loss of acceptor capacity (ω^{π} = -0.331). These results can be rationalized as follows: when trans-$PdL_2(Ph)_2$ loses a ligand and the two phenyl rings approach to form the y-shaped transition state, the electron density on the palladium decrases, and, in order to stabilize the palladium center, the ligand is forced to increase its donor ability. Furthermore, since the palladium increases its donor ability toward the two phenyl rings, it loses the ability to transfer electronic density toward the ligand in π-symmetry. These electronic rearrangements, as already seen for the oxidative addition, are more remarkable for the NHC ligands, but, contrary to what was observed for the oxidative addition (see Chapter 5) are not correlated. In the oxidative addition process, the bigger the increase of the L→Pd σ-donation, the lower the L←Pd π-backdonation, and the linear correlation between these electronic rearrangements was satisfying. In the reductive elimination process, the correlation between ω^{σ} and ω^{π} is not observed. In addition, among the two processes, the ranges of variation ω^{σ} and ω^{π} are quite different. In the oxidative addition process, the ω^{σ} values range from -0.027 to 0.267, while in the reductive elimination from -0.043 to 0.137. Similarly, the ω^{π} values range from -0.250 to -0.380 in the oxidative addition process, and from -0.201 to -0.364 in the reductive elimination process. This suggests that the ligands are more able to change their donor-acceptor properties in the oxidative addition, since in such process the coordination of PhBr fragment on palladium is involved.

7.5.1 How Ligand-Palladium bond influences the energetic barriers ($\Delta E^{\ddagger}$)

In the previous section we have shown how different ligands, in the process of reductive elimination of Ph_2 from trans-$Pd_2(Ph)_2$ change their donor-acceptor abilities. In particular, we analyzed the nature of these variations in terms of charge transfers toward the palladium (σ-donation) and from the palladium (π-backdonation). We now extend the analysis to the energetic barriers ($\Delta E^{\ddagger}$) of the process. $\Delta E^{\ddagger}$ were calculated without the inclusion of the dispersion corrections, since we were interested only to the electronics effects of the ligand in the process. The values of $\Delta E^{\ddagger}$ are reported in Table 7.4, and range from 51.7 kcal mol^{-1}(P1) to 64.0 kcal mol^{-1}(C3). In general the phosphines exhibit lower values with respect to NHC ligands. C2 and C2 systems have the same $\Delta E^{\ddagger}$ values (59.1 kcal $mol^{-1}$and 59.0 kcal mol^{-1}respectively), despite they have a different electronic structure. In this section we analyze the $\Delta E^{\ddagger}$ values on the basis of CD-NOCV analysis of L-Pd bonds.

In Figures 7.9 and 7.10 are shown the $\Delta E^{\ddagger}$ values versus the ω^{σ} and ω^{π} values.

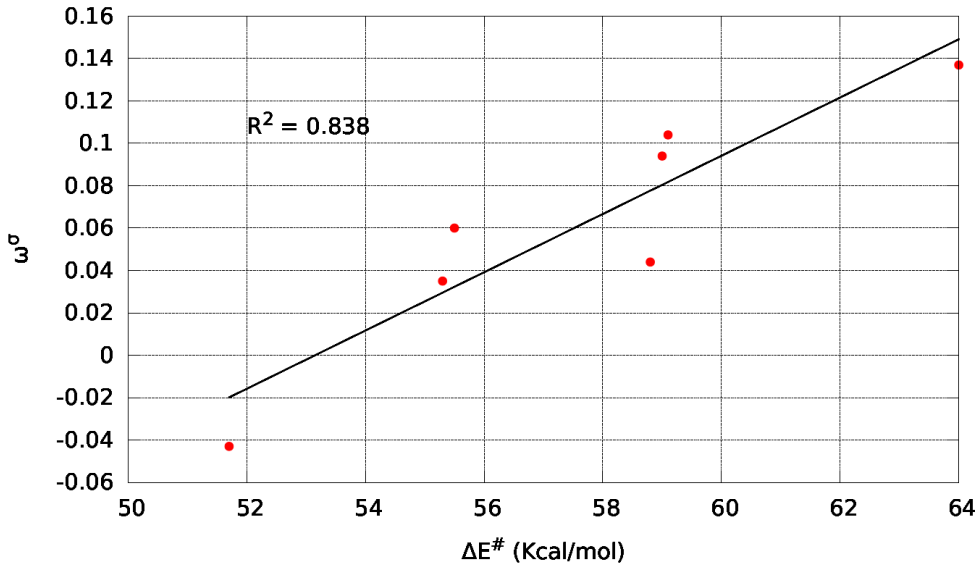

Figure 7.9: *Correlation between $\Delta E^{\ddagger}$ (kcal mol^{-1}) and ω^{σ} values for each analyzed ligand.*

Figure 7.9 (R^2 = 0.838) shows a correlation between the energetic barriers of the process ($\Delta E^{\ddagger}$) and the capacity of the ligand to increase its donor power (ω^{σ}). The bigger the capacity of the ligand to increase its donor power, the higher the activation barrier will be. The ligands that exhibit low ω^{σ} values (negative in the case of P1) show lower values of $\Delta E^{\ddagger}$. Another correlation between $\Delta E^{\ddagger}$ and ω^{π} can be observed in Figure 7.10.

Figure 7.10 shows that all the ligands lose their π-acceptor capacity in the process. The higher the loss of accepting capacity (ω^{π} negative) , such as NHCs, the higher the activation barrier will be. More generally, the ligand that exhibits the

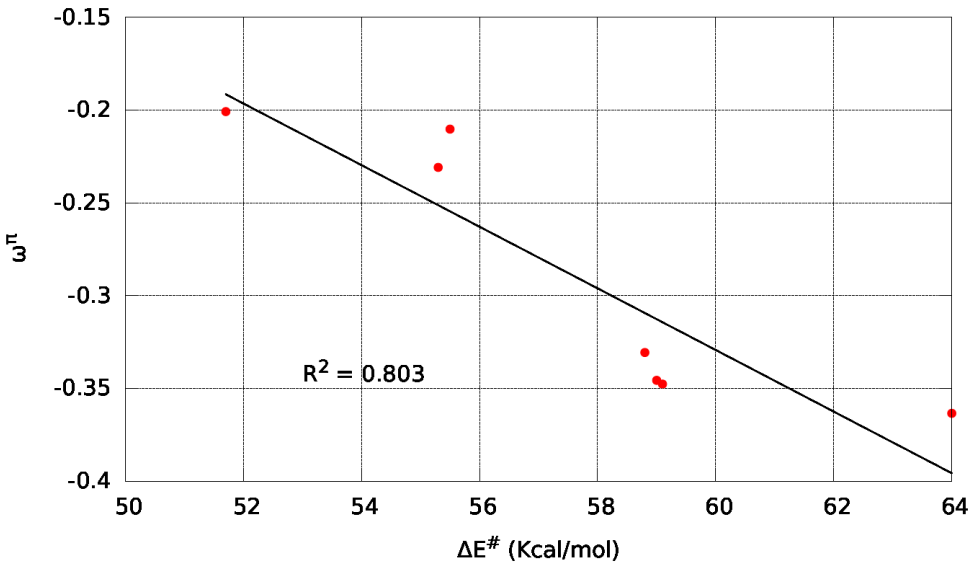

Figure 7.10: *Correlation between* $\Delta E^{\ddagger}$ *(kcal* mol^{-1}*) and* ω^{π} *values for each analyzed ligand.*

larger change in their electronic influences (NHC) are associated with larger activation energies.

No correlation between the electronic rearrangmets and K_{L-Pd} could be observed.

These results, similarly to what observed for the oxidative addition, can be qualitatively rationalized as follows: when *trans*-$L_2Pd(Ph)_2$ loses a ligand, the $Pd(Ph)_2$ fragment is more able to accept electronic density from the palladium center. Therefore the ligand, in order to stabilize the palladium center, is forced to increase its donor ability. Furthermore, upon the loss of a second ligand in *trans* to the first one, the latter loses the ability to transfer electronic density toward the ligand in π-symmetry.

These results need a parallel analysis on the Pd-C bonds, as already done for the oxidative addition on the basis of the NBO methodology. Unfortunately, the NBO analysis has not given satisyting data.

	$\Delta E^{\ddagger}$	r(L-Pd) (Å)	$CT_{\sigma}^{(0)}$ (e)	$CT_{\pi}^{(0)}$ (e)	$CT_{net}^{(0)}$ (e)
L_2PdPh_2-Tr					
P1	-	2.264	-0.185	0.225	0.0395
P2	-	2.282	-0.201	0.210	0.0091
P3	-	2.285	-0.202	0.220	0.0175
P4	-	2.316	-0.206	0.199	-0.0067
C1	-	2.018	-0.173	0.204	0.0309
C2	-	2.018	-0.180	0.218	0.0378
C3	-	2.033	-0.161	0.209	0.0478
	$\Delta E^{\ddagger}$	r(L-Pd) (Å)	$CT_{\sigma}^{(TS)}$ (e)	$CT_{\pi}^{(TS)}$ (e)	$CT_{net}^{(TS)}$ (e)
TSL-Cis					
P1	51.7	2.330	-0.177	0.179	0.002
P2	55.5	2.338	-0.213	0.166	-0.047
P3	55.3	2.354	-0.209	0.169	-0.040
P4	58.8	2.394	-0.215	0.133	-0.082
C1	59.1	2.088	-0.191	0.133	-0.058
C2	59.0	2.086	-0.197	0.143	-0.055
C3	64.0	2.087	-0.183	0.133	-0.050

Table 7.3: *Activation energies ($\Delta E^{\ddagger}$), ligand-Palladium bond distances (in Angstrom) and charge transfers results (e) obtained from the CD-NOCV analysis for the considered series of L_2PdPh_2-Tr and TSL-Cis systems.*

	$\Delta E^{\ddagger}$	ω^{σ}	ω^{π}	K_{L-Pd}
P1	51.7	-0.043	-0.201	0.029
P2	55.5	0.060	-0.210	0.025
P3	55.3	0.035	-0.231	0.030
P4	58.8	0.044	-0.331	0.034
C1	59.1	0.104	-0.348	0.035
C2	59.0	0.094	-0.346	0.034
C3	64.0	0.137	-0.364	0.027

Table 7.4: *Activation energies ($\Delta E^{\ddagger}$), ω^{σ}, ω^{π}, and K_{L-Pd} values obtained from the CD-NOCV analysis.*

7.6 Conclusions

In this chapter, we have carried out a computational analysis on the reductive elimination of biphenyl (Ph-Ph) from $L_2Pd(Ph)_2$ complexes with different ligands. Between the two possible pathways, the direct pathway, from *cis*-$L_2Pd(Ph)_2$, is more favorable for the aliphatic systems (as Ipr_3P, PH_3, and Cy_3P), while it is disfavored for the phosphites and the aromatic systems (except for PPh_3). This pathway is not possible for the systems bearing bulky ligands ($Ptbu_3$ and the biggest carbenes). The smallest carbenes show the highest energetic barriers for such process ($\Delta G^{\ddagger}$ = 22-23 kcal mol^{-1}), making such ligands not suitable for the direct reductive elimination. The dissociative pathway, involving the loss of a ligand from *cis*-$L_2Pd(Ph)_2$ and *trans*-$L_2Pd(Ph)_2$, leads to the formation of *cis*-$LPd(Ph)_2$, while *trans*-$LPd(Ph)_2$ are destabilized for all the ligand series. The energetic barriers for such process are very close among them ($\Delta G^{\ddagger}$ = 2-5 kcal mol^{-1}). *cis*-$LPd(Ph)_2$ are more stabilized when L = PH_3, $PIpr_3$ Ph_3P and OEt_3P. Conversely, such species are much more destabilized when the ligand is a carbene.

This study shows that it is not possible to predict *a priori* which kind of ligand favors the reductive elimination without a detailed analysis of the L-Pd bond. We have carried out such an analysis, for seven representative ligands, on the basis of NOCV-CD analysis. The purpose of this study was to show that the donor-acceptor power of a ligand can not be rationalized only on the basis of the nature of the ligand and many other factors can be considered (the metal center, the oxidative state of the metal, the species surrounding the ligand, *etc.*). For example, differently to what can be found in the literature, we have shown that, in *trans*-$PdL_2(Ph)_2$, the phosphine ligands have an higher donor power toward the palladium center and an higher acceptor power than the carbenes (excpet for tbu_3P). The same analysis in TSL-Cis gives the same quantitative results. This suggests that, more than focusing on the analysis of one species in a process, one could analyze the electronic rearrangement of a ligand going from a reactant to a transition state. In the case of the reductive elimination from *trans*-$PdL_2(Ph)_2$ to TSL-Cis, we have shown that the ligands are forced to increase their donor ability toward the palladium to stabilize the system, and in addition they lose their acceptor capacity from the palladium. These electronic rearrangements are more remarkable for the carbenes, to which are associated the highest electronic barriers (calculated without dispersion corrections and Gibbs corrections). There are satysfsing correlations between these rearrangements (ω^{σ} and ω^{π}) and the electronic barriers, suggesting that this methodology, can provide several tools to a better design of ligand in chemical processes.

Bibliography

[1] Bonney, K.; F., S. *Chem.Soc.Rev.* **2014**, *43*, 6609–6638.

[2] Perdew, J.; Burke, K.; Ernzerhof, M. *Phys. Rev. Lett.* **1996**, *77*, 3865–3868.

[3] Perdew, J.; Burke, K.; Ernzerhof, M. *Phys. Rev. Lett.* **1997**, *78*, 1396.

[4] Andrae, D.; Haubermann, U.; Dolg, M.; Stoll, H.; Preub, H. *Theor. Chim. Acta* **1990**, *77*, 123.

[5] Ehlers, A.; Bohme, M.; Dapprich, S.; Gobbi, A.; Hollwarth, A.; Jonas, V.; Kohler, K.; Stegmann, F.; Veldkamp, A.; Frenking, G. *Chem.Phys.Lett.* **1993**, *208*, 111.

[6] Neese, F. *Comput. Mol. Sci.* **2012**, *2*, 73.

[7] Grimme, S.; Antony, J.; Ehrlich, S.; Krieg, H. *J. Chem. Phys.* **2010**, *132*, 1456.

[8] Grimme, S.; Ehrlich, S.; Goerigk, L. *J.Comput.Chem.* **2011**, *32*, 1456.

[9] Fonseca Guerra, C.; Snijders, J.; de Velde, G.; Baerends, E. *Theor. Chem. Acc.* **1998**, *99*, 391.

[10] te Velde, G.; Bickelhaupt, F.; Baerends, C., E.J. Fonseca Guerra; van Gisbergen, J., S.J.A. Snijders; Ziegler, T. *J. Comp. Chem.* **2001**, *22*, 931.

[11] Van Lenthe, E.; Baerends, E.; Snijders, J. *J. Chem. Phys.* **1993**, *99*, 4597.

[12] Van Lenthe, E.; Baerends, E.; Snijders, J. *J. Chem. Phys.* **1994**, *101*, 9783.

[13] Van Lenthe, E.; Ehlers, A.; Baerends, E. *J. Chem. Phys.* **1999**, *110*, 8943.

General Conclusions

In this thesis we provided theoretical studies on several palladium catalyzed cross-coupling processes, with the goal to gain a better understanding of such reactions using the tools of computational chemistry. In the first chapter we provided an historical overview of the palladium cross-coupling processes, pointing out the importance of this kind of catalysis, the features of the palladium and the reasons for which this metal is preferred over the others metals of groups 10 and 11 in the cross-coupling processes.

In the second chapter we presented the theoretical models considered for our analysis. The most essentially tools used in this work are:

- *Density Functional Theory* (DFT) for the characterization of the energetic paths with the relative stationary points.
- *Dispersion correction to the energy*, based on the Grimme model, in order to analyze how such corrections change the relative energies of the stationary points along the energetic paths and, consequentely, the activation barriers of the different processes.
- *Charge Displacement Analysis by Natural Orbital for Chemical Valence* (CD-NOCV) for a detailed study of the L-Pd chemical bond, by which we obtained reliable and consistent measures of σ-donation and π-backdonation charges.
- *Natural Bond Orbital Analysis* (NBO), to quantify the interactions between the palladium and the organo-halide substrate, in the oxidative addition and reductive elimination processes, in order to investigate how these interactions are influenced by changing the auxiliary ligand bounded to palladium.

The thesis was divided in two main parts. The first one, called *REAL SYSTEMS* was devoted to a mechanistic investigation, at the DFT level, on experimental processes with the goal of reproducing experimental parameters and of clarifying their origin. The second one, called *MODEL SYSTEMS*, was devoted to a better understanding of the effect of different ligands on the most common steps of Pd-catalyzed processes.

As first example of *REAL SYSTEMS* we have studied the Pd-catalyzed hydrophosphonylation of alkenes with dialkyl H-phosphonates (Chapter 3). For this reaction, experimentally, a completely different regioselectivity of the two possible products, highly dependent on the nature of dialkyl-H phosphonate substrates, was

found. The theoretical mecanistic study of this reaction was complicated by the several different conformations of the L-Pd(styrene) species, very close in relative energy among them, which led to different energetic pathways with the relative regioselectivity. Since a rationalization of the different regioselectivities on the base of a pure mecanistic study was problematic, we carried out a theoretical kinetic model, using the COPASI software and the Eyring model. The goal of this study was to reproduce the experimental ratio of the two possible products and individuating the most accesible energetic pathways. The results were in a very good agreement with the experiments, showing how this kind of kinetic models can be of great help in absence of mecanistic data.

The second example of *REAL SYSTEMS* studied was the arylation of fluorobenzene mediated by Pd(0) catalyst (Chapter 4). The experimental results show that the C-H bond activation of the fluorinated substrate is the rate determining step of the whole process. Our theoretical investigation was devoted to clarify which energetic pathway was preferred and to reproduce the activation barrier. In the process, the silver carbonate (Ag_2CO_3) was used as base, and, depending on its nature ($AgCO_3$ or $AgCO_3^-$) two energetic pathways are possible. Our calculations clearly suggest that the pathways involving $AgCO_3^-$ as base is preferred in terms of energy. In addition, we proved that the C-H bond activation is the rate determining step, with a relative energetic value that is in a very good agreement with the experiment.

As prototype of *MODEL SYSTEM* we performed calculations on the Negishi catalytic cycle with different ligands, among tertiary-phosphines and heterocyclic carbenes, with the goal of analyzing the effect of different ligands on the three main steps of the cycle. Moreover, a comparative mechanistic study, including and not including the dispersion correction to the energy was carried out.

In the case of oxidative addition (Chapter 5) two possible mechanisms are possible: associative and dissociative. The phosphines are much more efficient in favoring this step than the carbenes (except for the phosphites), showing lower activation barriers. The inclusion of the dispersion correction to the energy changes the energetic for the systems bearing bulky ligands, while for the small ligands such correction is essentially negligible. The dispersion corrections favor much more the associative pathway, because of the presence of a large number of pairwise interaction between non-bonded atoms.

For the transmetalation step (Chapter 6) a single mechanism for all the ligands was found. In absence of additional species, this step in many case is largely disfavored. This mechanism can occur with both the *cis* and *trans* isomers of Pd complex. The main effect of the dispersion corrections, especially on the bulky systems, is lowering the activation barriers. However, in some case (L = $P(iPr)_3$ for example), even if the dispersion corrections lower the barrier for the *trans* pathway, the *cis* one is still favored due to the relative positions of the stationary points.

For the reductive elimination step (Chapter 7), as seen for the oxidative addition, associative and dissociative pathways are possible. The phosphines are much more efficient in favoring this step than the carbenes showing lower activation

barriers. The inclusions of the dispersion corrections, especially for the bulky systems, favor the associative pathway. Summarizing the results for these three main steps, the nature of the ligand change the rate determining step of the whole cycle, and the lower values of the rate determining step are associated with the aromatic phosphines.

As additional study, we have carried out a theoretical investigation, on the dissociative pathways of oxidative addition, by using the CD-NOCV and NBO model on several ligands. The main goal of the study was to investigate how the bond components (σ-donation and π-backdonation) change going from the reactant to the transition states, and how these bond components influence the activation barriers. The prelimiary results show that, in the process, all the ligands (except PH_3 and $P(Me)_3$) increase their donor power, while their acceptor power decrease. These electronic rearrangements are more remarkably for the carbene ligands. The more important is the electronic rearrangement in the process, the highest the activation barrier will be.

Résumé en Français

Cette thèse est dédiée à l'étude, aux moyens des méthodes de la chimie computationnelle, de certains processus de formation de liaisons C-C catalysés par des complexes du palladium. L'objectif essentiel de ce travail est d'essayer de comprendre plus finement les influences électroniques et stériques des ligands ancillaires sur l'activité des catalyseurs.

Le premier chapitre de la thèse est consacré à une présentation du contexte expérimental associé aux processus de couplages C-C catalysés par le palladium. Un bref panorama historique de ce type de réaction est tout d'abord dressé en présentant les processus de couplage catalysés au cuivre (Glaser, Ullman), pour ensuite aborder une présentation des processus au palladium (Heck and Suzuki-Miyaura). Ceci permet d'avoir clair à l'esprit les étapes fondatrices ayant permis de développer ce champ de recherche. Ensuite une présentation générale de cycle catalytique de ces transformations permet de définir les trois grandes classes de réactions qui seront abordées dans ce travail doctoral :

- addition oxydante
- transmetallation
- élimination réductrice

Ce premier chapitre se termine par une description des atouts que revêt une approche théorique permettant de mieux comprendre les mécanismes de réaction. Il y est fait notamment mention de la capacité d'explorer différents chemins réactionnels afin de pouvoir déterminer lequel est le plus favorable. On peut notamment ainsi tester l'influence des propriétés électroniques et stériques des différents ligands autour du métal pour favoriser ou, au contraire, défavoriser une voie particulière.

Le second chapitre est essentiellement consacré à une présentation succinte des aspects théoriques associés aux différentes méthodes calculatoires utilisées. Comme la totalité des calculs de cette thèse ont été effectués grâce à la théorie de la fonctionnelle de la densité, un bref rappel des hypothèses de base de cette approche est présenté. Il ne s'agit pas ici d'être exhaustif, mais plutôt d'indiquer les points de repères cruciaux de la méthode. Comme ces dernières années se sont développées des méthodes permettant de prendre en compte les intéractions non-covalentes entre atomes, souvent mal représentées par des approches DFT, une

présentation rapide de l'approche de Grimme est donnée. Celà permet au lecteur de rapidement se faire une idée de comment ce type d'interactions peut être introduit à faible coût dans les calculs. L'objet de la thèse est d'obtenir des chemins réactionnels mais aussi d'essayer de comprendre pourquoi telle ou telle étape est plus ou moins difficile. Aussi avons nous utilisé deux méthodes d'analyses dans ce travail. La méthode NBO (Natural Bond Orbital) essaie de modéliser l'information contenue dans la fonction d'onde comme résultant d'une structure de Lewis. Ceci conduit à une représentation de la structure électronique d'une molécule au moyen de concepts familiers du chimiste. Une autre méthode d'analyse a été utilisée dans ce manuscript : la méthode CD-NOCV pour Charge Displacement Analysis via Natural Orbitals for Chemical Valence. Ici il s'agit plutôt d'essayer de quantifier les transferts électroniques entre deux fragments A et B lorsqu'une liaison est formée entre ces deux fragments. Sans tomber dans l'excès des développements méthodologiques, ce chapitre présente pour chacun des cas le contexte conceptuel permettant d'apprécier ce que l'on peut attendre des différentes méthodes.

Après ces deux chapitres introductifs, cinq chapitres différents présentent différents aspects du travail de thèse. Les chapitres 3 et 4 sont consacrés à l'étude de transformations effectuées par des groupes expérimentaux avec lesquels nous avons collaboré. Il s'agit d'études sur des systèmes réels. Les trois derniers chapitres quant à eux sont consacrés à des études sur des systèmes modèles dans l'objectif de comprendre plus finement l'interaction entre effets électroniques et stériques des ligands sur les trois grands types de réaction mentionnés ci-dessus.

Le chapitre trois est consacré à l'étude du mécanisme de réaction d'hydrophosphonylation des alcènes catalysée par un complexe du palladium portant une phosphine encombrée (DavePhos). Le travail expérimental, effectué dans le groupe du Prof. Jean-Marc Campagne (Ecole de Chimie) avait montré qu'avec le même catalyseur, la régiochimie des produits pour la réaction du styrène dépendait fortement du phosphonate utilisé. Les objectifs des calculs étaient tout d'abord de déterminer le mécanisme de réaction pour ensuite essayer de comprendre l'origine de l'inversion de régiochimie observée. Les calculs ont été effectués sur les systèmes réels avec prise en compte explicite des interactions non covalentes. Les calculs ont montré que l'addition oxydante P-H sur le palladium n'est pas possible sur le complexe PdL (L = DavePhos) mais en revanche est possible sur le complexe Pd(L)(L') (L = DavePhos, L' = Styrene). La coordination du substrat styrène est donc un prérequis pour que l'activation de la liaison P-H soit possible. En raison de la géométrie du ligand DavePhos et du styrène, il a fallu considérer huit complexes différents Pd(L)(L') comme reactifs potentiels pour l'activation P-H. La proximité énergétique de ces différents complexes n'a pas permis d'en sélectionner un en particulier (le plus stable) et nous avons donc considéré simultanément huit chemins réactionnels en parallèle pour chaque phosphonate, soit au total 16 chemins différents. Après l'addition oxydante de la liaison P-H, le styrène coordonné s'insère dans la liaison Pd-H et, après une isomérisation, le produit final est libéré après une élimination réductrice formant la liaison P-C. L'abondance des données calculatoires et la proximité d'un grand nombre de valeurs n'a pas permis de mettre en évidence un chemin particulier qui aurait permis d'expliquer les

observations expérimentales. En revanche, au moyen du logiciel COPASI, nous avons pu construire un modèle cinétique permettant de considérer simultanément les huit chemins. Quatre de ces chemins conduisent tous au même régioisomère, alors que les quatre autres fournissent l'autre régioisomère. Les résultats de cette modélisation cinétiques ont permis de reproduire, presque quantitativement, les ratio observés entre les deux régioisomères. Plus spécifiquement, l'inversion observée expérimentalement a été reproduite par les calculs. Cette étude montre, qu'en prenant en compte la complexité du système expérimental, les calculs peuvent reproduire finement les observations expérimentales.

Le chapitre 4 aborde une étude de la réaction d'arylation de fluorobenzene catalysée par un complexe de Pd(0). Les études expérimentales ont été effectuées dans le groupe du Prof. Robin Perutz (York). Ce processus consiste en trois étapes : addition oxydante C-I d'un iodure d'aryle, activation C-H du fluorbenzène par une base coordonnée au palladium, et finalement formation de la liaison C-C par élimination réductrice permettant de regénérer le Pd(0). L'étude de la réaction d'addition oxydante a montré que l'inclusion des corrections de dispersion a un effet sur la nature du chemin privilégié. En l'absence de ces corrections, l'addition oxydante de Ph-I est préférée sur $Pd(PPh_3)$, un catalyseur ne présentant qu'une phosphine. En revanche avec les corrections de dispersion, l'addition oxydante se fait préférentiellement sur $Pd(PPh_3)_2$, un catalyseur avec deux phosphines. Après l'addition oxydante, la substitution de l'iodure par $AgCO_3^-$ permet de générer l'espèce active pour activer la liaison C-H de C_6F_5H. Cette activation se fait selon un mécanisme de type AMLA et les calculs ont montré que la présence du cation argent favorise ce processus en créant des interactions avec les noyaux aromatiques de la phopshine. La fonctionalisation est effective grâce à l'élimination réductrice associée à la formation de la liaison C-C. Au final l'étape cinétiquement déterminante est l'activation C-H en accord avec les résultats expérimentaux et la barrière calculée est proche de la valeur déterminée par étude cinétique.

Le chapitre 5 est le premier chapitre qui aborde les systèmes modèles. Il concerne l'étude de la réaction d'addition oxydante de PhBr sur PdL_n (n = 1, 2). Pour cette réaction, la rupture de la liaison C-Br peut se faire soit sur une espèce mono-L ou bis-L. Nous avons considéré toute une série de ligand phosphine L = PR_3 et quelques ligands NHC (N-heterocyclic carbenes). Le résultat essentiel de ce chapitre concerne le nombre de ligands L en fonction de l'inclusion ou non des corrections de dispersion. Sans correction de dispersion le chemin préféré est associé à l'addition oxydante sur une espèce Pd-L. En revanche lorsque les corrections de dispersion sont introduites, alors l'addition oxydante devient préférée sur le système PdL_2. Ce changement de comportement est dû à la prise en compte de multiples interactions attractives entre atomes non liés lorsque les corrections de dispersion sont introduites. Plus les ligands seront encombrants, plus il y aura de telles attractions. La préférence pour un chemin d'addition oxydante avec deux ligands n'en sera alors que plus forte.

Dans le chapitre 6 est abordé la réaction de transmetallation dans le cas de la réaction de Negishi. Ici le substrat est ZnPhBr et la transmetallation se fait sur le complexe d'addition oxydante le plus stable trans-PdL_2(Ph)(Br). Ici encore les

chemins avec une phosphine ou deux phosphine ont été étudiés pour tous les ligands considérés. Comme dans le cas de l'addition oxydante, la prise en compte des interactions dispersives modifie profondément les préférences énergétiques entre les deux types de chemins. Pour des phosphines encombrées, les interactions de dispersion ont tendance à favoriser les structures compactes et donc les chemins avec deux phosphines.

Enfin le dernier chapitre concerne l'étude de la formation de la liaison C-C par élimination réductrice à partir de cis-PdL_2Ph_2. Là encore deux possibilités existent selon le nombre total de ligand L présents dans la sphère de coordination au moment de l'élimination réductrice. La prise en compte des interactions de dispersion est encore ici cruciale pour décider quel est le chemin préféré. Comme pour les deux autres trasnformations, les ligands encombrés favorise la transformation avec deux ligands L.

Une étude de l'ensemble des barrières d'activation pour chacun des trois processus lorsque les interactions de dispersion sont considérées ne montre pas de tendance claire parmi tous les ligands. En fait, il ne se dégage pas une tendance permettant de dire qu'une des trois étapes est l'étape cinétiquement déterminante et ainsi d'étudier l'effet de L sur cette étape. Selon la nature du ligand L, la nature de l'étape cinétiquement déterminante varie. On peut qualitativement identifier quel système sera le plus réactif. En revanche il sera difficile d'identifier un facteur qui permette d'améliorer l'activité des catalyseurs de manière globale puisque ce qui rend l'addition oxydante efficace n'est pas identique à ce qui rend l'élimination réductrice efficace. Selon la nature de l'étape cinétiquement déterminante, il faudra jouer sur l'un ou l'autre des aspects.

Acknowledgments

Many people, somehow, have contributed to the present thesis. First of all I would express my gratitude to my supervisor, Eric Clot, for everything he taught me, for his support and, above all, for his patience. Merci beaucoup. Thanks also to Odile Eisenstein, for the collaboration and the interesting scientific discussions. Thanks to the people of CTMM group who aided me in these years. In particular many thanks to Fabrice for having solved all my "informatic problems "and Thibaud for his support in the last months. Thank to those who shared the office with me: Gerard, David, Simona, Emmeline and Gudrun. Thanks to Prof. Francesco Tarantelli, Dr. Leonardo Belpassi, Giovanni Bistoni and Carlo Gaggioli for their support from Perugia and for the opportunity to collaborate together once again in using the Charge Displacement analysis. Thanks to all the people with which I shared this experience, not only from a scientific point of view. My gratitude goes to the "team of the first floor": Fabrizio, Stefano ("che muscoli") , Filippo, Luca, Elia, Francesco ("the French"), Giorgio, Simona, Lorenzo, Sara. Thank you for the time spent together. My wide gratitude goes to my mother and my brother for their constant support and to the people that, even if not present here, did not miss their support from Italy. In particular my uncles, my cousins, Gianni and Ivan.